



MINISTÉRIO DA CIÊNCIA, TECNOLOGIA E INOVAÇÃO
INSTITUTO NACIONAL DE PESQUISAS ESPACIAIS

sid.inpe.br/mtc-m21d/2024/02.22.12.30-TDI

**DEVELOPMENT OF UNINTERRUPTED
CORRELATIONS OF WORKING FLUID PROPERTIES
FOR PASSIVE TWO-PHASE HEAT TRANSFER
DEVICES WITHIN AND OUT OF OPERATING
TEMPERATURE LIMITS**

Alan Felipe Castilho Maia

Master's Dissertation of the Graduate Course in Engineering and Space Technology/ Engineering and Space Systems Management, guided by Drs. Valeri Vlassov Vladimirovich, and Rafael Lopes Costa, approved in February 20, 2024.

URL of the original document:

<<http://urlib.net/8JMKD3MGP3W34T/4AQ4ASL>>

INPE
São José dos Campos
2024

PUBLISHED BY:

Instituto Nacional de Pesquisas Espaciais - INPE
Coordenação de Ensino, Pesquisa e Extensão (COEPE)
Divisão de Biblioteca (DIBIB)
CEP 12.227-010
São José dos Campos - SP - Brasil
Tel.:(012) 3208-6923/7348
E-mail: pubtc@inpe.br

**BOARD OF PUBLISHING AND PRESERVATION OF INPE
INTELLECTUAL PRODUCTION - CEPPII (PORTARIA Nº
176/2018/SEI-INPE):****Chairperson:**

Dra. Marley Cavalcante de Lima Moscati - Coordenação-Geral de Ciências da Terra
(CGCT)

Members:

Dra. Ieda Del Arco Sanches - Conselho de Pós-Graduação (CPG)
Dr. Evandro Marconi Rocco - Coordenação-Geral de Engenharia, Tecnologia e
Ciência Espaciais (CGCE)
Dr. Rafael Duarte Coelho dos Santos - Coordenação-Geral de Infraestrutura e
Pesquisas Aplicadas (CGIP)
Simone Angélica Del Ducca Barbedo - Divisão de Biblioteca (DIBIB)

DIGITAL LIBRARY:

Dr. Gerald Jean Francis Banon
Clayton Martins Pereira - Divisão de Biblioteca (DIBIB)

DOCUMENT REVIEW:

Simone Angélica Del Ducca Barbedo - Divisão de Biblioteca (DIBIB)
André Luis Dias Fernandes - Divisão de Biblioteca (DIBIB)

ELECTRONIC EDITING:

Ivone Martins - Divisão de Biblioteca (DIBIB)
André Luis Dias Fernandes - Divisão de Biblioteca (DIBIB)



MINISTÉRIO DA CIÊNCIA, TECNOLOGIA E INOVAÇÃO
INSTITUTO NACIONAL DE PESQUISAS ESPACIAIS

sid.inpe.br/mtc-m21d/2024/02.22.12.30-TDI

**DEVELOPMENT OF UNINTERRUPTED
CORRELATIONS OF WORKING FLUID PROPERTIES
FOR PASSIVE TWO-PHASE HEAT TRANSFER
DEVICES WITHIN AND OUT OF OPERATING
TEMPERATURE LIMITS**

Alan Felipe Castilho Maia

Master's Dissertation of the Graduate Course in Engineering and Space Technology/ Engineering and Space Systems Management, guided by Drs. Valeri Vlassov Vladimirovich, and Rafael Lopes Costa, approved in February 20, 2024.

URL of the original document:

<<http://urlib.net/8JMKD3MGP3W34T/4AQ4ASL>>

INPE
São José dos Campos
2024

Cataloging in Publication Data

Maia, Alan Felipe Castilho.

Ma28d Development of uninterrupted correlations of working fluid properties for passive two-phase heat transfer devices within and out of operating temperature limits / Alan Felipe Castilho Maia. – São José dos Campos : INPE, 2024.
xxxvi + 269 p. ; (sid.inpe.br/mtc-m21d/2024/02.22.12.30-TDI)

Dissertation (Master in Engineering and Space Technology/ Engineering and Space Systems Management) – Instituto Nacional de Pesquisas Espaciais, São José dos Campos, 2024.

Guiding : Drs. Valeri Vlassov Vladimirovich, and Rafael Lopes Costa.

1. Heat Pipes. 2. Operating temperature limits. 3. Working fluid properties. 4. Uninterrupted correlations. 5. Thermo-physical properties of water. I.Title.

CDU 536.5:629.7



Esta obra foi licenciada sob uma Licença [Creative Commons Atribuição-NãoComercial 3.0 Não Adaptada](https://creativecommons.org/licenses/by-nc/3.0/).

This work is licensed under a [Creative Commons Attribution-NonCommercial 3.0 Unported License](https://creativecommons.org/licenses/by-nc/3.0/).



MINISTÉRIO DA
CIÊNCIA, TECNOLOGIA
E INOVAÇÃO



INSTITUTO NACIONAL DE PESQUISAS ESPACIAIS

DEFESA FINAL DE DISSERTAÇÃO ALAN FELIPE CASTILHO MAIA BANCA Nº 014/2024, REG. 277894/2021

No dia 20 de fevereiro de 2024, às 09:30h, por teleconferência, o(a) aluno(a) mencionado(a) acima defendeu seu trabalho final (apresentação oral seguida de arguição) perante uma Banca Examinadora, cujos membros estão listados abaixo. O(A) aluno(a) foi APROVADO(A) pela Banca Examinadora, por unanimidade, em cumprimento ao requisito exigido para obtenção do Título de Mestre em Engenharia e Tecnologia Espaciais / Engenharia e Gerenciamento de Sistemas Espaciais, com a exigência de que o trabalho final a ser publicado deverá incorporar as correções sugeridas pela Banca Examinadora, com revisão pelo(s) orientador(es).

Título: "Development of uninterrupted correlations of working fluid properties for passive two-phase heat transfer devices within and out of operating temperature limits."

Membros da Banca:

Dr. Valeri Vlassov Vladimirovich – Orientador / Presidente - INPE

Dr. Rafael Lopes Costa - Orientador - INPE

Dr. Evaldo José Corat - Membro Interno - INPE

Dr. Gustavo Adolfo Ronceros Rivas - Membro Externo - UNILA



Documento assinado eletronicamente por **Valeri Vlassov Vladimirovich, Tecnologista**, em 22/02/2024, às 09:00 (horário oficial de Brasília), com fundamento no § 3º do art. 4º do [Decreto nº 10.543, de 13 de novembro de 2020](#).



Documento assinado eletronicamente por **Evaldo José Corat, Pesquisador Titular**, em 22/02/2024, às 12:30 (horário oficial de Brasília), com fundamento no § 3º do art. 4º do [Decreto nº 10.543, de 13 de novembro de 2020](#).



Documento assinado eletronicamente por **Gustavo Adolfo Ronceros Rivas (E), Usuário Externo**, em 26/02/2024, às 12:41 (horário oficial de Brasília), com fundamento no § 3º do art. 4º do [Decreto nº 10.543, de 13 de novembro de 2020](#).



Documento assinado eletronicamente por **Rafael Lopes Costa, Chefe da Divisão de Mecânica Espacial e Controle**, em 05/03/2024, às 07:47 (horário oficial de Brasília), com fundamento no § 3º do art. 4º do [Decreto nº 10.543, de 13 de novembro de 2020](#).



A autenticidade deste documento pode ser conferida no site <https://sei.mcti.gov.br/verifica.html>, informando o código verificador **11726867** e o código CRC **79A42441**.

Referência: Processo nº 01340.001286/2024-38

SEI nº 11726867

“Доверяй, но проверяй.” (Trust, but verify.)

Russian proverb

To Maria Fernanda, my pillar of strength and source of unwavering support; your love has been the guiding light throughout this academic endeavor. Your patience, encouragement, and belief in me have made this journey not only bearable but also incredibly rewarding. Thank you for being my constant inspiration. And, to my dog Rute, your wagging tail and comforting presence have added joy and warmth to every moment.

ACKNOWLEDGMENT

I would like to express my deepest gratitude to my wife, Maria Fernanda. Her understanding and encouragement have been invaluable, and to our beloved dog, Rute.

I am also immensely thankful to my parents for their constant love and support, which has been the foundation of my perseverance. Also, to my friend Dr. Paulo Caixeta, his belief in my abilities has been a driving force.

Special thanks go to my dedicated advisors, Dr. Valeri, and Dr. Rafael, for their exceptional guidance, mentorship, and tireless commitment. Their expertise and encouragement have played a pivotal role in helping me achieve the title of Master. I am profoundly grateful for the knowledge and skills they have imparted to me.

This accomplishment would not have been possible without the collective support of these amazing individuals. Thank you all for being an integral part of this significant milestone in my academic journey.

ABSTRACT

The rapid evolution of computational technology leads widespread use of numerical simulations in projects. These simulations offer cost-effective alternatives to extensive experimental work, using advanced mathematical models to represent complex physical phenomena. The focus of this work is on two-phase heat transfer devices, specifically heat pipes, whose performance depends on thermo-physical properties taking water as a working fluid. In this work it is proposed new-type approximations of 13 thermo-physical properties of water needed for heat pipes complex mathematical models, which could be able to simulate transient modes over the entire temperature range without interruptions either in value or derivative, including start-up from freeze or supercritical conditions. All property formats are unified to be dimensionless and to have values 0 at the triple point and 1 at the critical point to all 13 properties. For the first time, the approximations are presented not in the commonly used format of closed-form empirical correlations, but in the form of pseudo-code, which can be implemented in any programming language. Smoothing within the piecewise functions and between matter states is performed by an interfacing algorithm with application of the Heaviside functions. Optimal parameters of some approximations are obtained with a developed random-search algorithm completed with a feature of interactive bounds reduction. A criterion which combines minimal average absolute deviation and minimal maximal deviation, factored with dimensionless weights, was used. Despite the significance of this topic for heat pipe numerical simulations, no prior publications have been found. The work presented is groundbreaking, linking all three major states of matter (freezing, saturation, and supercritical zones) and using water as working fluid for heat pipe.

Keywords: Heat Pipes. Operating temperature limits. Working fluid properties. Uninterrupted correlations. Thermo-physical properties of water.

DESENVOLVIMENTO DE CORRELAÇÕES CONTÍNUAS DE PROPRIEDADES DO FLUIDO DE TRABALHO PARA DISPOSITIVOS PASSIVOS DE TRANSFERÊNCIA DE CALOR BIFÁSICO DENTRO E FORA DOS LIMITES DE TEMPERATURA DE OPERAÇÃO

RESUMO

A rápida evolução da tecnologia computacional conduz ao amplo uso de simulações numéricas em projetos. Essas simulações oferecem alternativas economicamente viáveis para extenso trabalho experimental, utilizando modelos matemáticos avançados para representar fenômenos físicos complexos. O foco deste trabalho está voltado para dispositivos de transferência de calor de duas fases, especificamente tubos de calor, cujo desempenho depende de propriedades termo físicas considerando a água como fluido de trabalho. Neste trabalho, são propostas novas aproximações de 13 propriedades termo físicas da água necessárias para modelos matemáticos complexos de tubos de calor, que podem ser capazes de simular modos transitórios em toda a faixa de temperatura sem interrupções, seja no valor ou na derivada, incluindo a inicialização a partir de condições de congelamento ou supercríticas. Todos os formatos de propriedades são unificados para serem adimensionais e terem valores 0 no ponto triplo e 1 no ponto crítico para todas as 13 propriedades. Pela primeira vez, as aproximações são apresentadas não no formato comumente usados de correlações empíricas em forma fechada, mas na forma de pseudocódigo, que pode ser implementado em qualquer linguagem de programação. O suavizamento dentro das funções e entre estados da matéria é realizado por um algoritmo de interface com a aplicação de funções de Heaviside. Parâmetros ótimos de algumas aproximações são obtidos com um algoritmo de busca aleatória desenvolvido com uma característica de redução interativa de limites. Um critério que combina desvio médio absoluto mínimo e desvio máximo mínimo, ponderado com pesos adimensionais, foi utilizado. Apesar da importância desse tópico para simulações numéricas de tubos de calor, nenhuma publicação anterior foi encontrada. O trabalho apresentado é

inovador, vinculando os três principais estados da matéria (sólido, saturação e zonas supercríticas) e utilizando a água como fluido de trabalho para tubos de calor.

Palavras-chave: Tubos de calor. Limites de temperatura operacional. Propriedades dos fluidos de trabalho. Correlações ininterruptas. Propriedades termo físicas d'água.

FIGURE LIST

	<u>Page</u>
Figure 1.1 – Heat pipe schematic.....	1
Figure 1.2 – Comparative simulation analyzes: CBERS3 Satellite panel with and without embedded heat pipe.	2
Figure 2.1 – c_{pV} polynomial approximation behavior within and out of the specified range.	9
Figure 2.2 – Difference between tabled saturation pressure and Clausius-Clapeyron equation.	12
Figure 4.1 – Working fluids grading results.	15
Figure 4.2 – Figure of merit (liquid based) for different fluids.	17
Figure 4.3 – Figure of merit (vapor based) for different fluids.....	17
Figure 4.4 – Vapor Pressure as a Function of Temperature, Potential Heat Pipe or LHP Working Fluids.	18
Figure 4.5 – Vapor pressure of ice versus inverse temperature for selected experimental data.....	21
Figure 4.6 – The ratio of selected ice vapor pressure data.	22
Figure 4.7 – Ratios of various parametrizations of the vapor pressure of ice to the nominal thermodynamic solution proposed by (MURPHY; KOOP, 2005).	23
Figure 4.8 – Discontinuity in the changing phase.....	27
Figure 4.9 – Result deviation by comparison between Equation (4.17) and (4.18).	28
Figure 4.10 – Correlation between thermal conductivity and temperature.	35
Figure 4.11 – Correlation between vapor heat capacity and temperature.	38
Figure 4.12 – Comparative study of c_p made by (MURPHY; KOOP, 2005).....	39
Figure 4.13 – Comparative study of c_p developed by (MURPHY; KOOP, 2005) continuation.....	39
Figure 4.14 – Correlation between density and temperature.....	42
Figure 4.15 – Correlation between dynamic viscosity and temperature.	44
Figure 4.16 – Correlation between specific heat and temperature.	50

Figure 5.1 – Correlation between water surface tension and saturation temperature.....	56
Figure 5.2 – Example of function tendency for different “a” value.	56
Figure 5.3 – Two equations of fluid properties at T_3	59
Figure 5.4 – Interfacing example around $\tau=0$	60
Figure 5.5 – Interfacing example around $\tau=1$	62
Figure 5.6 – Interfacing for general case.	66
Figure 5.7 – Example of piecewise function with conjugation by Heaviside function.....	70
Figure 5.8 – The impact of a Heaviside function on an approximation curve. ..	71
Figure 5.9 – Algorithm block diagram.	73
Figure 5.10 – Excel Sheet function mapping.	76
Figure 5.11 – Cases with more iteration.	77
Figure 5.12 – Compilations of all cases number of iterations.	78
Figure 6.1 – Water vapor pressure data.	79
Figure 6.2 – Faghri polynomial approximation.....	80
Figure 6.3 – Vapor pressure approximation result in saturated zone “as is”. ...	82
Figure 6.4 – Logarithm Vapor pressure approximation in saturated zone.	83
Figure 6.5 – Deviation of Data and Clausius–Clapeyron equation for saturated zone.	84
Figure 6.6 – Property data in freezing (sublimation) zone.	85
Figure 6.7 – Vapor pressure approximation result in freezing zone.	86
Figure 6.8 – Final Result to interfacing below sub freezing point.	88
Figure 6.9 – Correlation between dimensionless pressure and dimensionless temperature for water above critical point and with a density equal to 322 kg/m^3	90
Figure 6.10 – Property data in supercritical zone.	91
Figure 6.11 – Vapor pressure approximation result in supercritical zone by density.....	93
Figure 6.12 – Final result with interfacing at critical point.	95
Figure 6.13 – Interfacing supercritical region details.	95

Figure 6.14 – Final result to vapor pressure approximation in the entire temperature range.....	96
Figure 6.15 – Water vapor density data.	98
Figure 6.16 – Faghri polynomial approximation.....	99
Figure 6.17 – Vapor density approximation result in saturated zone.....	100
Figure 6.18 – Approximation by three piecewise functions.	101
Figure 6.19 – Detail of Heaviside function application in approximation for saturated zone.....	102
Figure 6.20 – Vapor density in freezing zone.	103
Figure 6.21 – Result to the interface around the triple point.....	105
Figure 6.22 – Final result for the interface above the critical point.	107
Figure 6.23 – Final result for liquid density approximation for the entire temperature range.....	108
Figure 6.24 – Water vapor dynamic viscosity tabulated data.	110
Figure 6.25 – Vapor dynamic viscosity approximation result in saturation zone....	112
Figure 6.26 – Heaviside function in approximation for saturated zone.....	113
Figure 6.27 – Zoom on Heaviside function conjugate points.....	113
Figure 6.28 – Property value prediction below the triple point.....	114
Figure 6.29 – Final Result to interfacing below freezing point.	116
Figure 6.30 – Water dynamic viscosity data at critical pressure [220.64 bar].	117
Figure 6.31 – Final result to interfacing above critical point.....	118
Figure 6.32 – Final Result to vapor dynamic viscosity approximation in the entire temperature range.....	119
Figure 6.33- Thermal Conductivity Schematics.	120
Figure 6.34 – Water vapor thermal conductivity tabled data.....	121
Figure 6.35 – Faghri polynomial approximation.....	122
Figure 6.36 – Vapor thermal conductivity approximation result in saturated zone.	123
Figure 6.37 – Approximation for saturated zone by combination of three functions.	124

Figure 6.38 – Zoom on the conjugation points in approximation for the saturation zone.	124
Figure 6.39 – Vapor thermal conductivity data in freezing zone.	125
Figure 6.40 – Final Result to interfacing below sub-freezing point.	127
Figure 6.41 – Property data in supercritical zone.	128
Figure 6.42 – Final result to interfacing at critical point.	129
Figure 6.43 – Final result for vapor thermal conductivity approximation over entire temperature range.	130
Figure 6.44 – Water vapor specific heat capacity number data.	132
Figure 6.45 – Faghri polynomial approximation.	133
Figure 6.46 – Vapor specific heat capacity approximation in saturated zone.	134
Figure 6.47 – Heaviside function in approximation for saturated zone.	135
Figure 6.48 – Property data in freezing zone.	136
Figure 6.49 – Property dimensionless data and approximation in freezing zone.	136
Figure 6.50 – Final result to interfacing around the freezing triple point.	138
Figure 6.51 – Property data in supercritical zone.	139
Figure 6.52 – Final result to interfacing around critical point.	140
Figure 6.53 – Final approximation for Vapor specific heat capacity in the entire temperature range.	141
Figure 6.54 – Water vapor Prandtl number Data.	143
Figure 6.55 – Water vapor Prandtl number after logarithm application.	143
Figure 6.56 – Prandtl approximation result.	145
Figure 6.57 – Interfacing n1-Prandtl number linking subcooled zone with saturated zone.	147
Figure 6.58 – Approximation of n1-Prandtl number as a function of temperature and pressure.	148
Figure 6.59 – Prandtl number behavior above critical point dependent of temperature and pressure (BEATON, 1986).	149
Figure 6.60 – Approximation of n1-Prandtl number as a function of dimensionless pressure.	150

Figure 6.61 – Interfacing Prandtl number example to $P=300$ [bar] or $p[-]=1.3581..$	152
Figure 6.62 – Final Result to Prandtl number approximation in the entire temperature and pressure range.	153
Figure 6.63 – Interfacing n_l Prandtl number around critical temperature.	153
Figure 6.64 – Water liquid density data.	155
Figure 6.65 – Faghri polynomial approximation.....	156
Figure 6.66 – Liquid Density approximation result in saturated zone.	157
Figure 6.67 – Two- functions approximation for saturated zone.....	158
Figure 6.68 – Water liquid density data before triple point.	159
Figure 6.69 – Final result to interfacing below freezing point.	161
Figure 6.70 – Final result to interfacing above critical point.....	163
Figure 6.71 – Final result for liquid density approximation over entire temperature range.	164
Figure 6.72 – Water liquid dynamic viscosity number data.	166
Figure 6.73 – Faghri polynomial approximation.....	167
Figure 6.74 – Liquid Dynamic Viscosity approximation result in saturated zone using additive technique of approximate functions.	168
Figure 6.75 – Approximation for saturated zone using additive technique of piece- wise functions.....	169
The result approximation is shown in Figure 6.76.	170
Figure 6.76 – Liquid Dynamic Viscosity approximation result in saturated zone using substitution of approximate functions.....	170
Figure 6.77 – Components adding used in the approximation using substitution of approximate functions.	171
Figure 6.78 – Step by step components adding used in the approximation ...	172
Figure 6.79 – Compare between Heaviside substitution and Heaviside addition techniques.....	173
Figure 6.80 – Final Result to interfacing below freezing point.	176
Figure 6.81 – Water dynamic viscosity data at critical pressure [220.64 bar].	177
Figure 6.82 – Final result to interfacing above critical point.....	178

Figure 6.83 – Result to liquid dynamic viscosity approximation in saturated range and super critical.	179
Figure 6.84 – Water liquid thermal conductivity numerical data.	181
Figure 6.85 – Faghri polynomial approximation.....	182
Figure 6.86 – Liquid thermal conductivity approximation results in saturated zone.	183
Figure 6.87 –Approximation by two functions for saturated zone.	184
Figure 6.88 – Zoom on conjugate point in the approximation.....	185
Figure 6.89 - Liquid thermal conductivity tabled data in freezing zone.	186
Figure 6.90 – Final Result to interfacing below freezing point.	188
Figure 6.91 – Liquid thermal conductivity data under the critical pressure.	189
Figure 6.92 – Final result to interfacing above critical point.....	191
Figure 6.93 – Final result to liquid thermal conductivity approximation in the entire temperature range.....	192
Figure 6.94 – Water Liquid specific heat capacity number data.	194
Figure 6.95 – Faghri polynomial approximation.....	195
Figure 6.96 – Liquid specific heat capacity approximation results in saturated zone.	196
Figure 6.97 – Heaviside function in approximation for saturated zone.....	197
Figure 6.98 – Property data in freezing zone.....	198
Figure 6.99 – Final Result to interfacing below freezing point.	199
Figure 6.100 – Property data in super critical zone.	200
Figure 6.101 – Final result to interfacing above critical point.....	202
Figure 6.102 – Final result for liquid specific heat capacity approximation in the entire temperature range.....	203
Figure 6.103 – Water liquid Prandtl number Data.	205
Figure 6.104 – Liley approximation.	206
Figure 6.105 – Liquid reduced Prandtl number approximation in saturated zone..	208
Figure 6.106 – Contributions of approximation functions to final approximation for saturated zone.....	209

Figure 6.107 – Zoom on individual functions in approximation for saturated zone.	209
Figure 6.108 – Reduced Prandtl number calculated.	210
Figure 6.109 – Prandtl number data compare with approximation and calculation.	211
Figure 6.110 – Prandtl Number in freezing zone.	212
Figure 6.111 – Final result to interfacing below freezing point.....	214
Figure 6.112 – Approximation of reduced Prandtl number as a function of dimensionless temperature and pressure for super-critical zone.	215
Figure 6.113 – Final result to interfacing above critical point.....	216
Figure 6.114 – Final result for liquid reduced Prandtl number approximation in the entire temperature range.....	217
Figure 6.115 – Water Latent Heat Data. (LEMMON et al., 2023; LILEY, 2005).....	219
Figure 6.116 – Faghri polynomial approximation.....	220
Figure 6.117 – Latent Heat approximation result in saturated zone.	222
Figure 6.118 – Two-functions approximation for saturated zone.....	223
Figure 6.119 – Property data in freezing zone. (LILEY, 2005).....	224
Figure 6.120 – Final Result to interfacing below freezing point.	225
Figure 6.121 – Final result to interfacing above critical point.....	227
Figure 6.122 – Final result to latent heat approximation in the entire temperature range.	228
Figure 6.123 – Water surface tension data.....	229
Figure 6.124 – Faghri approximation available range.	230
Figure 6.125 – Surface tension approximation result in saturated zone.....	231
Figure 6.126 – Final Result to interfacing below freezing point.	233
Figure 6.127 – Final result to interfacing above the critical point.....	234
Figure 6.128 – Final result to surface tension approximation in the entire temperature range.....	235
Figure B.1 – Equation behavior example $y = ax^n$ (Function meets conditions $y(0)=0$; $y'(0)=0$ at $n>\sim 1.5$).....	248

Figure B.2 – Equation behavior example $y = \frac{ax^n}{1-bx^m}$, Function meets conditions $y(0)=0$; $y'(0)=0$ at $n \sim 1.5$; $0.1 < b < 0.9$	249
Figure B.3 – Equation behavior example, $y = a_2x^2 + a_3x^3 + a_4x^4$, Function meets conditions $y(0)=0$; $y'(0)=0$	249
Figure B.4 – Equation behavior example $y = aTanh^n(ex)$, Function meets conditions $y(0)=0$; $y'(0)=0$ at $n \sim 1.5$	250
Figure B.5 – Equation behavior example $y = aSinh^n(x)$, Function meets conditions $y(0)=0$; $y'(0)=0$ at $n \sim 1.5$	250
Figure B.6 – Equation behavior example $y = a \left(\frac{1-Cos(\pi x)}{2} \right)^n$, Function meets conditions $y(0)=0$; $y'(0)=0$	251
Figure B.7 – Equation behavior example $y = ax^b e^{cx^n}$, Function meets conditions $y(0)=0$; $y'(0)=0$ at $b \sim 1.5$ & $n > 0$	251
Figure B.8 – Equation behavior example $y = Tanh^n(ex)$	252
Figure B.9 – Equation behavior example $y = 1 - Tanh^n(ex)$	252
Figure B.10 – Equation behavior example $y = (1 - Tanh^n(ex))^n$	253
Figure B.11 – Equation behavior example $y = \frac{1}{2} (1 + Tanh(n(x - 0.5)))$	253
Figure B.12 – Equation behavior example $y = (1 - x)^n$	254
Figure B.13 – Equation behavior example $y = \frac{1-x}{1-x^n}$	254
Figure B.14 – Equation behavior example $y = Sech^n(x)$	255
Figure B.15 – Equation behavior example $y(x) = a \left(1 - \frac{(x-b)^2}{c^2} \right)^n$	255
Figure B.16 – Equation behavior example $y(x) = Ln \left(a \cdot Exp \left(b \cdot \left(1 - \frac{c}{nx} \right) \right) + e \right)$	256

TABLE LIST

	<u>Page</u>
Table 4.1 – Intermediate Temperature Fluids.....	16
Table 4.2 – Equation (4.2) coefficients value.....	19
Table 4.3 – Equation (4.2) coefficients values.....	19
Table 4.4 – Equation (4.4) & (4.5) coefficients value.....	20
Table 4.5 – Equation (4.9) coefficients value.....	20
Table 4.6 – Equation (4.7) coefficients value.....	21
Table 4.7 – Equation (4.8) coefficients value.....	22
Table 4.8 – Coefficient values of Equation (4.9).....	24
Table 4.9 – Coefficient values of Equation (4.10).....	24
Table 4.10 – Coefficient values of Equation (4.11).....	24
Table 4.11 – Coefficient values of Equation (4.12).....	25
Table 4.12 – Coefficient values of Equations (4.13) and (4.14).....	25
Table 4.13 – Coefficient values of Equation (4.15).....	26
Table 4.14 – Coefficient values of Equation (4.16).....	26
Table 4.15 – Coefficient values of Equation (4.17).....	27
Table 4.16 – Equation (4.18) coefficients value.....	28
Table 4.17 – Coefficient values of Equation (4.20).....	29
Table 4.18 – Coefficient values of Equation (4.21).....	30
Table 4.19 – Coefficient values of Equation (4.22).....	30
Table 4.20 – Coefficient values of Equation (4.23).....	30
Table 4.21 – Coefficient values of Equation (4.24).....	31
Table 4.22 – Coefficient values of Equation (4.25).....	31
Table 4.23 – Coefficient values of Equation (4.26).....	31
Table 4.24 – Coefficient values of Equation (4.35).....	33
Table 4.25 – Coefficient values of Equation (4.35).....	33
Table 4.26 – Coefficient values of Equation (4.36).....	34
Table 4.27 – Coefficient values of Equation (4.37).....	34
Table 4.28 – Coefficient values of Equation (4.38).....	35
Table 4.29 – Coefficient values of Equation (4.39).....	35

Table 4.30 – Coefficient values of Equation (4.40).....	36
Table 4.31 – Coefficient values of Equation (4.41).....	36
Table 4.32 – Coefficient values of Equation (4.42).....	37
Table 4.33 – Coefficients suggestion for Equation (4.43).....	37
Table 4.34 – Equation (4.44) coefficients value.....	40
Table 4.35 – Equation (4.45) coefficients value.....	40
Table 4.36 – Equation (4.46) coefficients value.....	40
Table 4.37 – Equation (4.47) coefficients value.....	41
Table 4.38 – Coefficient values of Equation (4.48) and (4.49).....	42
Table 4.39 – Coefficient values of Equation (4.50).....	43
Table 4.40 – Coefficient values of Equation (4.50).....	43
Table 4.41 – Coefficient values of Equation (4.51).....	43
Table 4.42 – Coefficient values of Equation (4.52).....	44
Table 4.43 – Coefficient values of Equation (4.55).....	45
Table 4.44 – Coefficient values of Equation (4.56).....	45
Table 4.45 – Coefficient values of Equation (4.57).....	46
Table 4.46 – Coefficient values of Equation (4.58).....	46
Table 4.47 – Coefficient values of Equation (4.59).....	47
Table 4.48 – Coefficient values of Equation (4.60).....	47
Table 4.49 – Coefficient values of Equation (4.61).....	47
Table 4.50 – Coefficient values of Equation (4.62).....	48
Table 4.51 – Coefficient values of Equation (4.64).....	48
Table 4.52 – Coefficient values of Equation (4.65).....	49
Table 4.53 – Coefficient values of Equation (4.66).....	49
Table 4.54 – Coefficient values of Equation (4.67).....	50
Table 4.55 – Coefficient values of Equation (4.68).....	51
Table 4.56 – Coefficient values of Equation (4.69).....	51
Table 4.57 – Coefficient values of Equation (4.70).....	51
Table 4.58 – Coefficient values of Equation (4.71).....	52
Table 4.59 – Coefficient values of Equation (4.75).....	53
Table 4.60 – Coefficient values of Equation (4.76).....	53
Table 4.61 – Coefficient values of Equation (4.79).....	54

Table 6.1 – Coefficients “a” and “b” expressed by polynomial coefficients.	89
Table 6.2 – Result algorithm values for density of 350kg/m ³	97
Table 6.3 – Result liquid density algorithm values for the case $\bar{\rho}_{ch} = 1$	109
Table 6.4 – Result of vapor dynamic viscosity algorithm values.	120
Table 6.5 –Vapor thermal conductivity pseudo-code values.	131
Piece-wise functions y_i are defined by Equation (6.87)	142
Table 6.6 – Result values of vapor specific heat capacity pseudo-code.	142
Table 6.7 –vapor Prandtl number pseudo-code values.	154
Table 6.8 – Result algorithm values for the case of $\bar{\rho}_{ch} = 1$	165
Table 6.9 – Result liquid dynamic viscosity pseudo-code values.	180
Table 6.10 – Heaviside Addition coefficient value for liquid dynamic viscosity....	180
Table 6.11 – Result of liquid thermal conductivity the algorithm values.	193
Table 6.12 – Resulting liquid specific heat capacity pseudo code values.	204
Table 6.13 – Resulting liquid reduced Prandtl number approximation parameters.	218
Table 6.14 – Resulting latent heat approximation parameters.	229
Table 6.15 – Resulting to surface tension approximation parameters.	236

ABBREVIATION LIST

ASHRAE	American Society of Heating, Refrigerating and Air-Conditioning Engineers
CC	Clausius – Clapeyron
CLHP	Cryogenic Loop Heat Pipe
HP	Heat Pipe
INPE	<i>Instituto Nacional de Pesquisas Espaciais</i>
MS	Microsoft
SI	International System of Measurement
USA	United States of America
UK	United Kingdom
VBA	Visual Basic for Applications

SYMBOL LIST

a_n	Variable
a, b, c, d, e, f	Variables
$^{\circ}\text{C}$	Celsius degree
c_p	Specific heat capacity [J/kg/K]
D_{av}	Average deviation
D_{max}	Maximum deviation
D_p	Final deviation combining two optimization criteria
kJ	Kilojoule
kg	Kilogram
K	Kelvin
k	Thermal conductivity [W/m/K]
Ln	Natural logarithm
M	Variable
m	Mass [kg]
N	Number of points available in a table of the given thermo-physical property.
P	Pressure [Pa]
p	Dimensionless pressure
$p(T, q)$	Expressions for any property
Pa	Pascal
p_v	Dimensionless vapor pressure
Pr	Prandtl number
p_r	Reduced pressure
Q	Energy released or absorbed during the change of phase of the substance [J/kg/K]
q	Vector of approximation parameters
R_u	Universal gas constant [J/mol/K]

R	Specific gas constant [J/kg/K]
T	Temperature [K]
T_i	Temperatures presented in tabulated data
t_r	Reduced temperature
V	Volume [m ³]
W	Optimization weight
x	Abscissa axis of example
y	Ordered axis of example
y	Property approximation
y'	Derivative of property approximation
$y(T)$	Fluid property function temperature dependent
$y(q, \tau_i)$	Function of parameter vector and dimensionless temperature
y_{lt}	Property approximation on the left side
y_{rt}	Property approximation on the right side
y_i	Interfacing property approximation
\hat{y}_i	Dimensionless property example
\hat{Y}_i	Property example with dimension
z	Abbreviation deviation subtraction
α	Thermal diffusivity [m ² /s]
τ	Dimensionless temperature
τ_i	Dimensionless temperature data
τ_H	Heaviside dimensionless temperature point
τ_{lt}	Dimensionless temperature on the left side of function
τ_{rt}	Dimensionless temperature on the right side of function
τ_1	Interfacing temperature at freezing zone
τ_2	Interfacing temperature at saturation zone near 0
τ_3	Interfacing temperature at saturation zone near 1
τ_4	Interfacing temperature at supercritical zone

χ	Heaviside function
σ	Surface tension [N/m]
$\psi(p)$	Property function dependent by dimensionless pressure
$\varphi(\tau)$	Property function dependent by dimensionless temperature
ρ_{ch}	Charged density [kg/m ³]
ρ	Density [kg/m ³]
ω	Variable
λ	Fluid latent heat [J/kg]
μ	Dynamic viscosity [Pa*s]
ν	Momentum diffusivity [N/m ²]

Subscribes

A	Freeze zone
AB	Interfacing zone between freeze zone and saturated
B	Saturated zone
BC	Interfacing zone between saturated zone and supercritical
C	Super critical zone
cc	Clausius-Clapeyron
ch	Charge
cr	Critical
H	Heaviside interruption point
HP	Heat Pipe
l	Liquid
v	Vapor
0	Reference point
3	Triple Point

SUMMARY

	<u>Page</u>
1 INTRODUCTION	1
2 MOTIVATION	7
3 OBJECTIVES	14
4 LITERATURE REVIEW	15
4.1 Fluid properties for heat pipes	15
4.2 Vapor pressure	18
4.3 Vapor density	33
4.4 Vapor dynamic viscosity	34
4.5 Vapor thermal conductivity	35
4.6 Vapor specific heat capacity	36
4.7 Vapor Prandtl number	41
4.8 Liquid density	41
4.9 Liquid dynamic viscosity	44
4.10 Liquid thermal conductivity	46
4.11 Liquid specific heat capacity	48
4.12 Liquid Prandtl number	50
4.13 Latent heat (enthalpy) of vaporization	51
4.14 Surface tension	52
5 METHODOLOGY	55
5.1 Building equations	55
5.2 Interfacing	59
5.2.1 Interfacing around T_3 ($\tau = 0$)	59
5.2.2 Interfacing around T_{CR} ($\tau = 1$)	62
5.2.3 Interfacing at any point of temperature	66
5.3 Piecewise approach using Heaviside functions	68
5.4 Final format	72
5.5 The best approximation by optimization algorithm of random search	72
6 RESULTS	79
6.1 Approximations for vapor pressure	79

6.1.1	Approximations for saturated zone.....	79
6.1.2	Approximations for freezing zone or sublimation zone.....	84
6.1.3	Approximations for super-critical zone	88
6.1.4	Final approximation and pseudo code	96
6.2	Approximations for vapor density.....	97
6.2.1	Approximations for saturated vapor density	97
6.2.2	Approximations for freezing zone and interfacing	103
6.2.3	Approximations for supercritical zone and interfacing.....	105
6.2.4	Final approximation and pseudo code	107
6.3	Approximations for vapor dynamic viscosity	109
6.3.1	Approximations for saturated zone.....	109
6.3.2	Approximations for freezing zone.....	114
6.3.3	Approximations for super-critical zone	116
6.3.4	Final approximation and pseudo code	118
6.4	Approximations for vapor thermal conductivity	120
6.4.1	Approximations for saturated zone.....	120
6.4.2	Approximations for freezing zone and interfacing	125
6.4.3	Approximations for supercritical zone and interfacing.....	127
6.4.4	Final approximation and pseudo code	130
6.5	Approximations for vapor specific heat capacity	131
6.5.1	Approximations for saturated zone.....	131
6.5.2	Approximations for freezing zone and interfacing	135
6.5.3	Approximations for supercritical zone and interfacing.....	138
6.5.4	Final approximation and pseudo code	141
6.6	Approximations for vapor Prandtl number.....	142
6.6.1	Approximations for saturated zone.....	142
6.6.2	Approximations for freezing zone.....	145
6.6.3	Approximations for super critical zone	147
6.6.4	Final approximation and pseudo code	152
6.7	Approximations for liquid density	154
6.7.1	Approximations for saturated zone.....	154
6.7.2	Approximations for freezing zone.....	158

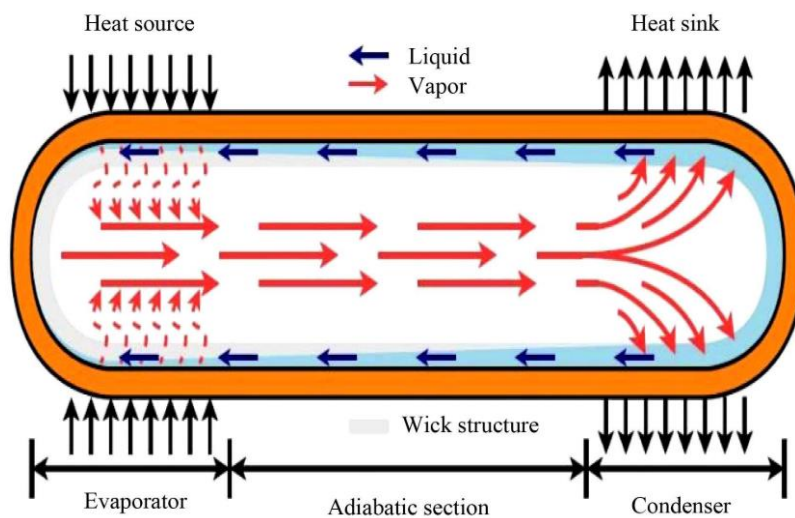
6.7.3	Approximations for super critical zone	161
6.7.4	Final approximation and pseudo code	163
6.8	Approximations for liquid dynamic viscosity	165
6.8.1	Approximations for saturated zone.....	165
6.8.2	Approximations for freezing zone and interfacing	173
6.8.3	Approximations for supercritical zone and interfacing	176
6.8.4	Final approximation and pseudo code	179
6.9	Approximations for liquid thermal conductivity	180
6.9.1	Approximations for saturated zone.....	180
6.9.2	Approximations for freezing zone and interfacing	185
6.9.3	Approximations for supercritical zone and interfacing	188
6.9.4	Final approximation and pseudo code	191
6.10	Approximations for liquid specific heat capacity	193
6.10.1	Approximations for saturated zone.....	193
6.10.2	Approximations for freezing zone and interfacing	197
6.10.3	Approximations for supercritical zone and interfacing	200
6.10.4	Final approximation and pseudo code	202
6.11	Approximations for liquid Prandtl number	204
6.11.1	Approximations for saturated zone.....	204
6.11.2	Approximations for freezing zone and interfacing	211
6.11.3	Approximations for supercritical zone and interfacing	214
6.11.4	Final approximation and pseudo code	216
6.12	Approximations for latent heat	218
6.12.1	Approximations for saturated zone.....	218
6.12.2	Approximations for freezing zone and interfacing	223
6.12.3	Approximations for supercritical zone and interfacing	225
6.12.4	Final approximation and pseudo code	227
6.13	Approximations for surface tension.....	229
7.	CONCLUSIONS	237
8.	PROPOSAL FOR NEW RESEARCH.....	239
	REFERENCES.....	240
	APPENDIX A – EQUATIONS AND ITS DERIVATIVES	247

APPENDIX B – FUNCTIONS AND GRAPHS FOR THE APPROXIMATIONS ...	
.....	248
APPENDIX C – EXCEL VISUAL BASIC CODE FOR RANDOM SEARCH .	257

1 INTRODUCTION

Any electronic equipment produces heat while running. The satellite thermal control subsystem manages the heat distribution in the satellite and the heat pipes are widely applied for this purpose. Shukla (2015) explained the concept of heat pipes: “A typical heat pipe comprises a sealed pipe or tube made of a material that is compatible with the working fluid such as Copper for water heat pipes, or Aluminum for ammonia heat pipes. It is a simple construction that makes a heat pipe to allow high heat transfer rates over considerable distances, with minimum temperature drops...”.

Figure 1.1 – Heat pipe schematic.



Source: Shukla (2015).

The heat pipe keeps vapor-liquid equilibrium with the saturated liquid and its vapor. The saturated liquid vaporizes and flows to the condenser part, where it is cooled and turned back to the saturated liquid. In a standard heat pipe, the condensate is returned to the evaporator by capillary force through a wick structure. Good wettability of the liquid phase of the working fluid with the material of the capillary structure is a main condition of such a capillary return.

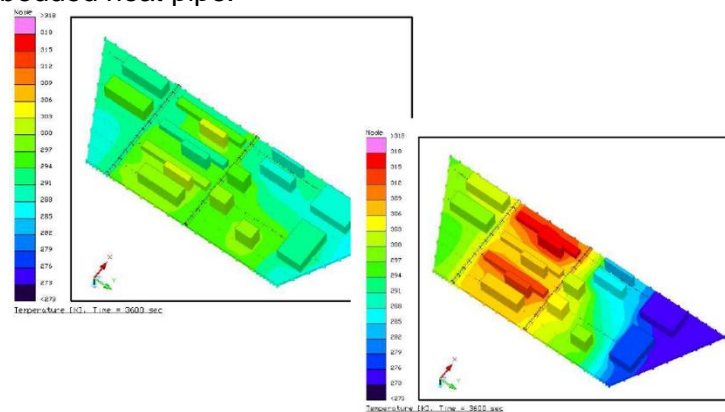
The concept of heat pipes traces its roots back to the early 1960s when the aerospace industry sought innovative ways to address thermal challenges in spacecraft. In 1963, the idea of using a capillary-driven heat transfer device to

manage the extreme temperatures gradient experienced by a satellite in outer space was proposed by George Grover (BRENNAN; KROLICZEK, 1979).

The first designs of heat pipes focused on space applications, aiming to dissipate the heat generated by electronic components in spacecraft. The first functional heat pipe was developed and proven in 1964 by Grover and his coworkers (BRENNAN; KROLICZEK, 1979).

Grover baptized the name “heat pipe” and characterized it as a “synergetic engineering structure which is equivalent to a material having a thermal conductivity exceeding that of any known metal.” These early heat pipes used water working fluid with copper mesh as a capillary structure and the case made by cooper. Soon later he manufactured a high-temperature HP with a sodium as a working fluid to operate above 1100K. The first cryogenic HP with nitrogen as a working fluid was developed by Haskin Brennan and Kroliczek (1979) at Wright-Patterson Air Force Base, USA. The success of this demonstrations paved the way for further exploration of heat pipe technology in the aerospace sector. Figure 1.2 shows the effect of heat pipe typical application to reduce the temperature gradients over a satellite honeycomb panel with installed electronic equipment.

Figure 1.2 – Comparative simulation analyzes: CBERS3 Satellite panel with and without embedded heat pipe.



Source: Vlassov (2021).

As the benefits of heat pipes in space applications became clear, researchers and engineers explored their potential in other industrial fields. By the 1970s, heat pipes found applications in cooling systems for electronic devices, such as

computers and radar systems (BRENNAN; KROLICZEK, 1979). The versatility of heat pipes in transferring heat efficiently with no external power sources contributed to their widespread adoption in various thermal management scenarios. Brennan and Kroliczek (1979) argued in his word "...the capability of have a fixed and variable conductance heat pipes are being developed or proposed for various shuttle mission, including thermal canister."

The oil crisis of the 1970s ("Energy crisis") spurred interest in energy-efficient technologies, leading to increased research on heat pipes to improve energy efficiency in heating and cooling systems. Heat pipes became integral components in solar collectors, where they efficiently transferred heat from the absorber plate to the working fluid, enhancing the overall performance of solar thermal systems "...the demand for alternated energy sources had led to the development of innovative intermediate and high temperature heat pipes for solar collection and coal gasification."

Heat pipes can be used in a wide variety of applications, besides satellites, solar energy, and coal mining application. Those categories of uses can be since satellites applications to medicine and human body temperature control, "Depending on their intended use, heat pipes can in the temperature range from 4 to 3000K (FAGHRI, 2016). Furthermore, Faghri (2016) divided heat pipes into three major categories, firstly separation of heat source and sink, due to its efficiency of transport heat; followed by temperature equalization and temperature control. The temperate equalization is linked to the high thermal conductivity and the temperature control is linked to the capability of heat pipes transport copious quantities of heat rapidly. Some applications were listed by Faghri as following:

- Electronic and electrical equipment cooling – the heat density of electronic and electrical equipment is rising by the miniaturization of components. Because of their sensitive operating temperature, the design is choosing to improve heat dissipation in its components by incorporating heat pipes.
- Energy systems – the use of heat pipes and thermosiphons draws more attention of their efficiency of using energy conservation and cost.

According to Faghri (2016), a few systems have been used thermosiphons as an implementation on building heating seeking thermal comfort. Shortly, the system absorbs solar energy using a heat pipe and transports that energy to a living space. That space is heated by air convection or that energy is stored as hot water. And at night, those thermosiphons act like a one-way valve to that heat that energy only can be transferred from inside to outside by axial conduction through the pipe walls.

- Aerospace and Avionics – some characteristics such as weight, maintenance, and reliability are decisive factors for the success or a potential disaster of the project, and heat pipes are an incredibly attractive choice because it has all those three characteristics. This occurs because of the simplicity of the object, with no moving parts to transport the energy, lightweight, and no maintenance, which enhances the reliability.
- Medicine and human body temperature control. Faghri (2016) suggested that using of heat pipes relates to human physiology, the proposal is to incorporate a cryogenic heat pipe to destroy tumors in human body, using this technique, the tissue is freezing rather than irradiated, and as a result the surrounding tissue sustains no damage.

Closed passive evaporation-condensation cycle and temperature-induced capillary pumping principle have given an impulse for developing of similar like-HP heat transfer devices; they belong to a class of passive two-phase heat transfer devices.

These two-phase heat transfer devices are important components for thermal control systems in the aerospace industry and terrestrial applications. It includes not only heat pipes but also thermosiphons, capillary pumped loops, looped heat pipes and advanced capillary pumped systems of complex networks. The performance of such devices depends on fluid properties at saturation conditions. Such devices cannot run out of temperature limits. When the temperature is below the triple point, the working fluid freezes. When the temperature is above the critical conditions, two phases cannot coexist anymore. However, for many

applications, such devices may temporarily be exposed to non-operational conditions but may resume normal operation afterwards.

Experimental studies and tests are an important part of satellites development, but they are usually expensive and time consuming. Because of that, numerical simulations play a vital role. Numerical models can be very reality-representative and simulate many phenomena and particular cases within a fraction of the experiment's cost and time.

As it was said, the performance and operation limits of heat pipes depend purely on thermo-physical properties. Any mathematical model must have an adequate treatment of such properties that critically depend on temperature. Applications of heat pipes in satellites, as well as in other applications, may call to a very wide operational temperature range, for example, start-up from super-critical states in cryogenic HPs, or start-up of water HP from freezing state. Therefore, it is particularly important to have correct correlations for the entire temperature two-phase range at saturation conditions and out of the saturation range. Simulation of HP transient modes needs smoothed property correlations without interruptions of value and derivatives. Commonly used tables or piece-wise linear interpolations between tabulated magnitudes are not acceptable. The most difficult problems come up in simulation of specific transient HP modes, like start-up from solid state (high-temperature and freezable HPs) and start-up from super-critical states in cryogenic loop heat pipe (CLHP). Such the applications demand all three states of matter to be simulated by mathematical model; any interruptions in properties values may cause numerical instabilities and failures. These smooth uninterrupted variations must pass through the freezing zone up to the super critical zone (LEE et al., 2020).

Jaworske et al. (2008) highlights the difficulty to perform start-up on a water heat pipe in space applications. This paper discusses the evaluation of panel performance under a Moon illumination for radiator panels equipped with titanium-water heat pipes. Authors study its behavior on the panel starts after freezing the water in the heat pipes under heater power applied. The modeling and investigation of lunar conditions confirmed that the heat pipes would be

freezing at lunar sunrise and would require more than one of sun illuminations to resume operation. This shows the importance and difficulty of transient simulation; part of this difficulty is placed in uninterrupted work fluid property models that cover all ranges with smooth transitions between freezing and saturation phases.

The study of Jouhara et al. (2017) concluded that heat pipes have a wide range of applications but exists a gap in research for different temperature patterns. Authors affirm that while the implementation of heat pipes in low-temperature applications has been studied extensively, but there is still a backlog of research to be conducted. The same applies to high temperature applications where heat pipes are commonly used in waste heat recovery and solar power and other energy sources. The author fell to the lack of the fluid properties approximations available from literature. Jouhara et al. (2017) emphasized that the properties of the working fluids, related to phase changes and heat transfer characteristics, play a crucial role in the performance of heat pipes. However, there may be a lack of available data and commercial models for certain fluids, which can hinder the modeling and simulation of heat pipe systems.

2 MOTIVATION

The mathematical modeling of heat pipes plays a key role in simulations of transient behavior and studies of operational failure risks as eventual dry-out and dynamic conditions for successful operational recuperation. Complex mathematical models include a complete system of fundamental differential equations of momentum, energy, mass conservation, as well as interfacing phenomena and multi-phase transitions (Bowman (1991), Faghri (2016), Tournier; El-Genk (1994) and Vlassov (2005, 2008)). One can extract the following thermo-physical properties from these fundamental equations; the list includes 13 parameters, namely c_{pl} , c_{pv} , k_l , k_v , λ , μ_l , μ_v , Pr_l , Pr_v , P_v , ρ_l , ρ_v and σ . It is a well-known fact that the performance and operational limits of any HP depends on temperature. The only reason for this dependence is that the values of all properties depend on temperature, moreover, by different manner.

Any mathematical model must have an adequate treatment of such properties that, as said, critically depends on temperature. Applications of heat pipes in aerospace industry, as well as in other applications, may call to extremely wide operational temperature range, for example, start-up from super-critical states in cryogenics HPs, or start-up of water HPs from freeze state. Therefore, it is especially important to have correct correlations for the entire temperature two-phase range at saturation conditions as well as out of the saturation range. Simulation of HP transient modes needs smoothed property correlations without interruptions of value and derivatives; commonly used tables or piece-wise linear interpolations between tabulated magnitudes are not acceptable. The most difficult problems come up in simulation of specific transient HP modes, like start-up from solid state (high-temperature and freezable HPs) and start-up from super-critical states in cryogenic heat pipe. Such the applications demand all three states of matter, if we put on a line this variation pass through freeze zone up to the supercritical zone (LEE et al., 2020). For example, Jaworske et al. (2008) highlights the difficulty of performing start-up on a water heat pipe in space application.

In order to property approximations be able to be implemented on a mathematical model, its behavior must be continuous and smooth, without sharp edges. Thus, to comply with those rules is common to see in literature thermos-physical data approximation in a strict range of temperature, mostly passing for only one state of matter and that behavior is described by a high polynomial equation, like shown in (2.1).

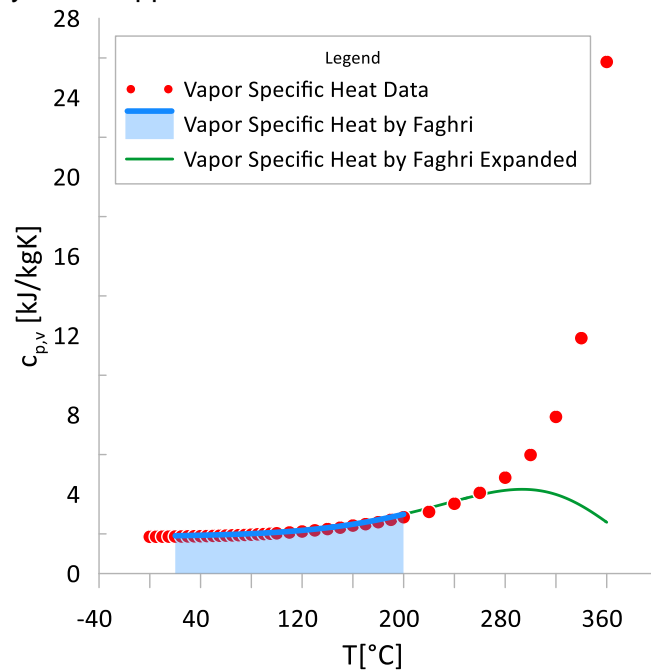
$$y(T) \approx a_0 + a_1T + a_2T^2 + a_3T^3 + \dots \quad | \quad T_1 \leq T \leq T_2 \quad (2.1)$$

Usually, this temperature range is narrower than the entire operating range even in saturation zone, and the calculated values by the polynomial approximation may run away from the physical sense and may get absurd magnitudes.

Using such a polynomial approximation, the iteration process in a numerical algorithm may temporarily get out of the expected temperature range, leading to numerical instability, false results and/or algorithm failure.

For example, a 5-order polynomial approximation for water vapor specific heat, suggested by Faghri (2016) is valid from 20°C to 200°C. However, out of the range, the approximation lost the physical sense, see Figure 2.1.

Figure 2.1 – $c_{p,v}$ polynomial approximation behavior within and out of the specified range.



Certainly, other functions but polynomials must be investigated for using in approximations.

Another drawback of commonly used polynomial approximation is that they usually depend on the system of units. The approximation coefficients will be different for the same fluid for SI Units, Imperial Units, US customary Units, etc. Moreover, the coefficients have dimensions. For example, a popular Faghri (2016) approximation plotted in the graph on Figure 2.1 in many handbooks is given exactly as follows in Equation (2.2).

$$\begin{aligned} \ln(c_{p,v}(T)) = & 6.3198 \cdot 10^{-1} + 6.7903 \cdot 10^{-4} \cdot T - 2.5923 \cdot 10^{-6} \cdot T^2 - \\ & 4.4936 \cdot 10^{-8} \cdot T^3 + 2.2606 \cdot 10^{-10} \cdot T^4 - 9.0694 \cdot 10^{-13} \cdot T^5 \end{aligned} \quad (2.2)$$

Where T is expressed in °C and $C_{p,v}$ in kJ/kg/K. (By the way, neither SI system of units is used here since kJ is used instead of J).

Let us examine the numerical coefficients. Their appearance may be unconventional, but each coefficient owns individual dimensions:

- The coefficient 0.63198 is of dimension $\ln(\text{kJ/kg/K})$.

- The coefficient $6.7903 \cdot 10^{-4}$ is of dimension $\text{Ln}(\text{kJ}/\text{kg}/\text{K})/\text{K}$.
- The coefficient $2.5923 \cdot 10^{-6}$ is of dimension $\text{Ln}(\text{kJ}/\text{kg}/\text{K})/\text{K}^2$.
- The coefficient $4.4936 \cdot 10^{-8}$ is of dimension $\text{Ln}(\text{kJ}/\text{kg}/\text{K})/\text{K}^3$.
- The coefficient $2.2606 \cdot 10^{-10}$ is of dimension $\text{Ln}(\text{kJ}/\text{kg}/\text{K})/\text{K}^4$.
- The coefficient $9.0694 \cdot 10^{-13}$ is of dimension $\text{Ln}(\text{kJ}/\text{kg}/\text{K})/\text{K}^5$.

Mathematically, this is not correct: numerical coefficients should not have dimensions.

To overcome this inconsistency, only dimensionless parameters should be used in approximations for fluid thermo-physical properties as well as for temperature. Literature research reveals that dimensionless approximations were never used for passive two-phase heat transfer device modeling. In conjugate areas like properties of steam and super-critical gases, rarely, in semi-empirical correlations, can be seen so named reduced parameters, like pressure and temperature:

$$t_r = \frac{T}{T_{cr}} \quad (2.3)$$

$$p_r = \frac{P}{P_{cr}} \quad (2.4)$$

Once again, in the expression of the reduced temperature, the components must have the dimension either R or K, while °C or °F are prohibiting (due to 0/0 risk).

Moreover, the reduced temperature t_r has a limited association with the state of fluid. For water, the two-phase zone started from a temperature of 0.42, while below the 0.42 is a freezing zone. Why do not create a much more informing dimensionless temperature which value varies from 0 to 1 over saturation zone, be negative in the freezing zone, and be >1 for supercritical zone? We suggest this form where this can be naturally achieved, as shown in Equation (2.5) for the dimensionless temperature.

$$\tau = \frac{T - T_3}{T_{cr} - T_3} \quad (2.5)$$

where T_3 - triple point temperature (temperature of freezing), and T_{cr} - critical temperature. This proposed temperature τ does not depend on the system of unity used for components. We did not find publications for the fluid properties with the use of such convenient dimensionless temperature in approximations. Therefore, we are going to use this temperature and the same type of all dimensionless fluid properties in our study.

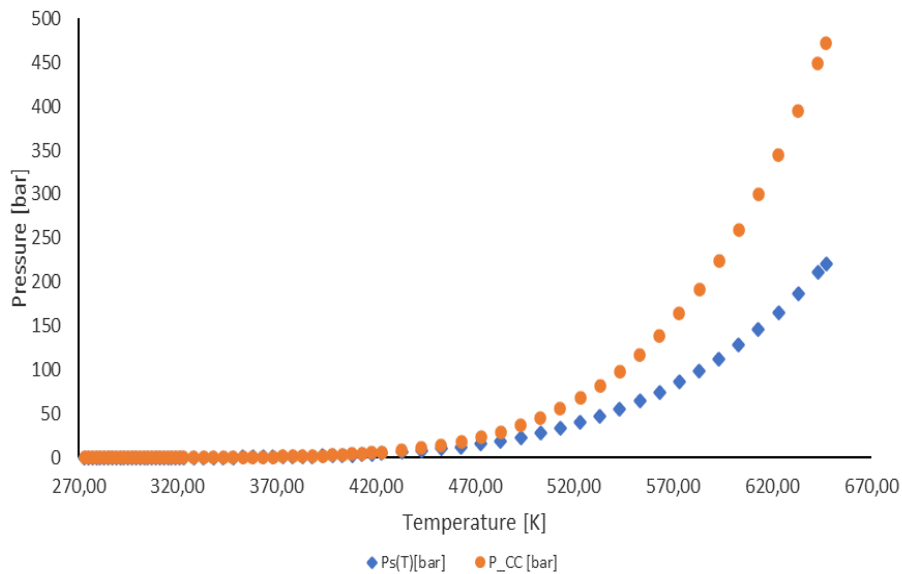
Another example usual correlation of limited temperature range is the saturation pressure, for which the widely used Clausius-Clapeyron integrated equation is employed:

$$P_{cc}(T) = P_0 e^{\frac{\lambda_0}{R} \left(\frac{1}{T_0} - \frac{1}{T} \right)} \quad (2.6)$$

The Clausius–Clapeyron of Equation (2.6) derives from entropy maximization, which determines the equilibrium between two phases of a substance. “Mathematically, it is expressed as the relationship between temperature, T , and pressure, P , at the equilibrium.” (KOUTSOYIANNIS, 2012).

However, the application of this equation directly causes a significant deviation from the table points far from the reference point 0. For example, for the reference point of $T_0=20$ °C, the C-C curve and the table points have visible deviations for elevated temperatures:

Figure 2.2 – Difference between tabled saturation pressure and Clausius-Clapeyron equation.



The possible approach to improve the approximation over the entire two-phase zone is trying to implement piecewise function for different intervals of the zone. In this case the crucial point is to assure smooth transitions over connection points; additional conditions shall be applied to approximation correlations at the edges of each function. They include the continuity of values and derivatives to fit the requirement of smooth uninterrupted conjunctions.

Through our literature review, we did not find such type of approximations for fluid properties used in heat pipes.

For many applications, heat pipes (HP) shall start from the non-operation temperature range. For example, high-temperature HP at the beginning may stay at normal ambient temperature such as sodium working fluid is solid in these conditions and when heated, the HP gradually enters its working regime. Another example – freezable water HP or freezable water thermal switch (KISEEV, et al, 2010), which may have a periodic operation with thawing-freeze cycles. Also, working fluids in cryogenic HPs (for example, nitrogen) are under over-critical conditions at normal ambient temperature; when cooled down, the HP gradually gets its nominal operation.

Numerical transient models shall simulate such start-up behavior from non-operational conditions. In this case the approximation of thermo-physical

properties shall include near-triple point region and near-critical region. For such a wide-range approximation, three temperature intervals shall be proved, and different correlations shall be used for each interval. Then, it is important to have smooth transitions between the intervals.

Detailed literature investigation did not reveal any type of uninterrupted approximations for fluid properties over the expanded full temperature range. Such the correlations should include both piecewise approximations with smooth conjunctions and representations of fluid state transitions with seamless interfacing. It should be noted that it is a difficult or even impossible task when thinking in a traditional manner - an approximation must look like a correlation. Let us doubt this postulate; our main question is: Does an approximation must look like a correlation? What about trying a novel approach: an approximation may be a pseudo-code. So, let us take a new way that no one has walked before.

3 OBJECTIVES

This work has the following main objectives:

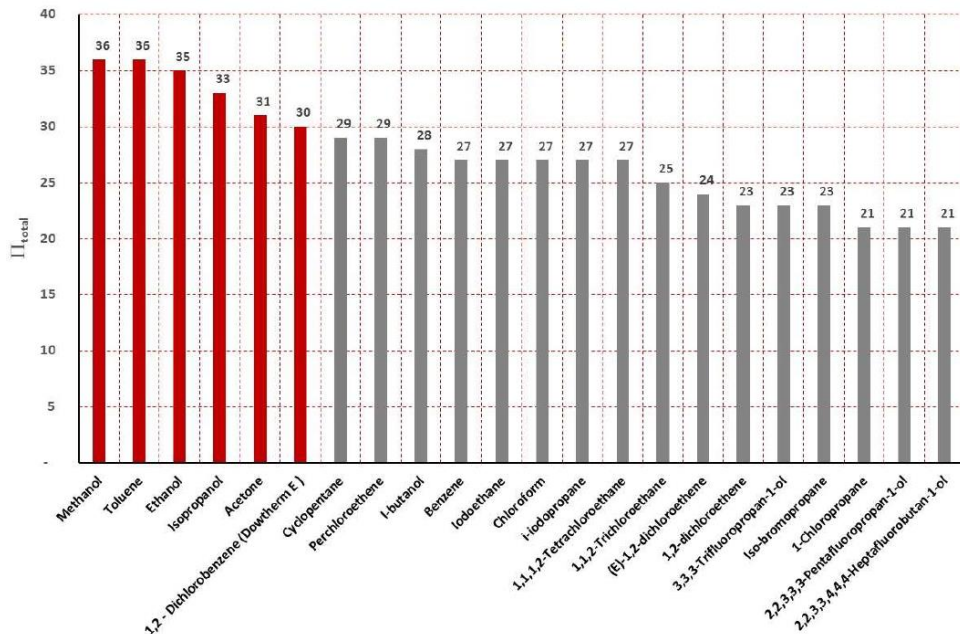
- 1) to prospect available all 13 thermo-physical properties of water, published in diverse sources and formats: tables, polynomials, empirical correlations, and transform all tables to dimensionless format;
- 2) to develop an adequate format of correlations of the properties for the entire two-phase zone and develop best dimensionless approximations following piecewise approach with smooth transition in conjunction points;
- 3) to develop approximations for freezing and super-critical zones and to develop a method of uninterrupted correlations on inter-zone interfacings, smooth approximations for values and the respective derivatives;
- 4) to develop uninterrupted approximations for all three phase zones for water, also revealing the errors of approximations for the entire temperature range typical for heat pipes of several types;
- 5) to present the results in the format of pseudo codes, being able to implement in any programming language, as universal dimensionless correlations;
- 6) to develop an optimization algorithm based on random parameters in a determinate range chosen by the User, to minimize approximation deviation; to develop a functional tool within EXCEL Visual Basic features, and to apply this tool to find optimal parameters and coefficients in pre-selected correlations for the approximations.

4 LITERATURE REVIEW

4.1 Fluid properties for heat pipes

In his study, Gakal et al. (2022) ranked the most common fluids, applicable to heat pipes, in strategic indicators, including the working fluid safety, working fluid melting temperature and working fluid critical temperature. They performed an evaluation in many indicators and plotted the result diagram shown in Figure 4.1.

Figure 4.1 – Working fluids grading results.



Source: Gakal et al. (2022).

In Figure 4.1 we have the higher scores fluids on 782 substances evaluated by Gakal et al. (2022), where Π_{total} is the sum of each fluid grade in each classification.

To make an efficient heat pipe project, the fluid choice is an important part of the process. As presented by Gakal et al. (2022), some fluid properties have more impact on the final design than others. As the heat pipe principle of function consists in liquid evaporation and condensation, naturally, melting point, boiling temperate, critical temperature, and critical pressure are variables that drive the main choice of the working for heat pipes.

Polasek and Stulc (1976), Ochterbeck and Mishkinis (2003) and Anderson et al. (2004) presented these main parameters for many fluids for intermediate temperatures, typical for aerospace applications (Table 4.1).

Table 4.1 – Intermediate Temperature Fluids.

Fluid		Melting Point, K	Boiling Temp., K	Critical Temp., K	Critical Pressure, MPa
Water	H ₂ O	273	373	647	22.12
Dowtherm A	Diphenyl/Diphenyl Oxide	285	530	770	3.135
Sulfur	S	386	718	1314	20.7
Sulfur/10% Iodine	S/10%I	-390	—	—	—
Iodine	I	387	458	785	11.6
Naphthalene	C ₁₀ H ₈	354	491	748	4.05
Phenol	C ₆ H ₆ O	314	455	694	6.13
Toluene	C ₆ H ₅ CH ₃	178	384	592	4.1
Hydrazine	N ₂ H ₄	275	387	653	14.7
Aniline	C ₆ H ₇ N	267	458	699	5.3
Titanium Tetrachloride	TiCl ₄	298	410	638	4.7
Titanium Tetrabromide	TiBr ₄	312	503	796	—
Titanium Tetraiodide	TiI ₄	423	650	1040	—

Source: Anderson et al. (2004).

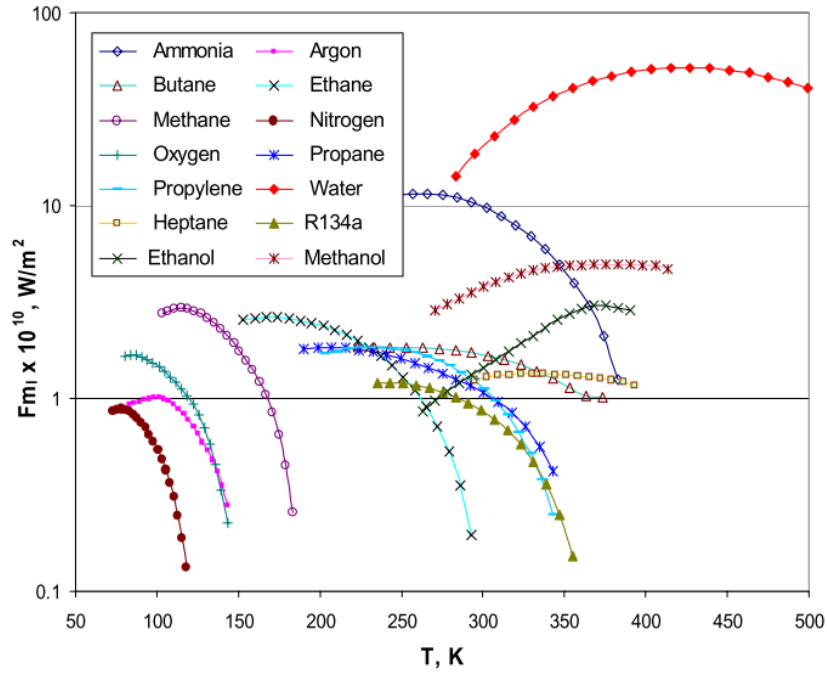
Ochterbeck and Mishkinis (2003) developed some criteria (Figures of Merit Fm) to expose in the best way possible efficiency of using the working fluid in heat pipes, see Figure 4.2 and Figure 4.3.

Figure 4.2 shows well-known Liquid Transport Factor criterion; the more its magnitude, the maximum theoretical heat transport capability the heat pipe may achieve.

One can see, water is the best working fluid to work in the temperature range above 20 °C for heat pipes.

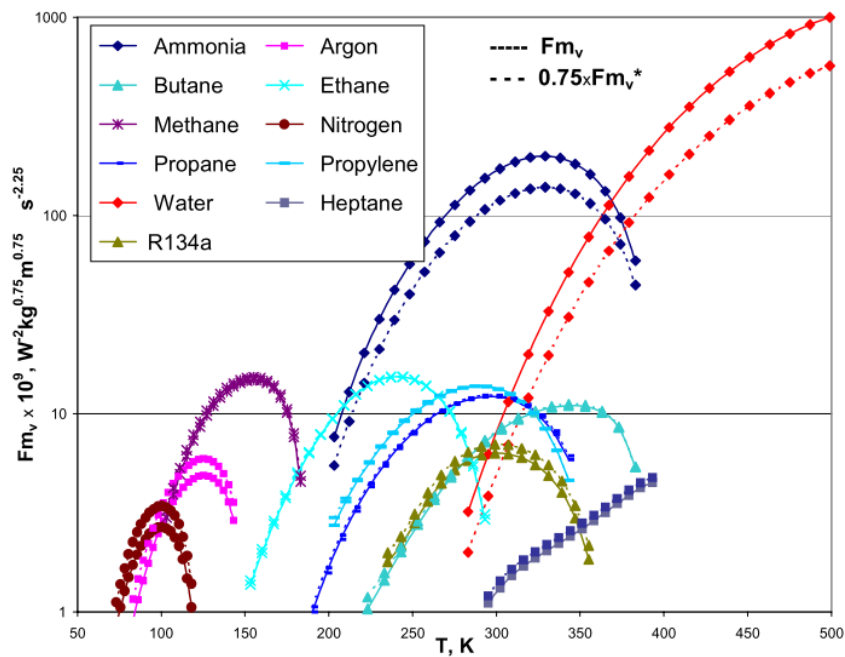
Additionally, they developed other figures of merits, such as presented in Figure 4.3 to characterize the vapor phase. Ammonia and water are the best working fluid according to this criterion.

Figure 4.2 – Figure of merit (liquid based) for different fluids.



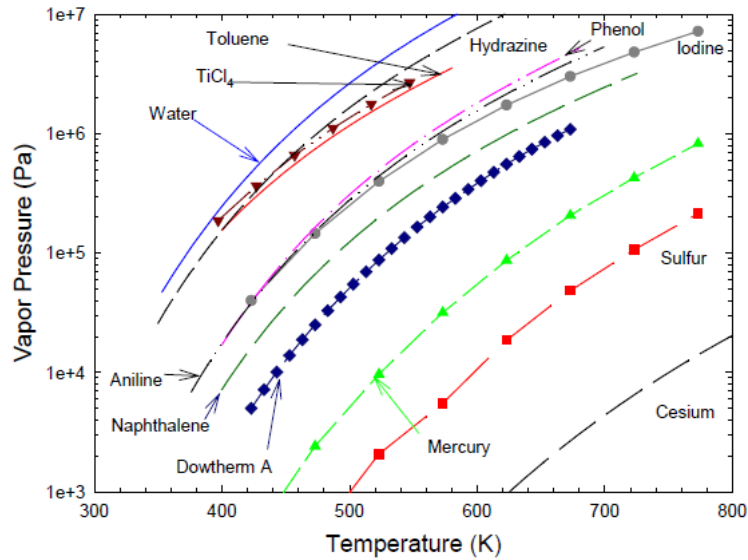
Source: Ochterbeck and Mishkinis (2003).

Figure 4.3 – Figure of merit (vapor based) for different fluids.



Source: Ochterbeck and Mishkinis (2003).

Figure 4.4 – Vapor Pressure as a Function of Temperature, Potential Heat Pipe or LHP Working Fluids.



Source: Anderson et al. (2004).

Many studies were performed to develop best approximations for different properties of working fluids. In many studies dimensionless parameters were used, for example Pátek et al. (2009) in equation below.

$$\tau = \frac{T}{T_R}, \quad \alpha = \frac{T_R}{T_a - T}, \quad \beta = \frac{T_R}{T - T_b} \quad (4.1)$$

where T is absolute temperature in K, $T_R=10$ K, $T_a=593$ K and $T_b=232$ K.

In the subsections 4.2 through 4.14, we show the review of typical approximations used in technical literature separately for each thermodynamic property.

4.2 Vapor pressure

Even though this work has a focus on heat pipe applications, the theme of vapor pressure approximations has a wide range of applications. We divide the review of water vapor pressure in three regions: sublimated vapor pressure above ice in freezing region below the triple point (0°C for water); saturated vapor pressure in two-phase region (between triple point and critical point) and super-critical region (temperatures above the critical point).

In their paper, Wagner and Pruss (1993) highlighted the importance of merging the experimental data collected for the freezing zone up to now. At that time, the work was the main reference in experimental data below 205K.

The authors in Murphy and Koop (2005) highlighted the importance of an effective technique to maintain the equation continuity: “The functional form was chosen to satisfy experimental constraints at the triple point as well as to have well-behaved vapor that simultaneously satisfy experimental data not only for vapor pressure and latent heat but also for other properties”. The authors also present several equations for the vapor pressure above ice (4.2) which depends on temperature (K) and pressure (Pa).

$$P_{v,ice} \approx \exp\left(a_A - \frac{b_A}{T}\right) \quad (4.2)$$

Table 4.2 – Equation (4.2) coefficients value.

$$a_A = 2.89074E1 \text{ [ln(Pa)]} \quad b_A = -6.1437E03 \text{ [K ln(Pa)]}$$

Source: Murphy and Koop (2005).

Once expressed the equation in the limited range, the authors tried to expand this range from 273K down to 111K, Equation (4.3). In this case the final expression was obtained through numerical solution provided by fourth order Runge-Kutta solver. It is possible to check the result in Figure 4.5.

$$P_{v,ice} = \exp\left(a_A + \frac{b_A}{T} + c_A \ln(T) + d_A T\right) \quad (4.3)$$

Table 4.3 – Equation (4.2) coefficients values.

$$\begin{aligned} a_A &= 9.550426E00 \text{ [ln(Pa)]} & c_A &= 3.53068E00 \text{ [ln(Pa)/ln(K)]} \\ b_A &= -5.723265E03 \text{ [K ln(Pa)]} & d_A &= -7.28332E-3 \text{ [ln(Pa)/K]} \end{aligned}$$

Source: Murphy and Koop (2005).

Through Figure 4.5, Jancso et al. (1970) expressed the formulation at temperature range from 195K to 273.16 K, pressure is in [Torr].

$$\ln p'_{v,ice} = \frac{a_A}{T} + b_A \quad (4.4)$$

$$P_{v,ice} = c_A \left(\frac{d_A}{e_A} \right) p'_{v,ice} \quad (4.5)$$

Table 4.4 – Equation (4.4) & (4.5) coefficients value.

$a_A = -2.668726E03$ [K exp(Torr)]	$d_A = 6.11657E02$
$b_A = 1.043112E00$ [exp(Torr)/K]	$e_A = 6.11283E02$
$c_A = 1.3332E02$	

Source: Jancso et al. (1970).

Also, Bryson et al. (1974), shared their approximation to vapor pressure, expressed in Torr. The temperature range for this approximation ranges from 153 to 183 K.

$$\ln P_{v,ice} = \frac{a_A}{RT} + b_A \quad (4.6)$$

Table 4.5 – Equation (4.9) coefficients value.

$a_A = 1.2E01$ [ln(Torr) kg/J]	$b_A = 2.4E02$ [exp(Torr)]
--------------------------------	----------------------------

Source: Bryson et al. (1974).

Where, R is the specific gas constant of sublimated wapor, and T is the absolute temperature in Kelvin. In lower temperature ranges, starting from 132 up to 153K, Bryson et al. (1974) suggested different coefficients.

The plotted curve available in Figure 4.5, Marti and Mauersberger (1993), ranges from 169K to 273K.

$$P_{v,ice} = \exp \left(a_A + \frac{b_A}{T} \right) \quad (4.7)$$

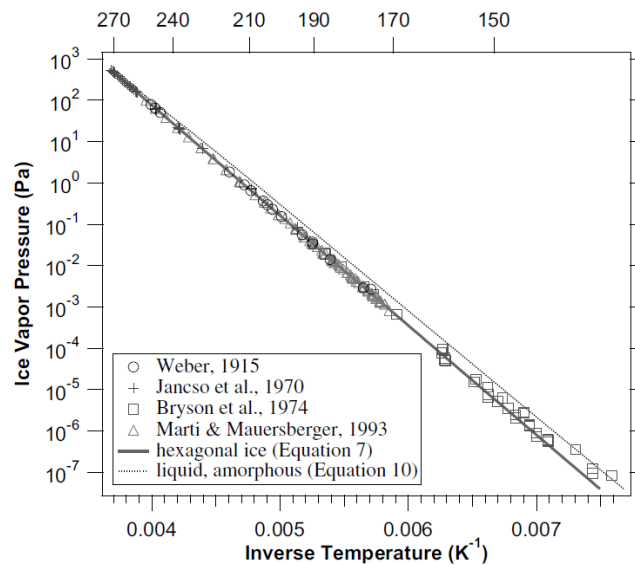
Table 4.6 – Equation (4.7) coefficients value.

$$a_A = 2.8868E01 [\ln(\text{Pa})]$$

$$b_A = -6.1329E03 [\text{K} \ln(\text{Pa})]$$

Source: Marti and Mauersberger (1993).

Figure 4.5 – Vapor pressure of ice versus inverse temperature for selected experimental data.

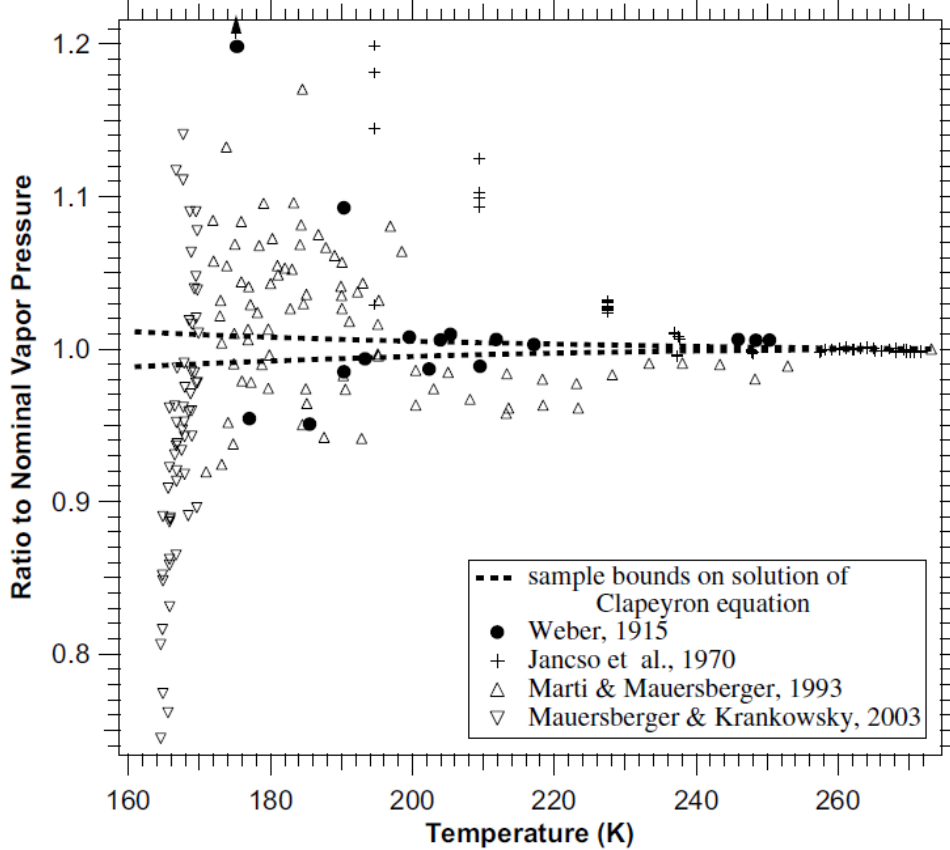


Source: Murphy and Koop (2005).

Each experimental strategy shows strengths and weaknesses (Figure 4.6). Also, this image is good to see the equation behavior when the temperature range is increased. For comparison, dimensionless pressure was represented by the ratio to nominal vapor pressure; this dimensionless property is a ratio by the result achieved by the approximation and tabled data. Figure 4.6 “shows a more detailed comparison of some experimental data on the vapor pressure of ice. Although the experimental data confirm the thermodynamic predictions, it is apparent that they do little to narrow the uncertainty compared to integrating the Clapeyron equation” (MURPHY; KOOP, 2005)

Their strategy was to validate their approximation tendency and quantify their advance in approximation rating their result by tabled data, the closer the tolerance, the better the result. Figure 4.6 has the main approximations considered in the study. Figure 4.7 presents the performance of such approach, including different references, data and equations.

Figure 4.6 – The ratio of selected ice vapor pressure data.



Source: Murphy and Koop (2005).

Murphy and Koop (2005) correlations are expressed in a common functional form:

$$\ln(P_{v,ice}) = a_A + \frac{b_A}{T} + c_A \ln(T) + d_A T \quad (4.8)$$

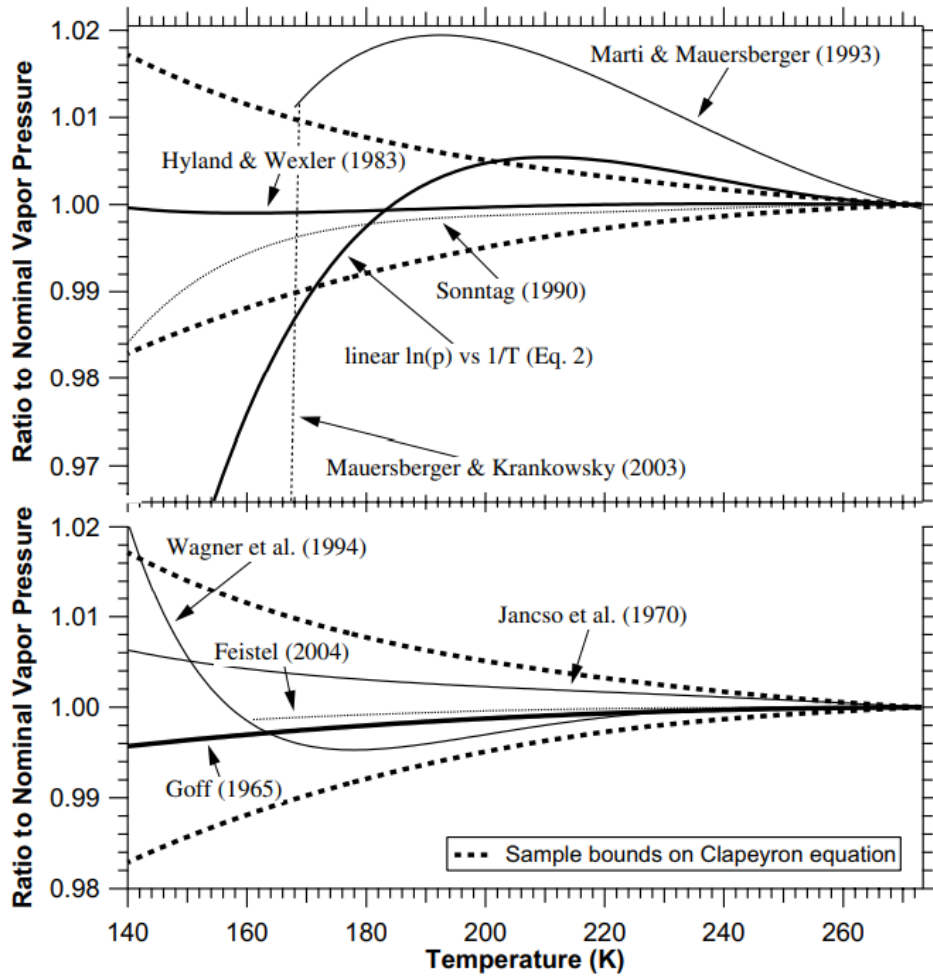
Table 4.7 – Equation (4.8) coefficients value.

$a_A = 9.550426E00$ [ln(Pa)]	$c_A = -3.53068E00$ [ln(Pa)/ln(K)]
$b_A = -5.723265E03$ [K ln(Pa)]	$d_A = -7.28332E-03$ [ln(Pa)/K]

Source: Murphy and Koop (2005).

Where P is vapor pressure in Pa and T is absolute temperature in Kelvin.

Figure 4.7 – Ratios of various parametrizations of the vapor pressure of ice to the nominal thermodynamic solution proposed by (MURPHY; KOOP, 2005).



Source: Murphy and Koop (2005).

Below we show a group of more equations that describes de vapor pressure in the freezing zone.

Correlation of Goff and Gratch (1946), valid within $184 \text{ K} < T < 273.16 \text{ K}$:

$$\ln(P_{v,ice}) = a_A \left[\left(\frac{b_A}{T} \right) - 1 \right] + c_A \ln \left(\frac{b_A}{T} \right) + d_A \left[1 - \left(\frac{T}{b_A} \right) \right] + \ln(e_A) \quad (4.9)$$

Table 4.8 – Coefficient values of Equation (4.9).

$$\begin{aligned} a_A &= -9.09718E00 \text{ [ln(Pa)]} & d_A &= 8.76793E-01 \text{ [ln(Pa)]}^2 \\ b_A &= 2.7316E02 \text{ [K ln(Pa)]} & e_A &= 6.1071E02 \text{ (Pa)} \\ c_A &= -3.56654E00 \end{aligned}$$

Source: Goff and Gratch (1946).

In other hand Goff (1957) expressed another correlation, valid within $180\text{K} < T < 273.16\text{ K}$,

$$\ln(P_{v,ice}) = \ln(a_A) + b_A \left(\frac{T_t}{T-1} \right) + c_A \ln \left(\frac{T_t}{T} \right) + d_A \left(\frac{1-T}{T_t} \right) \quad (4.10)$$

Table 4.9 – Coefficient values of Equation (4.10).

$$\begin{aligned} a_A &= 6.1114E02 \text{ [Pa]} & c_A &= -3.566506E00 \text{ [ln(Pa)]} \\ b_A &= -9.096853E00 \text{ [ln(Pa)]} & d_A &= 8.76812E-01 \text{ [ln(Pa)]} \end{aligned}$$

Source: Goff (1957).

Hyland and Wexler (1983) presented the following correlation, valid within $173.16\text{K} \leq T < 273.16\text{K}$,

$$\ln(P_{v,ice}) = \frac{a_A}{T} + b_A + c_A T + d_A T^2 + e_A T^3 + f_A T^4 + g_A \ln T \quad (4.11)$$

Table 4.10 – Coefficient values of Equation (4.11).

$$\begin{aligned} a_A &= -5.6745359E03 \text{ [K ln(Pa)]} & e_A &= 2.0747825E-09 \text{ [ln(Pa)]/K}^3 \\ b_A &= 6.3925247E00 \text{ [ln(Pa)]} & f_A &= -9.484024E-13 \text{ [ln(Pa)]/K}^4 \\ c_A &= -9.677843E-03 \text{ [ln(Pa)]/K} & g_A &= 4.1635019E00 \text{ [ln(Pa)]/ln(K)} \\ d_A &= 6.2215701E-07 \text{ [ln(Pa)]/K}^2 \end{aligned}$$

Source: Hyland and Wexler (1983).

Mauersberger (2003) developed exponential correlation for pressure [Pa], valid within $164.5\text{ K} < T < 169\text{ K}$:

$$P_{v,ice} = \exp\left(a_A + \frac{b_A}{T}\right) \quad (4.12)$$

Table 4.11 – Coefficient values of Equation (4.12).

$$a_A = 3.4262E01 \text{ [ln(Pa)]} \quad b_A = -7.044E03 \text{ [K ln(Pa)]}$$

Source: Mauersberger (2003).

Jancso et al. (1970), presented a mix correlation for the range $173\text{K} < T < 273.16\text{K}$:

$$\ln P'_{v,ice} = \frac{a_A}{T} + b_A \ln T + c_A T + d_A T^2 + e_A \quad (4.13)$$

$$P_{v,ice} = f_A \left(\frac{g_A}{h_A} \right) P'_{v,ice} \quad (4.14)$$

Table 4.12 – Coefficient values of Equations (4.13) and (4.14).

$$\begin{array}{ll} a_A = -2.481604E03 \text{ [K ln(Pa)]} & e_A = 1.901973E00 \text{ [ln(Pa)]} \\ b_A = 3.572198E00 \text{ [ln(Pa)/ln(K)]} & f_A = 1.3332E02 \\ c_A = 3.097203E-03 \text{ [ln(Pa)/K]} & g_A = 6.11657E02 \\ d_A = -1.7649E-07 \text{ [ln(Pa)/K}^2\text{]} & h_A = 6.11283E02 \end{array}$$

Source: Jancso et al. (1970).

Sonntag (1990) presented exponential correlation for iced vapor pressure [Pa] for $173.15\text{K} \leq T \leq 273.16\text{K}$:

$$P_{v,ice} = a_A \exp\left(b_A + \frac{c_A}{T} + d_A T + e_A T^2 f_A \ln(T)\right) \quad (4.15)$$

Table 4.13 – Coefficient values of Equation (4.15).

$$\begin{aligned}
 a_A &= 1\text{E}02 \text{ [Pa]} & d_A &= 1.0613868\text{E-}2 \text{ [ln(Pa)/K]} \\
 b_A &= 2.47219\text{E}01 \text{ [ln(Pa)]} & e_A &= -1.3198825\text{E-}05 \text{ [ln(Pa)/T}^2\text{]} \\
 c_A &= -6.0245282\text{E}03 \text{ [K ln(Pa)]} & f_A &= -4.9382577\text{E-}01 \text{ [ln(Pa)/ln(K)]}
 \end{aligned}$$

Source: Sonntag (1990).

Wagner et al. (1994) developed the following correlation, valid within $190\text{K} < T < 273.16\text{K}$:

$$\ln(P_{v,ice}) = \ln(a_A) + b_A \left(1 - \left(\frac{T_i}{T} \right)^{1.5} \right) + c_A \left(1 - \left(\frac{T_i}{T} \right)^{1.25} \right) \quad (4.16)$$

Table 4.14 – Coefficient values of Equation (4.16).

$$\begin{aligned}
 a_A &= 6.11657\text{E}02 \text{ [Pa]} & c_A &= 3.47078238\text{E}01 \text{ [ln(Pa)]} \\
 b_A &= -1.3928169\text{E}01 \text{ [ln(Pa)]}
 \end{aligned}$$

Source: Wagner et al. (1994).

Murphy and Koop (2005) extended upward from triple point using Wagner and Pruss (1993) results as a base and making this equation fitted from $123\text{K} < T < 322\text{K}$. It means the correlation becomes valid for two zones - freeze and two-phase one:

$$\begin{aligned}
 \ln(P_{liq}) &\approx a_B + \frac{b_B}{T} + c_B \ln(T) + d_B T + \\
 &\tanh\{e_B(T + f_B)\} \left(g_B + \frac{h_B}{T} + i_B \ln(T) + j_B T \right)
 \end{aligned} \quad (4.17)$$

In this correlation a hyperbolic tangent function first time was used.

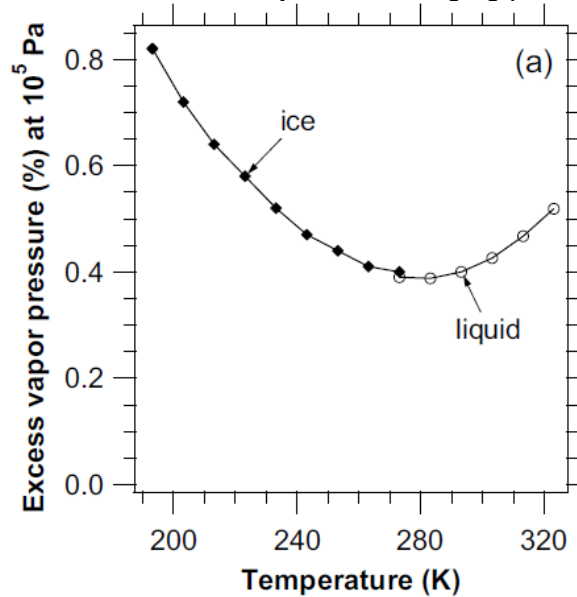
Table 4.15 – Coefficient values of Equation (4.17).

$a_B = 5.4842763E01$ [ln(Pa)]	$f_B = -2.188E02$ [K]
$b_B = -6.76322E03$ [K ln(Pa)]	$g_B = 5.3878E01$ [ln(Pa)]
$c_B = -4.21E00$ [ln(Pa)/ln(K)]	$h_B = -1.33122E03$ [ln(Pa)/K]
$d_B = -3.6E-04$ [ln(Pa)/K]	$i_B = -9.44523E00$ [ln(Pa)/ln(K)]
$e_B = -4.15E-02$ [1/K]	$j_B = 1.4025E-02$ [ln(Pa)/K]

Source: Murphy and Koop (2005).

Also, Murphy and Koop (2005) expressed his concerns about continuity; it is not necessarily those two equations will start or end in the same value, and this can be a numerical problem for the equation of continuity, translating in a problem to transient simulations. To build a bridge between vapor pressure below triple point and vapor pressure in saturation zone Murphy and Koop (2005) expressed their solution condensed in Figure 4.8.

Figure 4.8 – Discontinuity in the changing phase.



Source: Murphy and Koop (2005).

Kalova and Mares (2010) in their introduction mentioned the preferences of using water properties equation instead the using of experimental data due to the lack of quality in that range. In their work, they expressed the equation created by Saul

and Wagner (1987) and wrote below, valid from 123K to 332 K. They also highlighted the deviations associated.

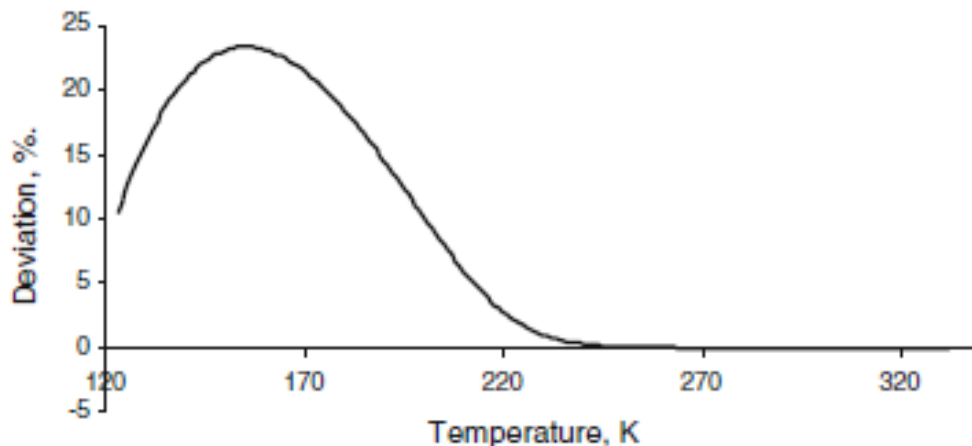
$$\ln(P_v) = \ln(P_C) + \left(\frac{T_C}{T}\right) \cdot (a_B T + b_B T^{1.5} + c_B T^3 + d_B T^{3.5} + e_B T^4 + f_B T^{7.5}) \quad (4.18)$$

Table 4.16 – Equation (4.18) coefficients value.

$a_B = -7.85951783E00$ [ln(Pa)/K]	$d_B = 2.26807411E01$ [ln(Pa)/K ^{3.5}]
$b_B = 1.84408259E00$ [ln(Pa)/K ^{1.5}]	$e_B = -1.59618718E01$ [ln(Pa)/K ⁴]
$c_B = -1.18766497E01$ [ln(Pa)/K ³]	$f_B = 1.80122502E00$ [ln(Pa)/K ^{7.5}]

Source: Saul and Wagner (1987).

Figure 4.9 – Result deviation by comparison between Equation (4.17) and (4.18).



Source: Kalova and Mares (2010).

In work Kalova and Mares (2010) shows the equation valid in the range of 120K to 270K.

Next a *potpourri* of equations designed to describe the vapor pressure of the saturated phase are shown. Popiel and Wojtkowiak (1998) exposed in their work a good approximation results to vapor pressure of water in temperatures from 0 to 150°C, reached by (SAUL; WAGNER, 1987).

$$P_v = P_{cr} \exp\left\{\left[\frac{T_c}{273.15+T}\right](a_B T + b_B T^{1.5} + c_B T^3 + d_B T^{3.5} + e_B T^4 + f_B T^{7.5})\right\} \quad (4.19)$$

Where P_c is water critical pressure (220.64 bar), T_c is water critical temperature (647.096K), and T is temperature in °C. The coefficients are the same as presented in

Table 4.16.

Goff and Gratch (1946), 273.15 < T < 373.15 K:

$$\ln(P_v) = a_B \left[\left(\frac{b_B}{T} \right) - 1 \right] + c_B \ln \left(\frac{b_B}{T} \right) + d_B \left(10^{\left(\frac{e_B}{b_B} \right) \left(\frac{1-T}{b_B} \right)} - 1 \right) + f_B \left(10^{g_B \left(\frac{b_B}{T-1} \right)} - 1 \right) + \ln(h_B) \quad (4.20)$$

Table 4.17 – Coefficient values of Equation (4.20).

$a_B = -7.90298E00$ [ln(Pa)]	$e_B = 1.011344E03$
$b_B = 3.7316E02$ [K]	$f_B = 8.1328E-03$ [ln(Pa)]
$c_B = 5.02808E00$ [ln(Pa)/ln(K)]	$g_B = -3.49149E00$
$d_B = -1.3816E-07$	$h_B = 1.01325E05$ [Pa]

Source: Goff and Gratch (1946).

Goff (1957), 273.15 < T < 373.15K:

$$\ln(P_v) = \ln(a_B) + b_B \left(\frac{1-T_t}{T} \right) + c_B \ln \left(\frac{T}{T_t} \right) + d_B \left(1 - 10^{\left(\frac{e_B}{T_t-1} \right) \left(\frac{T}{T_t} \right)} \right) + f_B \left(10^{g_B \left(\frac{1-T_t}{T} \right)} - 1 \right) \quad (4.21)$$

Table 4.18 – Coefficient values of Equation (4.21).

$a_B = 6.1114E02$ [Pa]	$e_B = -8.2969E00$
$b_B = 1.079574E01$ [ln(Pa)]	$f_B = 4.2873E-04$ [ln(Pa)]
$c_B = -5.028E00$ [ln(Pa)]	$g_B = 4.76955E00$
$d_B = 1.50475E-04$ [ln(Pa)]	

Source: Goff (1957).

Goff (1965), $180K < T < 273.16K$:

$$\ln(P_v) = \ln(a_B) + b_B \left(\frac{1 - T_t}{T} \right) + c_B \ln \left(\frac{T}{T_t} \right) + d_B \left(1 - 10^{e_B \left(\frac{T}{T_t - 1} \right)} \right) + f_B \left(10^{g_B \left(\frac{1 - T_t}{T} \right)} - 1 \right) \quad (4.22)$$

Table 4.19 – Coefficient values of Equation (4.22).

$a_B = 6.1114E02$ [Pa]	$e_B = -8.2969E00$
$b_B = 1.079574E01$ [ln(Pa)]	$f_B = 4.2873E-04$ [ln(Pa)]
$c_B = -5.028E00$ [ln(Pa)]	$g_B = 4.76955E00$
$d_B = 1.50475E-04$ [ln(Pa)]	

Source: Goff (1965).

Hyland and Wexler (1983), $173.16 \leq T < 273.16K$:

$$\ln(P_v) = \frac{a_B}{T} + b_B + c_B T + d_B T^2 + e_B T^3 + f_B \ln(T) \quad (4.23)$$

Table 4.20 – Coefficient values of Equation (4.23).

$a_B = -5.8002206E03$ [K ln(Pa)]	$d_B = 4.1764768E-05$ [ln(Pa)/K ²]
$b_B = 1.3914993E00$ [ln(Pa)]	$e_B = -1.4452093E-08$ [ln(Pa)/K ³]
$c_B = -4.8640239E-02$ [ln(Pa)/K]	$f_B = 6.5459673E00$ [ln(Pa)/ln(K)]

Source: Hyland and Wexler (1983).

Koop et al. (2000), $150 < T < 273$ K:

$$P_v \approx P_{v,ice} \exp\left(a_B + b_B T + \frac{c_B}{T} + d_B \frac{\ln(T)}{RT}\right) \quad (4.24)$$

Table 4.21 – Coefficient values of Equation (4.24).

$a_B = -2.10368E05$	$c_B = -3.32373E06$ [K]
$b_B = 1.31438E02$ [1/K]	$d_B = -4.17291E04$ [J/kg/ln(K)]

Source: Koop et al. (2000).

Sonntag (1990), $173.15K \leq T \leq 373.15K$:

$$P_v = \exp\left(a_B + \frac{b_B}{T} + c_B T + d_B T^2 + e_B \ln(T)\right) \quad (4.25)$$

Table 4.22 – Coefficient values of Equation (4.25).

$a_B = 1.6635764E01$ [ln(Pa)]	$d_B = 1.673952E-02$ [ln(Pa)/K ²]
$b_B = -6.0969385E03$ [K ln(Pa)]	$e_B = 2.433502E00$ [ln(Pa)/ln(K)]
$c_B = -2.711193E-02$ [ln(Pa)/K]	

Source: Sonntag (1990).

Wagner et al. (1994), $273.16K \leq T \leq 647$ K:

$$\ln\left(\frac{P_v}{a_B}\right) = \left(\frac{T_{cr}}{T}\right) \left(b_B \tau + c_B \tau^{1.5} + d_B \tau^3 + e_B \tau^{3.5} + f_B \tau^4 + g_B \tau^{7.5}\right) \quad (4.26)$$

Table 4.23 – Coefficient values of Equation (4.26).

$a_B = 2.2064E07$ [Pa]	$e_B = 2.26807411E01$
$b_B = -7.85951783E00$	$f_B = -1.59618719E01$
$c_B = 1.84408259E00$	$g_B = 1.80122502E00$
$d_B = -1.17866497E01$	

Source: Wagner et al. (1994).

where $\tau = 1 - \frac{T}{T_{cr}}$ and $T_{cr} = 647.096K$.

For temperatures above the critical point, Van der Waals pressure equation usually can be applied:

$$P = \frac{RT}{\frac{M}{\rho_{cr}} - b} - \frac{a}{\frac{M}{\rho_{cr}}^2} \quad (4.27)$$

$$a = \frac{27 \cdot R^2 \cdot T_{cr}^2}{64P_{cr}}; b = \frac{R \cdot T_{cr}}{8P_{cr}}; \quad (4.28)$$

Where P_{cr} and T_{cr} are pressure and temperature at critical point, respectively, T is absolute temperature in Kelvin, M is the molar mass and R is the universal gas constant.

Redlich and Kwong (1949) have improved the Van der Waals (4.27) Equation:

$$P = \frac{RT}{\frac{M}{\rho_{cr}} - b} - \frac{a}{\frac{M}{\rho_{cr}} \left(\frac{M}{\rho_{cr}} + b \right) T^{1/2}} \quad (4.29)$$

$$a = \frac{R^2 \cdot T_{cr}^{5/2}}{2.3393P_{cr}}; b = \frac{R \cdot T_{cr}}{11.5420P_{cr}}; \quad (4.30)$$

Soave (1972) proposed a modification of equation presented Redlich and Kwong (1949) work, achieving a new concept of fluid characterization. At that time, the focus was on the improved temperature dependency of the attractive parameter “a”. Currently, the component “a” depends on the saturated vapor pressure (P_{vp}) in a reduced temperature characterized by $T_R = 0.7/T_{cr}$.

$$P = \frac{RT}{\frac{M}{\rho_{cr}} - b} - \frac{a}{\frac{M}{\rho_{cr}} \left(\frac{M}{\rho_{cr}} + b \right)} \quad (4.31)$$

$$a = \frac{R^2 \cdot T_{cr}^2}{2.3393P_{cr}} \left(1 + m \left(1 - T_R^{1/2} \right) \right)^2; b = \frac{R \cdot T_{cr}}{11.5420P_{cr}}; \quad (4.32)$$

$$m = 0.480 + 1.574\omega - 0.176\omega^2 \quad (4.33)$$

$$\omega = \log_{10} \left(\frac{P_{cr}}{P_{VP}} \right) - 1 \quad (4.34)$$

4.3 Vapor density

Saul and Wagner (1987) present a dimensionless density correlation based on data based on the thermal-physical properties on the saturation line of ordinary water substance. (273K<T<647.2K):

$$\ln \left(\frac{\rho_v}{\rho_{cr}} \right) = a_c \tau^{2/6} + b_c \tau^{4/6} + c_c \tau^{8/6} + d_c \tau^{18/6} + e_c \tau^{37/6} + f_c \tau^{71/6} \quad (4.35)$$

where $\tau = 1 - \frac{T}{T_{cr}}$.

Table 4.24 – Coefficient values of Equation (4.35).

$a_c = -2.02957$	$d_c = -17.3151$
$b_c = -2.68781$	$e_c = -44.6384$
$c_c = -5.38107$	$f_c = -64.3486$

Source: Saul and Wagner (1987).

Wagner et al. (1994) have slightly refined these coefficients:

Table 4.25 – Coefficient values of Equation (4.35).

$a_c = -2.03150240$	$d_c = -17.2991605$
$b_c = -2.68302940$	$e_c = -44.7586581$
$c_c = -5.38626492$	$f_c = -63.9201063$

Source: Wagner et al. (1994).

Faghri (2016) in his book also used a polynomial approximation 5th order instead.

$$\ln(\rho_v) = a_B + b_B T + c_B T^2 + d_B T^3 + e_B T^4 + f_B T^5 \quad (4.36)$$

where T is temperature in Celsius degree, from 20°C to 200°C.

Table 4.26 – Coefficient values of Equation (4.36).

$a_B = -5.3225E+00$ [ln(kg/m ³)]	$d_B = 8.4522E-07$ [ln(kg/m ³)/C ³]
$b_B = 6.8366E-02$ [ln(kg/m ³)/C]	$e_B = -1.6558E-09$ [ln(kg/m ³)/C ⁴]
$c_B = -2.7243E-04$ [ln(kg/m ³)/C ²]	$f_B = 1.5514E-12$ [ln(kg/m ³)/C ⁵]

Source: Faghri (2016).

4.4 Vapor dynamic viscosity

Xin et al. (2023) developed a polynomial approximation of 4th order for this property of water for heat pipe numerical models. This equation is valid for the temperature range from 20°C to 200°C.

$$\mu_v = a_B + b_B T + c_B T^2 + d_B T^3 + e_B T^4 \quad (4.37)$$

where T is temperature in Celsius degree and μ in N·s·m⁻²

Table 4.27 – Coefficient values of Equation (4.37).

$a_B = 2.37687E-05$ [N·s·m ⁻²]	$d_B = -1.24876E-12$ [N·s·m ⁻² /C ³]
$b_B = -1.94073E-07$ [N·s·m ⁻² /C]	$e_B = 7.2752E-16$ [N·s·m ⁻² /C ⁴]
$c_B = 8.02182E-10$ [N·s·m ⁻² /C ²]	

Source: Xin et al. (2023).

Faghri (2016) in his book also used a polynomial approximation of 5th order.

$$\ln(\mu_v) = a_B + b_B T + c_B T^2 + d_B T^3 + e_B T^4 + f_B T^5 \quad (4.38)$$

where T is temperature in Celsius degree, from 20°C to 200°C.

Table 4.28 – Coefficient values of Equation (4.38).

$a_B = -1.1596E+00$ [ln(N·s·m ⁻²)]	$d_B = -6.1035E-08$ [ln(N·s·m ⁻²)/C ³]
$b_B = 2.6382E-03$ [ln(N·s·m ⁻²)/C]	$e_B = 1.6844E-10$ [ln(N·s·m ⁻²)/C ⁴]
$c_B = 6.9205E-06$ [ln(N·s·m ⁻²)/C ²]	$f_B = -1.5910E-13$ [ln(N·s·m ⁻²)/C ⁵]

Source: Faghri (2016).

4.5 Vapor thermal conductivity

Qian et al. (2022) also achieved an approximation to water thermal conductivity; the result can be seen in graph below.

$$k_v = a_B + b_B T + c_B T^2 + d_B T^3 + e_B T^4 \quad (4.39)$$

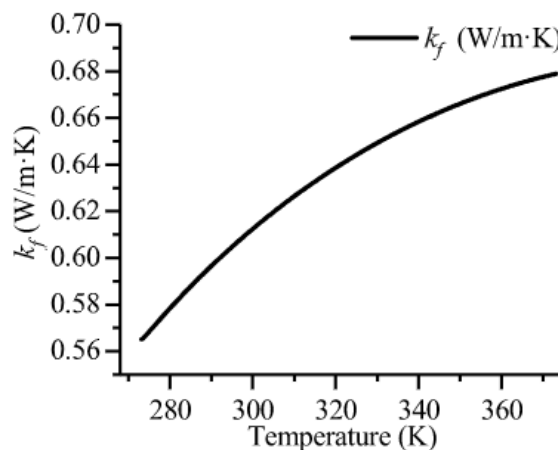
where T is temperature in Celsius degree.

Table 4.29 – Coefficient values of Equation (4.39).

$a_B = 5.650285E-01$ [W/m·K]	$d_B = -1.515492E-06$ [(W/m·K)/C ³]
$b_B = 2.6363895E-03$ [(W/m·K)/C]	$e_B = 9.412945E-04$ [(W/m·K)/C ⁴]
$c_B = -1.2516934E-04$ [(W/m·K)/C ²]	

Source: Qian et al. (2022).

Figure 4.10 – Correlation between thermal conductivity and temperature.



(d) Thermal conductivity

Source: Qian et al. (2022).

In a higher temperature range, Polasek and Stulc (1976), Saaski (1977) and Mishkinis et al. (2009) have reached a linear equation which presents a good property accuracy.

$$k_{sat,v} = a_B + b_B T \quad (4.40)$$

where T is temperature in Celsius degree.

Table 4.30 – Coefficient values of Equation (4.40).

$$a_B = -6.99E+00 \text{ [W/m}\cdot\text{K]} \quad b_B = -6.2E-02 \text{ [(W/m}\cdot\text{K)/C]}$$

Source: Polasek and Stulc (1976), Saaski (1977) and Mishkinis et al. (2009).

Also, Xin et al. (2023) developed a polynomial approximation of 4th degree for this water property with the intention to use in heat pipe numerical model. This equation is valid in a temperature range of 20 to 200 °C.

$$k_v = a_B + b_B T + c_B T^2 + d_B T^3 + e_B T^4 \quad (4.41)$$

where T is temperature in Celsius degree and k in $\text{W}\cdot\text{m}^{-1}\cdot\text{K}^{-1}$

Table 4.31 – Coefficient values of Equation (4.41).

$$\begin{aligned} a_B &= -3.46E-03 \text{ [W/m}\cdot\text{K]} & d_B &= 1.55894E-09 \text{ [(W/m}\cdot\text{K)/C}^3\text{]} \\ b_B &= 1.79378E-04 \text{ [(W/m}\cdot\text{K)/C]} & e_B &= -7.6521E-13 \text{ [(W/m}\cdot\text{K)/C}^4\text{]} \\ c_B &= -7.50759E-07 \text{ [(W/m}\cdot\text{K)/C}^2\text{]} \end{aligned}$$

Source: Xin et al. (2023).

4.6 Vapor specific heat capacity

The equation below was developed by Giauque and Stout (1936) to be used from 15K to 273K (i.e., sublimated vapor over ice). That approximation was proven correct years later by data collected by Flubacher et al. (1960):

$$c_{p,ice} = a_A + b_A T + c_A T \exp\left[-\left(\frac{T}{d_A}\right)^2\right] \quad (4.42)$$

where T is absolute temperature in Kelvin.

Table 4.32 – Coefficient values of Equation (4.42).

$a_A = -2.0572E00$ [J/kg/K]	$c_A = 6.6163E-02$ [J/kg/K ²]
$b_A = 1.4644E-01$ [J/kg/K ²]	$d_A = 1.251E02$ [K]

Source: Giauque and Stout (1936).

Murphy and Koop (2005) approximation can be written similar as the equation above (4.42), using different coefficients:

$$c_{p,ice} = a_A + b_A T + c_A T^2 + d_A T \exp\left[-\left(\frac{T}{e_A}\right)^2\right] \quad (4.43)$$

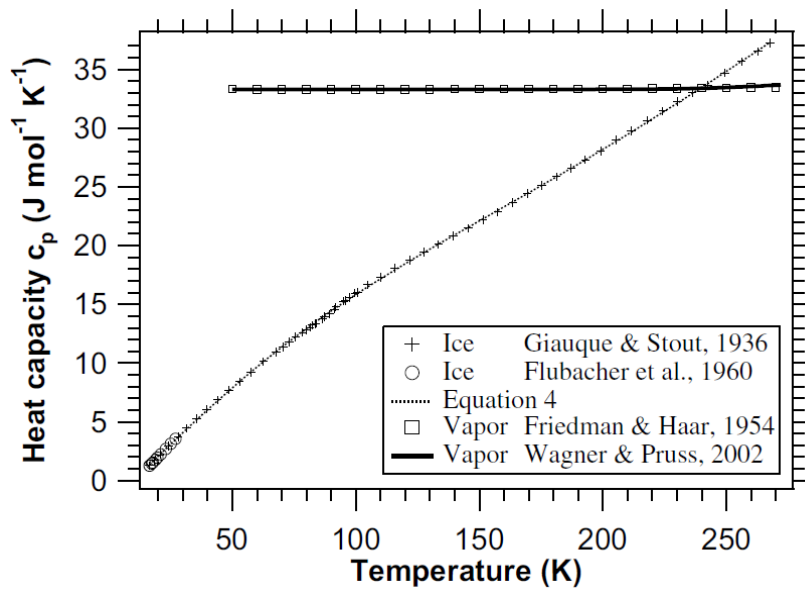
Table 4.33 – Coefficients suggestion for Equation (4.43).

$a_A = 4.67825E04$ [J/mol/K]	$d_A = 5.415E02$ [J/mol/K ²]
$b_A = 3.58925E01$ [J/mol/K ²]	$e_A = 1.2375E02$ [K]
$c_A = -7.414E-02$ [J/mol/K ³]	

Source: Murphy and Koop (2005).

“The last term is good for fitting the nonlinear portion because it goes to zero at both low and elevated temperatures and can be integrated analytically. The same form can be used for the difference in heat capacity between vapor and ice.”
Murphy and Koop (2005).

Figure 4.11 – Correlation between vapor heat capacity and temperature.

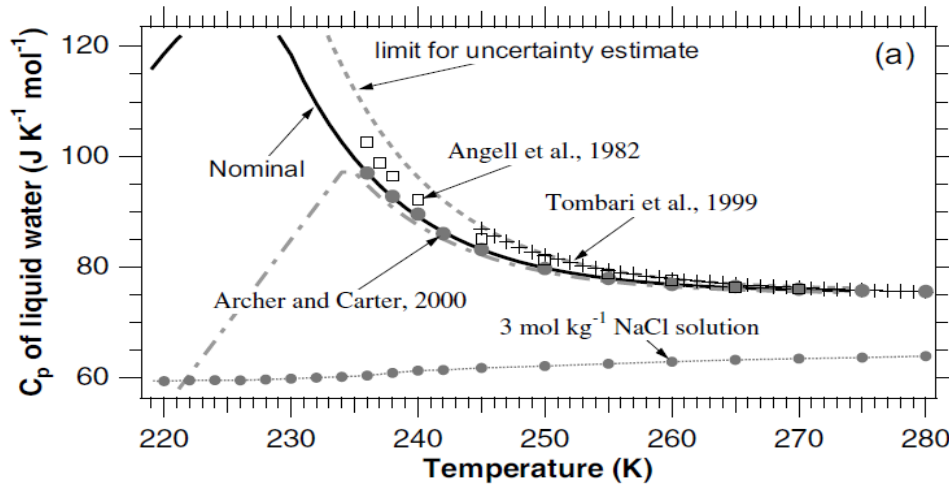


Source: Murphy and Koop (2005).

The same extrapolation, mentioned in vapor pressure topic, was made for the heat capacity; the author exposed and compared different equations in a wider range. It is important to highlight the limits of uncertainty of estimated curve and its behavior with temperature variation. Above the specified range, this limit becomes more permissible as is possible to see in Figure 4.12.

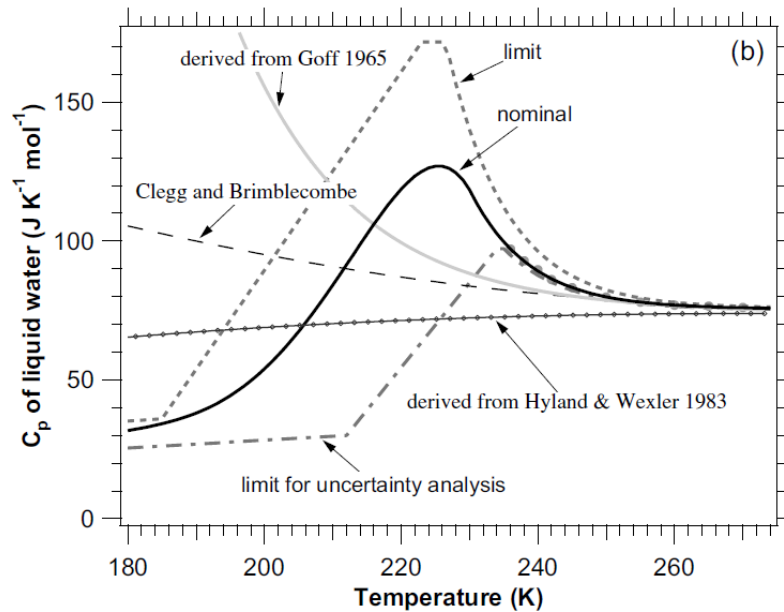
Murphy and Koop (2005) confronted their approximation result with experimental data obtain by Angell et al. (1982), Tombari (1999), Archer and Carter (2000); the result is shown in Figure 4.12.

Figure 4.12 – Comparative study of c_p made by (MURPHY; KOOP, 2005).



Source: Murphy and Koop (2005).

Figure 4.13 – Comparative study of c_p developed by (MURPHY; KOOP, 2005) continuation.



Source: Murphy and Koop (2005).

The next part this work will show a *potpourri* of equations developed to describe the specific heat capacity reached by Murphy and Koop (2005). He in his work shows a relation for $c_{p,ice}$, from 123K up to 155K, achieved by Giaque and Stout (1936) mentioned above in Equation (4.42) whose also built an equation to describes sublimated vapor $c_{p,ice}$, from 123K to 167 K, and in Equation (4.45) is possible to see the result reached by Giaque and Stout (1936) for water in vapor phase.

$$c_{p,ice} = a_A + b_A T + c_A T \exp\left[-\left(\frac{T}{d_A}\right)^2\right] \quad (4.44)$$

Table 4.34 – Equation (4.44) coefficients value.

$$\begin{aligned} a_A &= -5.72E-02 \text{ [J/mol/K]} & c_A &= 6.6163E-02 \text{ [J/mol/K}^2\text{]} \\ b_A &= 1.4644E-01 \text{ [J/mol/K}^2\text{]} & d_A &= 1.251E02 \text{ [K]} \end{aligned}$$

Source: Murphy and Koop (2005).

$$c_{p,vap} = a_B + b_B T + c_B T \exp\left[-\left(\frac{T}{d_B}\right)^2\right] + e_B T \exp\left[-\left(\frac{T}{f_B}\right)^2\right] \quad (4.45)$$

Table 4.35 – Equation (4.45) coefficients value.

$$\begin{aligned} a_B &= 3.326182E01 \text{ [J/kg/K]} & d_B &= 1.2985E02 \text{ [K]} \\ b_B &= 1.87E-03 \text{ [J/kg/K}^2\text{]} & e_B &= 6.6163E-02 \text{ [J/kg/K}^2\text{]} \\ c_B &= 6.165E-02 \text{ [J/kg/K}^2\text{]} & f_B &= 1.251E02 \text{ [K]} \end{aligned}$$

Source: Giauque and Stout (1936).

Faghri (2016) also made his contribution using a 5th degree polynomial approximation for saturated range of temperature.

$$\ln(c_{p,v}) = a_B + b_B T + c_B T^2 + d_B T^3 + e_B T^4 + f_B T^5 \quad (4.46)$$

where T is temperature in Celsius degree; the approximation is valid from 20°C to 200°C.

Table 4.36 – Equation (4.46) coefficients value.

$$\begin{aligned} a_B &= 6.3198E-01 \text{ [ln(J/kg/K)]} & d_B &= 4.4936E-08 \text{ [ln(J/kg/K)/C}^3\text{]} \\ b_B &= 6.7903E-04 \text{ [ln(J/kg/K)/C]} & e_B &= 2.2606E-10 \text{ [ln(J/kg/K)/C}^4\text{]} \\ c_B &= -2.5923E-06 \text{ [ln(J/kg/K)/C}^2\text{]} & f_B &= -9.0694E-13 \text{ [ln(J/kg/K)/C}^5\text{]} \end{aligned}$$

Source: Faghri (2016).

4.7 Vapor Prandtl number

This property is the combination of others three properties, vapor specific heat, vapor thermal conductivity and vapor dynamic viscosity; so, many authors choose to use those property approximations to build a dedicated approximation of the Pr number instead.

4.8 Liquid density

Now we are going to look to liquid density. In their study, Qian et al. (2022) used all fluid properties in two-phase range limited by (270K – 370 K) interval. They used 4th polynomial approximation, Equation (4.47). Out of this range, the equation is not accurate enough to be used in mathematical models:

$$\rho_l(T) = a_B + b_B T + c_B T^2 + d_B T^3 + e_B T^4 \quad (4.47)$$

where T is absolute temperature in Kelvin.

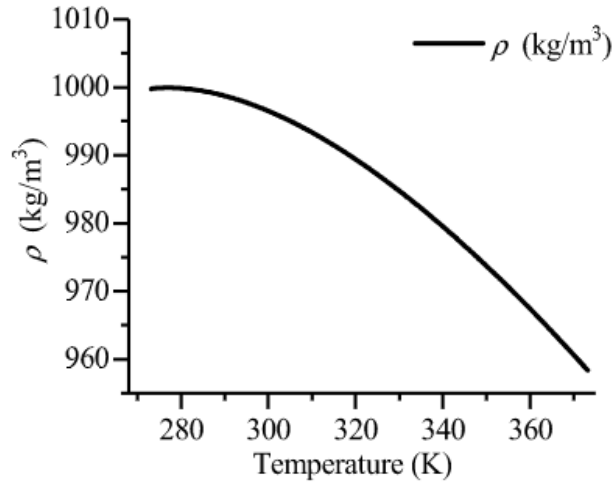
Table 4.37 – Equation (4.47) coefficients value.

$a_B = 9.997968E03$ [kg/m ³]	$d_B = 8.2140905E-04$ [kg/m ³ /K ³]
$b_B = 6.8317355E-02$ [kg/m ³ /K]	$e_B = 2.303988E-05$ [kg/m ³ /K ⁴]
$c_B = -1.0740248E-02$ [kg/m ³ /K ²]	

Source: Qian et al. (2022).

This approximation results in graph below, given in Figure 4.14.

Figure 4.14 – Correlation between density and temperature.



(a) Density

Source: Qian et al. (2022).

Le bideau et al. (2019) used the following approximation for liquid density.

$$\rho_l(T) = (a_B T^2 + b_B T + c_B) \exp(d_B Y_{KOH}) \quad (4.48)$$

where Y is coefficient of approximation and T is temperature in Celsius degree. The approximation coefficients are available in

Table 4.38.

In spite of the work made by Le bideau et al. (2019) refers to an aqueous solution, to reach this result, the authors started from a water liquid density, using a 2nd degree polynomial equation to model this behavior:

$$\rho_l = \rho_{H_2O} \exp(d_B Y_{KOH}) \quad (4.49)$$

Table 4.38 – Coefficient values of Equation (4.48) and (4.49).

$a_B = -3.25E-03$ [kg/m ³ /K ²]	$c_B = 1.00171E03$ [kg/m ³]
$b_B = 1.11E-01$ [kg/m ³ /K]	$d_B = 8.6E-01$

Source: Le bideau et al. (2019).

In their work Saul and Wagner (1987) proposed his contribution to discretize the water density for saturated liquid also using like-polynomial equation and they further have updated that work (WAGNER; SAUL; PRUSS, 1994):

$$\ln\left(\frac{\rho_l}{\rho_{cr}}\right) = 1 + a_B \tau^{1/3} + b_B \tau^{2/3} + c_B \tau^{5/3} + d_B \tau^{16/3} + e_B \tau^{43/3} + f_B \tau^{110/3} \quad (4.50)$$

where $\tau = 1 - \frac{T}{T_c}$ ($273.15 < T < 423.15$ K). Differently to the classic polynomial functions, authors used not-integer powers for dimensionless temperature.

Table 4.39 – Coefficient values of Equation (4.50).

$a_B = 1.99206$	$d_B = -1.75263$
$b_B = 1.10123$	$e_B = -45.4485$
$c_B = -0.512506$	$f_B = -6.75615E5$

Source: Saul and Wagner (1987).

Table 4.40 – Coefficient values of Equation (4.50).

$a_B = 1.99274064$	$d_B = -1.75493479$
$b_B = 1.09965342$	$e_B = -45.5170352$
$c_B = -0.510839303$	$f_B = -6.74694450E5$

Source: Wagner et al. (1994).

Popiel and Wojtkowiak (1998) also recommended the use of Saul and Wagner (1987) equation. Faghri (2016) in his book used a classical polynomial approximation 5th order instead:

$$\ln(\rho_l) = a_B + b_B T + c_B T^2 + d_B T^3 + e_B T^4 + f_B T^5 \quad (4.51)$$

where T is temperature in Celsius degree, from 20°C to 200°C.

Table 4.41 – Coefficient values of Equation (4.51).

$a_B = 6.9094E+00$ [ln(kg/m ³)]	$d_B = 2.5921E-08$ [ln(kg/m ³)/C ³]
$b_B = -2.0146E-05$ [ln(kg/m ³)/C]	$e_B = -9.3244E-11$ [ln(kg/m ³)/C ⁴]
$c_B = -5.9868E-06$ [ln(kg/m ³)/C ²]	$f_B = 1.2103E-13$ [ln(kg/m ³)/C ⁵]

Source: Faghri (2016).

4.9 Liquid dynamic viscosity

Qian et al. (2022) gave contribution to this topic, and in the analogous way said above reached his formulation for liquid dynamic viscosity:

$$\mu_l(T) = a_B + b_B T + c_B T^2 + d_B T^3 \quad (4.52)$$

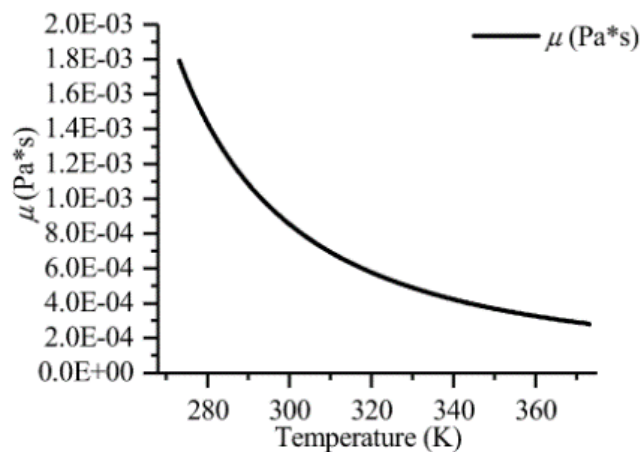
where T is absolute temperature in Kelvin.

Table 4.42 – Coefficient values of Equation (4.52).

$a_B = 5.5782468E02$ [N·s·m ⁻²]	$c_B = 1.360459E-01$ [N·s·m ⁻² /K ²]
$b_B = 1.9408782E01$ [N·s·m ⁻² /K ²]	$d_B = 3.1160832E-04$ [N·s·m ⁻² /K ³]

Source: Qian et al. (2022).

Figure 4.15 – Correlation between dynamic viscosity and temperature.



(b) Dynamic viscosity

Source: Qian et al. (2022).

Kestin et al. (1978) made their contribution presenting the following approximation using logarithm for reduced (i.e. dimensionless) dimensionless dynamic viscosity.

$$\bar{\mu}_l = \frac{\mu}{\mu(T_0)} \quad (4.53)$$

$$\ln \left\{ \frac{\mu(T)}{\mu(20^\circ\text{C})} \right\} = \frac{20-T}{T+96} \left\{ 1.2364 - 1.37 \cdot 10^{-3}(20-T) + 5.7 \cdot 10^{-6}(20-T)^2 \right\} \quad (4.54)$$

where T is measured in Celsius degree; the approximation has a limited range that goes from 0°C up to 40 °C.

Le bideau et al. (2019) used a 2nd order polynomial for approximation under exponential function; the approximation range is 15 °C to 60°C:

$$\mu_l(T) = \exp(a_B + b_B T + c_B T^2 + d_B C) \quad (4.55)$$

where T is temperature in Celsius degree, and C is molarity (mol/L), a correlation between mass fraction, density and molar mass.

Table 4.43 – Coefficient values of Equation (4.55).

$a_B = 4.3\text{E-}01$ [ln(N·s·m ⁻²)]	$c_B = 1.\text{E-}04$ [ln(N·s·m ⁻²)/C ²]
$b_B = -2.51\text{E-}02$ [ln(N·s·m ⁻²)/C]	$d_B = 1.3\text{E-}01$ [ln(N·s·m ⁻²) · L/mol]

Source: Le bideau et al. (2019).

Qian et al. (2022) also presented specific correlation for this property, developed by Popiel and Wojtkowiak (1998):

$$\mu_l(T) = \frac{1}{a_B + b_B T + c_B T^2 + d_B T^3} \quad (4.56)$$

where T is temperature in Celsius degree.

Table 4.44 – Coefficient values of Equation (4.56).

$$\begin{aligned} a_B &= 5.5782468E02 [1/(N \cdot s \cdot m^{-2})] & c_B &= 1.360459E-01 [1/(N \cdot s \cdot m^{-2})/C^2] \\ b_B &= 1.9408782E01 [1/(N \cdot s \cdot m^{-2})/C] & d_B &= -3.1160832E-04 [1/(N \cdot s \cdot m^{-2})/C^3] \end{aligned}$$

Source: Qian et al. (2022).

And Faghri (2016) made his traditional contribution using a 5th degree polynomial approximation:

$$\ln(\mu_l) = a_B + b_B T + c_B T^2 + d_B T^3 + e_B T^4 + f_B T^5 \quad (4.57)$$

where T is temperature in Celsius degree, from 20°C to 200°C.

Table 4.45 – Coefficient values of Equation (4.57).

$$\begin{aligned} a_B &= -6.3530E+00 [\ln(N \cdot s \cdot m^{-2})] & d_B &= -1.1559E-06 [\ln(N \cdot s \cdot m^{-2})/C^3] \\ b_B &= -3.1540E-02 [\ln(N \cdot s \cdot m^{-2})/C] & e_B &= 3.7470E-09 [\ln(N \cdot s \cdot m^{-2})/C^4] \\ c_B &= 2.1670E-04 [\ln(N \cdot s \cdot m^{-2})/C^2] & f_B &= -5.2189E-12 [\ln(N \cdot s \cdot m^{-2})/C^5] \end{aligned}$$

Source: Faghri (2016).

4.10 Liquid thermal conductivity

Mondal et al. (2021) developed a linear correlation to thermal conductivity for liquid phase.

$$k_l = a_B + b_B T \quad (4.58)$$

where T is temperature in Celsius degree and k is thermal conductivity in $W m^{-1}K^{-1}$.

Table 4.46 – Coefficient values of Equation (4.58).

$$\begin{aligned} a_B &= 1.3572E02 [W/m \cdot C] & b_B &= -2.15E-01 [W/m \cdot C^2] \end{aligned}$$

Pátek et al. (2009) presented the following approximation for liquid thermal conductivity.

$$k_l(T) = a_B (T^*)^{b_B} + c_B (T^*)^{d_B} + e_B (T^*)^{f_B} + g_B (T^*)^{h_B} \quad (4.59)$$

where T is absolute temperature in Kelvin, T* is dimensionless temperature T*=T/300K and k is given in W m⁻¹K⁻¹.

Table 4.47 – Coefficient values of Equation (4.59).

a _B = 8.0201E-01 [W/m·K]	e _B = 1.0024E-01 [W/m·K]
b _B = -3.2E-01	f _B = -1.2E01
c _B = -2.5992E-1 [W/m·K]	g _B = -3.2005E-02 [W/m·K]
d _B = -5.7E00	h _B = -1.5E01

And Faghri (2016) has performed a 5th degree polynomial approximation:

$$\ln(k_l) = a_B + b_B T + c_B T^2 + d_B T^3 + e_B T^4 + f_B T^5 \quad (4.60)$$

where T is temperature in Celsius degree, from 20°C to 200°C.

Table 4.48 – Coefficient values of Equation (4.60).

a _B = -5.8220E-01 [ln(W/m·C)]	d _B = 6.5617E-08 [ln(W/m·C ⁴)]
b _B = 4.1177E-03 [ln(W/m·C ²)]	e _B = 4.1100E-11 [ln(W/m·C ⁵)]
c _B = -2.7932E-05 [ln(W/m·C ³)]	f _B = -3.8220E-13 [ln(W/m·C ⁶)]

Source: Faghri (2016).

Popiel and Wojtkowiak (1998) published in their work a polynomial equation that approximates this property behavior when temperature varieties.

$$k_l = a_B + b_B T + c_B T^{1.5} + d_B T^2 + e_B T^{0.5} \quad (4.61)$$

where T is temperature in Celsius degree, from 0°C to 150°C.

Table 4.49 – Coefficient values of Equation (4.61).

$$\begin{aligned} a_B &= 5.650285E-01 \text{ [W/m}\cdot\text{C]} & d_B &= -1.5154918E-06 \text{ [W/m}\cdot\text{C}^3] \\ b_B &= 2.6363895E-03 \text{ [W/m}\cdot\text{C}^2] & e_B &= -9.9412945E-04 \text{ [W/m}\cdot\text{C}^{1.5}] \\ c_B &= -1.2516934E-04 \text{ [W/m}\cdot\text{C}^{2.5}] \end{aligned}$$

4.11 Liquid specific heat capacity

Zaytsev and Aseyev (1992) used the following correlation to describe liquid specific heat capacity behavior with temperature, where Y is the molar mass of the solution:

$$c_{p,l} = a_B + b_B \ln\left(\frac{T}{100}\right) + (c_B + d_B Y + e_B T)Y_i \quad (4.62)$$

Table 4.50 – Coefficient values of Equation (4.62).

$$\begin{aligned} a_B &= 4.236E03 \text{ [J/kg/K]} & d_B &= 8E00 \\ b_B &= 1,075E00 \text{ [J/kg/K/ln(K)]} & e_B &= 8E00 \text{ [J/kg/K]} \\ c_B &= -4.831E03 \text{ [J/kg/K]} \end{aligned}$$

Source: Zaytsev and Aseyev (1992).

The approximation (4.62) can be generalizes to the following expression:

$$c_{p,l} = a_B + b_B T + c_B \ln(T) \quad (4.63)$$

Xin et al. (2023) developed a polynomial approximation of 4th order for this property for water:

$$c_{p,l} = a_B + b_B T + c_B T^2 + d_B T^3 + e_B T^4 \quad (4.64)$$

where T is temperature in Celsius degree from 20°C up to 200°C and c_p is given in $\text{J kg}^{-1} \text{K}^{-1}$.

Table 4.51 – Coefficient values of Equation (4.64).

$$\begin{aligned} a_B &= 8.356E03 \text{ [J/kg/K]} & d_B &= -3.478E-04 \text{ [(J/kg/K)/C}^3\text{]} \\ b_B &= -4.501E01 \text{ [(J/kg/K)/C]} & e_B &= 2.576E-07 \text{ [(J/kg/K)/C}^4\text{]} \\ c_B &= 1.848E-01 \text{ [(J/kg/K)/C}^2\text{]} \end{aligned}$$

And Faghri (2016) developed a 5th degree polynomial approximation using logarithm of the value:

$$\ln(c_{p,l}) = a_B + b_B T + c_B T^2 + d_B T^3 + e_B T^4 + f_B T^5 \quad (4.65)$$

where T is temperature in Celsius degree, from 20°C to 200°C.

Table 4.52 – Coefficient values of Equation (4.65).

$$\begin{aligned} a_B &= 1.4350E+00 \text{ [ln(kJ/kg/K)]} & d_B &= -4.4099E-08 \text{ [ln((kJ/kg/K)/C}^3\text{)]} \\ b_B &= -3.2231E-04 \text{ [ln((kJ/kg/K)/C)]} & e_B &= 2.0968E-10 \text{ [ln((kJ/kg/K)/C}^4\text{)]} \\ c_B &= 6.1633E-06 \text{ [ln((kJ/kg/K)/C}^2\text{)]} & f_B &= -3.0400E-13 \text{ [ln((kJ/kg/K)/C}^5\text{)]} \end{aligned}$$

Source: Faghri (2016).

In a similar way Qian et al. (2022) reached his formulation for water liquid specific heat:

$$c_{p,l} = a_B + b_B T + c_B T^2 + d_B T^3 + e_B T^4 \quad (4.66)$$

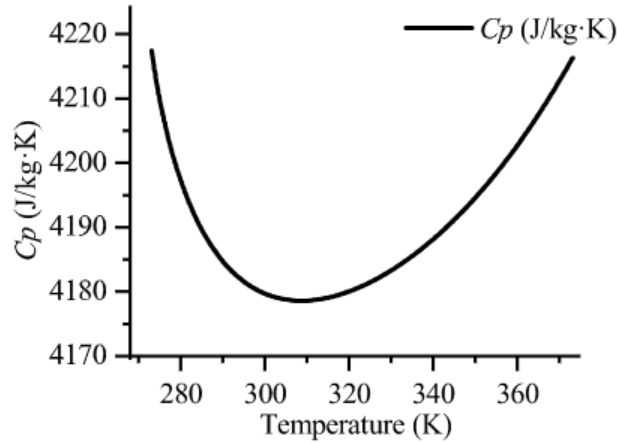
where T is absolute temperature in Kelvin.

Table 4.53 – Coefficient values of Equation (4.66).

$$\begin{aligned} a_B &= 4.2174356E03 \text{ [J/kg/K]} & d_B &= -1.115353E-01 \text{ [J/kg/K}^4\text{]} \\ b_B &= -5.6181625E00 \text{ [J/kg/K}^2\text{]} & e_B &= 4.14964E-03 \text{ [J/kg/K}^5\text{]} \\ c_B &= 1.2992528E00 \text{ [J/kg/K}^3\text{]} \end{aligned}$$

Source: Qian et al. (2022).

Figure 4.16 – Correlation between specific heat and temperature.



(c) Specific heat capacity

Source: Qian et al. (2022).

Popiel and Wojtkowiak (1998) published in their work a polynomial equation that approximates this property behavior when temperature variates.

$$c_{p,l} = a_B + b_B T + c_B T^{1.5} + d_B T^{2.5} + e_B T^3 \quad (4.67)$$

where T is temperature in Celsius degree, from 0°C to 90°C.

Table 4.54 – Coefficient values of Equation (4.67).

$a_B = 4.2174365E00$ [(J/kg/K)/C]	$d_B = -1.1535353E-4$ [(J/kg/K)/C ^{3.5}]
$b_B = -5.6181625E-03$ [(J/kg/K)/C ²]	$e_B = 4.14964E-06$ [(J/kg/K)/C ⁴]
$c_B = 1.2992528E-03$ [(J/kg/K)/C ^{2.5}]	

4.12 Liquid Prandtl number

Popiel and Wojtkowiak (1998) suggested an equation to approximate this water property by an inverse polynomial function:

$$Pr_l = \frac{1}{a_B + b_B T + c_B T^2 + d_B T^3} \quad (4.68)$$

where T is temperature in Celsius degree.

Table 4.55 – Coefficient values of Equation (4.68).

$$\begin{aligned} a_B &= 7.4763403E-02 & c_B &= 2.8606181E-05 [1/C^2] \\ b_B &= 2.9020983E-03 [1/C] & d_B &= -8.1395537E-08 [1/C^3] \end{aligned}$$

Source: Popiel and Wojtkowiak (1998).

4.13 Latent heat (enthalpy) of vaporization

Faghri (2016) also contributed using a 5th degree polynomial approximation.

$$\ln(\lambda) = \exp(a_B + b_B T + c_B T^2 + d_B T^3 + e_B T^4 + f_B T^5) \quad (4.69)$$

where T is temperature in Celsius degree, from 20 to 200°C.

Table 4.56 – Coefficient values of Equation (4.69).

$$\begin{aligned} a_B &= 7.8201E+00 [\ln(\text{kJ/kg})] & d_B &= 8.4738E-08 [\ln(\text{kJ/kg})/C^3] \\ b_B &= -5.8906E-04 [\ln(\text{kJ/kg})/C] & e_B &= -3.9635E-10 [\ln(\text{kJ/kg})/C^4] \\ c_B &= -9.1355E-06 [\ln(\text{kJ/kg})/C^2] & f_B &= -5.9150E-13 [\ln(\text{kJ/kg})/C^5] \end{aligned}$$

Source: Faghri (2016).

Popiel and Wojtkowiak (1998) published in their work a polynomial equation that approximates this property behavior when temperature variates.

$$\lambda = a_B + b_B T + c_B T^{1.5} + d_B T^{2.5} + e_B T^3 \quad (4.70)$$

where T is temperature in Celsius degree, from 0 to 150°C.

Table 4.57 – Coefficient values of Equation (4.70).

$$\begin{aligned} a_B &= 2.500304E+03 [\text{kJ/kg}] & d_B &= 3.1750163E-04 [\text{kJ/kg}/C^{2.5}] \\ b_B &= -2.2521025E00 [\text{kJ/kg}/C] & e_B &= -2.867959E-05 [\text{kJ/kg}/C^3] \\ c_B &= -2.1465847E-02 [\text{kJ/kg}/C^{1.5}] \end{aligned}$$

4.14 Surface tension

Vargaftik et al. (1983) developed a more advanced approximation valid from 0.01 to 185°C.

$$\sigma = a_B \left[\frac{T_{cr} - T}{T_{cr}} \right]^{b_B} \left[1 + c_B \left(\frac{T_{cr} - T}{T_{cr}} \right) \right] \quad (4.71)$$

Table 4.58 – Coefficient values of Equation (4.71).

$$a_B = 2.358E-01 \text{ [N/m]}$$

$$b_B = -6.25E-01$$

$$c_B = 1.256E00$$

Also, Poling et al. (2001) presented an approximation of the following format:

$$\sigma \propto (1 - T_R)^n \quad (4.72)$$

Where “n” is a local variable that can vary from 0.8 to 1.22 and T_R , also known as reduced temperature, is a dimensionless result from T/T_{cr} .

Devarakonda (2005), presented the following approximation:

$$\sigma = Q \cdot (P_{cr})^{2/3} (T_{cr})^{1/3} \left(1 - \frac{1}{T_{cr}} \right)^{11/9} \cdot 10^{-3} \quad (4.73)$$

Where, P_{cr} and T_{cr} are critical pressure in bar and critical temperature in Kelvin respectively, resulting in surface tension in N m^{-1} .

$$Q = 0.1196 \left(1 + \frac{\frac{T_{boil}}{T_{cr}} \cdot \ln(P_C)}{1 - \frac{T_{boil}}{T_{cr}}} \right) \quad (4.74)$$

Qasem et al. (2021) presented the correlation for pure water:

$$\sigma = a_B \left(1 - \frac{T}{b_B}\right)^{c_B} \left(1 - d_B \left(1 - \frac{T}{b_B}\right)^{c_B}\right) \quad (4.75)$$

where T is absolute temperature in Kelvin.

Table 4.59 – Coefficient values of Equation (4.75).

$a_B = 2.358E02$ [N/m]	$c_B = 1.256E00$
$b_B = 6.47096E02$ [K]	$d_B = 6.25E-01$

Source: Qasem et al. (2021).

And Faghri (2016) also made his contribution using a 5th degree polynomial approximation.

$$\ln(\sigma) = a_B + b_B T + c_B T^2 + d_B T^3 + e_B T^4 + f_B T^5 \quad (4.76)$$

where T is temperature in Celsius degree, from 20°C to 200°C.

Table 4.60 – Coefficient values of Equation (4.76).

$a_B = 4,3438E+00$ [ln(N/m)]	$d_B = -2,5499E-07$ [ln(N/m)/C ³]
$b_B = -3,0664E-03$ [ln(N/m)/C]	$e_B = 1,0377E-09$ [ln(N/m)/C ⁴]
$c_B = 2,0743E-05$ [ln(N/m)/C ²]	$f_B = -1,7156E-12$ [ln(N/m)/C ⁵]

Source: Faghri (2016).

Straub (1980) developed an approximation using dimensionless temperature:

$$\sigma = a_b \tau^{b_b} \left(1 + c_b \tau^{d_b}\right) \quad (4.77)$$

$$\tau = 1 - \frac{T}{T_{cr}} \quad (4.78)$$

Where sigma is the surface tension, T_c is the critical temperature, and T is the temperature (in K).

Popiel and Wojtkowiak (1998) published a polynomial equation that approximates this property behavior when temperature varies .

$$\sigma = a_B + b_B T + c_B T^2 + d_B T^3 \quad (4.79)$$

where T is temperature in Celsius degree, valid from 0°C to 150°C.

Table 4.61 – Coefficient values of Equation (4.79).

$a_B = 7.5652711E-02$ [N/m]	$c_B = -3.0842103E-07$ [N/m/C ²]
$b_B = -1.3936856E-04$ [N/m/C]	$d_B = 2.7588435E-10$ [N/m/C ³]

5 METHODOLOGY

5.1 Building equations

Polynomial equations are widely used to build approximations for fluid properties. It is quite common to find the following expressions for any property (p):

$$p(T, q) = a + bT + cT^2 + dT^3 + eT^4 + fT^5 + \dots \quad (5.1)$$

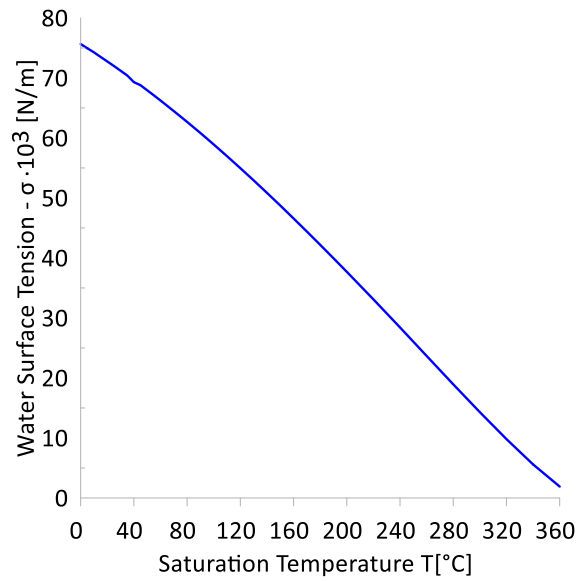
where q - is a vector of approximation parameters (coefficients):

$$q = \{a, b, c, d, e, f, \dots\} \quad (5.2)$$

This type of correlation is usually only valid within well-defined limits. The higher the order, the higher the precision of the approximation. However, out of the range, the behavior of the polynomial may get a significant deviation away from the physical sense. The higher the order of this polynomial equation applied in a wide range of temperature implies into an unstable behavior.

Usually, a polynomial approximation does not reflect the physical nature of the property behavior. To avoid this drawback, it is suggested for any thermo-physical property p that the main component of approximation would follow the main tendency of fluid behavior with temperature whenever possible. After that, the approximation may be improved by adding auxiliary terms or coefficients. To choose a suitable basic correlation, a collection of distinct functions shall be preliminarily created and plotted with variation of key parameters (such a study is presented in APPENDIX A – Equations and its derivatives). For example, for the water surface tension, the original curve looks like in Figure 5.1.

Figure 5.1 – Correlation between water surface tension and saturation temperature.

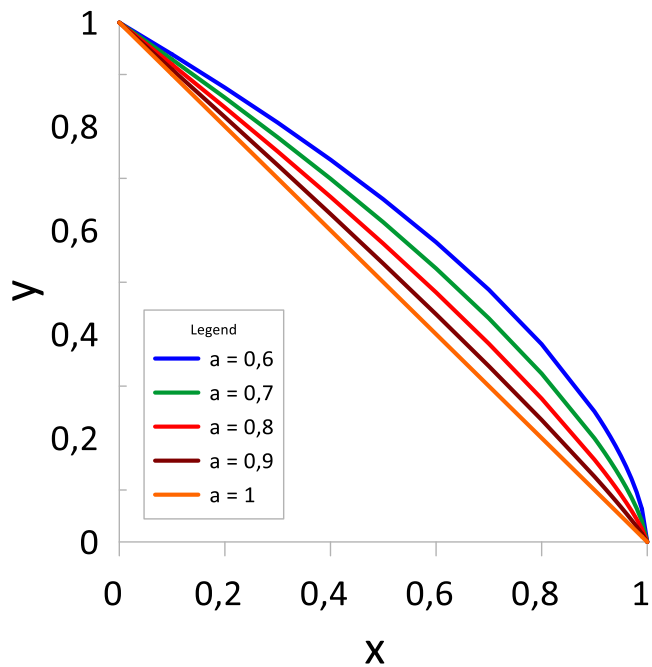


A similar tendency is seen for the following function type.

$$y = (1 - x)^a \quad (5.3)$$

When x varies from 0 to 1 and $a \leq 1$:

Figure 5.2 – Example of function tendency for different “a” value.



One can see that when a is adjusted between 0.6 and 0.9, the tendency in function y follows the tendency of surface tension. This approach is not new, and some correlations already have been elaborated by this manner. For example, a correlation of this type for surface tension as a function of relative temperature can be found in the technical literature:

$$\sigma(T) = \sigma_0 \left(1 - \frac{T}{T_{cr}} \right)^a \quad (5.4)$$

The parameters T_{cr} , σ_0 and a – are different for each specific fluid.

One of the drawbacks of the usual approach with polynomial is that the approximations coefficients “ q ” has dimensions, and those dimensions are dependent on the system of units. To avoid this and for generality, we will use dimensionless properties and temperature:

$$\tau = \frac{T - T_3}{T_{cr} - T_3} \quad (5.5)$$

$$p = \frac{P - P_3}{P_{cr} - P_3} \quad (5.6)$$

The example of Equation (5.6) is shown for pressure. However, the same approach will be applied to all properties.

Wherefore, for the two-phase zone, the values for both τ and p may vary from 0 to 1. For sublimation, τ and p are negative, and for the one-phase supercritical zone (i.e., gas), the values are above 1. We expect such an approach will help to elaborate universal correlations with close coefficients for different working fluids. Moreover, the approximation parameters (coefficients) are also dimensionless.

The properties shall include saturated pressure, latent heat of vaporization and surface tension for interface conditions, as well as density, dynamic viscosity, specific heat, and thermal conductivity for both vapor and liquid phases.

The correlation for the approximation includes approximation parameters “ q ,” whose values shall be obtained from the conditions of the best fitting of known

tabulated data for different temperatures T_i . We denote such parameter vector “q.” These components of vector “q” shall be obtained by a minimization of deviations from tabulated data. To implement this for the dimensionless variables, the first tabulated data shall be recalculated and passed to the dimensionless format as a function of dimensionless temperature:

$$\hat{Y}_i(T_i) \Rightarrow \hat{y}_i(\tau_i) \quad (5.7)$$

When the least-square technique may work fine. In mathematic terms it can be expressed as minimization of average absolute deviation or minimization of maximum absolute deviation:

$$\min_q D_{av} = \frac{1}{N} \sum_{i=1}^N |y(q, \tau_i) - \hat{y}_i(\tau_i)| \quad (5.8)$$

$$\min_q D_{max} = \max_i |y(q, \tau_i) - \hat{y}_i(\tau_i)| \quad (5.9)$$

where N – number of points available in a table of the given thermo-physical property.

These two criteria of optimization can be combined in one by applied dimensionless wights which reflect the relative important of each criterion.

$$\min_q D_p = W_1 D_{max} + W_2 D_{av} \quad (5.10)$$

$$W_1 + W_2 = 1 \quad (5.11)$$

After performing the optimization by any this technique, the best values of the vector “q” components, which provide a better fitting to the tabulated values, will be obtained. The methods for best fitting may be different, starting from try-and-error methods within EXCEL features, or using known search algorithms, beginning from random search to some kinds of genetic optimization algorithms.

When we use the dimensionless properties, those values vary around 0-1 interval, the relative error for optimization is not recommended, once in the zone where the parameter values are near to 0, the uncertainty 0/0 may lead to artificial

exaggerated giant relative errors. Therefore, the absolute deviations are preferable for the dimensionless parameters. This dimensionless absolute deviation makes sense for relative error, referred to the entire two-phase interval. For example, the absolute dimensionless deviation of 0.01 means 1% of the interval ($P_{cr}-P_3$). To be within this sense we will use % (factor of 100) to handle the dimensionless absolute deviations.

5.2 Interfacing

5.2.1 Interfacing around T_3 ($\tau = 0$)

Usually, it is easy to find in technical literature approximations for two different zones:

- for the sublimation zone, at $\tau < 0$, let denote as $y_A(\tau)$;
- for two-phase zone, let denote as $y_B(\tau)$.

However, at $\tau=0$ we have an interruption, as illustrated on the curve of

Figure 5.3, for the magnitude and for derivatives for both sides: from the left and from the right:

$$y_A(0) \neq y_B(0) \quad (5.12)$$

$$y'_A(0) \neq y'_B(0) \quad (5.13)$$

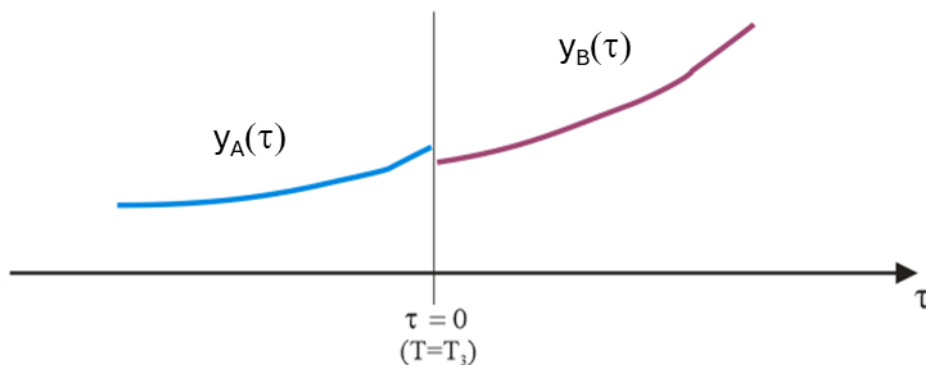
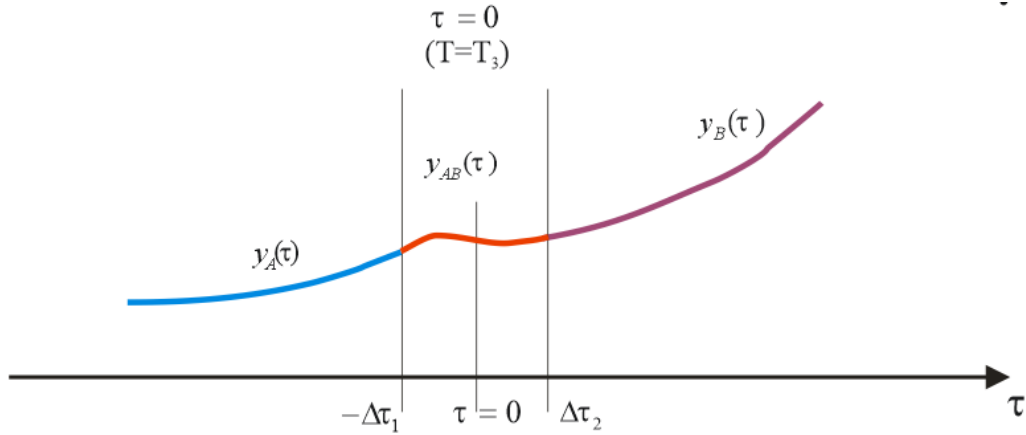


Figure 5.3 – Two equations of fluid properties at T_3 .

Such interruptions are not acceptable for HP numerical modeling for simulation of transient behavior over a wide range of temperatures. To solve this problem, the idea is to introduce a small interface zone (AB) around T_3 temperature to smooth these interruptions, as illustrated in Figure 5.4.

Figure 5.4 – Interfacing example around $\tau=0$.



This zone is bounded by small deviations, say $\Delta\tau_1$ and $\Delta\tau_2$. The magnitude of these variations must be set to a small value of temperature difference, say ~ 0.005 (it corresponds to about ~ 1 °C in absolute temperature scale). The approximation in this interfacing zone, $y_{AB}(\tau)$, must eliminate the non-continuity and smooth these interruptions. To do this, some additional constrains are imposed to the approximation (conditions of smoothing in interfacing zone), considering that we already have the approximations $y_A(\tau)$ and $y_B(\tau)$ and its derivatives:

$$\begin{cases} y_{AB}(-\Delta\tau_1) = y_A(-\Delta\tau_1) \\ y'_{AB}(-\Delta\tau_1) = y'_A(-\Delta\tau_1) \\ y_{AB}(\Delta\tau_2) = y_B(\Delta\tau_2) \\ y'_{AB}(\Delta\tau_2) = y'_B(\Delta\tau_2) \end{cases} \quad (5.14)$$

It was assumed that we already have satisfactory approximations $y_A(\tau)$ and $y_B(\tau)$ and its derivatives in the curves before and after this interfacing zone around the triple point temperature $T=T_3$ (i.e., $\tau=0$). Therefore, there are 4 conditions, and

we can build a function for the interface zone with 4 variables. In general, it could be done by any type of function, but a 3rd order polynomial function of is more appropriate.

$$y_{AB}(x) = a + bx + cx^2 + dx^3 \quad (5.15)$$

The derivative is following:

$$y'_{AB}(x) = b + 2cx + 3dx^2 \quad (5.16)$$

After substitution of this approximation into the conditions, we have.

$$\begin{cases} a + b(-\Delta\tau_1) + c(-\Delta\tau_1)^2 + d(-\Delta\tau_1)^3 = y_A(-\Delta\tau_1) \\ b + 2c(-\Delta\tau_1) + 3d(-\Delta\tau_1)^2 = y'_A(-\Delta\tau_1) \\ a + b\Delta\tau_2 + c\Delta\tau_2^2 + d\Delta\tau_2^3 = y_B(\Delta\tau_2) \\ b + 2c\Delta\tau_2 + 3d\Delta\tau_2^2 = y'_B(\Delta\tau_2) \end{cases} \quad (5.17)$$

Here $\Delta\tau$ is always positive.

$$\begin{cases} a - b\Delta\tau_1 + c\Delta\tau_1^2 - d\Delta\tau_1^3 = y_A(-\Delta\tau_1) \\ b - 2c\Delta\tau_1 + 3d\Delta\tau_1^2 = y'_A(-\Delta\tau_1) \\ a + b\Delta\tau_2 + c\Delta\tau_2^2 + d\Delta\tau_2^3 = y_B(\Delta\tau_2) \\ b + 2c\Delta\tau_2 + 3d\Delta\tau_2^2 = y'_B(\Delta\tau_2) \end{cases} \quad (5.18)$$

Therefore, we have a system of 4 algebraic equations of 4 unknowns a, b, c, and d, which can be resolved by several appropriate methods.

To simplify the representation, we denote:

$$\begin{aligned} -\Delta\tau_1 &\equiv \tau_1 \\ \Delta\tau_2 &\equiv \tau_2 \end{aligned} \quad (5.19)$$

We can derive analytical solution for the polynomial coefficients for the interfacing around $\tau=0$, as presented below:

$$a_{AB} = \frac{\tau_2(\tau_1(\tau_1 - \tau_2)(y'_A\tau_2 - y'_B\tau_1) + y_A\tau_2(3\tau_1 + \tau_2)) + y_B\tau_1^2(\tau_1 + 3\tau_2)}{(\tau_1 - \tau_2)^3} \quad (5.20)$$

$$b_{AB} = \frac{y'_B\tau_1(\tau_1 - 2\tau_2)(\tau_1 + \tau_2) - y'_A\tau_2(2\tau_1 - \tau_2)(\tau_1 + \tau_2) + 6\tau_1\tau_2(y_B - y_A)}{(\tau_1 - \tau_2)^3} \quad (5.21)$$

$$c_{AB} = \frac{y'_A(\tau_1 - 2\tau_2)(\tau_1 + \tau_2) + y'_B(2\tau_1 - \tau_2)(\tau_1 + \tau_2) + 3(\tau_1 - \tau_2)(y_A - y_B)}{(\tau_1 - \tau_2)^3} \quad (5.22)$$

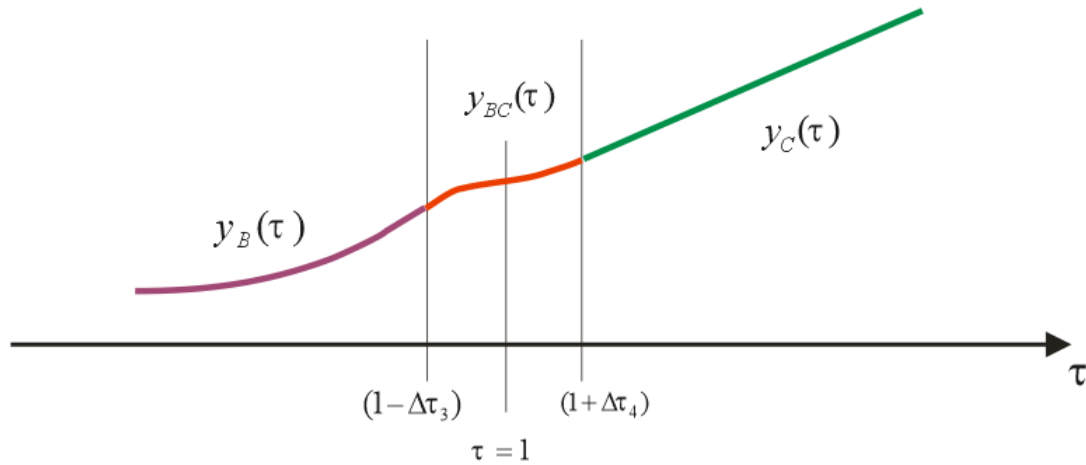
$$d_{AB} = \frac{(y'_A + y'_B)(\tau_1 + \tau_2) + 2(y_A - y_B)}{(\tau_1 - \tau_2)^3} \quad (5.23)$$

The same approach may be used for interfacing of approximations around the critical temperature T_{cr} ($\tau = 1$), presented in next sub-section.

5.2.2 Interfacing around T_{CR} ($\tau = 1$)

The same approach may be used for interfacing of approximations around critical temperature T_{cr} ($\tau = 1$), illustrated in Figure 5.5.

Figure 5.5 – Interfacing example around $\tau=1$.



For the small temperature deviations, we will use $\Delta\tau_3$ and $\Delta\tau_4$ instead of $\Delta\tau_1$ and $\Delta\tau_2$:

$$\begin{cases} y_{BC}(1 - \Delta\tau_3) = y_B(1 - \Delta\tau_3) \\ y'_{BC}(1 - \Delta\tau_3) = y'_B(1 - \Delta\tau_3) \\ y_{BC}(1 + \Delta\tau_4) = y_C(1 + \Delta\tau_4) \\ y'_{BC}(1 + \Delta\tau_4) = y'_C(1 + \Delta\tau_4) \end{cases} \quad (5.24)$$

If we apply the polynomial approximation of 3rd order over the interfacing zone, the basic system of the equation will be the following.

$$\begin{cases} a + b(1 - \Delta\tau_3) + c(1 - \Delta\tau_3)^2 + d(1 - \Delta\tau_3)^3 = y_B(1 - \Delta\tau_3) \\ b + 2c(1 - \Delta\tau_3) + 3d(1 - \Delta\tau_3)^2 = y'_B(1 - \Delta\tau_3) \\ a + b(1 + \Delta\tau_4) + c(1 + \Delta\tau_4)^2 + d(1 + \Delta\tau_4)^3 = y_C(1 + \Delta\tau_4) \\ b + 2c(1 + \Delta\tau_4) + 3d(1 + \Delta\tau_4)^2 = y'_C(1 + \Delta\tau_4) \end{cases} \quad (5.25)$$

Therefore, we have 4 conditions. In this case a polynomial function of 3rd order is adequate.

$$p_{BC}(z) = a + bz + cz^2 + dz^3 \quad (5.26)$$

The derivative is the following.

$$p'_{BC}(z) = b + 2cz + 3dz^2 \quad (5.27)$$

Where z tends to $(1 - \Delta\tau)$ for the case of interfacing around T_{CR} .

After the substitution of the argument z to $(1 - \Delta\tau)$ of this approximation into the system of the smooth interfacing conditions, $\Delta\tau$ is replaced by coefficients in Equation system (5.28).

$$\begin{cases} a + b\tau_3 + c\tau_3^2 + d\tau_3^3 = p_B(\tau_3) \\ b + 2c\tau_3 + 3d\tau_3^2 = p'_B(\tau_3) \\ a + b\tau_4 + c\tau_4^2 + d\tau_4^3 = p_C(\tau_4) \\ b + 2c\tau_4 + 3d\tau_4^2 = p'_C(\tau_4) \end{cases} \quad (5.28)$$

Therefore, we have a system of 4 algebraic equations of 4 unknowns a, b, c, and d, which can be solved by any method.

Solving the system above, the parameters values are available below.

The analytical solution of the system of the Equation (5.28) was obtained for the polynomial coefficients of the interfacing curve.

$$a_{BC} = \frac{\tau_4(\tau_3(\tau_3 - \tau_4)(y'_B\tau_4 - y'_C\tau_3) + y_B\tau_4(3\tau_3 + \tau_4)) + y_C\tau_3^2(\tau_3 + 3\tau_4)}{(\tau_3 - \tau_4)^3} \quad (5.29)$$

$$b_{BC} = \frac{y'_C\tau_3(\tau_3 - 2\tau_4)(\tau_3 + \tau_4) - y'_B\tau_4(2\tau_3 - \tau_4)(\tau_3 + \tau_4) + 6\tau_3\tau_4(y_C - y_B)}{(\tau_3 - \tau_4)^3} \quad (5.30)$$

$$c_{BC} = \frac{y'_B(\tau_3 - 2\tau_4)(\tau_3 + \tau_4) + y'_C(2\tau_3 - \tau_4)(\tau_3 + \tau_4) + 3(\tau_3 - \tau_4)(y_B - y_C)}{(\tau_3 - \tau_4)^3} \quad (5.31)$$

$$d_{BC} = \frac{(y'_B + y'_C)(\tau_3 + \tau_4) + 2(y_B - y_C)}{(\tau_3 - \tau_4)^3} \quad (5.32)$$

These solutions can be implemented into MS Excel spreadsheets.

In the case where fluid property not only depends on temperature but also on pressure, especially in the region above the critical point, the approach may be similar. However, the two-arguments approximation shall be presented as a product of two functions:

$$y_c(\tau, p) = \psi(p)\varphi(\tau) \quad (5.33)$$

The function $\psi(p)$ does not depend on temperature. Therefore, it can be treated as a constant factor in the interfacing equations and will not interfere on the solution of algebraic equations system. However, in this case, the polynomial coefficients a, b, c, d will be functions of pressure. When value of pressure is known, the value of these coefficients can be calculated at different magnitudes of pressure.

The conjugate conditions for this case will be as following:

$$\begin{cases} y_{BC}(1 - \Delta\tau_3) = y_B(1 - \Delta\tau_3) \\ y'_{BC}(1 - \Delta\tau_3) = y'_B(1 - \Delta\tau_3) \\ y_{BC}(1 + \Delta\tau_4) = y_C(1 + \Delta\tau_4, p) \\ y'_{BC}(1 + \Delta\tau_4) = y'_C(1 + \Delta\tau_4, p) \end{cases} \quad (5.34)$$

The basic system of equations, after substitution the expression for $y_C(\tau, p)$ looks like the following.

$$\begin{cases} a + b(1 - \Delta\tau_3) + c(1 - \Delta\tau_3)^2 + d(1 - \Delta\tau_3)^3 = y_B(1 - \Delta\tau_3) \\ b + 2c(1 - \Delta\tau_3) + 3d(1 - \Delta\tau_3)^2 = y'_B(1 - \Delta\tau_3) \\ a + b(1 + \Delta\tau_4) + c(1 + \Delta\tau_4)^2 + d(1 + \Delta\tau_4)^3 = \psi(p)\varphi(1 + \Delta\tau_4) \\ b + 2c(1 + \Delta\tau_4) + 3d(1 + \Delta\tau_4)^2 = \psi(p)\varphi'(1 + \Delta\tau_4) \end{cases} \quad (5.35)$$

Once we have a function of the variable “p” in the system, its solution shall be obtained analytically.

To simplify the representation, we denote:

$$\begin{aligned} (1 - \Delta\tau_3) &\equiv \tau_3 \\ (1 + \Delta\tau_4) &\equiv \tau_4 \end{aligned} \quad (5.36)$$

The analytical solution for the system of Equations (5.35) was obtained for the polynomial coefficients of the interfacing curve:

$$a = \frac{\varphi(\tau_4)\psi(p)\tau_3^2(\tau_3 - 3\tau_4) + \tau_4(\varphi'(\tau_4)\psi(p)\tau_3^2(\tau_4 - \tau_3) - \tau_4(\tau_4 - 3\tau_3)y_B(\tau_3) + \tau_3\tau_4(\tau_4 - \tau_3)y'_B(\tau_3))}{(\tau_3 - \tau_4)^3} \quad (5.37)$$

$$b = \frac{\varphi'(\tau_4)\psi(p)\tau_3(\tau_3 - \tau_4)(\tau_3 + 2\tau_4) + 6\tau_3\tau_4(\varphi(\tau_4)\psi(p) - y_B(\tau_3)) - \tau_4(\tau_4^2 + \tau_3\tau_4 - 2\tau_3^2)y'_B(\tau_3)}{(\tau_3 - \tau_4)^3} \quad (5.38)$$

$$c = \frac{-3\varphi(\tau_4)\psi(p)(\tau_3 + \tau_4) + \varphi'(\tau_4)\psi(p)(\tau_4^2 + \tau_3\tau_4 - 2\tau_3^2) + 3(\tau_3 + \tau_4)y_B(\tau_3) - (\tau_3 - \tau_4)(\tau_3 + 2\tau_4)y'_B(\tau_3)}{(\tau_3 - \tau_4)^3} \quad (5.39)$$

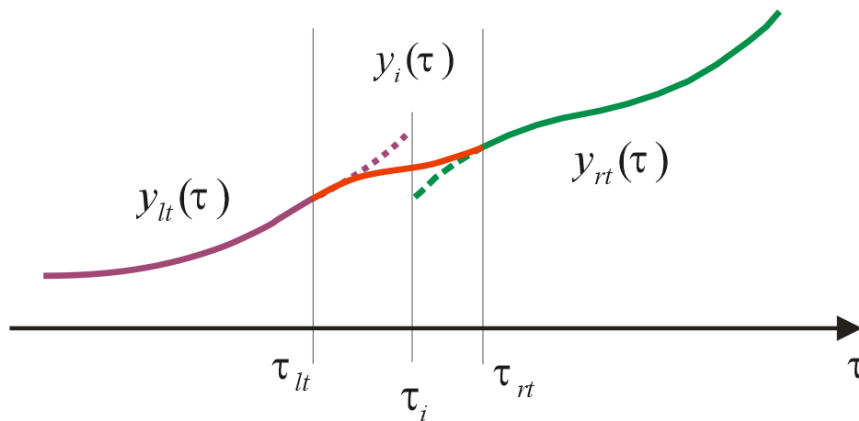
$$d = \frac{2\varphi(\tau_4)\psi(p) - 2y_B(\tau_3) + (\tau_3 - \tau_4)(\varphi'(\tau_4)\psi(p) + y'_B(\tau_3))}{(\tau_3 - \tau_4)^3} \quad (5.40)$$

The solution can be also implemented into an EXCEL spreadsheet. Then, a linear approximation of coefficients a,b,c,d as functions of pressure can be realized.

5.2.3 Interfacing at any point of temperature

By the same manner, the general interfacing algorithm can be used at any point of the temperature axis. In this case we need to define the bound not by $\Delta\tau_1$ and $\Delta\tau_2$ around 0 (or $\Delta\tau_3$ and $\Delta\tau_4$ around 1) but by the values from both sides of an arbitrary conjugation (interruption) point τ_i , let be τ_{lt} on the left side and τ_{rt} - on the right side. This nomenclature is shown in Figure 5.6.

Figure 5.6 – Interfacing for general case.



The conjugate conditions include continuity on function values and on its derivatives from both sides of the interruption point τ_i .

$$\begin{cases} y_i(\tau_{lt}) = y_{lt}(\tau_{lt}) \\ y'_i(\tau_{lt}) = y'_{lt}(\tau_{lt}) \\ y_i(\tau_{rt}) = y_{rt}(\tau_{rt}) \\ y'_i(\tau_{rt}) = y'_{rt}(\tau_{rt}) \end{cases} \quad (5.41)$$

Note, that the interruption points position τ_i are not important anymore, only left, and right bounds are considered.

These conditions are universal and are applicable for any point on the temperature axis. Then we perform the following substitutions.

$$\{\tau_{lt} \rightarrow -\Delta\tau_1; \tau_{rt} \rightarrow \Delta\tau_2; y_{lt} \rightarrow y_A; y_{rt} \rightarrow y_B; y_i \rightarrow y_{AB}\} \quad (5.42)$$

In Equation (5.42), we obtain the conditions for the interfacing between freezing and saturation zones.

$$\{\tau_{lt} \rightarrow 1-\Delta\tau_3; \tau_{rt} \rightarrow 1+\Delta\tau_4; y_{lt} \rightarrow y_B; y_{rt} \rightarrow y_C; y_i \rightarrow y_{BC}\} \quad (5.43)$$

In Equation (5.43), we obtain the conditions for the interfacing between saturation and super-critical zones.

As it has been proven, a polynomial function of 3rd order can be used in the interval of the interfacing:

$$y_i(\tau) = a_i + b_i\tau + c_i\tau^2 + d_i\tau^3 \quad (5.44)$$

After substitution, we obtain the system of equation which must be solved to get the polynomial coefficients a, b, c, and d of the interfacing curve:

$$\begin{cases} a_i + b_i\tau_{lt} + c_i\tau_{lt}^2 + d_i\tau_{lt}^3 = y_{lt}(\tau_{lt}) \\ b_i + 2c_i\tau_{lt} + 3d_i\tau_{lt}^2 = y'_{lt}(\tau_{lt}) \\ a_i + b_i\tau_{rt} + c_i\tau_{rt}^2 + d_i\tau_{rt}^3 = y_{rt}(\tau_{rt}) \\ b_i + 2c_i\tau_{rt} + 3d_i\tau_{rt}^2 = y'_{rt}(\tau_{rt}) \end{cases} \quad (5.45)$$

The parts on the right side are numerical values. Therefore, we have a linear system of 4 equations with 4 unknowns, which in general case has a unique solution. This solution can be obtained analytically manually or with the help of MATHEMATICA[®] or similar tool.

The analytical solution of the system of Equations (5.45) was obtained for the polynomial coefficients of the interfacing curve and shown below.

$$a_i = \frac{(\tau_{rt}(\tau_{lt}(\tau_{rt} - \tau_{lt}))(y'_{rt}\tau_{lt} + y'_{lt}\tau_{rt}) - \tau_{rt}(\tau_{rt} - 3\tau_{lt})y_{lt}) + \tau_{lt}^2(\tau_{lt} - 3\tau_{rt})y_{rt}}{(\tau_{lt} - \tau_{rt})^3} \quad (5.46)$$

$$b_i = \frac{(y'_r \tau'_l (\tau_l - \tau_r)(\tau_l + 2\tau_r) - \tau_r (y'_l (\tau_r^2 + \tau_l \tau_r - 2\tau_l^2) + 6\tau_l (y_l - y_r)))}{(\tau_l - \tau_r)^3}, \quad (5.47)$$

$$c_i = \frac{(-(y'_l (\tau_l - \tau_r)(\tau_l + 2\tau_r)) + y'_r (\tau_r^2 + \tau_l \tau_r - 2\tau_l^2) + 3(\tau_l + \tau_r)(y_l - y_r))}{(\tau_l - \tau_r)^3} \quad (5.48)$$

$$d_i = \frac{((y'_l + y'_r)(\tau_l - \tau_r) - 2y_l + 2y_r)}{(\tau_l - \tau_r)^3} \quad (5.49)$$

The nomenclature is also not important; we may use any customized definition, for example.

$$\begin{aligned} \tau_l &\rightarrow \tau_{H1}; & \tau_r &\rightarrow \tau_{H2}; \\ y_l &\rightarrow y_{H1}; & y_r &\rightarrow y_{H2}; \\ y'_l &\rightarrow y'_{H1}; & y'_r &\rightarrow y'_{H2}; \end{aligned} \quad (5.50)$$

5.3 Piecewise approach using Heaviside functions

The main aim of the research is to develop the approximations which are valid within the entire interval of temperature. It may be exceedingly difficult to elaborate a unique correlation which may be valid for the entire interval, even from 0 to 1 of dimensionless temperature. In this case it is worth to break the interval in few parts where good approximations can be found separately. In this case it is particularly important that in the conjugate point τ_H , the smooth transition must be provided. The condition for the smooth transition is that the values and derivatives of the right and left functions must be equal:

$$\begin{cases} y_2(\tau_H) = y_1(\tau_H) \\ y'_2(\tau_H) = y'_1(\tau_H) \end{cases} \quad (5.51)$$

Where y_1 and y_2 are the components of piecewise functions used for approximation in two conjugate subintervals in this example.

To implement this feature, we propose to use Heaviside functions, defined as:

$$\chi(\tau - \tau_H) = \begin{cases} 0: \tau \leq \tau_H \\ 1: \tau > \tau_H \end{cases} \quad (5.52)$$

We will also use the reverse Heaviside function:

$$\chi^{-1}(\tau - \tau_H) = \begin{cases} 1: \tau < \tau_H \\ 0: \tau \geq \tau_H \end{cases} \quad (5.53)$$

Obviously:

$$\chi^{-1}(\tau - \tau_H) = 1 - \chi(\tau - \tau_H) \quad (5.54)$$

$$\chi(\tau - \tau_H) + \chi^{-1}(\tau - \tau_H) = 1 \quad (5.55)$$

For example, for the case when piecewise function has two components y_1 and y_2 , the approximation over entire interval of temperature can be expressed as:

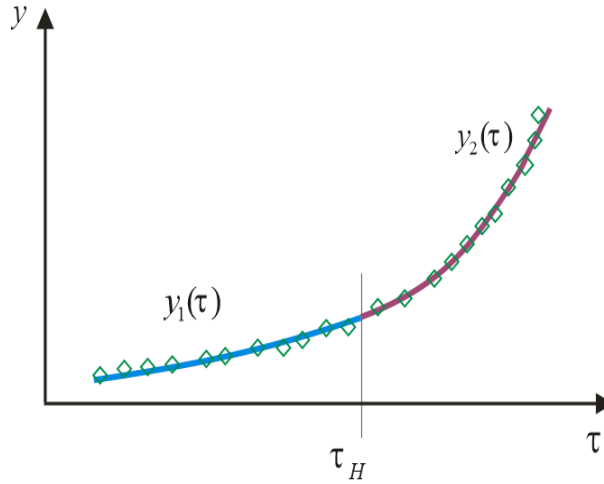
$$\begin{aligned} y(q, \tau) &= (1 - \chi(\tau - \tau_H))y_1(q_1, \tau) + \chi(\tau - \tau_H)y_2(q_2, \tau) \\ &\equiv \chi^{-1}(\tau - \tau_H)y_1(q_1, \tau) + \chi(\tau - \tau_H)y_2(q_2, \tau) \end{aligned} \quad (5.56)$$

In this expression, the sub-vectors of approximation parameters q_1 and q_2 are included:

$$q = \{q_1, q_2\} \quad (5.57)$$

Figure 5.7 illustrates the use of piecewise function with conjugation by Heaviside function.

Figure 5.7 – Example of piecewise function with conjugation by Heaviside function.



The expression for using 3 functions with two conjugate points is similar.

$$y(q, \tau) = \chi^{-1}(\tau - \tau_{H1})y_1(q_1, \tau) + \chi(\tau - \tau_{H1})\chi^{-1}(\tau - \tau_{H2})y_2(q_2, \tau) + \chi(\tau - \tau_{H2})y_3(q_3, \tau) \quad (5.58)$$

$$q = \{q_1, q_2, q_3\} \quad (5.59)$$

Obviously, the approach can be expanded up to any number of components in the piecewise function.

The approach may be called as piecewise approximation by substitution (one function by another). However, this approach has a certain drawback: the solution of the system of equations of smooth transition, Equation (5.60), may be difficult for nonlinear functions.

In this case we propose the conjugation by addition.

For the case of two functions and one conjugate point it can be defined as follows.

$$y(\tau) = \begin{cases} y_1(\tau) : & \tau \leq \tau_H \\ y_1(\tau) + y_2(\tau) : & \tau > \tau_H \end{cases} \quad (5.60)$$

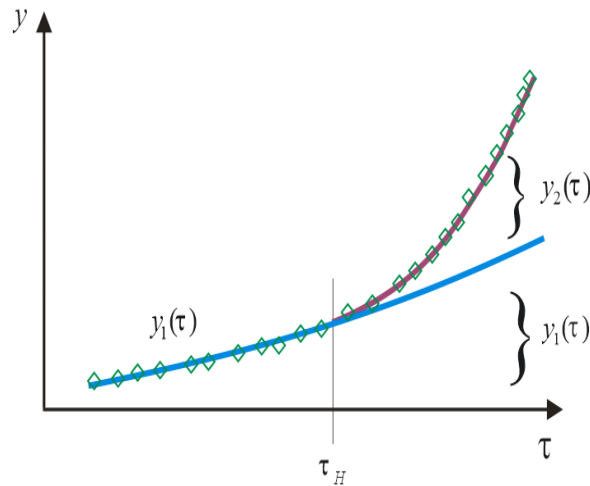
It means the first function provide rough approximation over entire interval, while the second function then add in the point τ_H to improve the approximation. Using the Heaviside functions, the approximation by addition is expressed as:

$$y(\tau, q) = y_1(\tau, q_1) + \chi(\tau - \tau_H)y_2(\tau, q_2) \quad (5.61)$$

$$q = \{q_1, q_2\} \quad (5.62)$$

Next Figure 5.8 illustrates the use of piecewise function with conjugation by addition.

Figure 5.8 – The impact of a Heaviside function on an approximation curve.



The conditions for the smooth transitions become simpler:

$$\begin{cases} y_2(q_2, \tau_H) = 0 \\ y_2'(q_2, \tau_H) = 0 \end{cases} \quad (5.63)$$

This approach also has the drawback that not all candidates for the approximation functions y_2 can be used. A collection for such functions which satisfy the conditions for using in piecewise approximations by addition must be previously created.

5.4 Final format

The results of the approximation over entire temperature range in the format of an algorithm written in pseudo-code, which is quite easy to implement in any programming language, can look like following:

$$y(\tau) = \begin{cases} \text{if } \tau \leq \tau_1 \text{ then } y_A(\tau) \\ \text{if } \tau_1 \leq \tau \leq \tau_2 \text{ then } y_{AB}(\tau) \\ \text{if } \tau_2 \leq \tau \leq \tau_3 \text{ then } y_B(\tau) \\ \text{if } \tau_3 < \tau < \tau_4 \text{ then } y_{BC}(\tau) \\ \text{if } \tau \geq \tau_4 \text{ then } y_C(\tau) \end{cases} \quad (5.64)$$

Where any function “y” could have a shape like this

$$y(q, \tau) = \chi^{-1}(\tau - \tau_{H1})y_1(q_1, \tau) + \chi(\tau - \tau_{H1})\chi^{-1}(\tau - \tau_{H2})y_2(q_2, \tau) \quad (5.65)$$

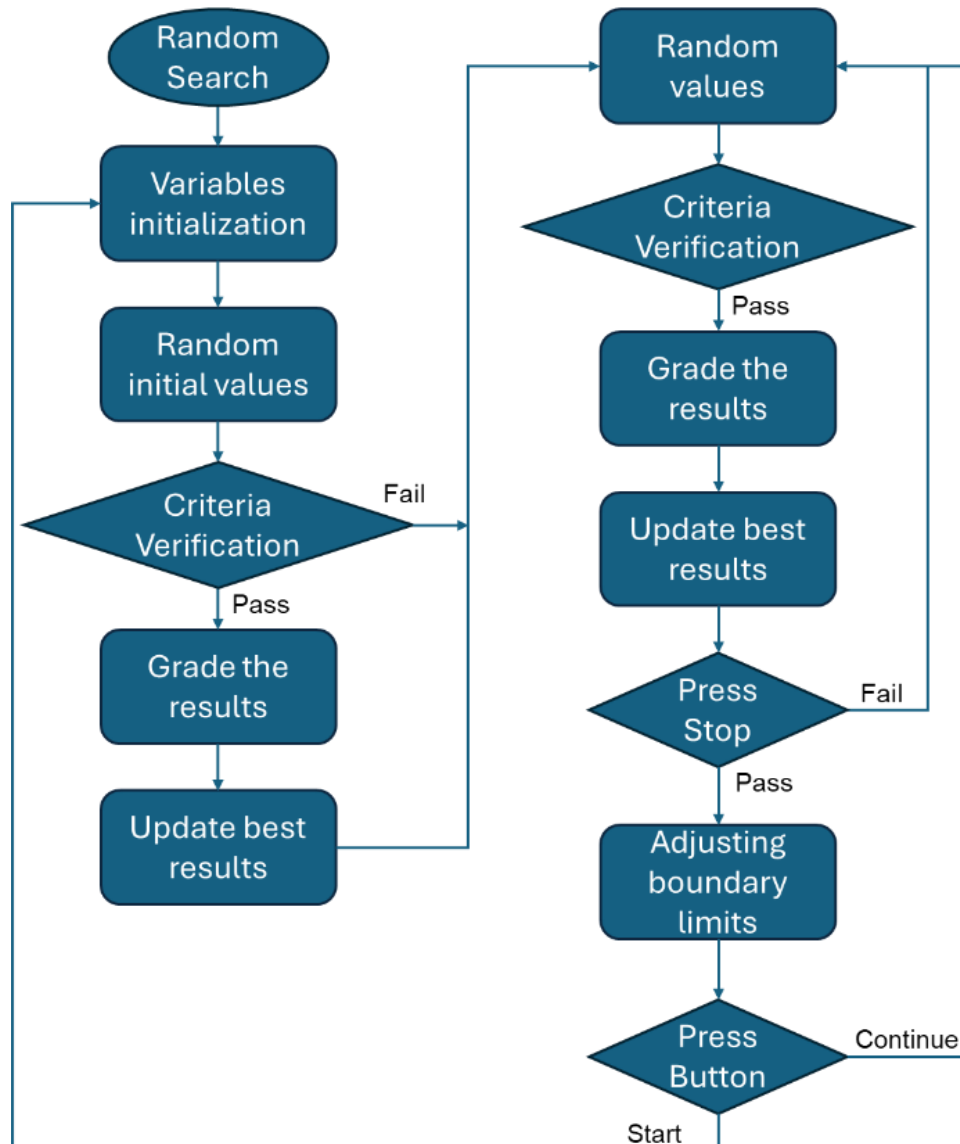
All approximations of all properties will be presented in this format.

5.5 The best approximation by optimization algorithm of random search

As a scientific contribution, this works proposes an optimization algorithm based on applying random values within a specific range chosen by User. The algorithm was developed by author in MS Visual Basic programming language, then implemented, tested and validated within the MS Excel tool.

This algorithm can be checked in block diagram in Figure 5.9 below.

Figure 5.9 – Algorithm block diagram.



The developed tool has several interesting features. It reveals ten best results achieved during iterations and reveals left and right boundaries for all best approximation parameters, including conjugation points positions. At any moment, the User may interrupt calculation and adjust the boundaries to reduce diapason of optimization parameters variations and then continue the calculation. It allows to reduce overall number of iterations and improves the quality of approximation by achieving a better magnitude of the minimization criterion (total deviation). The tool has e visualization of current curve of approximation and best curve achieved.

In our work we choose the liquid Prandtl number of waters to trim our optimization technique. This will be detailed along this work, but Equation (5.66) introduces the format of this dimensionless property by dimensionless temperature. Our program optimizes thirteen variables available in Equation (5.67) using random values in determinate ranges.

The optimization variables are the parameters of approximations.

$$\overline{\text{Pr}}_L(\tau) = y_1(\tau) - \chi(\tau - \tau_{H1})y_2(\tau) + \chi(\tau - \tau_{H2})y_3(\tau) \quad (5.66)$$

$$\begin{cases} y_1 = a_B + b_B\tau + c_B\tau^2 + d_B\tau^3 + e_B\tau^4 + f_B\tau^5 + g_B\tau^6 \\ y_2 = h_B(\tau - \tau_{H1})^{i_B} \\ y_3 = j_B\left(\frac{1 - \text{Cos}(\pi(\tau - \tau_{H2}))}{2}\right)^{k_B} \end{cases} \quad (5.67)$$

Here we have the approach of three piecewise functions combined by addition manner through two conjugate points, τ_{H1} and τ_{H2} . The vector of optimization variables (i.e., approximation parameters) has the following components:

$$q = \{q_1, q_2, q_3\} \quad (5.68)$$

$$\begin{aligned} q_1 &= \{a_B, b_B, c_B, d_B, e_B, f_B, g_B\} \\ q_2 &= \{h_B, i_B\} \\ q_3 &= \{j_B, k_B\} \end{aligned} \quad (5.69)$$

The algorithm used to develop this optimization is based on the deviation of the approximation when it's compared with the property table data., In

Figure 5.10 this value D_P is expressed by name "DesP", this parameter must be minimized and can be defined as weighted sum of the maximum absolute deviation of the approximation from data, and the average deviation in all the temperature range.

$$\min_q D_p = W_1 D_{\max} + W_2 D_{av} \quad (5.70)$$

$$D_{av} = \frac{1}{N} \sum_{i=1}^N |y(q, \tau_i) - \hat{y}_i(\tau_i)| \quad (5.71)$$

$$D_{\max} = \max_i |y(q, \tau_i) - \hat{y}_i(\tau_i)| \quad (5.72)$$

where, W_1 and W_2 are weights of importance applied by user to achieve the best approximation result; the combination of those two always result in one.

$$W_1 + W_2 = 1 \quad (5.73)$$

When the start button is pressed, the algorithm applies random values on each optimization variable; then the result of this operation is evaluated, and the ten best results are ranked. After that, the program applies a routine that set random values on each variable again within the established boundary limits and the result is verified if it could be inserted in the rank of ten best results.

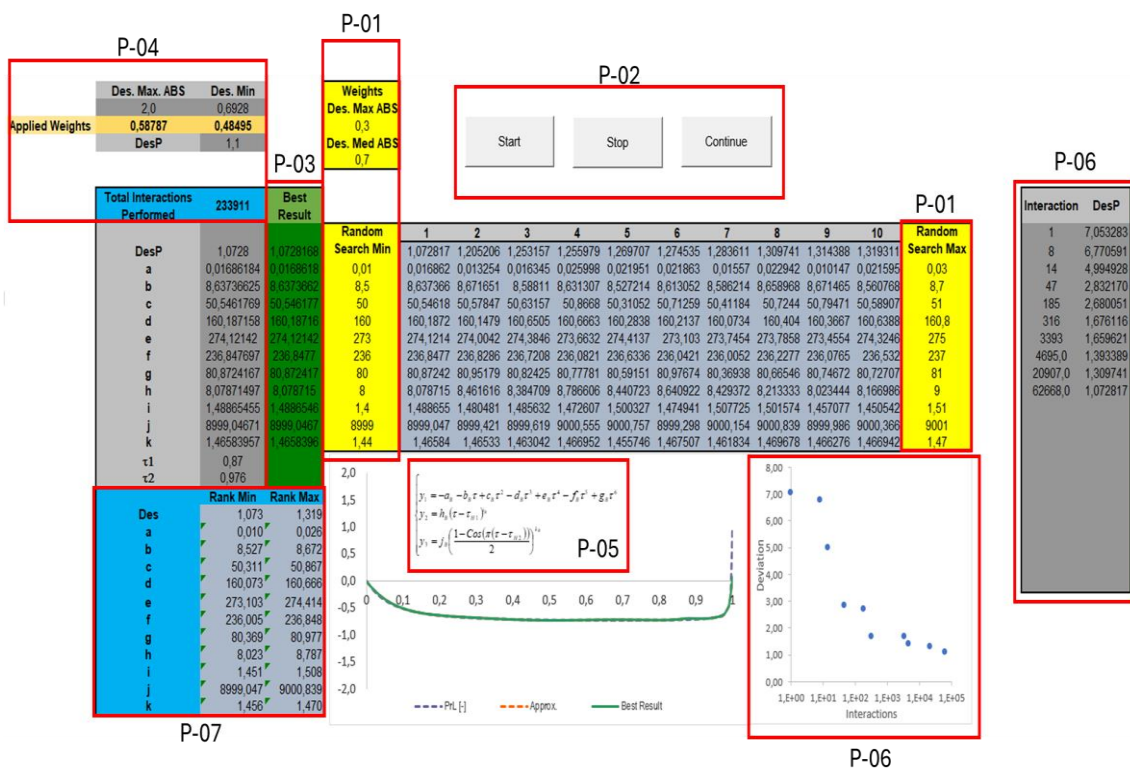
This code provides an iteration counter to observe the process of calculations. Reinforcing that, the User may interrupt iterations at any moment and restrict the range of each variable by readjusting the boundary limits. It may decrease the overall numbers of iteration and may reach a much better approximation.

Figure 5.10 presents an overview of the User Interface within MS Excel spreadsheet used to perform the optimization and a map of all components. Everything in yellow (marked as P-01) is a user input since each error weight, until boundaries of each variable, limiting the range of approximation parameter variations. In box P-02 we have the command buttons (Start, Stop and Continue), the start button initiated the approximation algorithm and the iteration counter. Random values will be assigned to each variable, within the previously determined range. The Stop button pauses the iterations, which allows the User, if necessary, to adjust anything in yellow cells. The Continue button returns to iterations with the modified variables (if applicable), but this button does not reset

the ranking previously placed. The Start button restarts the algorithm, resetting the counter and the ranking.

The green collum (P-03) shows the best result found after all iterations followed by the ten best results ranking. The blue cells display the number of iterations followed by error maximum; the average deviation after weight applied is marked as box P-04. A possible check the approximation components, followed by the chart, shows a visual comparison between data, best results and current approximation curve. An important feature to evaluate the optimization performance is the relationship between deviation and the number of iterations. The box P-06 shows a table that update itself on each deviation achieved the better result in a way to minimize this criterion. The chart of this table is automatically updated to make the evaluation easier. And in box P-07 we have the minimum and maximum values of each variable in rank, in ways to help the adjusting of boundary limits.

Figure 5.10 – Excel Sheet function mapping.



Besides the algorithm works automatically, it is possible to achieve a more efficient way to get a satisfactory result working with each variable limit of approximation. As an example, we set a satisfactory DesP (D_P) value and executed twenty times the algorithm to show how efficient the algorithm can be trimming with the variable limits. Out of those 20 runs, 10 times was running without adjustments and the other 10 was doing after the adjustments. Our DesP target was set as any value be less or equal to 1.30. In Figure 5.11 it is possible to see the worst cases of each of the 20 rounds; the blue line without adjustments demanded 38489 iterations and the orange line with adjustments demanded 1132 iterations to reach our DesP target.

Some more cases have been run to test the efficiency of the adjusting procedure. In Figure 5.12 it is possible to see the result of each case to evaluate the impact of the adjustments on the total number of iterations. The test results show that the adjustments can help to get result faster. Using no adjustments, the user will need on average of 18290 iterations to get the deviation under 1.30, as shown in Figure 5.12 in green line. On the other hand, if the user trims the variables operational limits, the user will need on average of 967 iterations (in red line) to get the same results.

Figure 5.11 – Cases with more iteration.

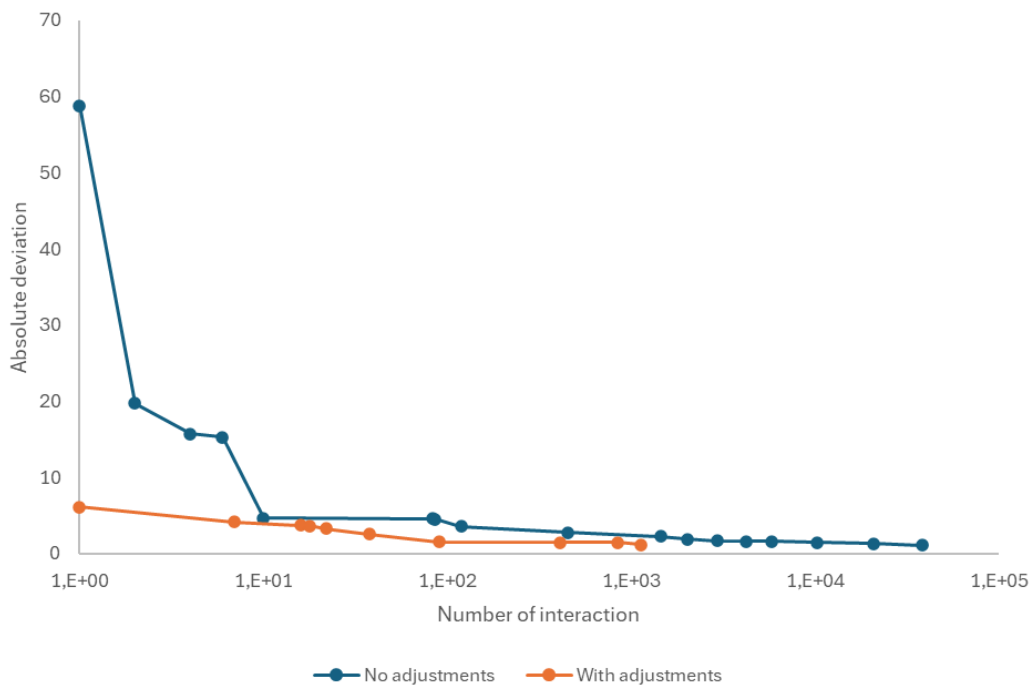
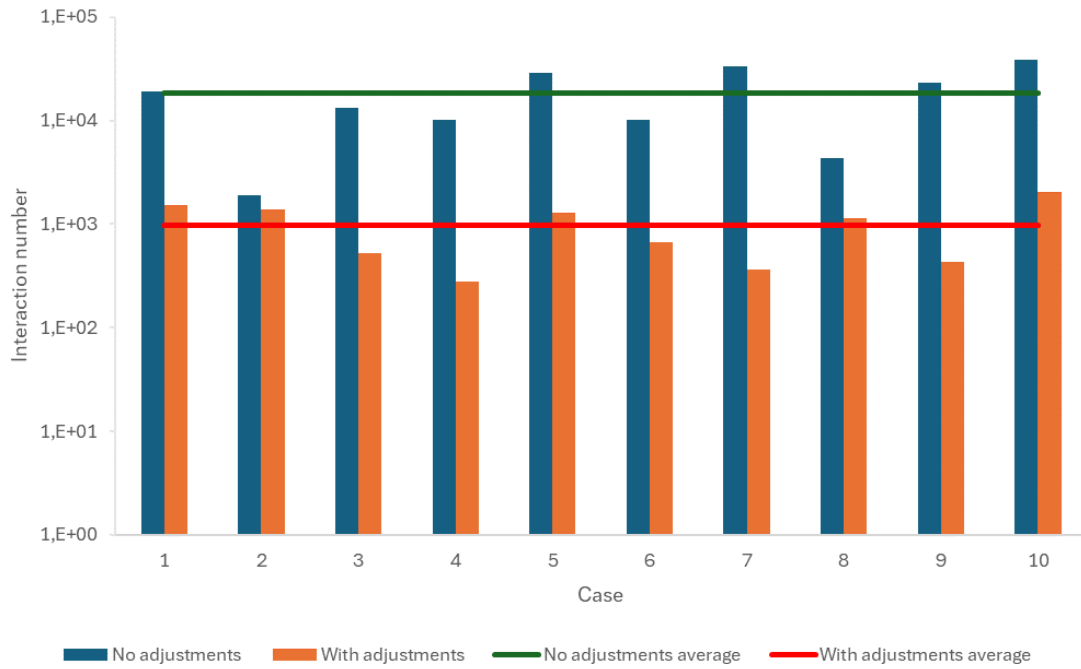


Figure 5.12 – Compilations of all cases number of iterations.



The tool performs about 1200 iterations per minute on the usual desktop home PC. The efficiency can be improved by limitation of the visualization function of current curve be exposed at each iteration.

6 RESULTS

6.1 Approximations for vapor pressure

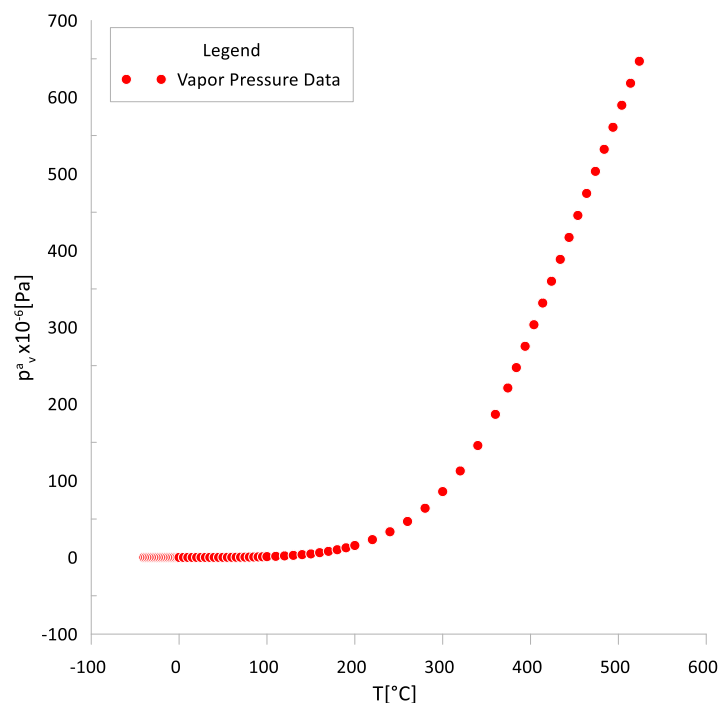
6.1.1 Approximations for saturated zone

Vapor pressure under saturation conditions can be defined as the pressure of vapor applied to a surface when a closed system is in thermodynamic equilibrium with its condensed phase. It means the liquid tends to evaporate until the equilibrium is achieved.

In general, the pressure is the force perpendicularly applied to the surface of an object per unit area over which that force is distributed. Dimension is N/m^2 or Pa.

The original data of the water vapor pressure behavior with temperature is presented in Figure 6.1 (LEMMON et al., 2023). Also, the figure has vapor pressure data in sub-freezing zone compiled from (TURNS et al., 2007). In that case, these data start in $-40\text{ }^\circ\text{C}$ and go to critical temperature.

Figure 6.1 – Water vapor pressure data.



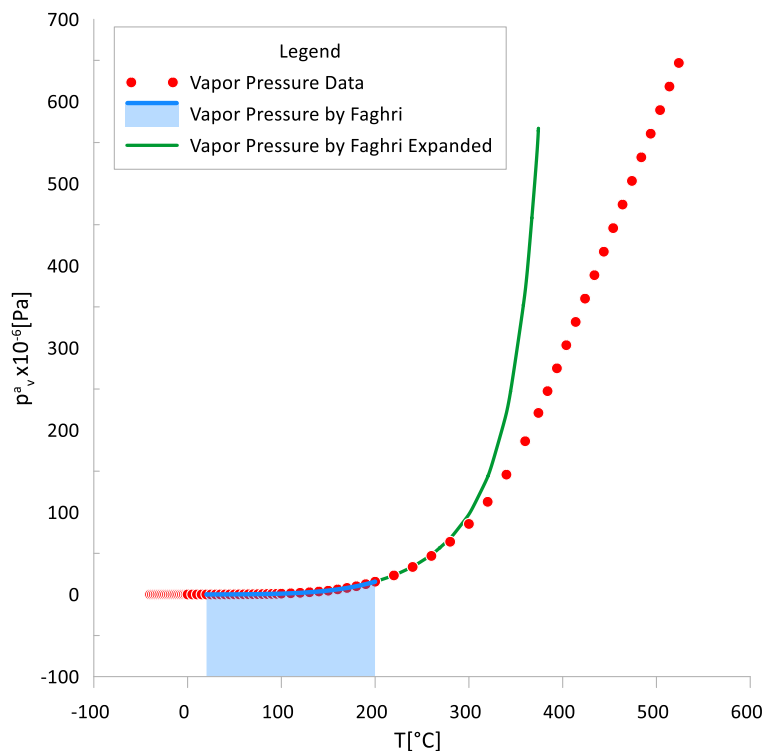
Faghri (2016) in his book suggested the Equation (6.1) to approximate this water property by polynomial function.

$$\begin{aligned} \ln(p_v(T)) = & -5.0945 + 7.228 \cdot 10^{-2} \cdot T - 2.8625 \cdot 10^{-4} \cdot T^2 + \\ & 9.2341 \cdot 10^{-7} \cdot T^3 - 2.02955 \cdot 10^{-9} \cdot T^4 + 2.1645 \cdot 10^{-12} \cdot T^5 \end{aligned} \quad (6.1)$$

where T is expressed in °C and pressure in Pa.

This equation is valid between 20°C and 200°C and can be used for HP modeling with no concern once the approximation error mentioned in Faghri (2016) is 0.03%. The equation covers up to 48% of the entire two-phase temperature range. However, when we try using this polynomial equation out of established range, the result is not acceptable. The green line in Figure 6.2 expresses this deviation from the real values.

Figure 6.2 – Faghri polynomial approximation.



However, we will use the dimensionless vapor pressure following our general approach:

$$p(\tau) = \frac{P - P_3}{P_{cr} - P_3} \quad (6.2)$$

For the saturation interval (i.e., two-phase zone, $0 < \tau < 1$), the main idea is work with the deviation from well-known Clausius–Clapeyron Equation (6.3). This equation determines the equilibrium between the two phases of a substance:

$$P_{cc}(T) = P_0 e^{\frac{\lambda_0}{R} \left(\frac{1}{T_0} - \frac{1}{T} \right)} \quad (6.3)$$

The Clausius–Clapeyron equation has solid theoretical base, but it deviates from the original table data at distant points from the reference point (T_0 & P_0). The deviation increases as distances from (T_0 & P_0) increases.

Firstly, it is important to present the Clausius-Clapeyron equation at the dimensionless format. This dimensionless Clapeyron-Clausius equation includes dimensionless saturations pressure at reference point and dimensionless triple point respectively (p_0 & p_3); then dimensionless reference temperature (τ_0), constant temperatures at triple point and critical point respectively (T_3 & T_{CR}), and latent heat at reference point (λ_0):

$$p_{CC} = (p_0 + p_3) \text{Exp} \left[\frac{\lambda_0}{R(T_3 + \tau_0(T_{cr} - T_3))} \left(1 - \frac{T_3 + \tau_0(T_{cr} - T_3)}{T_3 + \tau(T_{cr} - T_3)} \right) \right] - p_3 \quad (6.4)$$

Finally, the Equation (6.4) is dimensionless.

To build an adequate approximation for vapor pressure, we have two main ways to work with that property. The first one is trying to build a curve with property value “as is,” and the second one is to work with the natural logarithm of that property.

The best results have been obtained the following approximate functions, “as is”, Equation(6.5). The results for the natural logarithm approximation are given by Equation (6.6):

$$p_{Sat}(\tau) = p_{cc} + a + b\tau + c\tau^2 + d\tau^3 \quad (6.5)$$

$$\ln(p_{Sat}(\tau)) = \ln\left(\frac{p_{cc}}{p_0}\right) - \frac{a}{(b+c\tau)^n} + d \quad (6.6)$$

Figure 6.3 – Vapor pressure approximation result in saturated zone “as is”.

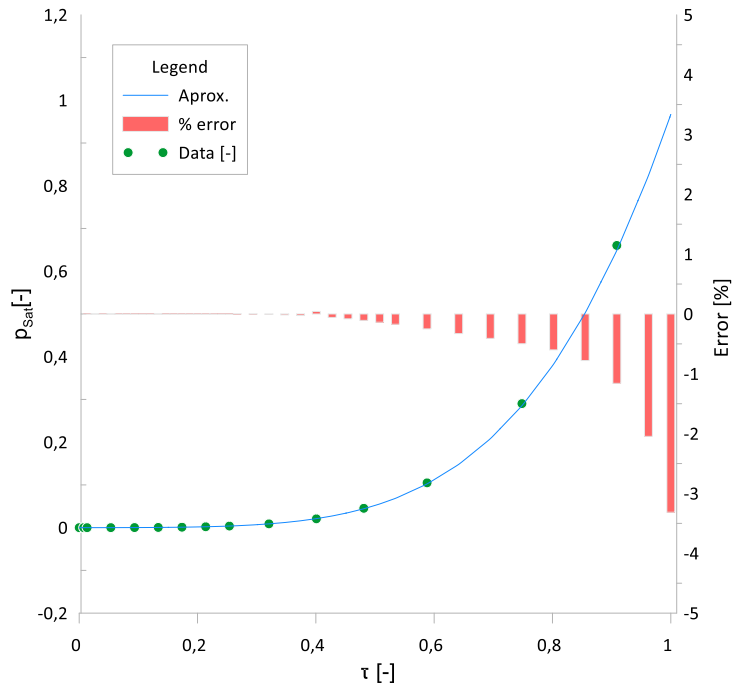
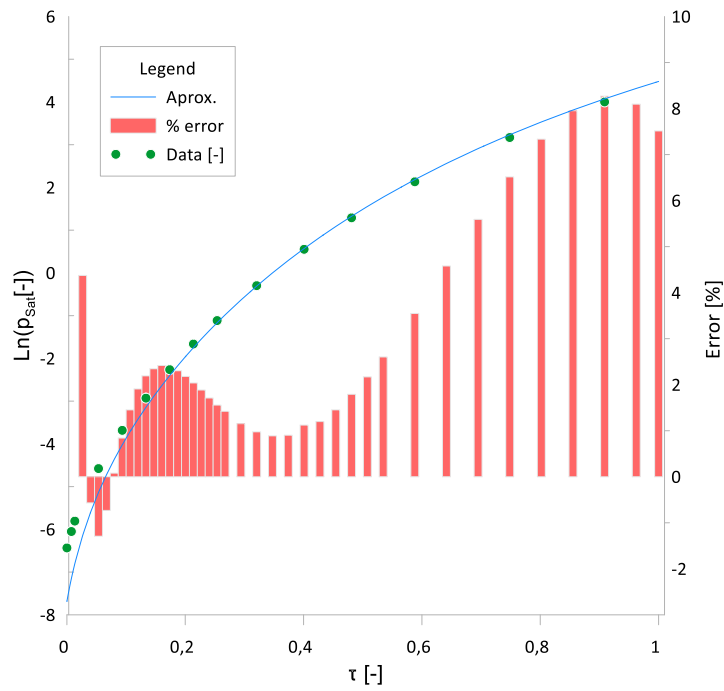


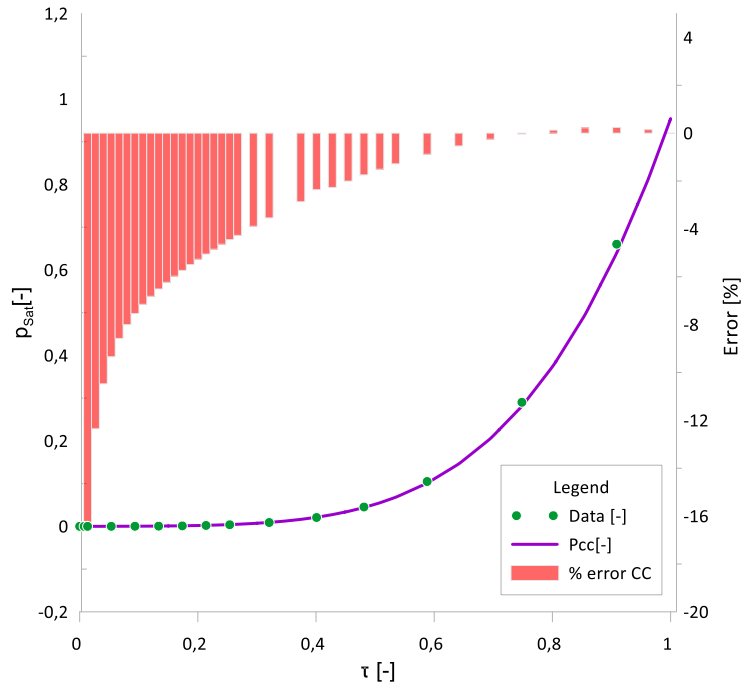
Figure 6.4 – Logarithm Vapor pressure approximation in saturated zone.



We observe the deviation from data by approximation “as is” lies within the usual acceptance criteria in 5% of deviation.

Figure 6.5 shows the difference between real data and the result that Clausius-Clapeyron achieved to vapor pressure.

Figure 6.5 – Deviation of Data and Clausius–Clapeyron equation for saturated zone.



6.1.2 Approximations for freezing zone or sublimation zone

To approximate the pressure of sublimated vapor in freezing zone, some results have been published. The work of Liley (2005) uses an equation, which starts in $-20\text{ }^{\circ}\text{C}$ and go up to $0\text{ }^{\circ}\text{C}$. The approximation is expressed in Equation (6.7), where P is pressure in kPa.

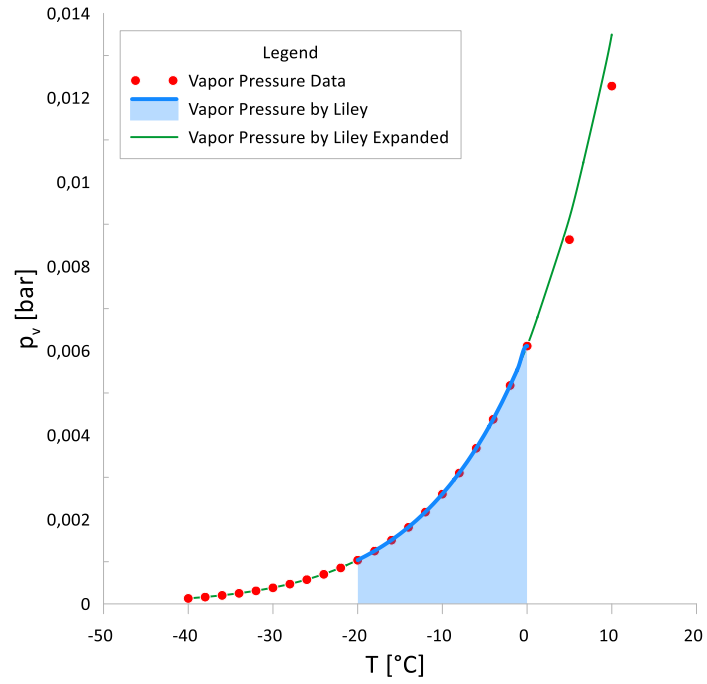
$$\ln(p_{ice}(T)) = 22.01251 - \frac{6166.44}{T + 274.005} \quad (6.7)$$

Marti and Mauersberger (1993) developed the Equation (6.8) with the temperature ranging from $-105\text{ }^{\circ}\text{C}$ to $0\text{ }^{\circ}\text{C}$, where P is in Pa.

$$P_{ice} = \exp\left(28.868 - \frac{61329}{T}\right) \quad (6.8)$$

In Figure 6.6 is possible to see the results of equation (6.5) for a wider temperature range.

Figure 6.6 – Property data in freezing (sublimation) zone.



In this work, we tried several types of approximations. The best results were achieved by the exponential function in freezing zone.

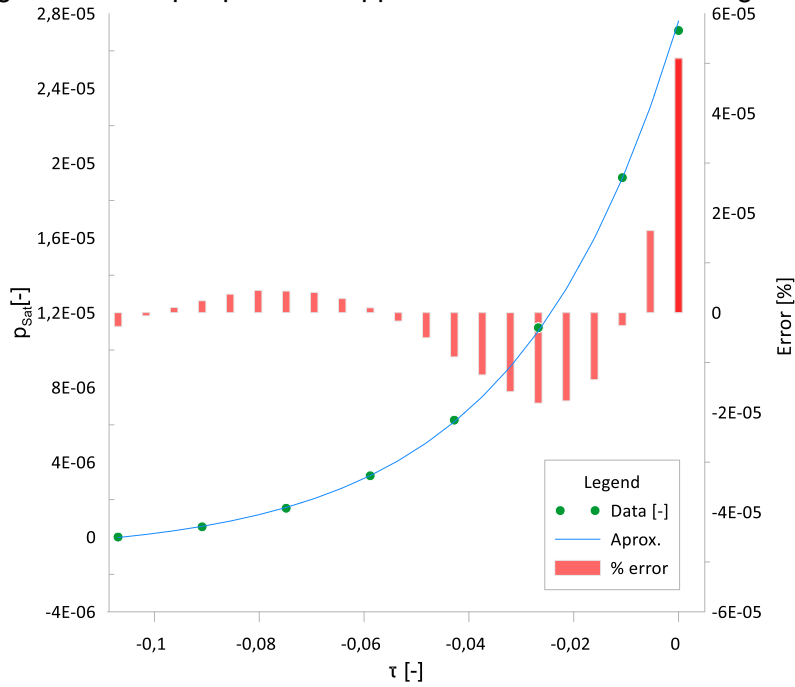
$$p_{sat_A}(\tau) = a_A e^{b_A \tau} + c_A \quad (6.9)$$

Finally, for freezing zone we have:

$$p_A(\tau) \Big|_{\tau < 0} = a_A e^{b_A \tau} + c_A \quad (6.10)$$

$$\left. \frac{d(p_A(\tau))}{d(\tau)} \right|_{\tau < 0} = a_A b_A e^{b_A \tau} \quad (6.11)$$

Figure 6.7 – Vapor pressure approximation result in freezing zone.



The interfacing equation joins subcooled zone with saturated zone.

Looking for a smooth transition between those two zones of Equations (6.5) and (6.9), it is used the third-degree polynomial (Equation (6.12)):

$$p_{AB}(\tau) = a_{AB} + b_{AB}\tau + c_{AB}\tau^2 + d_{AB}\tau^3 \quad (6.12)$$

Finally, the system will be of the following format to the interfacing equation performs tangency of both curves and makes a continuous smooth link.

$$\left\{ \begin{array}{l} \bar{p}_{v_A}(\tau_1) = a_{AB} + b_{AB}\tau_1 + c_{AB}\tau_1^2 + d_{AB}\tau_1^3 \\ \frac{d(\bar{p}_{v_A}(\tau_1))}{d(\tau_1)} = b_{AB} + 2c_{AB}\tau_1 + 3d_{AB}\tau_1^2 \\ \bar{p}_{v_B}(\tau_2) = a_{AB} + b_{AB}\tau_2 + c_{AB}\tau_2^2 + d_{AB}\tau_2^3 \\ \frac{d(\bar{p}_{v_B}(\tau_2))}{d(\tau_2)} = b_{AB} + 2c_{AB}\tau_2 + 3d_{AB}\tau_2^2 \end{array} \right. \quad (6.13)$$

Points of tangency were defined to optimize the approximation results. In this case dt is the distance between the points; the results are as follows.

$$\begin{aligned}
\Delta\tau_1 &= 0.003; \\
\Delta\tau_2 &= 0.01; \\
\tau_1 &= -\Delta\tau_1 \\
\tau_2 &= +\Delta\tau_2
\end{aligned}
\tag{6.14}$$

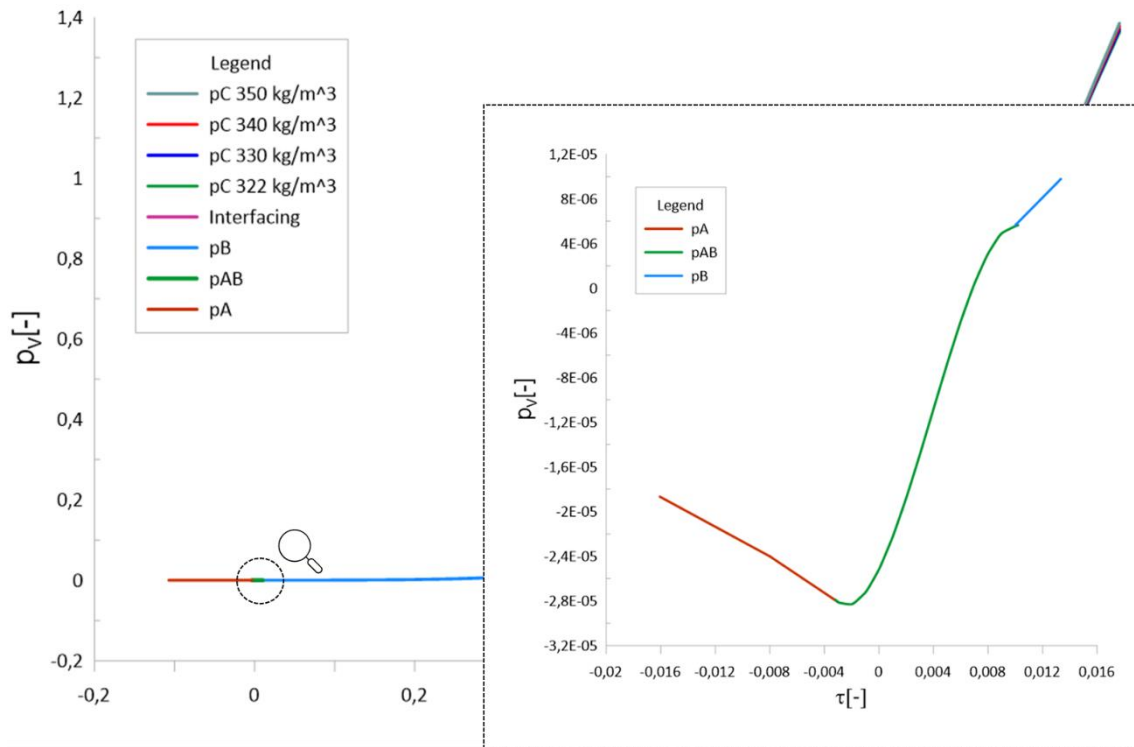
The analytical solution for the polynomial coefficients for the interfacing around $\tau=0$ is presented in the Methodology section.

The results are expressed below.

$$\begin{cases}
a_{AB} = -0.000025 \\
b_{AB} = 0.002519 \\
c_{AB} = 0.408934 \\
d_{AB} = -35.2521
\end{cases}
\tag{6.15}$$

The result approximation around triple point ($\tau=0$), including the interfacing curve, is shown in Figure 6.8.

Figure 6.8 – Final Result to interfacing below sub freezing point.



6.1.3 Approximations for super-critical zone

To obtain precision approximation the pressure above the critical point cannot be treated through a well-known ideal gas law. We will use a real gas approach based on the Van der Waals equation, Redlich-Kwong equation, and Soave-Redlich-Kwong equation. The best variant was selected for the approximation and interfacing at $\tau=1$.

Heat pipes have a peculiarity: the total density of working fluid, considering liquid and vapor phases together, is fixed and defined by the working fluid amount charged into the heat pipe during HP manufacturing. Then, the HP container is hermetically sealed, and the mass of working fluid does not change. By knowing the internal volume of heat pipe, total density can be easily calculated:

Therefore, the author chose more than one fluid density for the analysis, which varies from 332 kg/m^3 (critical density) to 350 kg/m^3 but in this study only the critical density will be analyzed. The Equation (6.16) can be expressed by the Van

der Waals equation, Redlich-Kwong Equation (6.19), and Soave Equation (6.28), Smith et al. (2013), Markočič and Knez (2016).

We transform the Van der Waals definition with the use of dimensionless temperature:

$$p = \frac{R \cdot (T_3 + \tau(T_{cr} - T_3))}{\left(\frac{M}{\rho_{cr}} - b\right)(P_{cr} - P_3)} - \frac{a}{\left(\frac{M}{\rho_{cr}}\right)^2(P_{cr} - P_3)} - \frac{P_3}{P_{cr} - P_3} \quad (6.16)$$

$$a(\tau) = \frac{(a_1(T_3 + \tau(T_{cr} - T_3)))^2 + b_1(T_3 + \tau(T_{cr} - T_3)) + c_1) \cdot R^2 \cdot T_{cr}^2}{P_{cr}} \quad (6.17)$$

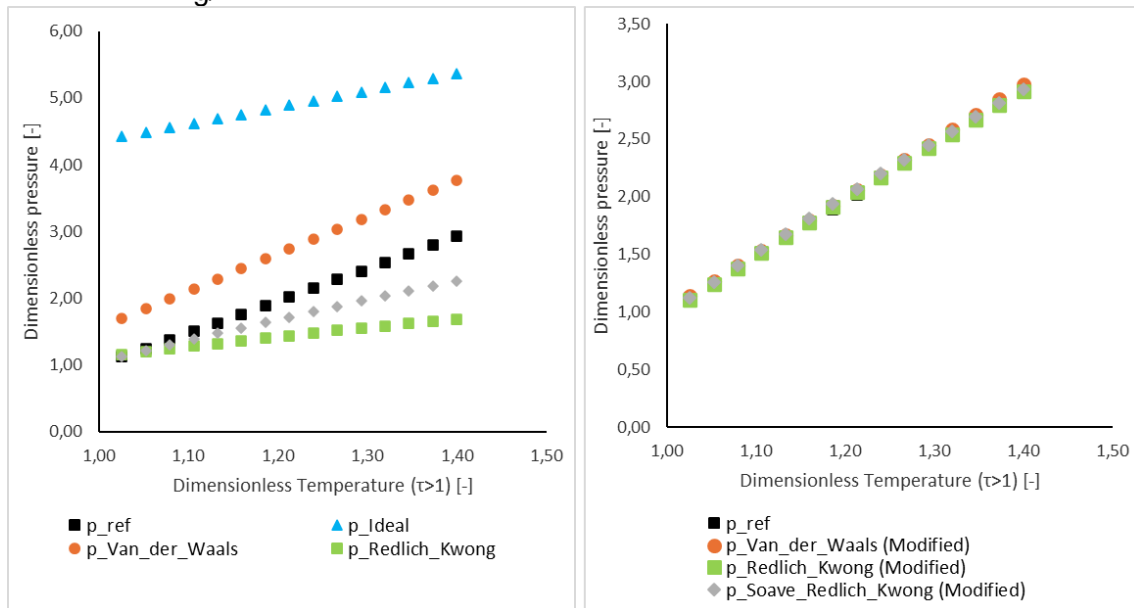
$$b(\tau) = \frac{R \cdot T_{cr}}{(a_1(T_3 + \tau(T_{cr} - T_3)))^2 + b_1(T_3 + \tau(T_{cr} - T_3)) + c_1)P_{cr}} \quad (6.18)$$

The statement summarizes intuitively the differences of vapor pressure equations and our goal, which is to modify the original equation to cover a wider range of temperatures.

Table 6.1 – Coefficients “a” and “b” expressed by polynomial coefficients.

		a1	a1 ρ= 322 kg/m3	b1	b1 ρ= 322 kg/m3	c1	c1 ρ= 322 kg/m3
Van der Waals	a	-	-6,00E-08	-	9,00E-05	4,22E+04	3,97E+02
	b	-	-	-	7,00E-04	8.00	7.81
Redlich-Kwong	a	-	-	-	2.4E-03	23.393	7,26E+02
	b	-	-	-	-9.6E-3	11.542	1,79E+05
Soave-Redlich-Kwong	a	-	-	-	1.3E-02	23.393	1.485
	b	-	-	-	-5.8E-3	11.542	1,54E+04

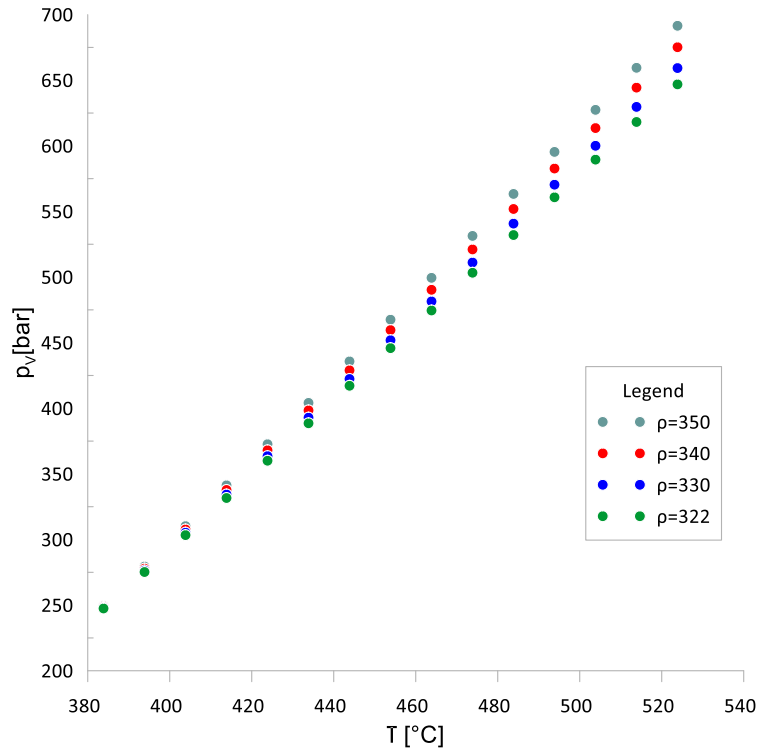
Figure 6.9 – Correlation between dimensionless pressure and dimensionless temperature for water above critical point and with a density equal to 322 kg/m³.



This property has behavior in super critical zone that will be considered in this study; figures below show data by (ACREE; CHICKOS, 2023). Considering that the charged density is an important parameter for HPs, in this case we get the saturation pressure behavior by temperature and density.

As mentioned above, at the supercritical region, the property not only depends on temperature, but also on density. The strategy adopted to this zone is to work of known equations available in literature, focused on Soave-Redlich-Kwong equation. We try to modify those equations to reach an approximation of the vapor pressure as more precise as possible. It is worth mentioning that choosing the Soave-Redlich-Kwong approximation is to obtain a vapor pressure value considering as a real gas; in other words, the compressibility effects must be included.

Figure 6.10 – Property data in supercritical zone.



Soave-Redlich-Kwong approximation is defined by:

$$P = \frac{RT}{M/\rho_{cr} - b} - \frac{a}{M/\rho_{cr} \left(M/\rho_{cr} + b \right) T^{1/2}} \quad (6.19)$$

$$a = \frac{R^2 \cdot T_{cr}^2}{2.3393P_{cr}} \left(1 + m \left(1 - T_R^{1/2} \right) \right)^2 \quad (6.20)$$

$$b = \frac{R \cdot T_{cr}}{11.5420P_{cr}} \quad (6.21)$$

$$m = 0.480 + 1.574\omega - 0.176\omega^2 \quad (6.22)$$

$$\omega = \log_{10} \left(\frac{P_{cr}}{P_{vp}} \right) - 1 \quad (6.23)$$

$$T_R = T / (T_{cr} + 8) \quad (6.24)$$

$$Z = \frac{M/\rho_{cr}}{M/\rho_{cr} - b} - \frac{a}{RT\left(M/\rho_{cr} + b\right)} \quad (6.25)$$

We changed “a” in Equation (6.20) format to adequate this approximation to values that pass in our acceptance criteria.

$$a(\tau, \rho) = \frac{R^2 \cdot T_{cr}^2}{(a_c(\rho) + b_c(\rho)T_{cr})P_{cr}} \left(1 + m\left(1 - T_R^{1/2}\right)\right)^2 \quad (6.26)$$

$$b(\tau, \rho) = \frac{R \cdot T_{cr}}{(c_c + d_c T_{cr})P_{cr}} \quad (6.27)$$

Rewriting the equation to be all dimensionless, we have:

$$p(\tau, \rho) = \frac{R \cdot (T_3 + \tau(T_{cr} - T_3))}{\left(M/\rho_{cr} - b\right)(P_{cr} - P_3)} - \frac{a(\tau, \rho)}{\left(M/\rho_{cr} \left(M/\rho_{cr} - b\right)\right)(P_{cr} - P_3)} - \frac{P_3}{(P_{cr} - P_3)} \quad (6.28)$$

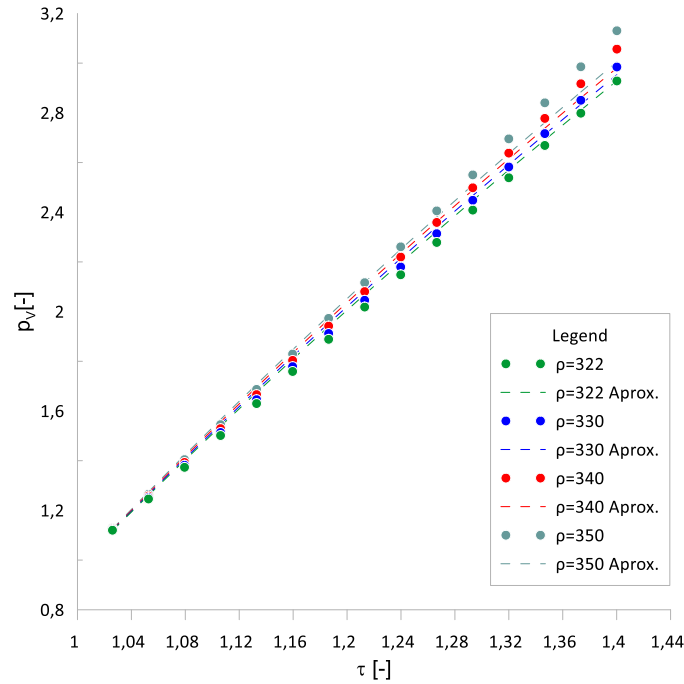
We can write $a_c(\rho)$ and $b_c(\rho)$ as:

$$a_c(\rho) = a_c + b_c \rho + c_c \rho^2 \quad (6.29)$$

$$b_c(\rho) = d_c + e_c \rho + f_c \rho^2 \quad (6.30)$$

These equations, given above, result in the graph of Figure 6.11.

Figure 6.11 – Vapor pressure approximation result in supercritical zone by density.



For super-critical zone:

$$\Psi_C(\tau, \rho) \Big|_{\tau < 1} = \frac{R \cdot (T_3 + \tau(T_{cr} - T_3))}{\left(\frac{M}{\rho_{cr}} - \frac{R \cdot T_{cr}}{(g_C + h_C T) P_{cr}} \right) (P_{cr} - P_3)} - \frac{\frac{R^2 \cdot T_{cr}^2}{(a_C(\rho) + b_C(\rho) T) P_{cr}} \left(1 + m \left(1 - T_R^{1/2} \right) \right)^2}{\left(\frac{M}{\rho_{cr}} \left(\frac{M}{\rho_{cr}} + \frac{R \cdot T_{cr}}{(g_C + h_C T) P_{cr}} \right) \right) (P_{cr} - P_3)} - P_3 \quad (6.31)$$

Looking for a smooth transition between those two zones in Equations (6.5) and (6.31), it is used a third-degree polynomial, Equation (6.32).

$$p_{BC}(\tau, \rho) = a_{BC} + b_{BC} \tau + c_{BC} \tau^2 + d_{BC} \tau^3 \quad (6.32)$$

Points of tangency can be defined trying to optimize the approximation result. In this case $\Delta\tau$ defines how far each point will be stay from the critical point, ($\tau=1$).

$$\begin{aligned}
\Delta \tau_3 &= 0.008; \\
\Delta \tau_4 &= 0.003; \\
\tau_3 &= 1 - \Delta \tau_3 = 0.992 \\
\tau_4 &= 1 - \Delta \tau_4 = 1.003
\end{aligned} \tag{6.33}$$

The system has the following format, built from the interfacing equation tangency when both curves make a continuous smooth link.

$$\left\{ \begin{array}{l}
\bar{p}_{V_{BC}}(\tau_3) = a_{BC} + b_{BC}\tau_3 + c_{BC}\tau_3^2 + d_{BC}\tau_3^3 \\
\frac{d(\bar{p}_{V_{BC}}(\tau_3))}{d(\tau_3)} = b_{BC} + 2c_{BC}\tau_3 + 3d_{BC}\tau_3^2 \\
\bar{p}_{V_{BC}}(\tau_4, \rho) = a_{BC}(\rho) + b_{BC}(\rho)\tau_4 + c_{BC}(\rho)\tau_4^2 + d_{BC}(\rho)\tau_4^3 \\
\frac{d(\bar{p}_{V_{BC}}(\tau_4, \rho))}{d(\tau_4)} = b_{BC}(\rho) + 2c_{BC}(\rho)\tau_4 + 3d_{BC}(\rho)\tau_4^2
\end{array} \right. \tag{6.34}$$

By solving the system above, the parameters values are available below, and we denoted here:

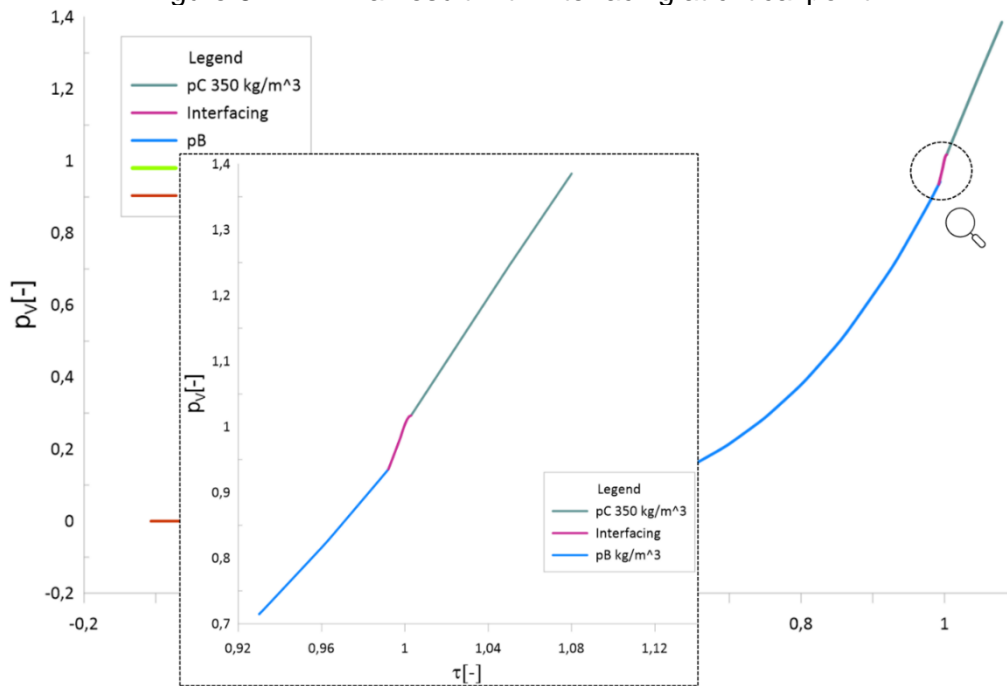
$$\begin{aligned}
y'_B(\tau) &= \frac{d(p_B(\tau))}{d(\tau)} \\
y_B(\tau) &= p_B(\tau) \\
y'_C(\tau, \rho) &= \frac{d(p_C(\tau, \rho))}{d(\tau)} \\
y_C(\tau, \rho) &= p_C(\tau, \rho)
\end{aligned} \tag{6.35}$$

Using the values mentioned above, the result is:

$$\left\{ \begin{array}{l}
a_{BC} = 122653.3 \\
b_{BC} = -368906 \\
c_{BC} = 369846.3 \\
d_{BC} = -123593
\end{array} \right. \tag{6.36}$$

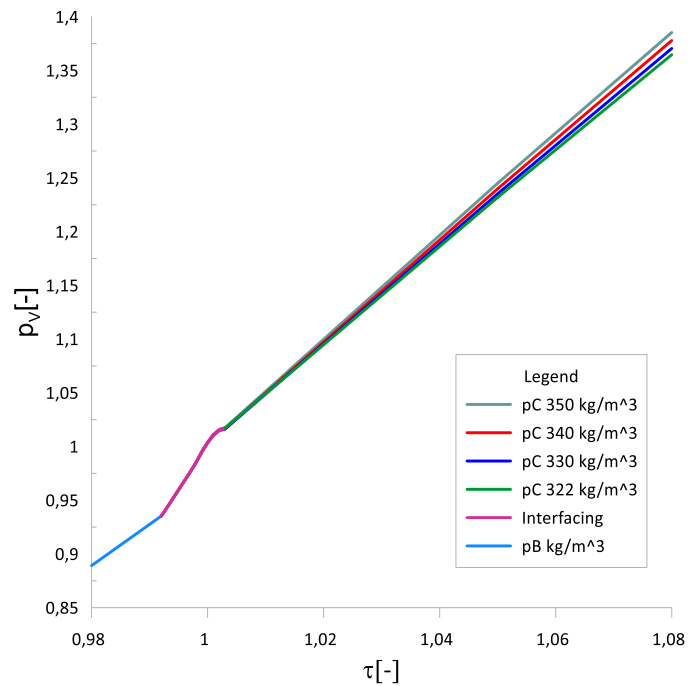
Figure 6.12 shows the result of the approximation.

Figure 6.12 – Final result with interfacing at critical point.



If we expand the idea of pressure as function of density in supercritical zone, we reach the behavior expressed in Figure 6.13.

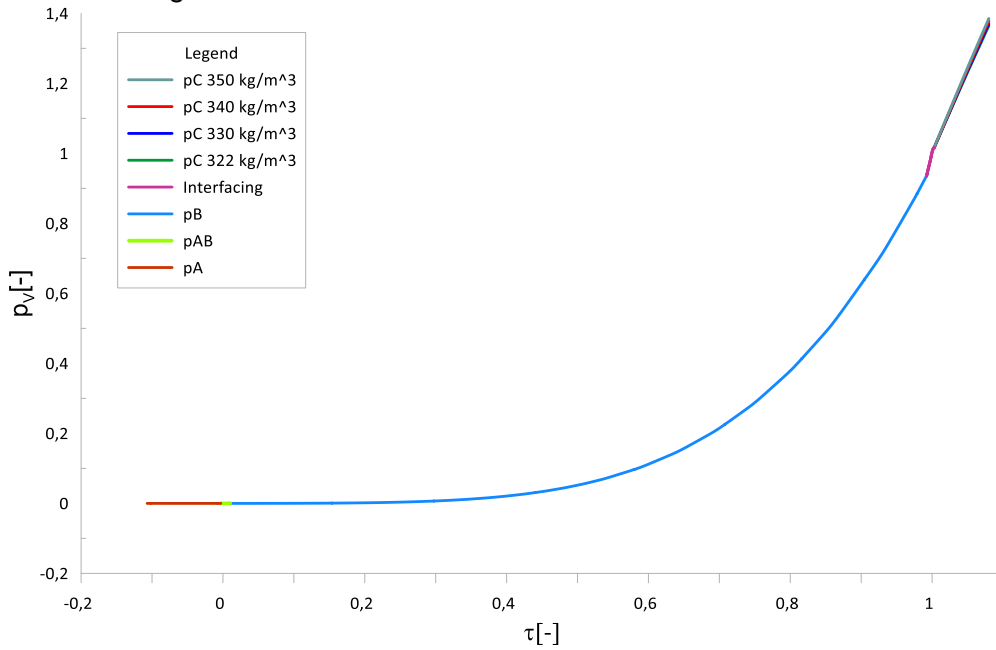
Figure 6.13 – Interfacing supercritical region details.



6.1.4 Final approximation and pseudo code

In this chapter we have reached an approximation in a wider range of temperature, managing the approximation error in satisfactory levels (no greater than 5%). The pseudo code provides fluid property values starting below triple point up to above critical point, Figure 6.14.

Figure 6.14 – Final result to vapor pressure approximation in the entire temperature range.



The interfacing technique provides softening and continuity in the conjugate points. It is possible to check the interfacing results in figures above (Figure 6.8 and Figure 6.13).

The all results are condensed together in a pseudo-code. This code can be implemented in any programming language:

$$\left\{ \begin{array}{ll} \text{if } (\tau \leq \tau_1) & \text{then } \bar{p}_A(\tau) = a_A e^{b_A \tau} + c_A \\ \text{if } (\tau_1 < \tau < \tau_2) & \text{then } \bar{p}_{AB}(\tau) = a_{AB} + b_{AB} \tau + c_{AB} \tau^2 + d_{AB} \tau^3 \\ \text{if } (\tau_2 \leq \tau \leq \tau_3) & \text{then } \bar{p}_B(\tau) = \bar{p}_{cc} + a_B + b_B \tau + c_B \tau^2 + d_B \tau^3 \\ \text{if } (\tau_3 < \tau < \tau_4) & \text{then } \bar{p}_{BC}(\tau) = a_{BC} + b_{BC} \tau + c_{BC} \tau^2 + d_{BC} \tau^3 \\ \text{if } (\tau \geq \tau_4) & \text{then } \bar{p}_C(\tau, \rho) = \Psi_C(\tau, \rho) \end{array} \right. \quad (6.37)$$

Table 6.2 – Result algorithm values for density of 350kg/m³.

$a_A = -3E-5$	$b_B = -5E-5$	$c_{BC} = 3.6985E5$	$g_C = -5.8E-3$
$b_A = 3.26E1$	$c_B = -1.02E-2$	$d_{BC} = -1.2359E5$	$h_C = 1.536E1$
$c_A = -9E-7$	$d_B = 2.33E-2$	$a_C = -5.991E-8$	$\Delta\tau_1 = 3E-3$
$a_{AB} = -2.5182E-5$	$\lambda_{0B} = 2.145E3$	$b_C = 5.0877E-5$	$\Delta\tau_2 = 1E-2$
$b_{AB} = 2.5185E-3$	$\rho_{0B} = 1.6329E-2$	$c_C = -8.694E-3$	$\Delta\tau_3 = 8E-3$
$c_{AB} = 4.089E-1$	$\tau_{0B} = 3.7417E-1$	$d_C = 4.093E-5$	$\Delta\tau_4 = 3E-3$
$d_{AB} = -3.5252E1$	$a_{BC} = 1.2265E5$	$e_C = -3.4385E-2$	
$a_B = -3E-5$	$b_{BC} = -3.6891E5$	$f_C = 8.3122$	

6.2 Approximations for vapor density

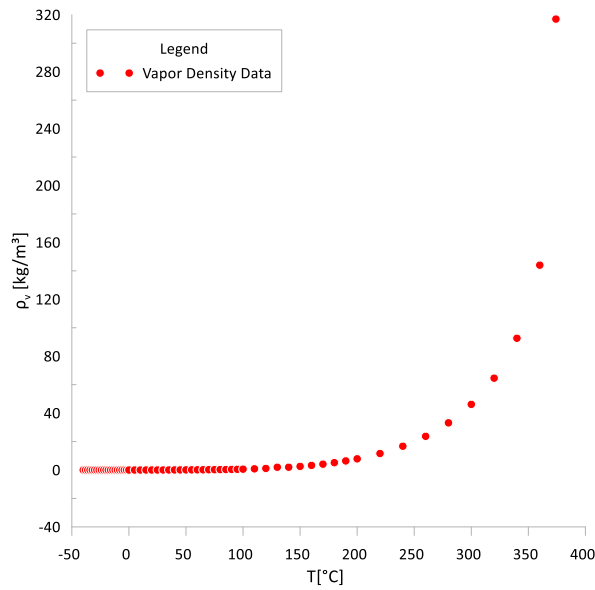
6.2.1 Approximations for saturated vapor density

Vapor density (ρ_v) can be defined the ratio between mass (m) and volume (V) and can be written by the following equation.

$$\rho_v = \frac{m}{V} \quad (6.38)$$

American Society of Heating, Refrigerating and Air-Conditioning Engineers (ASHRAE) Lemmon et al. (2023) presented the original data table of the saturated vapor density behavior with temperature, plotted in Figure 6.15.

Figure 6.15 – Water vapor density data.



The data covers freezing and saturated temperature regions.

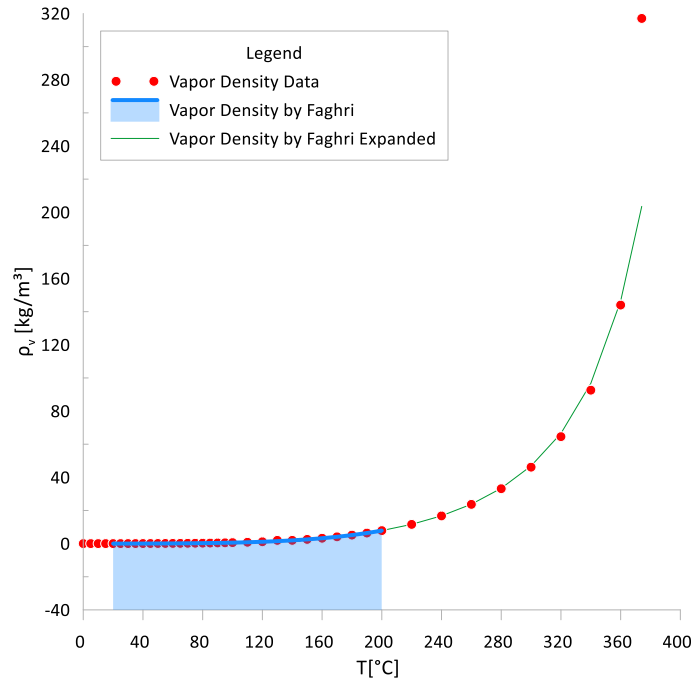
To use this property in the heat pipe modeling, Faghri (2016) in his book suggested a polynomial function over logarithm of the density, Equation (6.39), to approximate the water vapor in the two-phase saturated (i.e. phases coexisting) temperature region.

$$\begin{aligned} \ln(\rho_v(T)) = & -5.3225 + 6.8366 \cdot 10^{-2} \cdot T - 2.7243 \cdot 10^{-4} \cdot T^2 + \\ & 8.4522 \cdot 10^{-7} \cdot T^3 - 1.6558 \cdot 10^{-9} \cdot T^4 + 1.5514 \cdot 10^{-12} \cdot T^5 \end{aligned} \quad (6.39)$$

the Vapor density is expressed in kg/m³, and the temperature is in degrees of Celsius.

This equation is valid from 20°C to 200°C; and is widely used for HP modeling once the approximation error mentioned is 0.03% within this range. The equation covers up to 48% of the entire two-phase temperature range. However, when we try to use this polynomial equation out of the range established, the result can deviate from real behavior.

Figure 6.16 – Faghri polynomial approximation.



For the saturation interval (i.e., two-phase zone, $0 < \tau < 1$), the original curve has a sharp climb as it approaches the critical temperature. It is difficult to obtain a unique function which approximates the entire zone within acceptable error; therefore, we improve it with application of an interruption point (τ_H) and join two approximation functions in the interval $\tau_H \leq \tau < 1$ by application of the Heaviside function.

In the approximations, we will use dimensionless charged density defined by the same way:

$$\bar{\rho}_{ch} = \frac{\rho_{ch} - \rho_{v,3}}{\rho_{v,cr} - \rho_{v,3}} \quad (6.40)$$

The best results gave the following approximate functions:

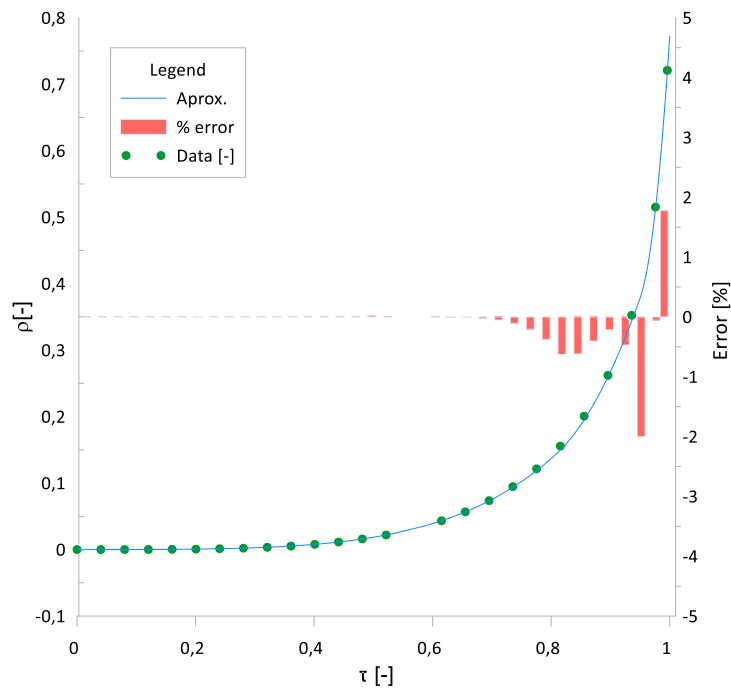
$$\begin{cases} y_1 = a_B + b_B \tau + c_B \tau^2 + d_B \tau^3 + e_B \tau^4 + f_B \tau^5 + g_B \tau^6 \\ y_2 = h_B (\tau - \tau_{H1})^{i_B} \\ y_3 = j_B (\tau - \tau_{H2})^{k_B} \end{cases} \quad (6.41)$$

These functions are used in an additive way: when $0 < \tau \leq \tau_{H1}$, then $y = y_1$; when $\tau_{H1} < \tau \leq \tau_{H2}$, then $y(\tau) = y_1(\tau) + y_2(\tau)$; when $\tau > \tau_{H2}$ then $y(\tau) = y_1(\tau) + y_2(\tau) + y_3(\tau)$ This can be condensed in a unique correlation for our property:

$$\rho_V(\tau) = y_1(\tau) + \chi(\tau - \tau_{H1})y_2(\tau) + \chi(\tau - \tau_{H2})y_3(\tau) \quad (6.42)$$

By applying the algorithm above, in the saturation interval of temperature we achieve the curve below. That chart shows data from ASHRAE using green circles in Figure 6.15 (LEMMON et al., 2023). The approximation results is in the blue line. In red bars we have the deviation error from property table data and approximation.

Figure 6.17 – Vapor density approximation result in saturated zone.



We observe the deviation from data by approximation lie within the usual acceptance criteria in 5% of deviation from the properties table data. In the beginning of approximation, the interface technique replaced the inaccurate data to a smooth link between the two approximations.

To develop this property approximation, we used a baseline curve (4th degree polynomial equation), and we add two auxiliary curves with the use of the Heaviside function, resulting in a final curve shown in

Figure 6.18. The main motive to use this technique is to reach an approximation curve be continuous and “smooth,” without sharp edges.

Figure 6.18 – Approximation by three piecewise functions.

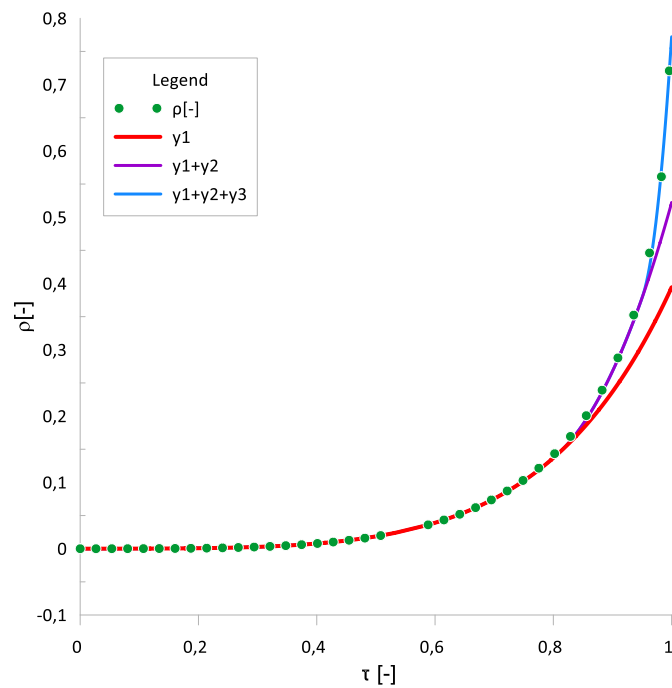
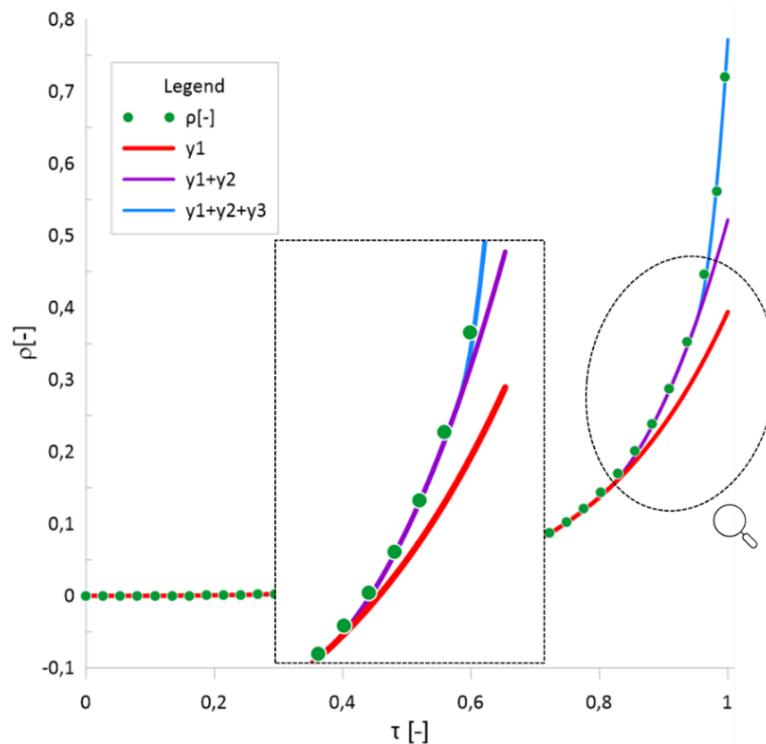


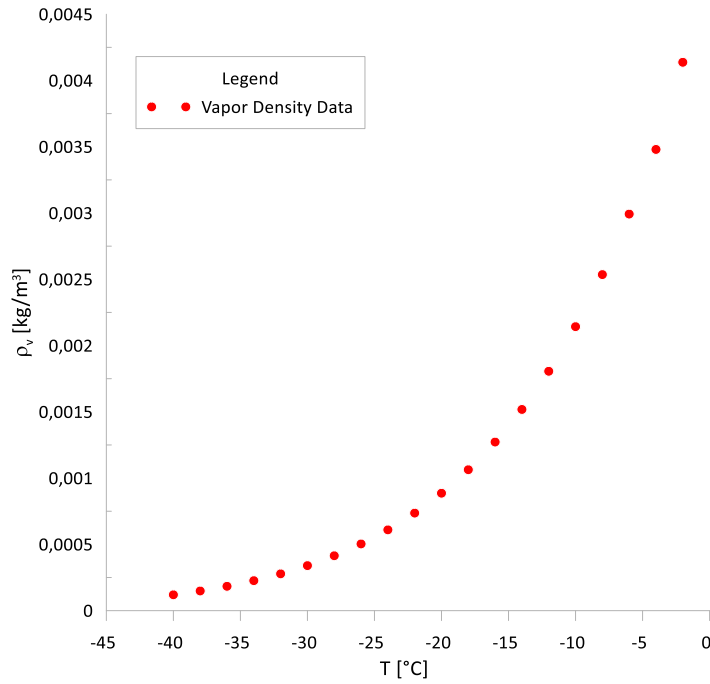
Figure 6.19 – Detail of Heaviside function application in approximation for saturated zone.



To reiterate the definitions, the critical point is where vapor and liquid are indistinguishable and triple point is where liquid phase (water), solid phase (ice) and vapor phase coexist in thermodynamic equilibrium. Therefore, in the zone below the triple point we will consider only vapor phase. Certainly, the Faghri's approximation does not cover these regions.

Turns et al. (2007) compiled in their book a liquid density behavior on freezing zone (Figure 6.20). In that case, this starts in -40 °C and go to 0°C.

Figure 6.20 – Vapor density in freezing zone.



6.2.2 Approximations for freezing zone and interfacing

We approximate the data in freezing zone by a second-degree polynomial Equation (6.42), using results of Turns et al. (2007).

$$\bar{\rho}_A(\tau) \Big|_{\tau < 0} = a_A + b_A \tau + c_A \tau^2 + d_A \tau^3 \quad (6.43)$$

$$\frac{d(\bar{\rho}_A(\tau))}{d(\tau)} \Big|_{\tau < 0} = b_A + 2c_A \tau + 3d_A \tau^2 \quad (6.44)$$

The interface between the freezing zone and saturated zone must meet the requirements of continuity and smoothness. It can be accomplished by using a third-degree polynomial Equation (6.45).

$$\bar{\rho}_{AB}(\tau) = a_{AB} + b_{AB} \tau + c_{AB} \tau^2 + d_{AB} \tau^3 \quad (6.45)$$

The system of equations is of the following format to yield continuity and smooth tangency of both curves.

$$\left\{ \begin{array}{l} \bar{\rho}_A(\tau_1) = a_{AB} + b_{AB}\tau_1 + c_{AB}\tau_1^2 + d_{AB}\tau_1^3 \\ \frac{d(\bar{\rho}_A(\tau_1))}{d(\tau_1)} = b_{AB} + 2c_{AB}\tau_1 + 3d_{AB}\tau_1^2 \\ \bar{\rho}_B(\tau_2) = a_{AB} + b_{AB}\tau_2 + c_{AB}\tau_2^2 + d_{AB}\tau_2^3 \\ \frac{d(\bar{\rho}_B(\tau_2))}{d(\tau_2)} = b_{AB} + 2c_{AB}\tau_2 + 3d_{AB}\tau_2^2 \end{array} \right. \quad (6.46)$$

Points of tangency can be defined by trying to optimize the approximation result, balancing between better smoothing and less error. In this case Δt defines how far each point will be away from the 0 (i.e., triple point).

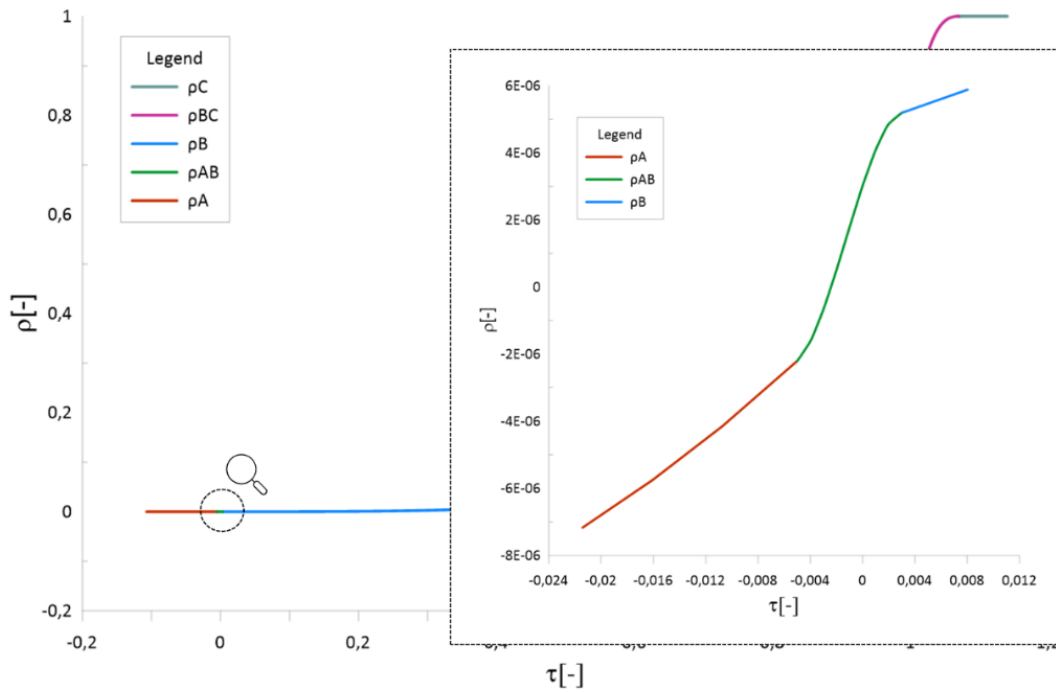
$$\left\{ \begin{array}{l} \Delta\tau_1 = 0.005; \\ \Delta\tau_2 = 0.01; \\ \tau_1 = -\Delta\tau_1 \\ \tau_2 = +\Delta\tau_2 \end{array} \right. \quad (6.47)$$

The solution is expressed below.

$$\left\{ \begin{array}{l} a_{AB} = 0.000000533 \\ b_{AB} = 0.0000675 \\ c_{AB} = 0.013846 \\ d_{AB} = -2.33408 \end{array} \right. \quad (6.48)$$

The result approximations around triple point ($\tau=0$), including the interfacing curve, is shown in Figure 6.21.

Figure 6.21 – Result to the interface around the triple point.



6.2.3 Approximations for supercritical zone and interfacing

As discussed in the introduction, for isochoric systems the density above the critical temperature is always constant and is equal to the “charged density.”

$$\bar{\rho}_v \Big|_{T \geq T_{cr}} = \bar{\rho}_{ch}$$

The smoothing is achieved using a polynomial function of third order. The result is presented below in a pseudo-code for the exponential approximation in the two-phase region and polynomial approximations for smoothed regions.

At the supercritical region, the property does not depend on either temperature, pressure, or any other property; it always constant and equal to charged density.

As said above, the properties values above the critical point are charged density constant value. Those can be expressed below.

For super-critical zone:

$$\bar{\rho}_{v_c}(\tau) \Big|_{\tau > 1} = \bar{\rho}_{ch} \quad \frac{d(\bar{\rho}_{v_c}(\tau))}{d(\tau)} \Big|_{\tau > 1} = 0 \quad (6.49)$$

A smoother transition between those two zones Equations (6.42) and (6.50) provides a third-degree polynomial, Equation (6.50).

$$\bar{\rho}_{BC}(\tau) = a_{BC} + b_{BC}\tau + c_{BC}\tau^2 + d_{BC}\tau^3 \quad (6.50)$$

Points of tangency can be defined by trying to optimize the approximation result. In this case $\Delta\tau$ is how far each point will be away from the critical point, ($\tau=1$).

$$\begin{aligned} \Delta\tau_3 &= 0.008; \\ \Delta\tau_4 &= 0.06913; \\ \tau_3 &= 1 - \Delta\tau_3 = 0.992 \\ \tau_4 &= 1 + \Delta\tau_4 = 1.06913 \end{aligned} \quad (6.51)$$

The system has the following format to the interfacing equations, when both curves make a continuous smoothie link.

$$\left\{ \begin{array}{l} \bar{\rho}_B(\tau_3) = a_{BC} + b_{BC}\tau_3 + c_{BC}\tau_3^2 + d_{BC}\tau_3^3 \\ \frac{d(\bar{\rho}_B(\tau_3))}{d\tau_3} = b_{BC} + 2c_{BC}\tau_3 + 3d_{BC}\tau_3^2 \\ \bar{\rho}_C(\tau_4) = a_{BC} + b_{BC}\tau_4 + c_{BC}\tau_4^2 + d_{BC}\tau_4^3 \\ \frac{d(\bar{\rho}_C(\tau_4))}{d\tau_4} = b_{BC} + 2c_{BC}\tau_4 + 3d_{BC}\tau_4^2 \end{array} \right. \quad (6.52)$$

We denote here:

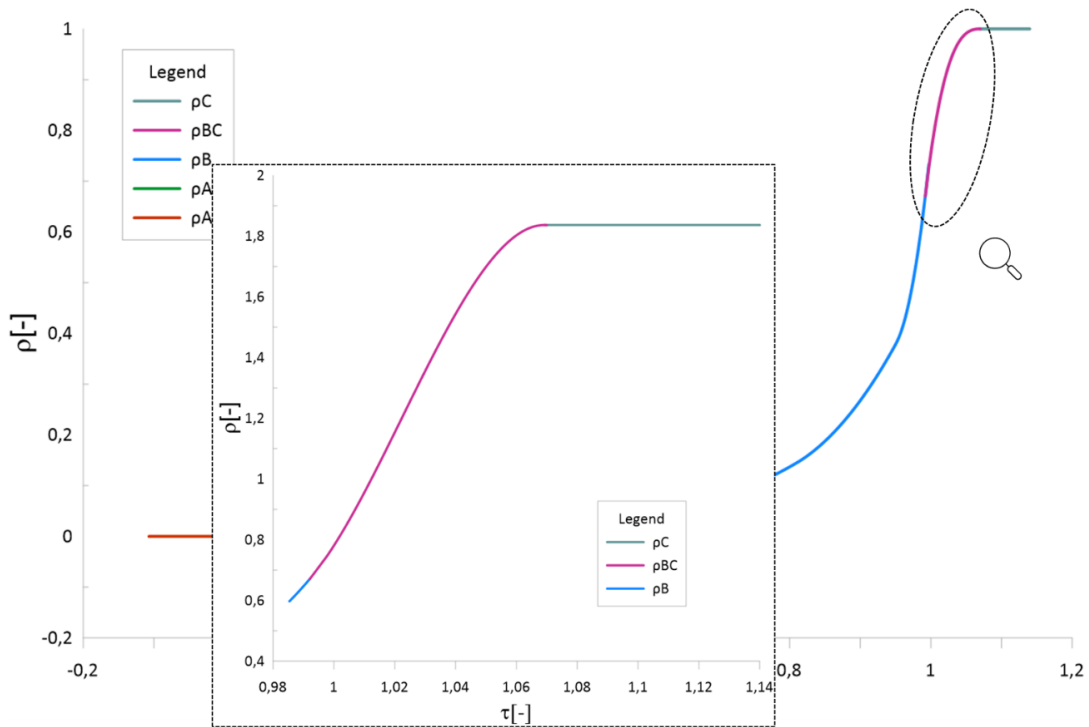
$$\bar{\rho}_C(\tau_4) = \bar{\rho}_{ch} \frac{d(\bar{\rho}_C(\tau_4))}{d(\tau_4)} = 0 \quad (6.53)$$

Therefore, the solution of the system (6.52) depends on the value of dimensionless charged density. Using the values mentioned above, the result for the case $\bar{\rho}_{ch} = 1$ is the following:

$$\begin{cases} a_{BC} = -676.914 \\ b_{BC} = 1887.644 \\ c_{BC} = -1751.94 \\ d_{BC} = 541.9615 \end{cases} \quad (6.54)$$

Figure 6.22 shows the result of the approximation.

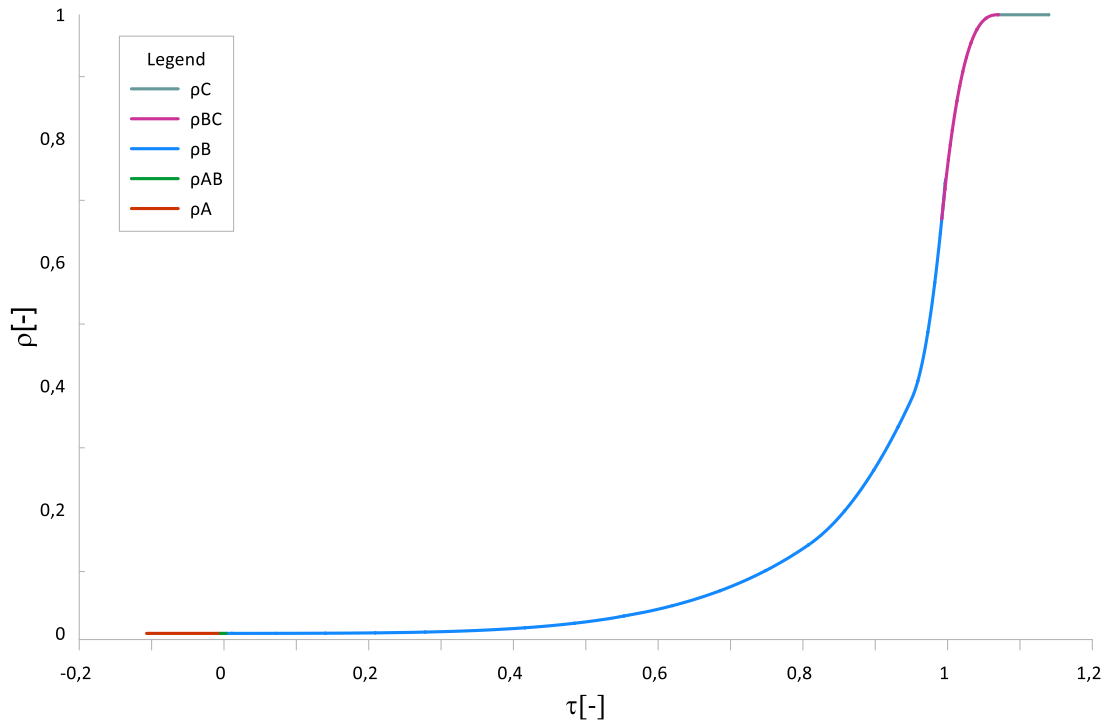
Figure 6.22 – Final result for the interface above the critical point.



6.2.4 Final approximation and pseudo code

The algorithm above that we proposed for the approximation of the entire region which includes below freezing point and above critical point regions is shown in Equation (6.55).

Figure 6.23 – Final result for liquid density approximation for the entire temperature range.



Therefore, in this chapter we have reached an approximation in a wider range of temperature, managing the approximation error in satisfactory levels (no greater than 5%).

This code can be implemented in any programming language:

$$\left\{ \begin{array}{ll} \text{if } (\tau \leq \tau_1) & \text{then } \bar{\rho}(\tau) = a_A + b_A \tau + c_A \tau^2 + d_A \tau^3 \\ \text{if } (\tau_1 < \tau < \tau_2) & \text{then } \bar{\rho}(\tau) = a_{AB} + b_{AB} \tau + c_{AB} \tau^2 + d_{AB} \tau^3 \\ \text{if } (\tau_2 \leq \tau \leq \tau_3) & \text{then } \bar{\rho}(\tau) = y_1(\tau) + \chi(\tau - \tau_{H1})y_2(\tau) + \chi(\tau - \tau_{H2})y_3(\tau) \\ \text{if } (\tau_3 < \tau < \tau_4) & \text{then } \bar{\rho}(\tau) = a_{BC} + b_{BC} \tau + c_{BC} \tau^2 + d_{BC} \tau^3 \\ \text{if } (\tau \geq \tau_4) & \text{then } \bar{\rho}(\tau) = \bar{\rho}_{ch} \end{array} \right. \quad (6.55)$$

Table 6.3 – Result liquid density algorithm values for the case $\bar{\rho}_{ch} = 1$.

$a_A = -3E-7$	$c_{AB} = 1.38E-2$	$e_B = 4.4E-1$	$k_B = 2.1$	$d_{BC} = 5.42E2$
$b_A = 4E-4$	$d_{AB} = -2.33$	$f_B = -3.48E-1$	$\tau_{H1} = 0.81$	$\Delta\tau_1 = 5E-3$
$c_A = 4E-3$	$a_B = 5.1E-6$	$g_B = 3.43E-1$	$\tau_{H2} = 0.95$	$\Delta\tau_2 = 1E-2$
$d_A = 1.41E-2$	$b_B = 1E-5$	$h_B = 3$	$a_{BC} = -6.77E2$	$\Delta\tau_3 = 8E-3$
$a_{AB} = 5.33E-7$	$c_B = 1.38E-2$	$i_B = 1.9$	$b_{BC} = 1.887E3$	$\Delta\tau_4 = 6.913E-2$
$b_{AB} = 6.75E-4$	$d_B = -5.49E-2$	$j_B = 1.35E2$	$c_{BC} = -1.751E3$	

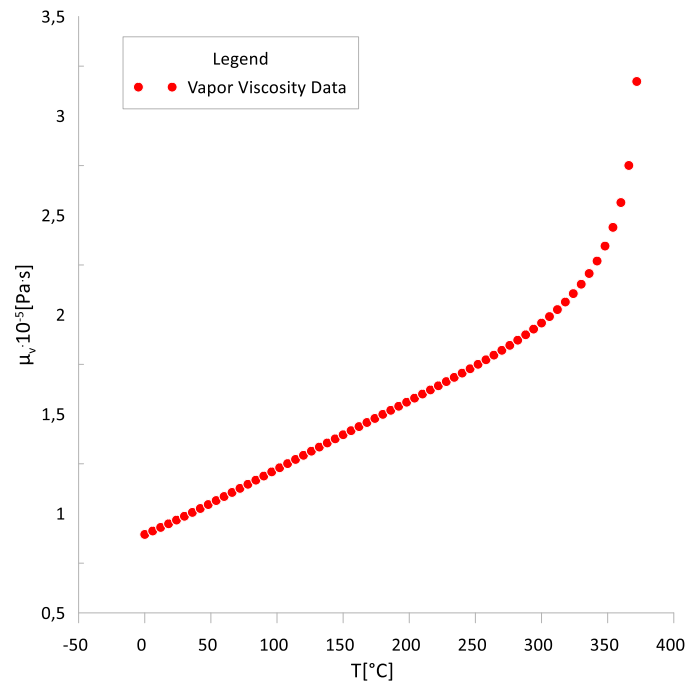
6.3 Approximations for vapor dynamic viscosity

6.3.1 Approximations for saturated zone

Liquid dynamic viscosity (μ_{lv}) is defined as the relation between shear stress and the fluid deformation velocity. This property is essential in determining how the flow is shaped. Therefore, this property is responsible for the fluid interface force between its layers or other fluid or solid surfaces in contact with that flow. This property is expressed mostly in $\mu\text{Pa}\cdot\text{s}$, where Pa is N/m^2 .

The presented data Huber et al. (2009) of the water vapor dynamic viscosity dependence with temperature for saturated conditions is shown in Figure 6.24.

Figure 6.24 – Water vapor dynamic viscosity tabulated data.



Faghri in his book Faghri (2016) suggested equation to approximate this water property (6.56). The dynamic viscosity is expressed in Pa*s and the temperature is in Celsius.

$$\begin{aligned} \ln(\mu_v(T)) = & -1.1596 + 2.6382 \cdot 10^{-3} \cdot T + 6.9205 \cdot 10^{-6} \cdot T^2 - \\ & 6.1035 \cdot 10^{-8} \cdot T^3 + 1.6844 \cdot 10^{-10} \cdot T^4 - 1.5910 \cdot 10^{-13} \cdot T^5 \end{aligned} \quad (6.56)$$

This equation is valid between 20°C and 200°C, the approximation error is 0.03%, and the equation covers up to 48% of the entire two-phase temperature range. Although Faghri (2016) suggested this equation, if we verify, the Equation (6.56) cannot reach a correct result; it is possible, that a new version of the equation need to be presented.

We use non-dimensional variables for both temperature and vapor dynamic viscosity:

$$\bar{\mu}_v(\tau) = \frac{\mu - \mu_{V_3}}{\mu_{V_{cr}} - \mu_{V_3}} \quad (6.57)$$

For the saturation interval (i.e., two-phase zone, $0 < \tau < 1$), the original curve has a sharp rise as it approaches the critical temperature. It is difficult to obtain a unique function which approximates the entire zone within acceptable error. Therefore, we improved it by applying interruption points (τ_{H1} and τ_{H2}) and joining three approximation functions in the interval $0 \leq \tau < 1$ by the application of Heaviside function.

The best results are the following.

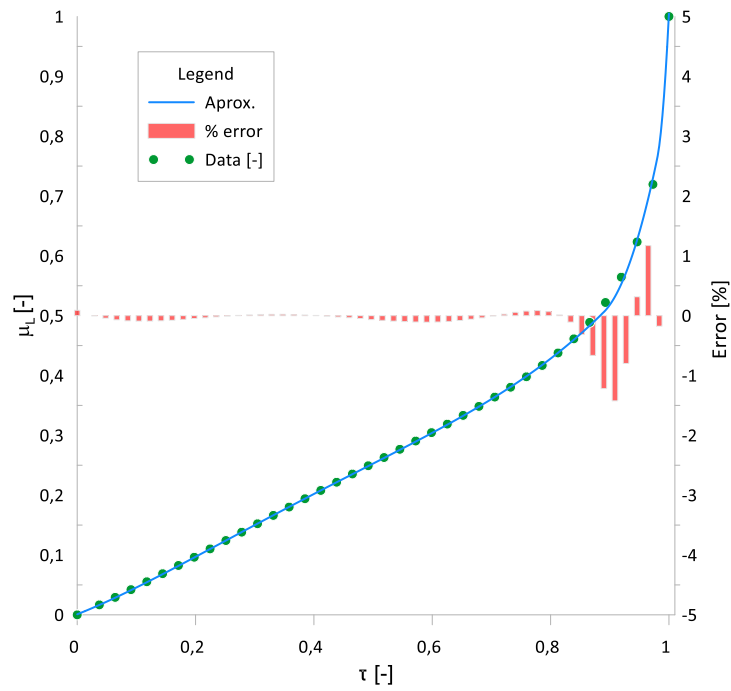
$$\begin{cases} y_1 = a_B + b_B \tau + c_B \tau^2 + d_B \tau^3 + e_B \tau^4 \\ y_2 = f_B (\tau - \tau_{H1})^{g_B} \\ y_3 = h_B (\tau - \tau_{H2})^{i_B} \end{cases} \quad (6.58)$$

These functions are used in an additive way: when $0 < \tau < \tau_{H1}$, then $y = y_1$; when $\tau_{H1} < \tau < \tau_{H2}$, then $y(\tau) = y_1(\tau) + y_2(\tau)$; when $\tau_{H2} < \tau < 1$, then $y(\tau) = y_1(\tau) + y_2(\tau) + y_3(\tau)$. This can be condensed in a unique correlation:

$$\bar{\mu}_{v_B}(\tau) = y_1(\tau) + \chi(\tau - \tau_{H1})y_2(\tau) + \chi(\tau - \tau_{H2})y_3(\tau) \quad (6.59)$$

Applying the algorithm above, in the saturation interval of temperature we achieve the curve shown below in Figure 6.25. That graph shows data from using green circles (HUBER et al., 2009). The approximation results in the blue line. In red bars we have the deviation error from property table data.

Figure 6.25 – Vapor dynamic viscosity approximation result in saturation zone.



We observed that the deviation from data by approximation lie within the ~2% compared to the properties table data.

Demonstration of Heaviside function application is shown in Figure 6.26.

Figure 6.26 – Heaviside function in approximation for saturated zone.

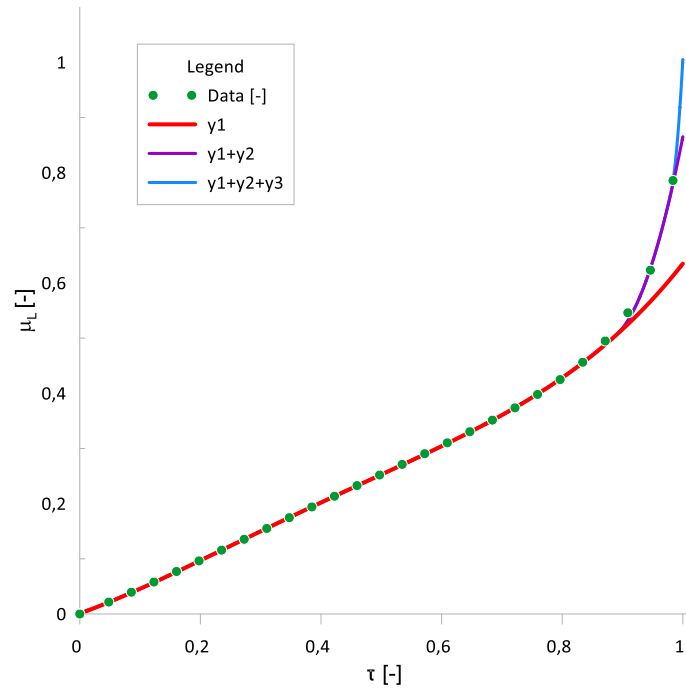
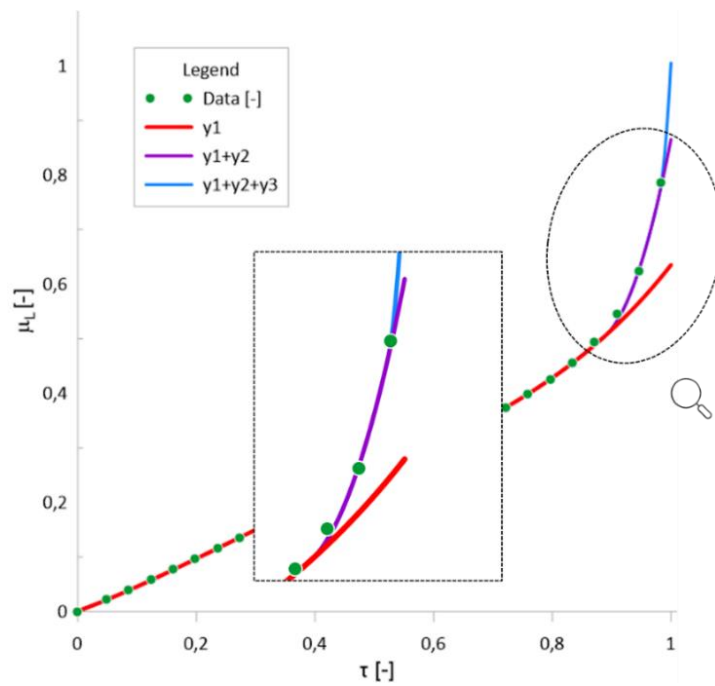


Figure 6.27 – Zoom on Heaviside function conjugate points



6.3.2 Approximations for freezing zone

Smith (1924) discovered a non-linear dependence of viscosity with temperature for this zone (6.60), where the dynamic viscosity is expressed in Pa·s and the temperature in K.

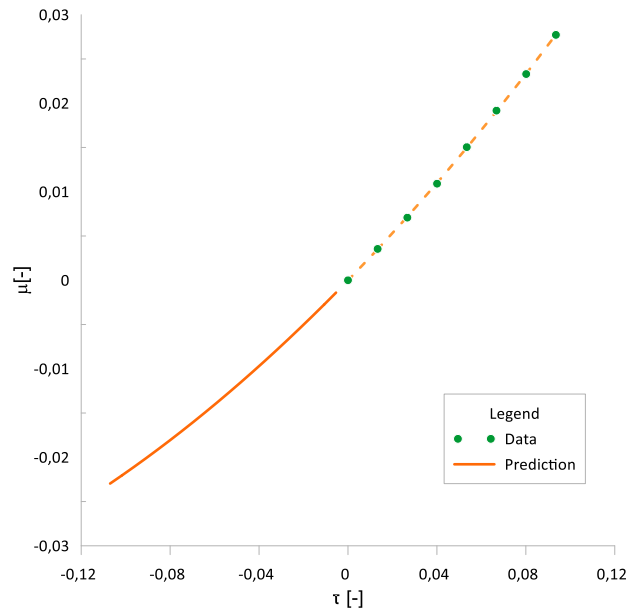
$$\mu \sim T^{\frac{3}{2}} \quad (6.60)$$

We used Smith (1924) data to fit a suggested approximation using a second-degree polynomial curve (6.61), as it is possible to see in

Figure 6.28.

$$\bar{\mu}_{v_A}(\tau) = a_A + b_A\tau + c_A\tau^2 \quad (6.61)$$

Figure 6.28 – Property value prediction below the triple point.



Looking for a smooth transition between those two zones it is used a third-degree polynomial Equation (6.62).

$$\bar{\mu}_{v_{AB}}(\tau) = a_{AB} + b_{AB}\tau + c_{AB}\tau^2 + d_{AB}\tau^3 \quad (6.62)$$

The system of equations of smoothing and uninterrupted conditions has the same format as for vapor density Equation (6.46) and does not present here points of tangency is defined by a similar manner:

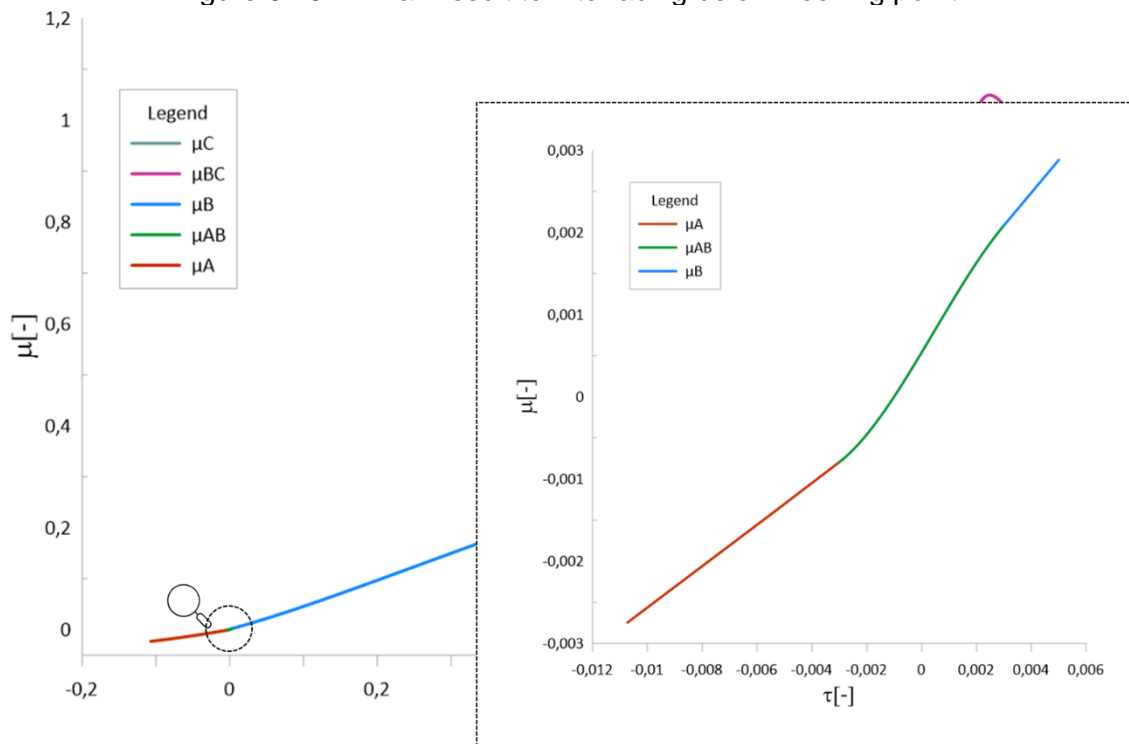
$$\begin{aligned}
 \Delta\tau_1 &= 0.003; \\
 \Delta\tau_2 &= 0.003; \\
 \tau_1 &= -\Delta\tau_1 \\
 \tau_2 &= +\Delta\tau_2
 \end{aligned}
 \tag{6.63}$$

The solution for the polynomial coefficients for the interfacing around $\tau=0$ is presented below.

$$\begin{cases}
 a_{AB} = 0.00053978 \\
 b_{AB} = 0.55665453 \\
 c_{AB} = 11.7682 \\
 d_{AB} = -8521.201
 \end{cases}
 \tag{6.64}$$

The result approximations around the triple point ($\tau=0$), including the interfacing curve, is shown in Figure 6.29.

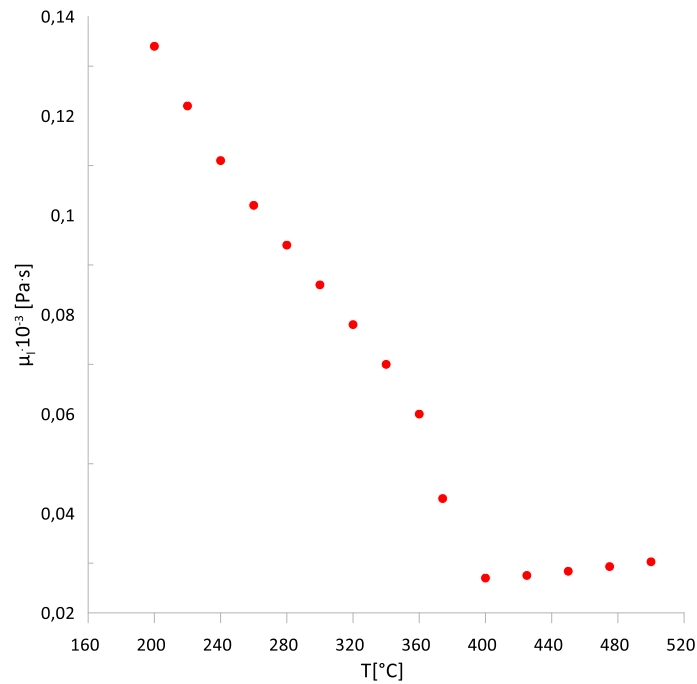
Figure 6.29 – Final Result to interfacing below freezing point.



6.3.3 Approximations for super-critical zone

In the super-critical zone, the viscosity suddenly drops and then gets a light permanent increasing. Moreover, the behavior above the critical point begins having a dependence of pressure, as shown in Figure 6.30.

Figure 6.30 – Water dynamic viscosity data at critical pressure [220.64 bar].



The property is pressure dependent. When we consider heat pipes, it is not expected much pressure variations as exceed the critical value at the critical temperature. Because of that, in the super critical zone our effort will be focused on property value at 220.64 bar (critical pressure).

For super-critical zone we also use second order polynomial approximation:

$$\bar{\mu}_{v_c}(\tau) \Big|_{\tau > 1} = (a_c + b_c \tau + c_c \tau^2) \quad (6.65)$$

We also use a third-degree polynomial Equation (6.66) for the interface:

$$\bar{\mu}_{v_{BC}}(\tau) = a_{BC} + b_{BC} \tau + c_{BC} \tau^2 + d_{BC} \tau^3 \quad (6.66)$$

Points of tangency at $\tau=1$ are defined by the following values

$$\begin{aligned}
\Delta\tau_3 &= 0.003; \\
\Delta\tau_4 &= 0.07; \\
\tau_3 &= 1 - \Delta\tau_3 = 0.997 \\
\tau_4 &= 1 - \Delta\tau_4 = 1.07
\end{aligned}
\tag{6.67}$$

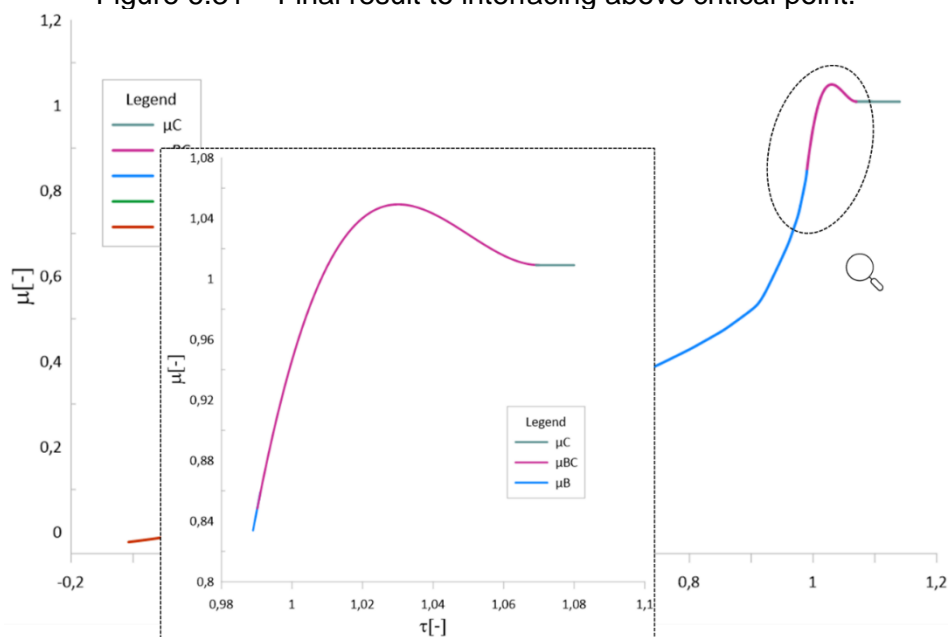
The system of equations of smoothing and uninterrupted conditions has the same format as for vapor density Equation (6.52) and does not present here.

Solving the system above, the parameters values are available below.

$$\begin{cases}
a_{BC} = -3375.60375 \\
b_{BC} = 9685.299 \\
c_{BC} = -9255.5652 \\
d_{BC} = 2946.8674
\end{cases}
\tag{6.68}$$

Figure 6.32 shows the result of the approximation around critical point.

Figure 6.31 – Final result to interfacing above critical point.

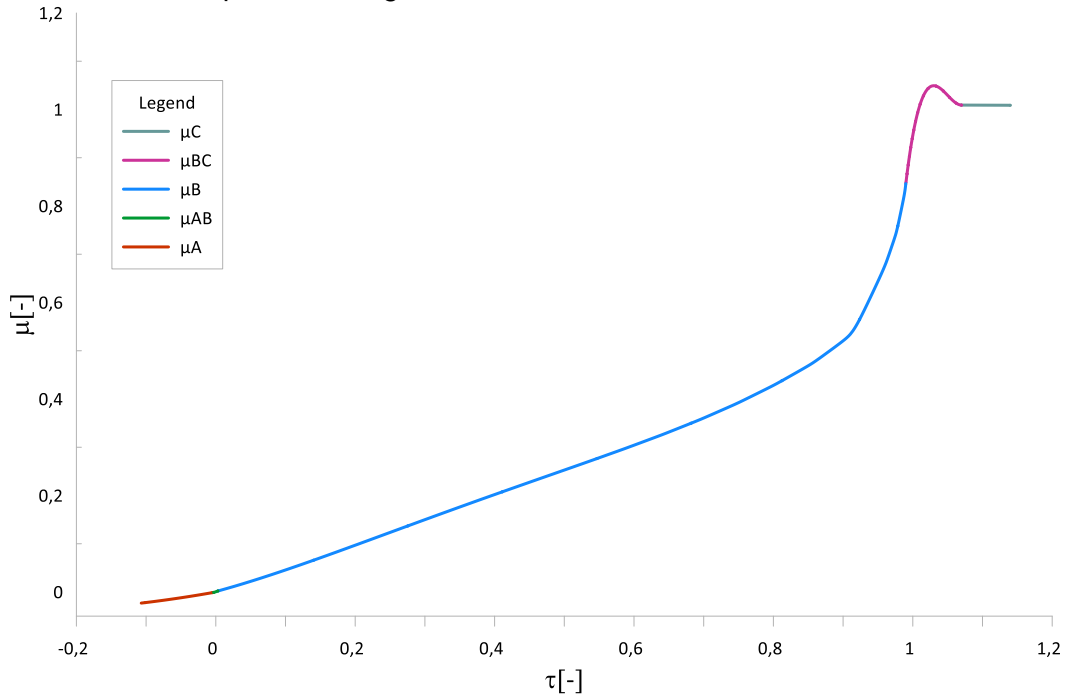


6.3.4 Final approximation and pseudo code

In this chapter we have reached an approximation in a wide range of temperature, managing the approximation error in satisfactory levels (usually no greater than

5%). The pseudo code provides a set of closed form approximations of the fluid property values starting below triple point and going up to above the critical point.

Figure 6.32 – Final Result to vapor dynamic viscosity approximation in the entire temperature range.



This pseudo-code for the entire temperature range is presented in (6.71) and can be implemented in any programming language:

$$\left\{ \begin{array}{ll} \text{if } (\tau \leq \tau_1) & \text{then } \bar{\mu}_v(\tau) = a_A + b_A \tau + c_A \tau^2 \\ \text{if } (\tau_1 < \tau < \tau_2) & \text{then } \bar{\mu}_v(\tau) = a_{AB} + b_{AB} \tau + c_{AB} \tau^2 + d_{AB} \tau^3 \\ \text{if } (\tau_2 \leq \tau \leq \tau_3) & \text{then } \bar{\mu}_v(\tau) = y_1(\tau) + \chi(\tau - \tau_{H1})y_2(\tau) + \chi(\tau - \tau_{H2})y_3(\tau) \\ \text{if } (\tau_3 < \tau < \tau_4) & \text{then } \bar{\mu}_v(\tau) = a_{BC} + b_{BC} \tau + c_{BC} \tau^2 + d_{BC} \tau^3 \\ \text{if } (\tau \geq \tau_4) & \text{then } \bar{\mu}_v(\tau) = (a_C + b_C \tau + c_C \tau^2) \end{array} \right. \quad (6.69)$$

Table 6.4 – Result of vapor dynamic viscosity algorithm values.

$a_A = -2.2577E-5$	$a_B = 1.22E-3$	$h_B = 1700$	$d_{BC} = -3.136E2$	$\Delta\tau_4 = 7E-2$
$b_A = 2.5844E-1$	$b_B = 2.118E-1$	$i_B = 1.5$	$a_C = 1.0038$	
$c_A = 4.1116E-1$	$c_B = 7.933E-1$	$\tau_{H1} = 0.95$	$b_C = 1.47E-2$	
$a_{AB} = 5.6374E-4$	$d_B = -1.53$	$\tau_{H2} = 0.997$	$c_C = -9.1E-3$	
$b_{AB} = 5.4605E-1$	$e_B = 1.005$	$a_{BC} = 2.862E2$	$\Delta\tau_1 = 1E-2$	
$c_{AB} = -3.2879$	$f_B = 25$	$b_{BC} = -8.9221E2$	$\Delta\tau_2 = 3E-3$	
$d_{AB} = -1.1474E4$	$g_B = 1.6$	$c_{BC} = 9.2039E2$	$\Delta\tau_3 = 3E-3$	

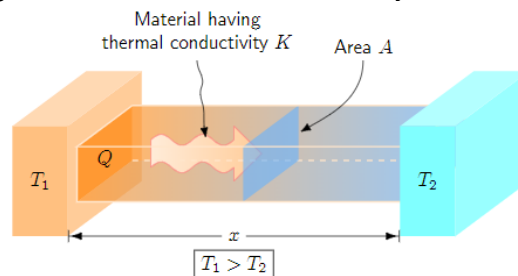
6.4 Approximations for vapor thermal conductivity

6.4.1 Approximations for saturated zone

Vapor thermal conductivity (k_v) is defined as the capacity of a solid or stationary fluid to conduct heat from one side to the other whenever a temperature difference occurs.

The property can be illustrated by the Figure 6.33.

Figure 6.33- Thermal Conductivity Schematics.

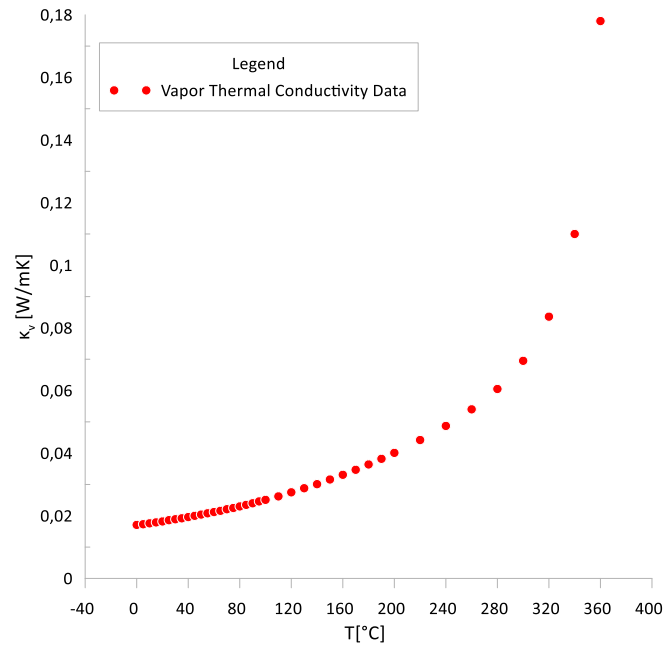


<https://www.concepts-of-physics.com/thermodynamics/heat-conduction.php>

Source: Singh (2019).

The thermal conductivity is measured in $W / (m K)$. This property is a key parameter in the fundamental Fourier's Law for heat conduction. The original data of the water vapor thermal conductivity behavior with temperature, published by American Society of Heating, Refrigerating and Air-Conditioning Engineers (ASHRAE), is presented in Figure 6.34.

Figure 6.34 – Water vapor thermal conductivity tabled data.

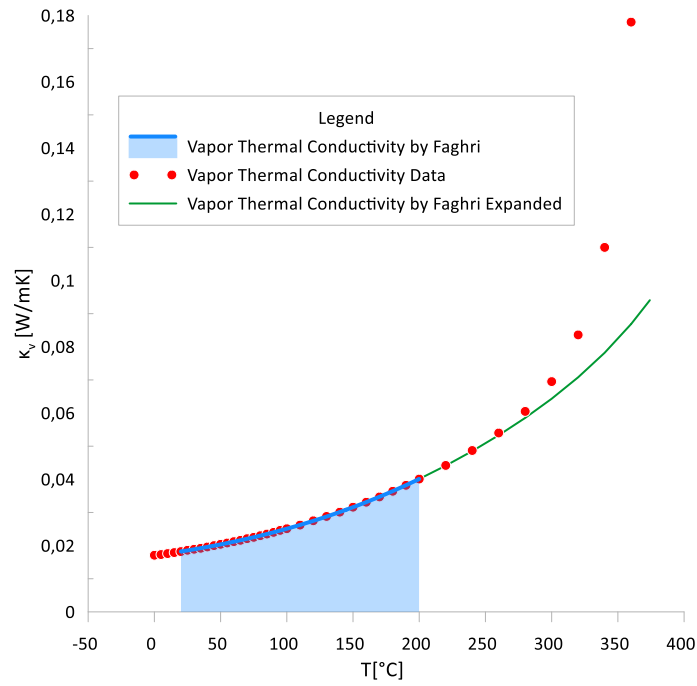


Faghri (2016) in his book, that serves as a reference for research in mathematical modeling of heat pipes, suggested a logarithm-polynomial expression (6.70) to approximate this water property. The vapor thermal conductivity is expressed in W/mK, and the temperature is in Celsius.

$$\begin{aligned} \ln(k_v(T)) = & -4.0722 + 3.2364 \cdot 10^{-3} \cdot T + 6.3860 \cdot 10^{-6} \cdot T^2 + \\ & 8.5114 \cdot 10^{-9} \cdot T^3 - 1.0464 \cdot 10^{-10} \cdot T^4 + 1.6481 \cdot 10^{-13} \cdot T^5 \end{aligned} \quad (6.70)$$

This equation is valid between from 20°C to 200°C and presents the approximation error of 0.03% in this range. The equation covers up to 48% of the entire two-phase temperature range. As an example, when we try to use this approximation out of range established, the result can be no tangible with real behavior. The green line in Figure 6.35 expresses this deviation from real value.

Figure 6.35 – Faghri polynomial approximation.



This deviation of Faghri's approximation at elevated temperatures shows that the approximation over entire two-phase range cannot be achieved with a unique polynomial function.

In our study we use non-dimensional variables for both temperature and vapor thermal conductivity:

$$k_v(\tau) = \frac{k_v - k_{v_3}}{k_{v_{CR}} - k_{v_3}} \quad (6.71)$$

The best results were obtained with the following combination of approximate functions:

$$\begin{cases} y_1 = a_B + b_B \tau + c_B \tau^2 + d_B \tau^3 + e_B \tau^4 \\ y_2 = f_B (\tau - \tau_{H1})^3 + g_B (\tau - \tau_{H1})^4 \\ y_3 = h_B (\tau - \tau_{H2})^{i_B} \end{cases} \quad (6.72)$$

These functions are used in an additive way: when $0 < \tau < \tau_{H1}$, then $y=y_1$; when $\tau_{H1} < \tau < \tau_{H2}$, then $y(\tau)=y_1(\tau)+y_2(\tau)$; when $\tau_{H2} < \tau < 1$, then $y(\tau)=y_1(\tau)+y_2(\tau)+y_3(\tau)$. This can be condensed in a unique correlation for our property:

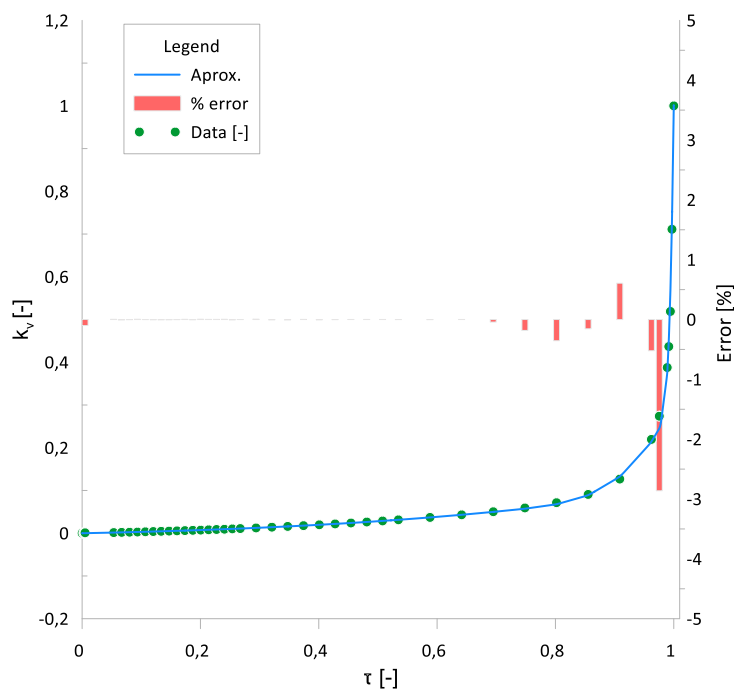
$$\bar{k}_{v_B}(\tau) = y_1(\tau) + \chi(\tau - \tau_{H1})y_2(\tau) + \chi(\tau - \tau_{H2})y_3(\tau) \quad (6.73)$$

The smoothing in the conjugate points (τ_{H1} & τ_{H2}) has been achieved by the application of the conditions of continuity of both function and its derivative.

Applying the algorithm above, in the saturation interval of temperature we achieved the approximation shown in Figure 6.36. That chart shows data from ASHRAE using green circles. The approximation result is shown in the blue line. In red bars we have the deviation error between property table data and the approximation.

The technique of the piece-wise technique with using the Heaviside function by addition is illustrated in Figure 6.37. As one can see, this technique allows reaching an approximation without sharp edges.

Figure 6.36 – Vapor thermal conductivity approximation result in saturated zone.



We observe the deviation from data by approximation lie within the acceptance criteria in 3% of deviation from the properties table data.

Figure 6.37 – Approximation for saturated zone by combination of three functions.

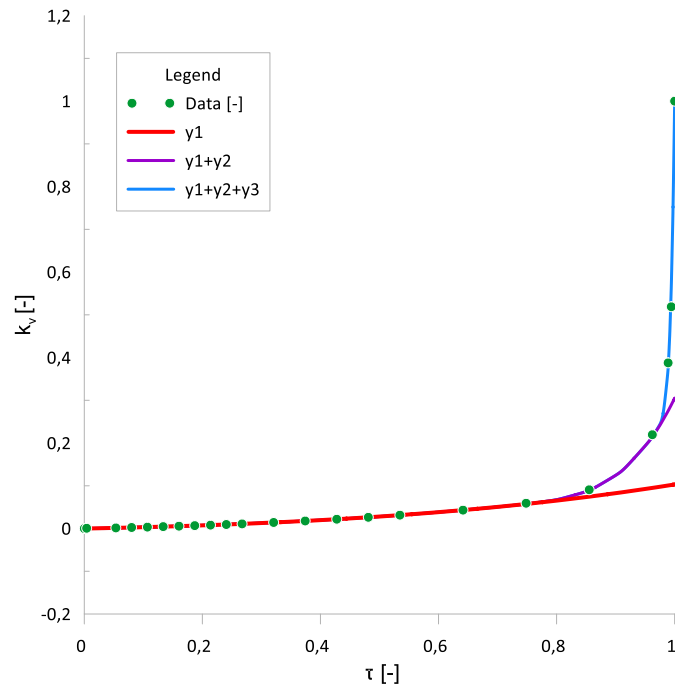
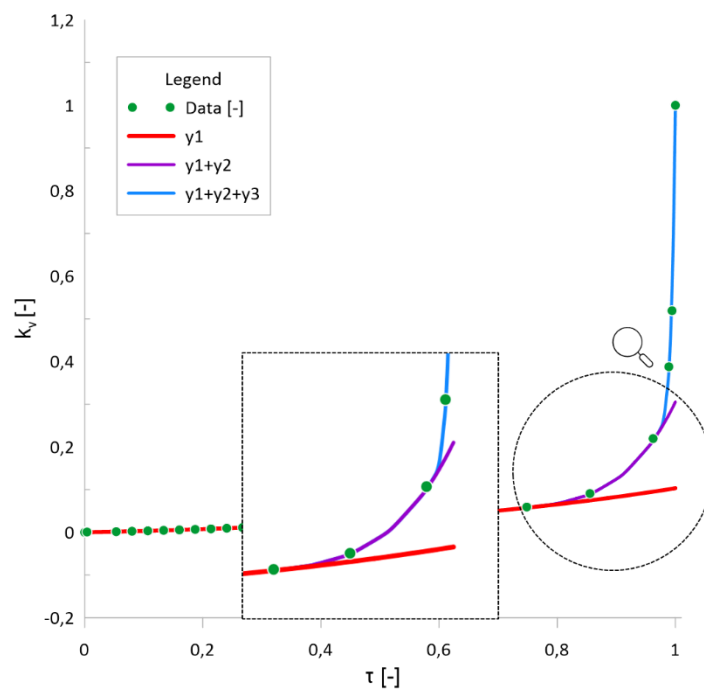


Figure 6.38 – Zoom on the conjugation points in approximation for the saturation zone.



6.4.2 Approximations for freezing zone and interfacing

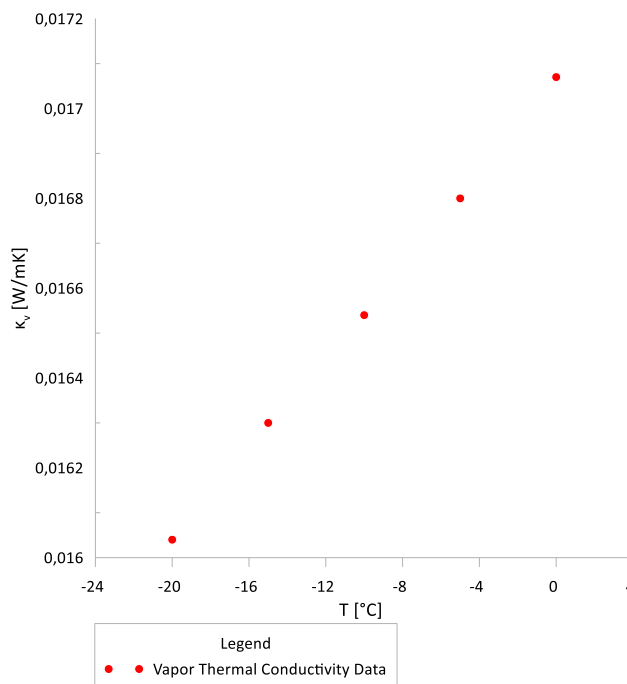
For freezing zone data, Liley (2005) arranged approximation results for water properties braking ranges of approximations in three zones A, B & C, whereas A is placed between -20 and 0°C, B in 0 up to 25°C and C starting in 25 reaching 50°C.

In this work we use the approximation in the freezing zone (range “A”) by (LILEY, 2005):

$$\bar{k}_{v_A}(T) = 2.216 - 0.0102T + 6.9444 \cdot 10^{-5} T^2 \quad (6.74)$$

Where k is in W/mK and T in Celsius degrees.

Figure 6.39 – Vapor thermal conductivity data in freezing zone.



Liley (2005) used the second order polynomial approximations, however in this work we will use 3rd order polynomial approximation aiming to improve the precision. After transformation of original data into dimensionless format, the proposed approximation is the following:

$$\bar{k}_{v_A}(\tau) = a_A + b_A \tau + c_A \tau^2 + d_A \tau^3 \quad (6.75)$$

The interfacing equations smoothly connect the subcooled zone with saturated zone. Following the general approach, the third-degree polynomial in Equation (6.76) is used.

$$\bar{k}_{v_{AB}}(\tau) = a_{AB} + b_{AB} \tau + c_{AB} \tau^2 + d_{AB} \tau^3 \quad (6.76)$$

The system of equations of smoothing and uninterrupted conditions has the same format as for vapor density Equation (6.46) and does not present here:

Points of tangency are defined by a similar manner

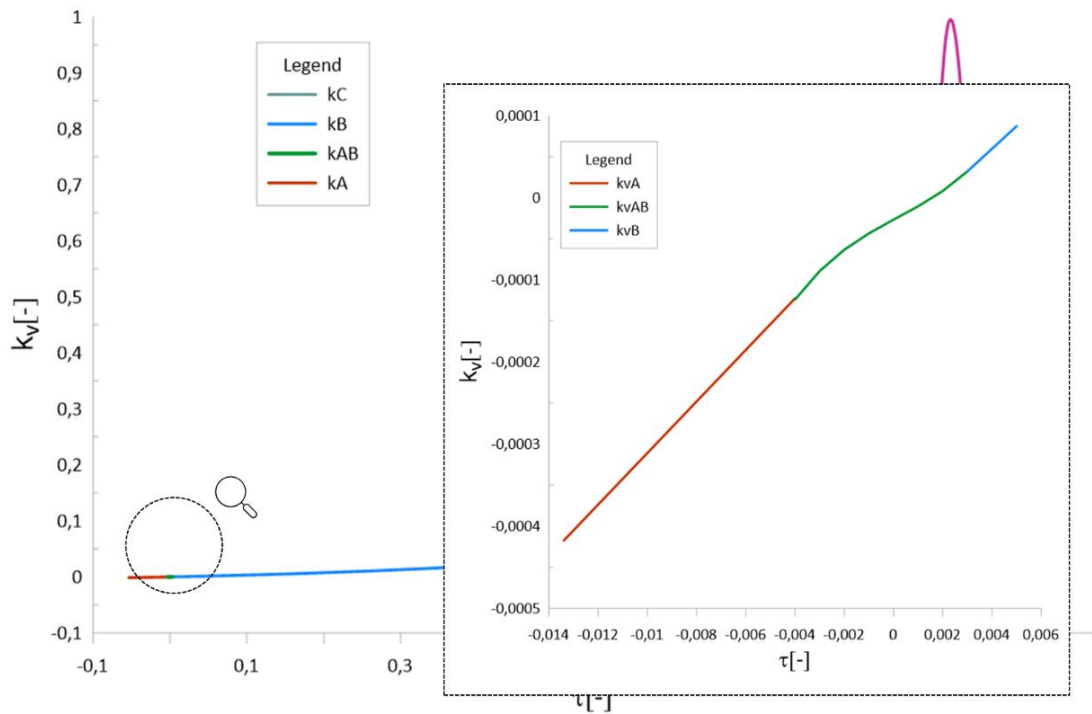
$$\begin{aligned} \Delta \tau_1 &= 0.0035; \\ \Delta \tau_2 &= 0.003; \\ \tau_1 &= -\Delta \tau_1 \\ \tau_2 &= +\Delta \tau_2 \end{aligned} \quad (6.77)$$

The solution of the system of the conjugate equations system is expressed below (6.78).

$$\begin{cases} a_{AB} = -2.6775 \cdot 10^{-5} \\ b_{AB} = 1.6029 \cdot 10^{-2} \\ c_{AB} = 2.0710 \cdot 10^{-1} \\ d_{AB} = 4.6490 \cdot 10^2 \end{cases} \quad (6.78)$$

The result approximations around triple point ($\tau=0$), including the interfacing curve, is shown in Figure 6.40.

Figure 6.40 – Final Result to interfacing below sub-freezing point.



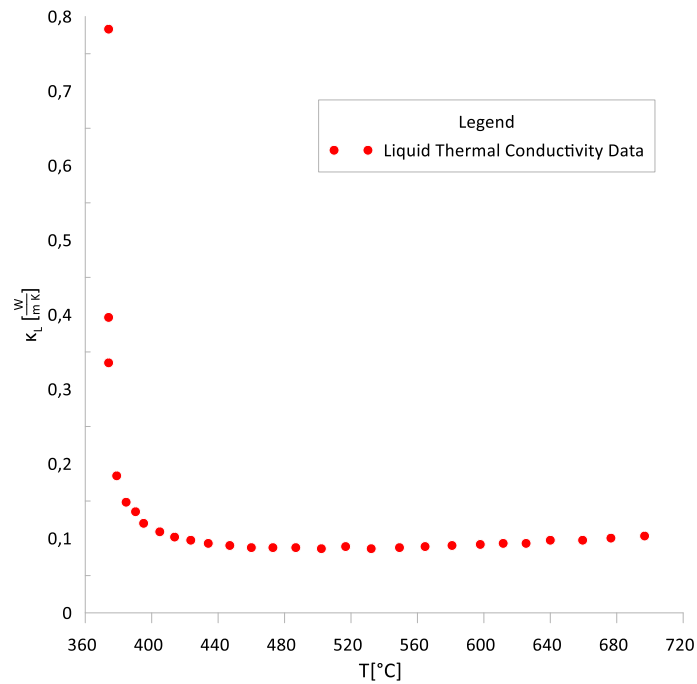
One can observe the interfacing curve links two approximation curves smoothly and tangentially. The value of dimensionless thermal conductivity of the vapor above ice is negative due to the absolute value of the conductivity is lower than in two-phase zone.

6.4.3 Approximations for supercritical zone and interfacing

In the super-critical zone, the behavior of the thermal conductivity is very complicated and very non-linear. Figure 6.41 presents original data for the water vapor in the supercritical region (gas). It is worthy to mention that in literature, the value of this property in the critical point is either not defined or considered infinity, so we decide to attribute a value for vapor thermal conductivity at critical point defined by an interpolation curve of the past four points. At temperature above the critical point, the thermal conductivity drops down to the value of about 0.09 W/m/K. Dhanuskodi et al (2011) showed the graph of such a sudden drop.

We can pick the curve which corresponds to the critical pressure (220.64 bar), as it is close to real heat pipe internal condition near critical point. The same behavior is presented in (PIORO, 2020).

Figure 6.41 – Property data in supercritical zone.



Another point which deserves attention is the continuity of the values and derivatives in the interface between curves, to guarantee that the interfacing technique provides a correct softening in the conjugate points. It was implemented and the result is possible to check in figures below, starting at the triple point and then at critical temperature point.

For super-critical zone we found that the polynomial curve of fifth order fits reasonable the tabled property data:

$$\bar{k}_{v_c}(\tau) = a_c + b_c \tau + c_c \tau^2 + d_c \tau^3 + e_c \tau^4 + f_c \tau^5 \quad (6.79)$$

Looking for a smoother transition between those two zones Equations (6.73) and (6.79), it is used a third-degree polynomial in Equation (6.80).

$$k_{v_{BC}}(\tau) = a_{BC} + b_{BC} \tau + c_{BC} \tau^2 + d_{BC} \tau^3 \quad (6.80)$$

Points of tangency can be defined trying to optimize the approximation result. In this case $\Delta\tau$ is how far each point will be away from the critical point, ($\tau=1$).

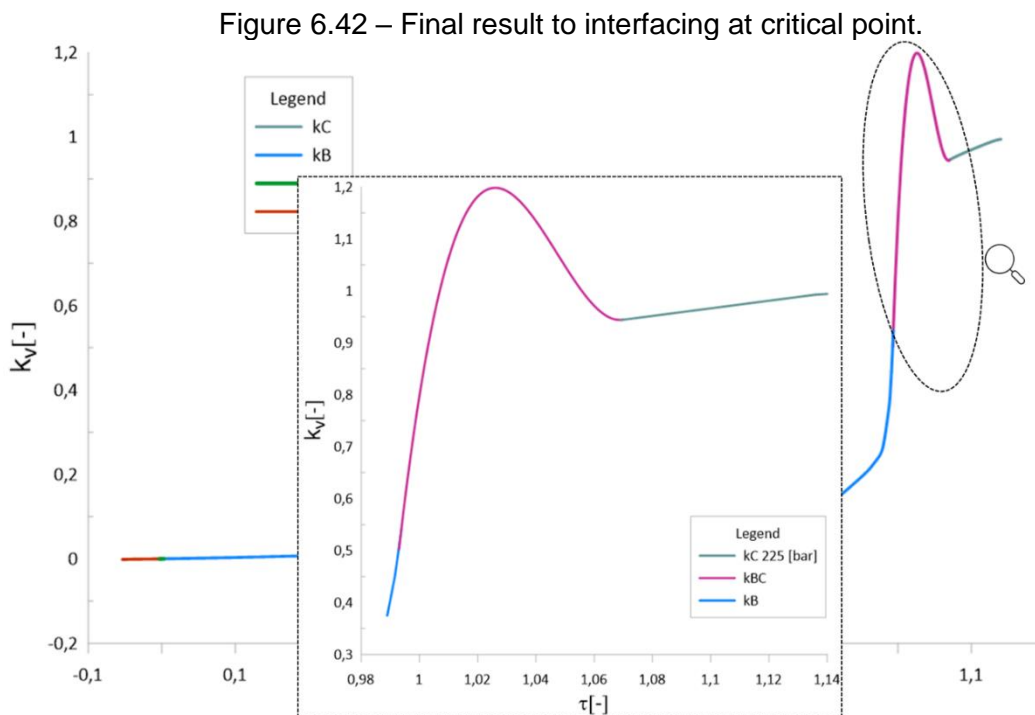
$$\begin{aligned}
 \Delta\tau_3 &= 0.0062; \\
 \Delta\tau_4 &= 0.07; \\
 \tau_3 &= 1 - \Delta\tau_3 = 0.9938 \\
 \tau_4 &= 1 + \Delta\tau_4 = 1.07
 \end{aligned}
 \tag{6.81}$$

The system of equation for smooth interfacing is similar to Equation (6.46) and does not present here.

Using the values mentioned above, the result is:

$$\begin{cases}
 a_{BC} = 7538.36 \\
 b_{BC} = 21613.62 \\
 c_{BC} = -20645 \\
 d_{BC} = 6570.554
 \end{cases}
 \tag{6.82}$$

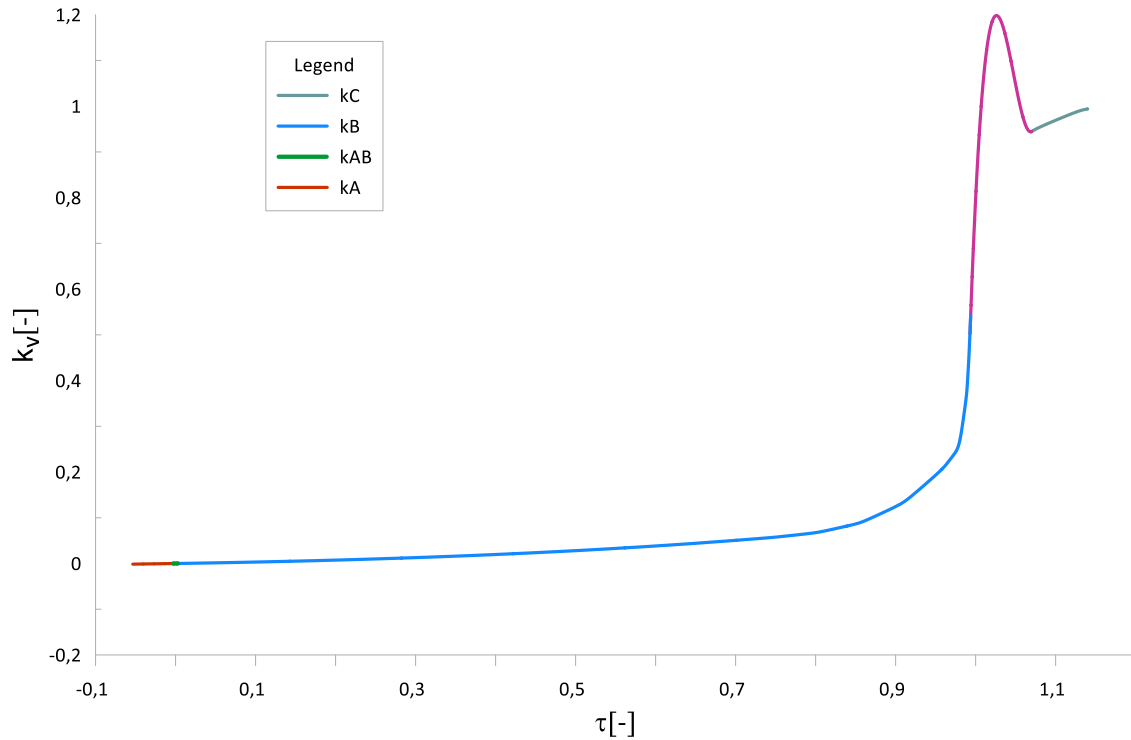
Figure 6.42 shows the result of approximation at the critical point and beyond it.



6.4.4 Final approximation and pseudo code

The algorithm that we proposed for the approximation of the entire region, which includes below freezing point and above critical point zones, provides the result curve shown in Figure 6.43.

Figure 6.43 – Final result for vapor thermal conductivity approximation over entire temperature range.



Therefore, in this chapter we have reached an approximation in the entire range of temperature, managing the approximation error in satisfactory levels (no greater than 5%). The pseudo-code (6.83) provides fluid property values starting below triple point up to above critical point.

$$\left\{ \begin{array}{ll} \text{if } (\tau \leq \tau_1) & \text{then } \bar{k}_v(\tau) = a_A + b_A \tau + c_A \tau^2 + d_A \tau^3 \\ \text{if } (\tau_1 < \tau < \tau_2) & \text{then } \bar{k}_v(\tau) = a_{AB} + b_{AB} \tau + c_{AB} \tau^2 + d_{AB} \tau^3 \\ \text{if } (\tau_2 \leq \tau \leq \tau_3) & \text{then } \bar{k}_v(\tau) = y_1(\tau) + \chi(\tau - \tau_{H1})y_2(\tau) + \chi(\tau - \tau_{H2})y_3(\tau) \\ \text{if } (\tau_3 < \tau < \tau_4) & \text{then } \bar{k}_v(\tau) = a_{BC} + b_{BC} \tau + c_{BC} \tau^2 + d_{BC} \tau^3 \\ \text{if } (\tau \geq \tau_4) & \text{then } \bar{k}_v(\tau) = a_C + b_C \tau + c_C \tau^2 + d_C \tau^3 + e_C \tau^4 + f_C \tau^5 \end{array} \right. \quad (6.83)$$

Table 6.5 –Vapor thermal conductivity pseudo-code values.

$a_A = 2E-5$	$d_{AB} = 4.65E2$	$g_B = 1.95E1$	$c_{BC} = -2.065E4$	$f_C = 1.525E1$
$b_A = 3.71E-2$	$a_B = -5E-5$	$h_B = 1.7E7$	$d_{BC} = 6.571E3$	$\Delta\tau_1 = 3.5E-3$
$c_A = 3.823E-1$	$b_B = 2.72E-2$	$i_B = 6$	$a_C = -1.018E2$	$\Delta\tau_2 = 3E-3$
$d_A = 3.811$	$c_B = 4.62E-2$	$\tau_{H1} = 0.73$	$b_C = 3.56E2$	$\Delta\tau_3 = 6.2E-3$
$a_{AB} = -2.6759E-5$	$d_B = 1.77E2$	$\tau_{H2} = 0.96$	$c_C = -4.895E2$	$\Delta\tau_4 = 7E-2$
$b_{AB} = 1.603E-2$	$e_B = 1.77E2$	$a_{BC} = -7.538E3$	$d_C = 3.342E2$	
$c_{AB} = 2.0710E-1$	$f_B = 5$	$b_{BC} = 2.161E4$	$e_C = -1.133E2$	

6.5 Approximations for vapor specific heat capacity

6.5.1 Approximations for saturated zone

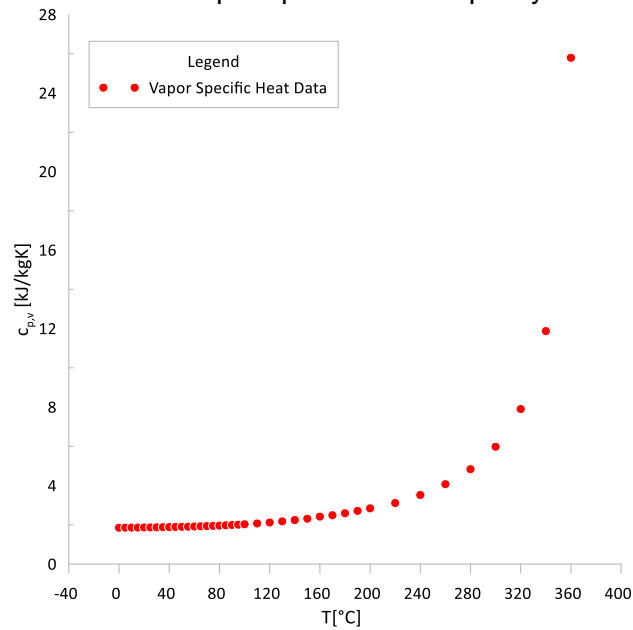
Liquid specific heat capacity ($c_{p,L}$) is defined as an amount of heat (dQ) needed to raise the temperature by an increment (dT) of a unity mass (M). (6.84).

$$c_{p,v} = \frac{1}{M} \cdot \frac{dQ}{dT} \quad (6.84)$$

The unity is J/kg/K.

The original data of the liquid specific heat capacity behavior with temperature in the two-phase zone, presented by ASHRAE, is shown in Figure 6.44 (LEMMON et al., 2023).

Figure 6.44 – Water vapor specific heat capacity number data.



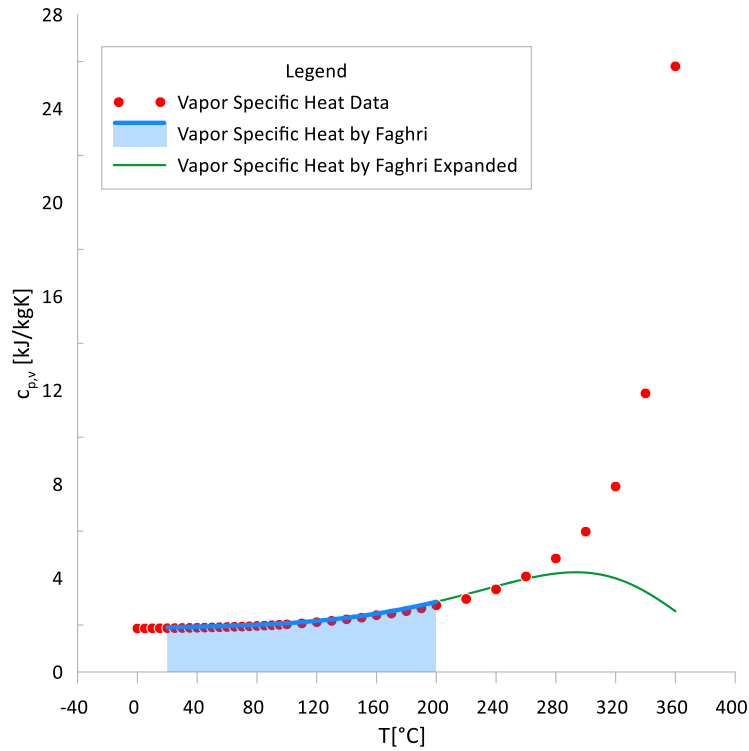
Faghri (2016) in his book suggested equation to approximate this water property by fifth order polynomial Equation (6.85) applied to logarithm of the specific heat.

$$\begin{aligned} \ln(c_{p,v}(T)) = & 6.3198 \cdot 10^{-1} + 6.7903 \cdot 10^{-4} \cdot T - 2.5923 \cdot 10^{-6} \cdot T^2 - \\ & 4.4936 \cdot 10^{-8} \cdot T^3 + 2.2606 \cdot 10^{-10} \cdot T^4 - 9.0694 \cdot 10^{-13} \cdot T^5 \end{aligned} \quad (6.85)$$

where T is expressed in °C and Cp_v in kJ/kg/K.

This equation is valid between 20°C and 200°C; in this range of temperature this equation can be used for HP modeling, because of the approximation error is 0.03%. The approximation covers up to 48% of the entire two-phase temperature range. However, when we try using this polynomial equation out of the range established, the result deviates from real behavior. The green line is expressed this deviation in Figure 6.45.

Figure 6.45 – Faghri polynomial approximation.



We use dimensionless vapor specific heat capacity, following our general approach:

$$\bar{c}_{p,v}(\tau) = \frac{c_{p,v} - c_{p,v_3}}{c_{p,v_{cr}} - c_{p,v_3}} \quad (6.86)$$

For the saturated interval (i.e., two-phase zone, $0 < \tau < 1$), the original curve has a sharp climb as it approaches the critical temperature. It is difficult to obtain a unique function which approximates the entire zone with acceptable error. Therefore, we improve it by applying three interruption points (τ_{H1} , τ_{H2} and τ_{H3}) and join three approximation functions in the interval $0 \leq \tau < 1$ by the application of the Heaviside function.

The best results were obtained using the following combination of four approximate functions:

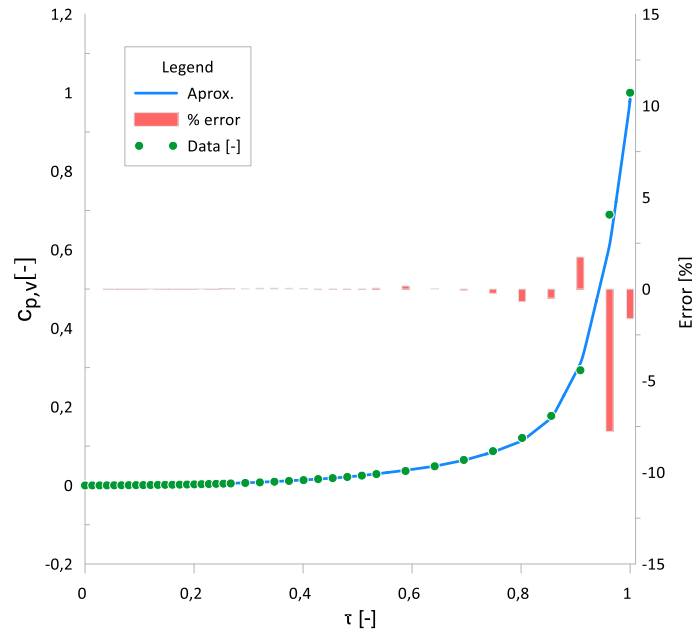
$$\begin{cases} y_1 = (a_B(1 + \text{Tanh}(b_B(\tau - c_B)))) - d_B \\ y_2 = e_B(\tau - \tau_{H1})^{f_B} \\ y_3 = g_B \text{Senh}^{h_B}(\tau - \tau_{H2}) \\ y_4 = i_B(\tau - \tau_{H3})^{j_B} \end{cases} \quad (6.87)$$

These functions are used in an additive way: when $0 < \tau < \tau_{H1}$, then $y=y_1$; when $\tau_{H1} < \tau < \tau_{H2}$, then $y(\tau)=y_1(\tau)-y_2(\tau)$; when $\tau_{H2} < \tau < 1$, then $y(\tau)=y_1(\tau)-y_2(\tau)-y_3(\tau)+y_4(\tau)$. This can be condensed in a unique correlation for our property:

$$\bar{c}_{p,v}(\tau) = y_1(\tau) - \chi(\tau - \tau_{H1})y_2(\tau) - \chi(\tau - \tau_{H2})y_3(\tau) + \chi(\tau - \tau_{H3})y_4(\tau) \quad (6.88)$$

By applying the algorithm above, we obtain the curve shown below in Figure 6.46 within the saturation interval of temperature. That graph shows data from ASHRAE using green circles (LEMMON et al., 2023). The approximation results are in the blue line. Red bars indicate the deviation error from the table data and the approximation.

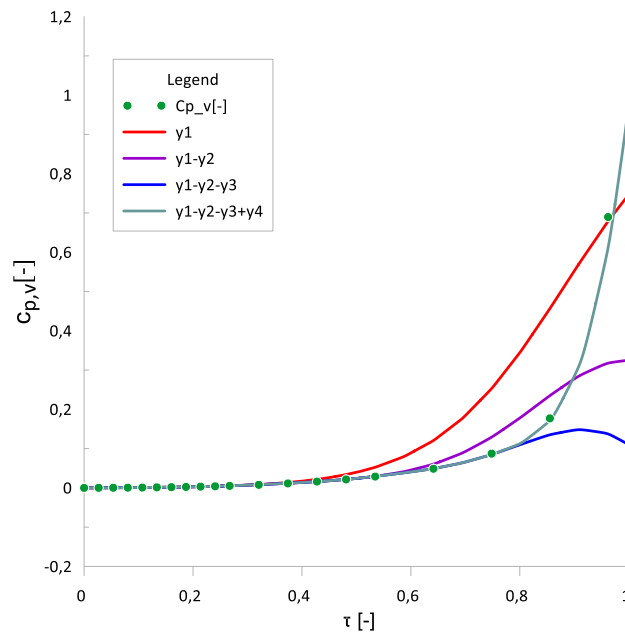
Figure 6.46 – Vapor specific heat capacity approximation in saturated zone.



We observe the deviation from data by approximation lies within the usual acceptance criteria in 5% of deviation from the properties table data; the only high error occurs near the critical point where initial data are not well defined.

To develop this property approximation, we used a baseline curve (fourth degree polynomial equation), and we add piece-wise functions to this curve with the use of the Heaviside function. It results in a final curve shown in Figure 6.47.

Figure 6.47 – Heaviside function in approximation for saturated zone.



6.5.2 Approximations for freezing zone and interfacing

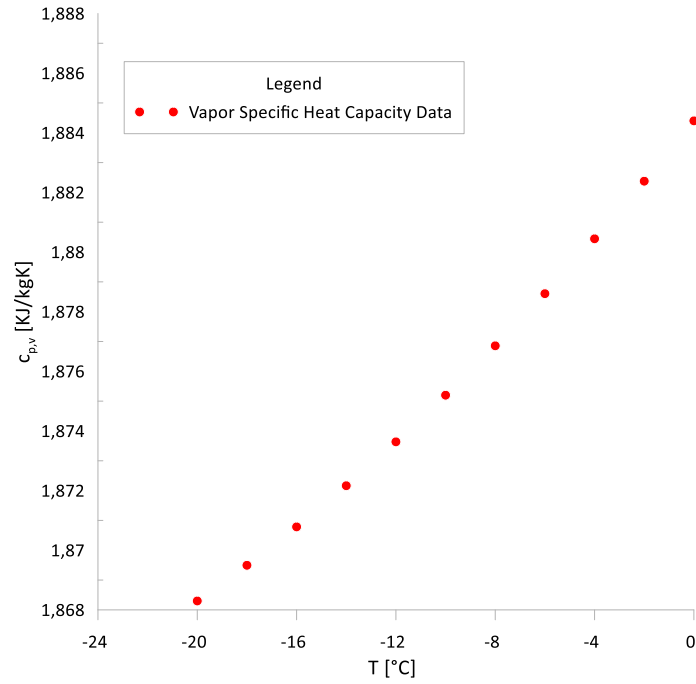
The algorithm above that we proposed for the approximation of the entire region includes zones below freezing and above critical point.

Below the saturation zone, in the freezing zone Liley (2005) proposed an equation which describes vapor specific heat capacity at constant pressure in temperatures below the triple point from 0 down to -20 °C, Equation (6.89).

$$c_{p,v}(T) = 1.8844 - 1.035 \cdot 10^{-3} T + 1.15 \cdot 10^{-5} T^2 \quad (6.89)$$

where T is expressed in °C and $C_{p,v}$ - in kJ/kg/K.

Figure 6.48 – Property data in freezing zone.

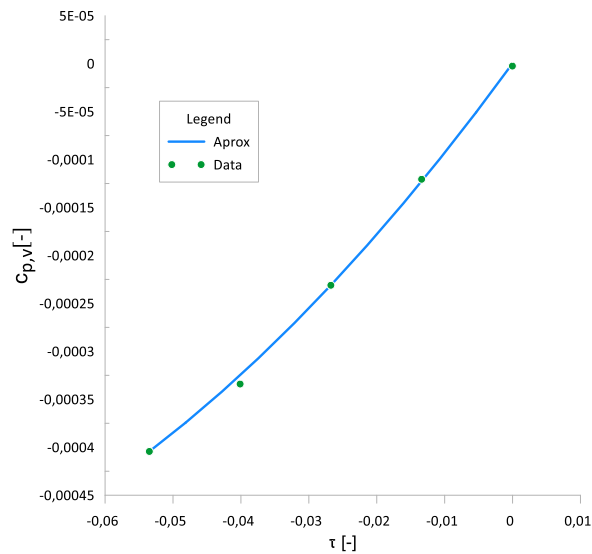


The best approximation for this region was provided by the 2nd order polynomial function.

$$\bar{c}_{p,v_A}(\tau)_{\tau < 0} = a_A + b_A \tau + c_A \tau^2 \quad (6.90)$$

Figure 6.49 shows this approximation curve as a solid blue line.

Figure 6.49 – Property dimensionless data and approximation in freezing zone.



Another point that deserves attention is the continuity of the values and derivatives at the intervening conjugate points (interfaces between curves) to guarantee perfect softening at these points.

The interfacing technique is the same that showed in others part of this work; we start with both equation that we want to link and the derivatives of each one, The interfacing equation joins the freezing zone with saturated zone.

For a smooth transition between these two zones, it is used a third-degree polynomial Equation (6.91).

$$\bar{c}_{p,v_A}(\tau) = a_{AB} + b_{AB}\tau + c_{AB}\tau^2 + d_{AB}\tau^3 \quad (6.91)$$

The conditions of continuity of values and derivatives have four unknowns and 4 equations, and the format similar to one presented in Equation (6.46) but.

Points of tangency can be defined through optimize of the approximation results. In this case Δt defines how far each point will be away from the other.

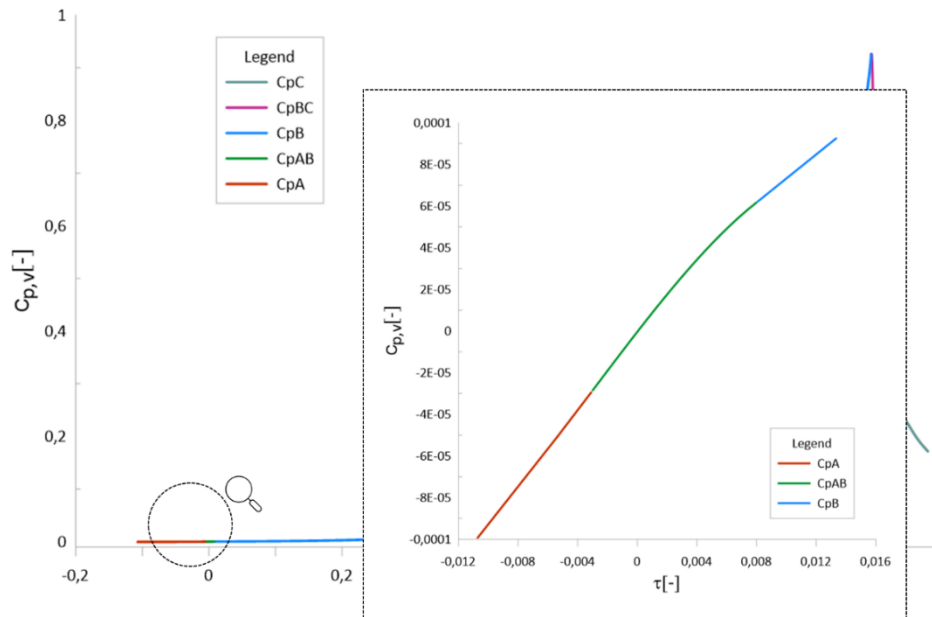
$$\begin{aligned} \Delta\tau_1 &= 0.003; \\ \Delta\tau_2 &= 0.008; \\ \tau_1 &= -\Delta\tau_1 \\ \tau_2 &= +\Delta\tau_2 \end{aligned} \quad (6.92)$$

Using the developed universal approach for any property, the result is:

$$\begin{cases} a_{AB} = -3.7991 \cdot 10^{-7} \\ b_{AB} = 9.2049 \cdot 10^{-3} \\ c_{AB} = -9.4741 \cdot 10^{-2} \\ d_{AB} = -1.0678 \cdot 10^1 \end{cases} \quad (6.93)$$

The result approximations around triple point ($\tau=0$), including the interfacing curve, is shown in Figure 6.50.

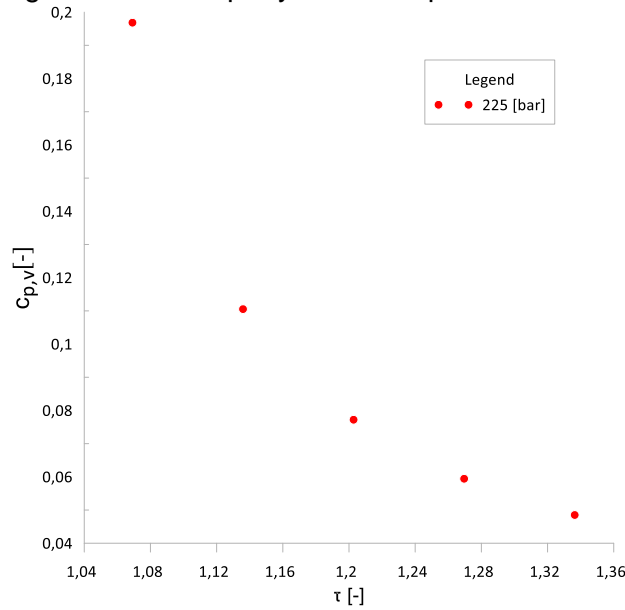
Figure 6.50 – Final result to interfacing around the freezing triple point.



6.5.3 Approximations for supercritical zone and interfacing

For the supercritical region, the difference between the liquid and vapor phases disappears. The c_{pv} behaves in a very complicated manner near the critical point: its values sharply decrease as τ approaches one from the left, and then gets sharp falling as τ slightly pass 1 to the right. The graph for near-critical pressure $P=250$ bar is shown in Figure 6.51. (adapted from DHANUSKODI; ARUNAGIRI; ANANTHARAMAN, 2011).

Figure 6.51 – Property data in supercritical zone.



Initially, the interfacing technique is the same that showed in others part of this work, we start with both equation that we want to link and their respective derivatives. For super-critical zone we found that the best result gave the approximation by the hyperbolic function:

$$\bar{c}_{p,v_c}(\tau) \Big|_{\tau>1} = \left((1 - \text{Tanh}(e\tau))^{a_c} \right) b_c + c_c \quad (6.94)$$

$$\frac{d(\bar{c}_{p,v_c}(\tau))}{d(\tau)} \Big|_{\tau>1} = \left(-a_c b_c e \text{Sech}(e\tau)^2 \right) \left(a_c b_c (1 - \text{Tanh}(e\tau))^{a_c} \right) \quad (6.95)$$

A smooth transition between these two zones is accomplished with a third-degree polynomial Equation (6.96).

$$\bar{c}_{p,v_{BC}}(\tau) = a_{BC} + b_{BC}\tau + c_{BC}\tau^2 + d_{BC}\tau^3 \quad (6.96)$$

Points of tangency around the critical point, ($\tau=1$) are the following.

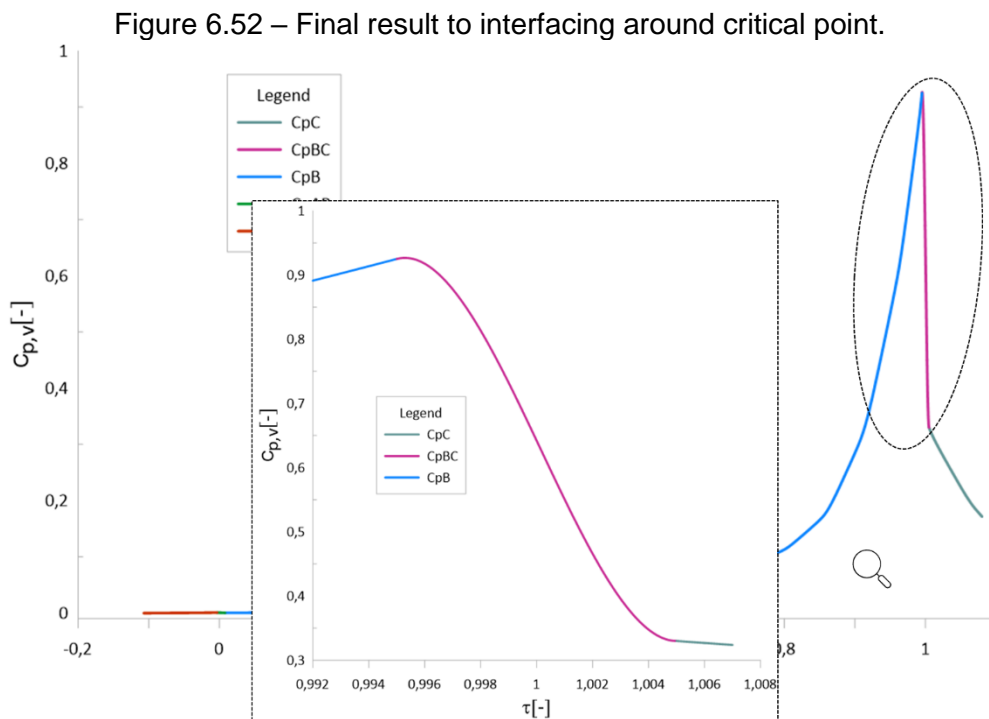
$$\begin{aligned}
\Delta\tau_3 &= 0.005; \\
\Delta\tau_4 &= 0.005; \\
\tau_3 &= 1 - \Delta\tau_3 = 0.995 \\
\tau_4 &= 1 + \Delta\tau_4 = 1.005
\end{aligned}
\tag{6.97}$$

The system has the usual format like in Equation (6.52) when both curves make a continuous smooth link.

By solving the system of continuity, the obtained parameters values are available below.

$$\begin{cases}
a_{BC} = -130298422 \\
b_{BC} = 390855571 \\
c_{BC} = -390806476 \\
d_{BC} = 130249392
\end{cases}
\tag{6.98}$$

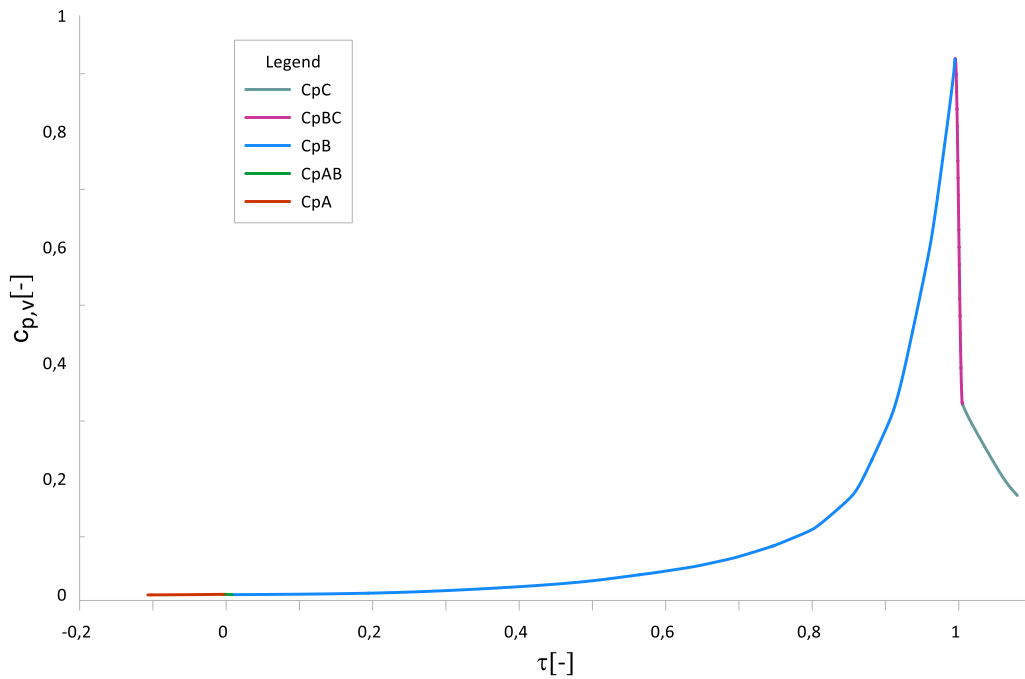
Figure 6.52 shows the result of the approximation.



6.5.4 Final approximation and pseudo code

Therefore, in this chapter we reached an approximation in the entire range of temperature, managing the approximation error in satisfactory levels (no greater than 5%). The pseudo code provides fluid property values starting below the triple point and going beyond the critical point.

Figure 6.53 – Final approximation for Vapor specific heat capacity in the entire temperature range.



This code can be implemented in any programming language:

$$\left\{ \begin{array}{ll}
 \text{if } (\tau \leq \tau_1) & \text{then } \bar{c}_{p,v}(\tau) = a_A + b_A \tau + c_A \tau^2 \\
 \text{if } (\tau_1 < \tau < \tau_2) & \text{then } \bar{c}_{p,v}(\tau) = a_{AB} + b_{AB} \tau + c_{AB} \tau^2 + d_{AB} \tau^3 \\
 \text{if } (\tau_2 \leq \tau \leq \tau_3) & \text{then } \bar{c}_{p,v}(\tau) = y_1(\tau) - \chi(\tau - \tau_{H1})y_2(\tau) - \chi(\tau - \tau_{H2})y_3(\tau) \\
 & \quad + \chi(\tau - \tau_{H3})y_4(\tau) \\
 \text{if } (\tau_3 < \tau < \tau_4) & \text{then } \bar{c}_{p,v}(\tau) = a_{BC} + b_{BC} \tau + c_{BC} \tau^2 + d_{BC} \tau^3 \\
 \text{if } (\tau \geq \tau_4) & \text{then } \bar{c}_{p,v}(\tau) = \left((1 - \text{Tanh}(e\tau))^{ac} \right) b_C + c_C
 \end{array} \right. \quad (6.99)$$

Piece-wise functions y_i are defined by Equation (6.87).

Table 6.6 – Result values of vapor specific heat capacity pseudo-code.

$a_A = 2.599E-7$	$a_B = 5.1E-1$	$g_B = 9E-1$	$\tau_{H3} = 7.4E-1$	$c_{BC} = -3.908E6$
$b_A = 9.727E-3$	$b_B = 4.2$	$h_B = 1.99$	$a_C = 6.358E4$	$d_{BC} = 1.302E6$
$c_A = 4.042E-2$	$c_B = 8.8E-1$	$i_B = 1.65E2$	$b_C = 1.405E-2$	$\Delta\tau_1 = 3E-2$
$a_{AB} = -3.79E-7$	$d_B = 6.1E-4$	$j_B = 3.89$	$c_C = 4.042E-2$	$\Delta\tau_2 = 8E-3$
$b_{AB} = 9.204E3$	$e_B = 1$	$\tau_{H1} = 2.5E-1$	$a_{BC} = -1.303E6$	$\Delta\tau_3 = 5E-3$
$c_{AB} = -9.474E-2$	$f_B = 3$	$\tau_{H2} = 5.3E-1$	$b_{BC} = 3.908E6$	$\Delta\tau_4 = 5E-3$
$d_{AB} = -1.06E1$				

6.6 Approximations for vapor Prandtl number

6.6.1 Approximations for saturated zone

The Prandtl number makes the correlation between the momentum diffusivity (ν) and the thermal diffusivity (α).

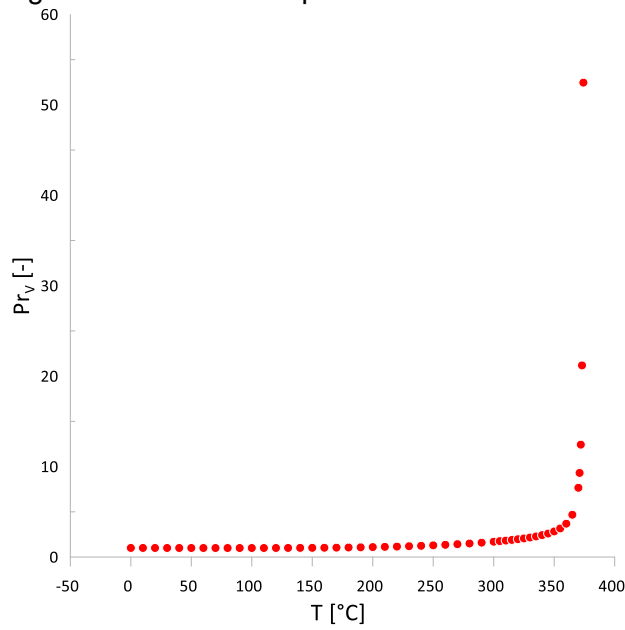
$$\text{Pr} = \frac{\nu}{\alpha} = \frac{\mu/\rho}{\kappa/(c_p\rho)} = \frac{c_p\mu}{\kappa} \quad (6.100)$$

The parameters are defined as following:

ν is momentum diffusivity or kinematic viscosity, α is thermal diffusivity, μ is dynamic viscosity, κ is thermal conductivity, c_p is specific heat and ρ is density.

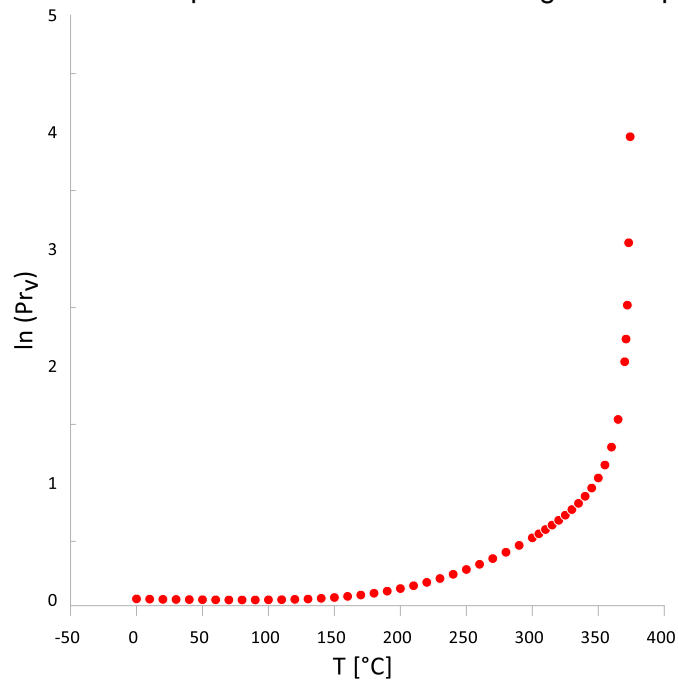
The Prandtl vapor number behavior with temperature in saturation zone is expressed in Figure 6.54 (BEATON, 1986).

Figure 6.54 – Water vapor Prandtl number Data.



This parameter has an abrupt increase value around 350 °C, near critical temperature. Direct approximation of such a function is a challenging task and may lead to elevated errors of the approximation. To minimize this peak, a natural logarithm was applied in tabled properties data to smooth this abruptness, Figure 6.55.

Figure 6.55 – Water vapor Prandtl number after logarithm application.



It is possible to notice in Figure 6.55 that the peak value was decreased from 52.4 down to ~4. To align with the methodology used in this work until now, we introduce a normalized function of $\ln(\text{Pr}_v)$, following our dimensionless parameters technique.

$$f(\ln \text{Pr}_v) = \frac{\ln(\text{Pr}_v) - \ln(\text{Pr}_{v3})}{\ln(\text{Pr}_{v,cr}) - \ln(\text{Pr}_{v3})} \quad (6.101)$$

We denote this function as normalized (and dimensionless) logarithmic Prandtl number (“nl-Pr”):

$$\overline{\text{Pr}}_v(\tau) = f(\ln \text{Pr}_v) \quad (6.102)$$

The curve in Figure 6.55 shows this function plotted over interval starting from $\tau=0$ and ending in $\tau=1$.

To perform the approximation, we divide the entire two-phase zone in three intervals, improving the approximation quality by adding new functions in each interval.

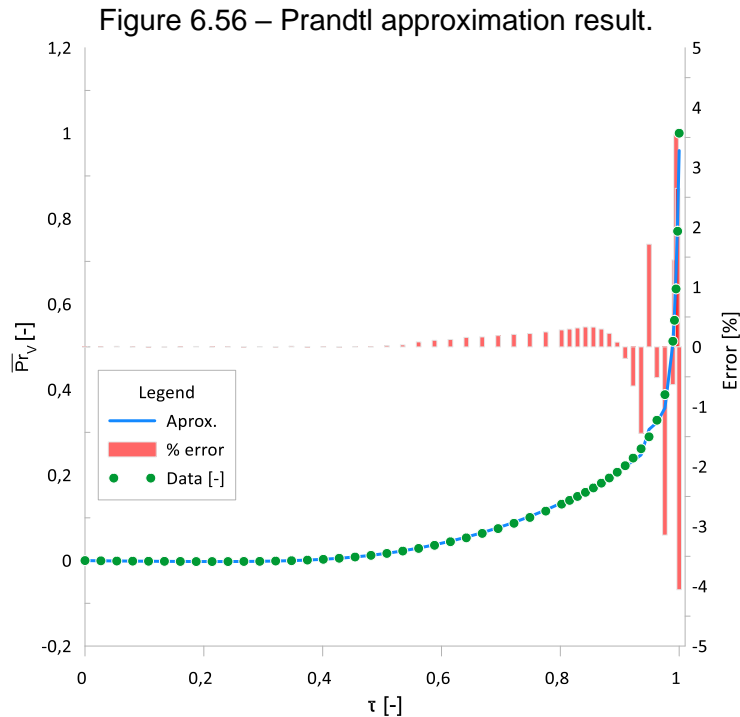
$$\begin{cases} y_1 = a_B + b_B \tau + c_B \tau^2 + d_B \tau^3 + e_B \tau^4 \\ y_2 = \left(f_B \text{Tanh}^{g_B}(\tau - \tau_{H1}) \right) \\ y_3 = \left(h_B (\tau - \tau_{H2}) \right)^{i_B} + j_B \end{cases} \quad (6.103)$$

The algorithm can be realized by using two Heaviside functions to build a unique approximation function over entire two-phase interval of τ from 0 to 1. (6.104).

$$\overline{\text{Pr}}_{v_B}(\tau) = y_1(\tau) + \chi(\tau - \tau_{H1})y_2(\tau) + \chi(\tau - \tau_{H2})y_3(\tau) \quad (6.104)$$

Applying the algorithm in the saturation interval of temperature we achieve an approximated curve to nl-Pr number in saturated range, Figure 6.56, which shows also tabled data from (BEATON, 1986) using green circles. The approximation

result function is shown in the blue line. In red bars we have the deviation error between property table data and the approximation.



In Figure 6.56, we have the deviation from data by the approximation ϵ delimited by a usual acceptance criterion of 4%. It is worth mentioning that when the n -Prandtl value is close to zero, an exceedingly small absolute deviation. In this case, the correct way to evaluate errors is by using the absolute deviations.

Like other properties, Prandtl number has different values above the critical point like exposed in Figure 6.57.

It is important to note that this parameter above the critical point varies with pressure and temperature and in that place demands more effort to build a robust approximation. In this case several interfacing curves might be created; each one to a different pressure level and in the end, all polynomial coefficients in the interfacing zones will be pressure functions.

6.6.2 Approximations for freezing zone

It is possible to demonstrate interfacing equation to joint subcooled zone with saturated zone.

$$\overline{\text{Pr}}_{v_A}(\tau) = 0 \quad (6.105)$$

$$\frac{d(\overline{\text{Pr}}_{v_A}(\tau))}{d(\tau)} = 0 \quad (6.106)$$

A smooth transition between A and B zones are accomplished with a third-degree polynomial function (6.107).

$$\overline{\text{Pr}}_{v_{AB}}(\tau) = a_{AB} + b_{AB}\tau + c_{AB}\tau^2 + d_{AB}\tau^3 \quad (6.107)$$

The system of continuity around the triple point has the following format to the interfacing tangency both curves, making a continuous smooth link.

$$\left\{ \begin{array}{l} \overline{\text{Pr}}_{v_A}(\tau_1) = a_{AB} + b_{AB}\tau_1 + c_{AB}\tau_1^2 + d_{AB}\tau_1^3 \\ \frac{d(\overline{\text{Pr}}_{v_A}(\tau_1))}{d(\tau_1)} = b_{AB} + 2c_{AB}\tau_1 + 3d_{AB}\tau_1^2 \\ \overline{\text{Pr}}_{v_B}(\tau_2) = a_{AB} + b_{AB}\tau_2 + c_{AB}\tau_2^2 + d_{AB}\tau_2^3 \\ \frac{d(\overline{\text{Pr}}_{v_B}(\tau_2))}{d(\tau_2)} = b_{AB} + 2c_{AB}\tau_2 + 3d_{AB}\tau_2^2 \end{array} \right. \quad (6.108)$$

Points of tangency is defined, trying to optimize the approximation results. In this case Δ defines how far each point is away from the other.

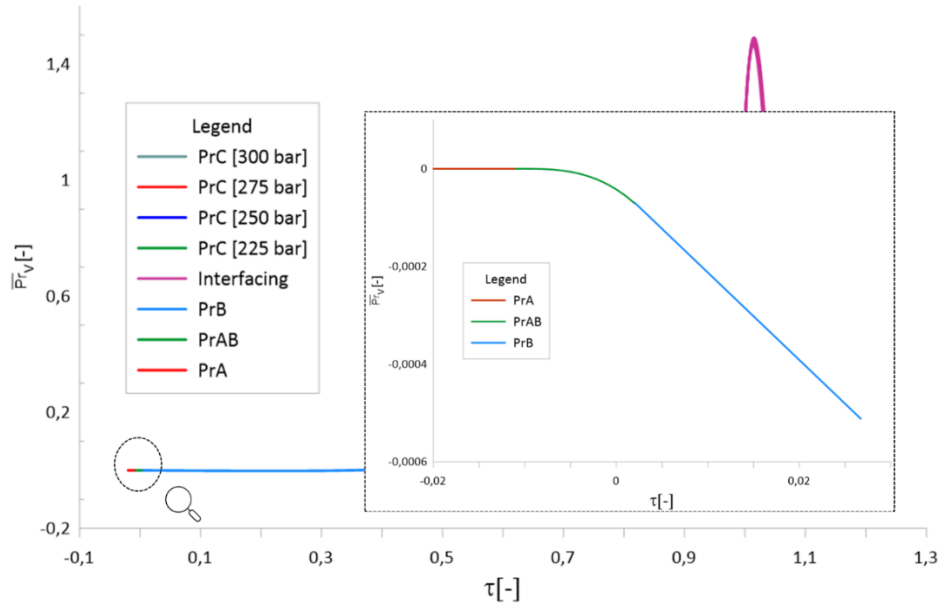
$$\begin{array}{l} \Delta\tau_1 = 0.01; \\ \Delta\tau_2 = 0.003; \\ \tau_1 = -\Delta\tau_1 \\ \tau_2 = +\Delta\tau_2 \end{array} \quad (6.109)$$

The result parameters of the interfacing curves are expressed below.

$$\left\{ \begin{array}{l} a_{AB} = -0.000042 \\ b_{AB} = -0.0199 \\ c_{AB} = -1.10528 \\ d_{AB} = -34.0329 \end{array} \right. \quad (6.110)$$

The result approximations around triple point ($\tau=0$), including the interfacing curve, shown in Figure 6.57.

Figure 6.57 – Interfacing nI-Prandtl number linking subcooled zone with saturated zone.



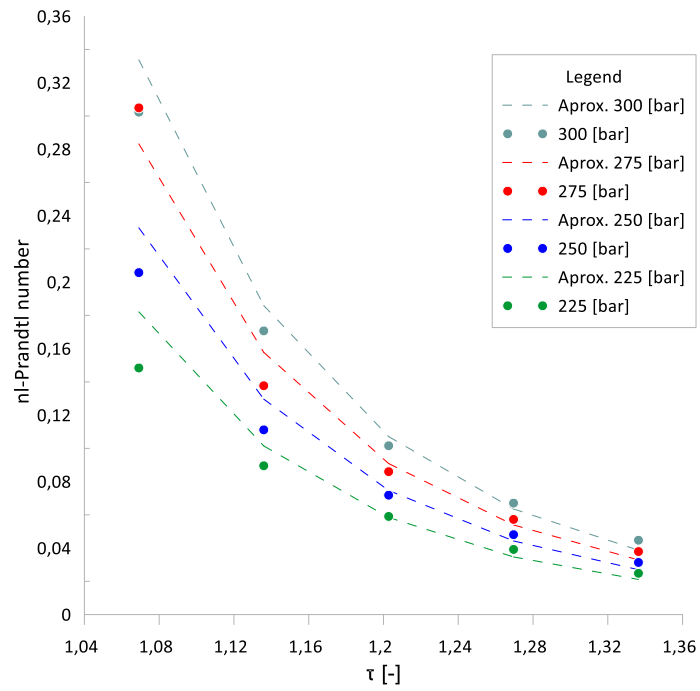
6.6.3 Approximations for super critical zone

As soon as the Pr number depends on pressure as well, we assume the two-arguments approximation shall be presented as a product of two functions, temperature and pressure:

$$\overline{\text{Pr}}_v(\tau, p) = \psi(p)\varphi(\tau) \quad (6.111)$$

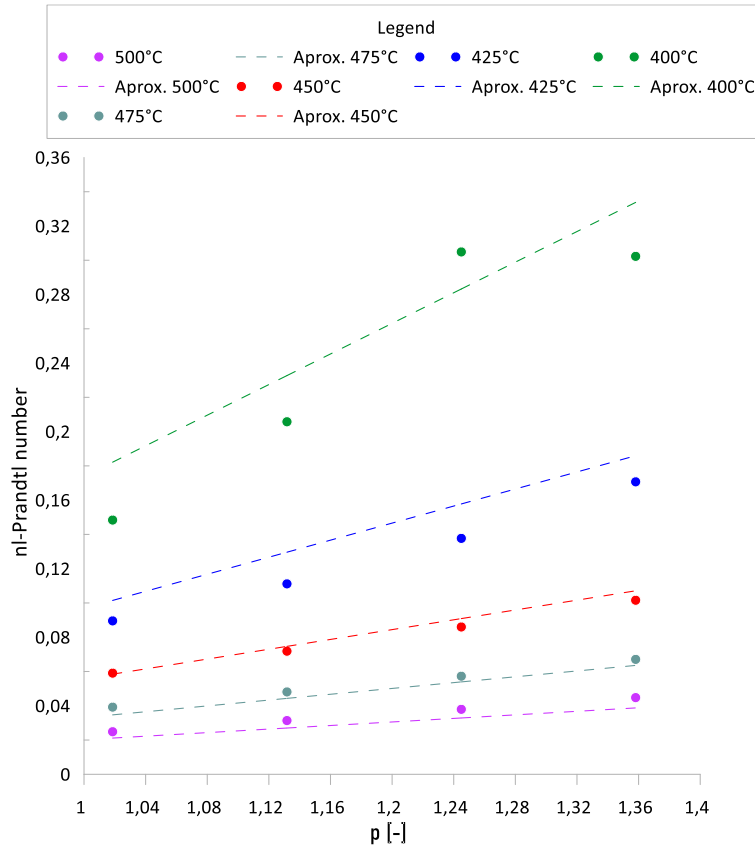
This splitting makes the approximation possible.

Figure 6.58 – Approximation of nl-Prandtl number as a function of temperature and pressure.



Beaton (1986) in his work demonstrates Prandtl number behavior varying with temperature above critical temperature.

Figure 6.60 – Approximation of nI-Prandtl number as a function of dimensionless pressure.



The interfacing technique is the same that showed in others part of this work, we start with both equations that we want to link and the derivative of each one, however assuming a linear approximation of pressure-dependent factor.

The Prandtl number approximation above critical point.

$$\overline{\text{Pr}}_{v_c}(p, \tau) = (a_c + b_c p) \cdot (c_c \tau^{d_c}) \quad (6.112)$$

$$\frac{d(\overline{\text{Pr}}_{v_c}(\tau))}{d(\tau)} = (a_c + b_c p) \cdot (c_c d_c \tau^{-1+d_c}) \quad (6.113)$$

As usual, a third-degree polynomial function is used for the interfacing:

$$\overline{\text{Pr}}_{v_{bc}}(\tau, p) = a_{BC}(p) + b_{BC}(p)\tau + c_{BC}(p)\tau^2 + d_{BC}(p)\tau^3 \quad (6.114)$$

Points of tangency can be defined optimizing the approximation result. In this case $\Delta\tau$ defines how far each point is departs from the critical point, ($\tau=1$).

$$\begin{aligned}\Delta\tau_3 &= 0.003; \\ \Delta\tau_4 &= 0.06913 \\ \tau_3 &= 1 - \Delta\tau_3 = 0.997 \\ \tau_4 &= 1 - \Delta\tau_4 = 1.06913\end{aligned}\tag{6.115}$$

The system has the following format to the interfacing equation tangency when both curves make a continuous smooth link. Note, the coefficients a_{bc} , b_{bc} , c_{bc} and d_{bc} become functions of pressure.

$$\left\{\begin{array}{l} \overline{\text{Pr}}_{vc}(\tau_3, p) = a_{BC}(p) + b_{BC}(p)\tau_3 + c_{BC}(p)\tau_3^2 + d_{BC}(p)\tau_3^3 \\ \frac{d(\overline{\text{Pr}}_{vc}(\tau_3, p))}{d(\tau_3)} = b_{BC}(p) + 2c_{BC}(p)\tau_3 + 3d_{BC}(p)\tau_3^2 \\ \overline{\text{Pr}}_{vc}(\tau_4, p) = a_{BC}(p) + b_{BC}(p)\tau_4 + c_{BC}(p)\tau_4^2 + d_{BC}(p)\tau_4^3 \\ \frac{d(\overline{\text{Pr}}_{vc}(\tau_4, p))}{d(\tau_4)} = b_{BC}(p) + 2c_{BC}(p)\tau_4 + 3d_{BC}(p)\tau_4^2 \end{array}\right.\tag{6.116}$$

Solving the system above for selected pressure magnitude, the parameters have the following values.

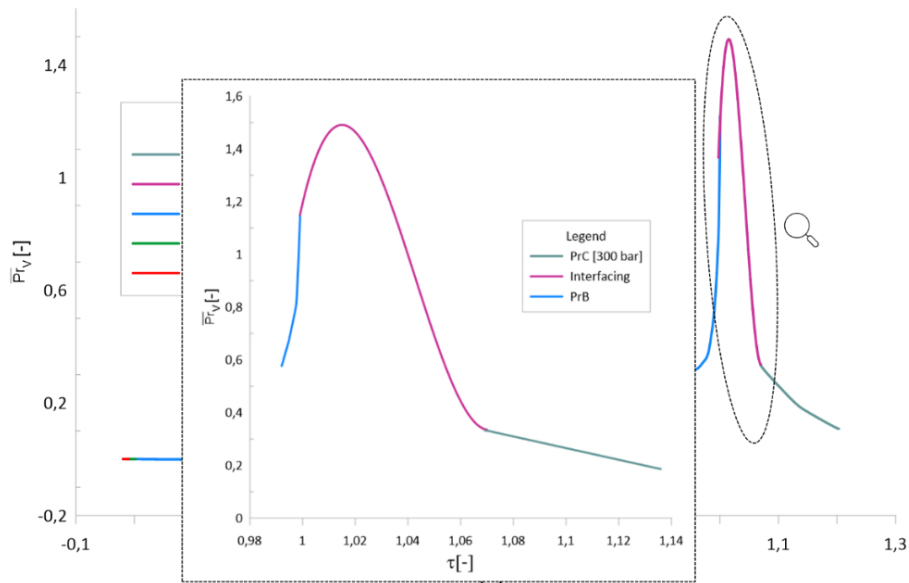
$$\left\{\begin{array}{l} a_{BC} = -16436.9 \\ b_{BC} = 47403.55 \\ c_{BC} = -45534.70 \\ d_{BC} = 14569.33 \end{array}\right.\tag{6.117}$$

Below, a solution of the system of interfacing equation (6.108) is presented. Since the method of solving is the same, with the only change being the pressure dependence, we set a particular pressure value as an example.

These coefficients were obtained for a particular value of the pressure: $p=1.3581$.

Figure 6.61 shows the result of the approximation.

Figure 6.61 – Interfacing Prandtl number example to P=300 [bar] or p[-]=1.3581.



The pressure value can be calculated from the known charging density.

6.6.4 Final approximation and pseudo code

The result above summarizes the approximations including the interfacing between subcooled zone and saturated zone. It also includes saturation zone and a part with the link between the saturated zone and supercritical zone. The last interfacing polynomial equation depends on two variables, dimensionless temperature, and dimensionless pressure, Figure 6.63 exposes a consistent result.

Figure 6.62 – Final Result to Prandtl number approximation in the entire temperature and pressure range.

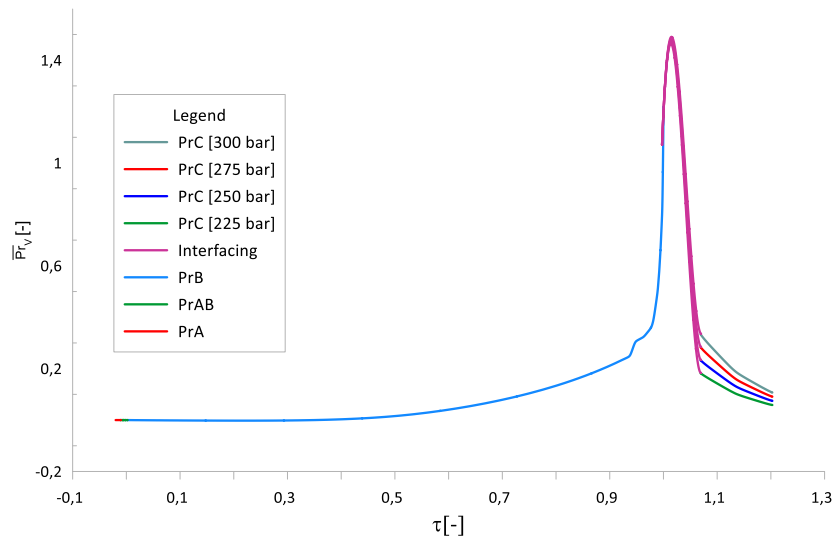
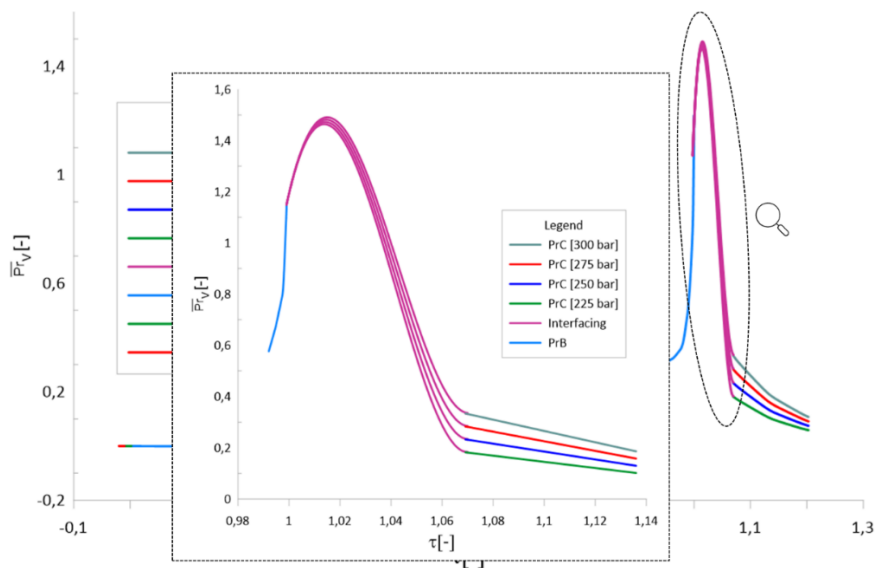


Figure 6.63 shows interfacing nl-Prandtl number linking saturated zone with supercritical zone under different values of pressure.

Figure 6.63 – Interfacing nl Prandtl number around critical temperature.



Final approximations over all three zones are shown below in Equation (6.118) as a pseudo-code.

$$\left\{ \begin{array}{ll} \text{if } (\tau \leq \tau_1) & \text{then } \overline{\text{Pr}}_v(\tau) = 0 \\ \text{if } (\tau_1 \leq \tau \leq \tau_2) & \text{then } \overline{\text{Pr}}_v(\tau) = a_{AB} + b_{AB}\tau + c_{AB}\tau^2 + d_{AB}\tau^3 \\ \text{if } (\tau_2 \leq \tau \leq \tau_3) & \text{then } \overline{\text{Pr}}_v(\tau) = y_1(\tau) + \chi(\tau - \tau_{H1})y_2(\tau) + \chi(\tau - \tau_{H2})y_3(\tau) \\ \text{if } (\tau_3 < \tau < \tau_4) & \text{then } \overline{\text{Pr}}_v(\tau) = a_{BC} + b_{BC}\tau + c_{BC}\tau^2 + d_{BC}\tau^3 \\ \text{if } (\tau \geq \tau_4) & \text{then } \overline{\text{Pr}}_v(p, \tau) = (a_C + b_C p) \cdot (c_C \tau^{d_C}) \end{array} \right. \quad (6.118)$$

Table 6.7 –vapor Prandtl number pseudo-code values.

$a_{AB} = -3.5E-5$	$c_B = 0.0770$	$i_B = 8.252$	$c_C = 0.5397$	$\Delta\tau_1 = 0.01$
$b_{AB} = -0.199$	$d_B = -0.3076$	$j_B = 0.045$	$d_C = -9.51$	$\Delta\tau_2 = 0.003$
$c_{AB} = -3.08$	$e_B = 0.7142$	$\tau_{HB1} = 0.50$	$a_{BC}(p) = 3915,7p - 27960$	$\Delta\tau_3 = 0.003$
$d_{AB} = -139.0$	$f_B = 1.41$	$\tau_{HB2} = 0.93$	$b_{BC}(p) = -11406p + 80662$	$\Delta\tau_4 = 0.06913$
$a_B = -3.0E-5$	$g_B = 3.00$	$a_C = -0.966$	$c_{BC}(p) = 11064p - 77511$	
$b_B = -0.0199$	$h_B = 2.0E-9$	$b_C = 1.580$	$d_{BC}(p) = -3574,3p + 24811$	

To return to original Prandtl number from the obtained approximations, the inverse expression must be used:

$$\text{Pr}_v(T) = \text{Pr}_v(T_3) + \text{aprx}(\overline{\text{Pr}}_v(\tau))(\text{Pr}_v(T_{cr}) - \text{Pr}_v(T_3)) \quad (6.119)$$

6.7 Approximations for liquid density

6.7.1 Approximations for saturated zone

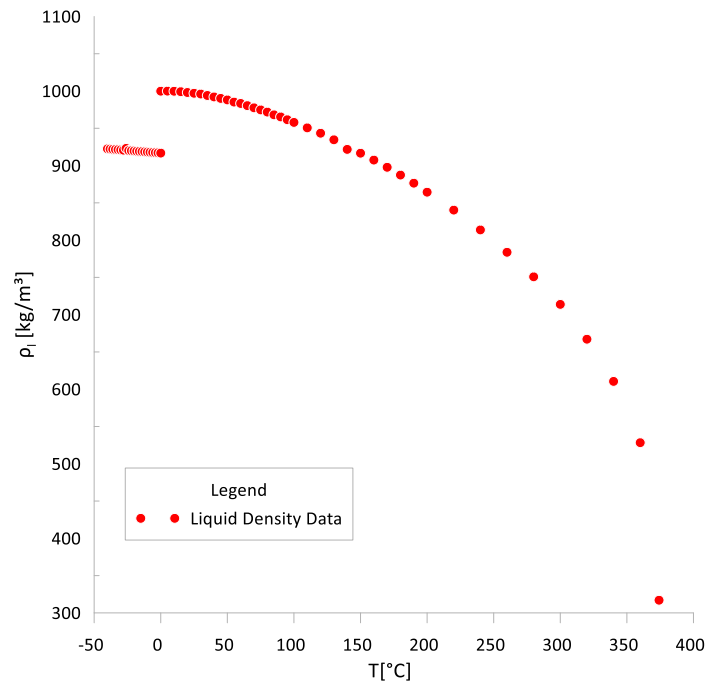
Liquid density (ρ_L) is defined as a relation between liquid mass (m) and volume (V) of that mass occupies:

$$\rho_L = \frac{m}{V} \quad (6.120)$$

where m is in kg, V is in m^3 and ρ is in kg/m^3 .

Liquid density behavior with temperature data, published by ASHRAE are presented in Figure 6.64 (LEMMON et al., 2023).

Figure 6.64 – Water liquid density data.



The data covers freezing and saturated temperature regions.

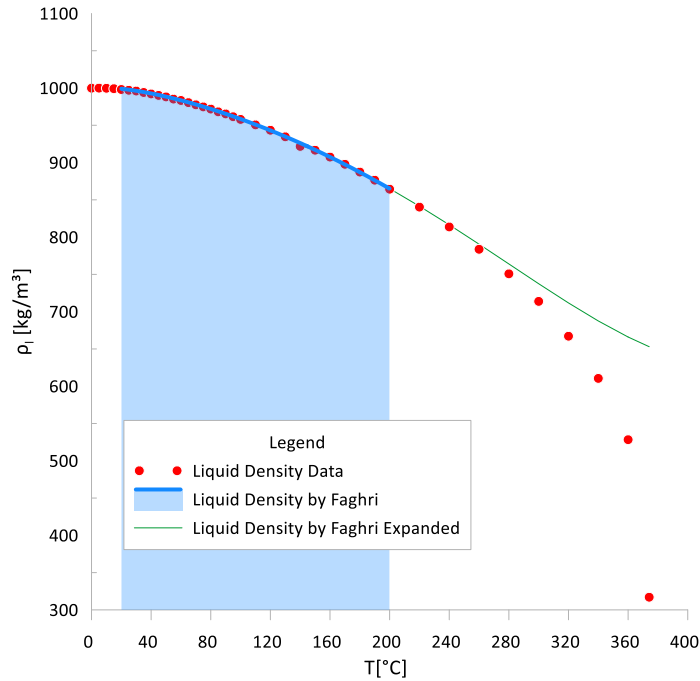
In HP modeling the approximations presented by Faghri (2016) are widely used. He suggested equation to approximate this water property by 5-order polynomial function (6.121), applied to the logarithm of the density.

$$\begin{aligned} \ln(\rho_l(T)) = & 6.9094 - 2.0146 \cdot 10^{-5} \cdot T - 5.9868 \cdot 10^{-6} \cdot T^2 + \\ & 2.5921 \cdot 10^{-8} \cdot T^3 - 9.3244 \cdot 10^{-11} \cdot T^4 + 1.2103 \cdot 10^{-13} \cdot T^5 \end{aligned} \quad (6.121)$$

The liquid density is expressed in kg/m³, and the temperature is in Celsius. For other unities, the polynomial coefficients must be redefined.

This equation is valid between 20°C and 200°C; in this range of temperature the approximation error mentioned in (FAGHRI, 2016) is 0.03% and the equation covers up to 48% of the entire two-phase temperature range. However, when we try to use this polynomial equation out of range established, the result can deviate from real behavior. The green line in Figure 6.65 expresses this deviation from real value.

Figure 6.65 – Faghri polynomial approximation.



Following the same approach, we expand the approximation over entire range for liquid density. Non-dimensional variables are used for both temperature and liquid density:

$$\bar{\rho}_l(\tau) = \frac{\rho_l - \rho_{l_3}}{\rho_{l_{cr}} - \rho_{l_3}} \quad (6.122)$$

For the saturation interval (i.e., two-phase zone, $0 < \tau < 1$), the original curve has a sharp climb as it approaches the critical temperature. It is difficult to obtain a unique function which approximates the entire zone within acceptable error: therefore, we will improve it with application of an interruption point (τ_H) and join two approximation functions in the interval $\tau_H \leq \tau < 1$ by application of Heaviside function.

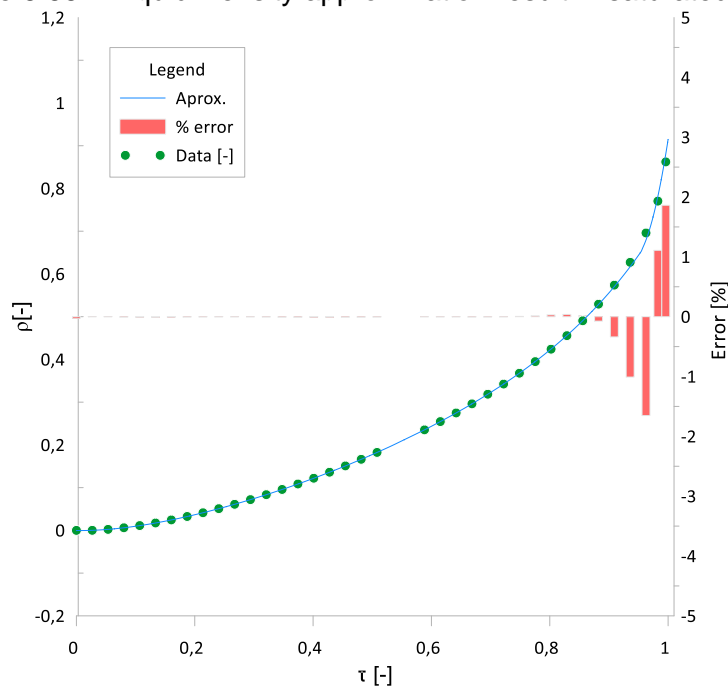
The best results gave the following approximate functions:

$$\begin{cases} y_1 = a_B + b_B \tau + c_B \tau^2 + d_B \tau^3 + e_B \tau^4 + f_B \tau^5 + g_B \tau^6 \\ y_2 = h_B (\tau - \tau_H)^{i_B} \end{cases} \quad (6.123)$$

$$\bar{\rho}_l(\tau) = y_1(\tau) + \chi(\tau_H)y_2(\tau) \quad (6.124)$$

By applying this technique, in the saturation interval of temperature we achieve the curve shown in Figure 6.66. The chart shows data from ASHRAE using green circles. The approximation results are given in the blue line. In red bars we have the deviation error from property table data and approximation.

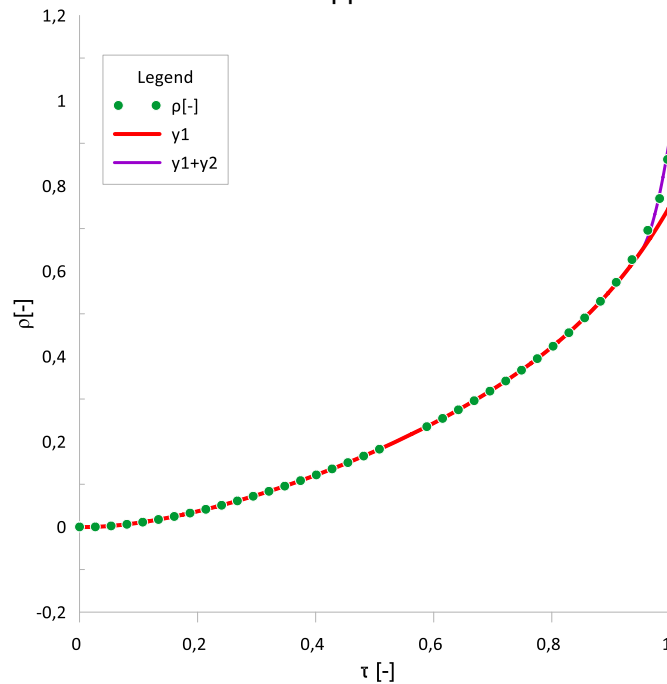
Figure 6.66 – Liquid Density approximation result in saturated zone.



We observe the deviation from data by approximation lies within the acceptance criteria in 2% of deviation from the properties table data.

To build this property approximation we used a baseline curve (fourth degree polynomial equation), and we add in these curves one that satisfies the condition of smooth transition using Heaviside function. The result is shown in Figure 6.67. The main motive to use this technique is reach and approximation curve continuous and “smooth,” without sharp edges.

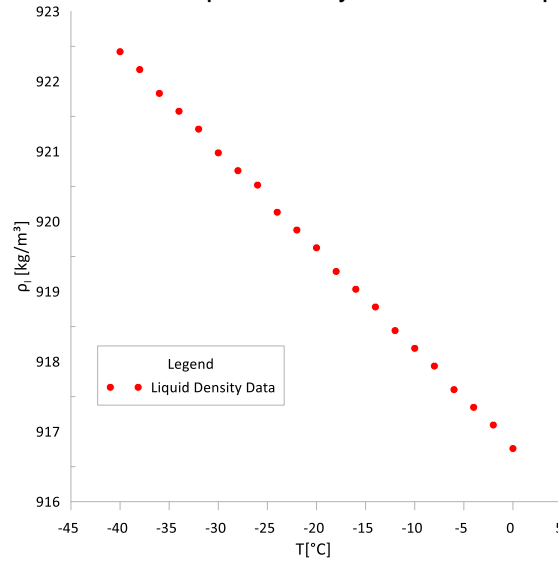
Figure 6.67 – Two- functions approximation for saturated zone.



6.7.2 Approximations for freezing zone

Under negative temperatures water turns into ice, and at positive temperatures it melts. Such behavior is typical for freezing HP start-up, therefore we continue referring ice as liquid in the freezing zone, Liquid density behavior with temperature data, published by ASHRAE Lemmon et al. (2023), are presented in Figure 6.64, and a closer look for the freezing zone (ice) is shown in Figure 6.68, where Turns et al. (2007) compiled in their book a liquid density behavior in freezing zone. In that case, the temperature ranges from -40 °C to 0°C.

Figure 6.68 – Water liquid density data before triple point.



The approximation must include a region below the freezing point (i.e., triple point), so for freezing zone the density is approximated very well by linear function:

$$\bar{\rho}_{l_A}(\tau)\Big|_{\tau < 0} = a_A + b_A \tau \quad (6.125)$$

The interfacing equation joints subcooled zone with saturated zone. as usual, we use a third-degree polynomial function (6.126).

$$\bar{\rho}_{l_A}(\tau) = a_{AB} + b_{AB} \tau + c_{AB} \tau^2 + d_{AB} \tau^3 \quad (6.126)$$

Choosing the third order polynomial functions is beneficial because here we have 4 unknown coefficients and 4 conditions for smooth interfacing: the equality of derivatives and values on both ends of the interface curve.

The system will be of the following format to the interface equation tangency both curves and makes a continuous smooth link.

$$\left\{ \begin{array}{l} \bar{\rho}_{l_A}(\tau_1) = a_{AB} + b_{AB}\tau_1 + c_{AB}\tau_1^2 + d_{AB}\tau_1^3 \\ \frac{d(\bar{\rho}_{l_A}(\tau_1))}{d(\tau_1)} = b_{AB} + 2c_{AB}\tau_1 + 3d_{AB}\tau_1^2 \\ \bar{\rho}_{l_B}(\tau_2) = a_{AB} + b_{AB}\tau_2 + c_{AB}\tau_2^2 + d_{AB}\tau_2^3 \\ \frac{d(\bar{\rho}_{l_B}(\tau_2))}{d(\tau_2)} = b_{AB} + 2c_{AB}\tau_2 + 3d_{AB}\tau_2^2 \end{array} \right. \quad (6.127)$$

Points of tangency can be defined by trying to optimize the approximation result. In this case Δt defines how far each point will be away from the other

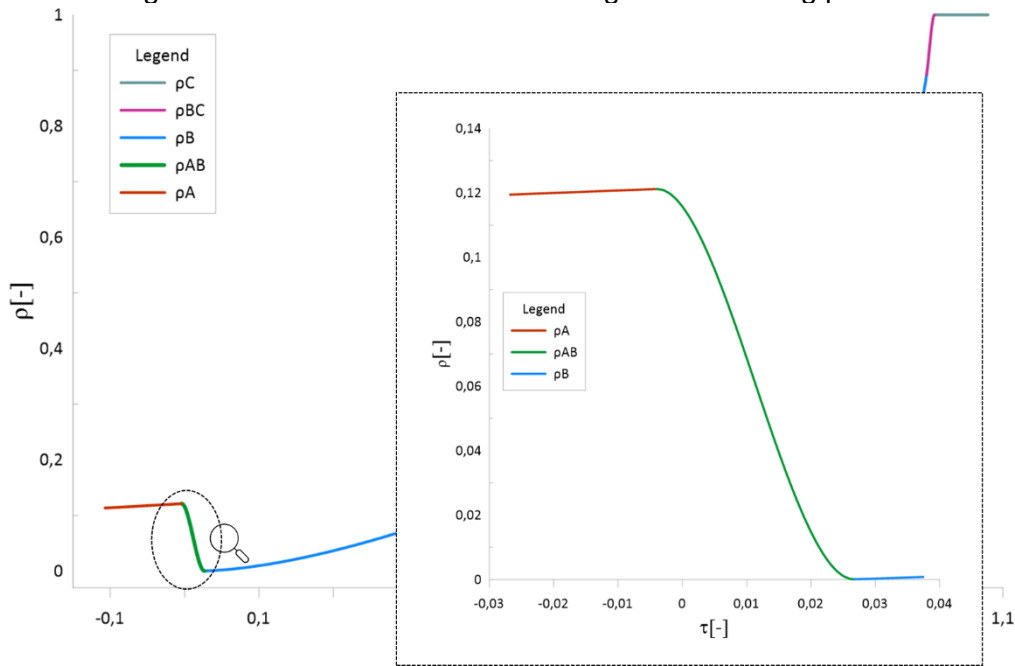
$$\left\{ \begin{array}{l} \Delta\tau_1 = 0.004; \\ \Delta\tau_2 = 0.0267; \\ \tau_1 = -\Delta\tau_1 \\ \tau_2 = +\Delta\tau_2 \end{array} \right. \quad (6.128)$$

The results are expressed below.

$$\left\{ \begin{array}{l} a_{AB} = 0.115772 \\ b_{AB} = -2.65106 \\ c_{AB} = -289.963 \\ d_{AB} = 8503.355 \end{array} \right. \quad (6.129)$$

The result approximations around triple point ($\tau=0$), including the interfacial curve, is presented in Figure 6.69.

Figure 6.69 – Final result to interfacing below freezing point.



6.7.3 Approximations for super critical zone

Just to remember the definitions, the critical point is where vapor and liquid are indistinguishable and triple point is where liquid phase (water), solid phase (ice) and vapor phase coexist in thermodynamic equilibrium.

As discussed in the introduction, for isochoric systems the density above the critical temperature is always constant and for HP is equal to the “charged density.”

$$\bar{\rho}_l \Big|_{T \geq T_{cr}} = \bar{\rho}_{ch} \quad (6.130)$$

The zone above the critical point corresponds to the situation of no vapor-liquid interface existence. i.e., only one unique phase exists denoted here as “gas.” Therefore, we have a transition from liquid phase to the gas phase at the critical temperature.

The interface conditions are the continuity of the values and derivatives in the interrupting points (interface between curves), used to guarantee that the interfacing technique provides perfect softening in the conjugate points.

The interfacing technique is the same that showed in others part of this work, we start with both equation that we want to link and the derivate of each one.

As said above, the properties values above the critical point are charged density constant value. Those can be expressed below:

$$\bar{\rho}_{l_c}(\tau)\Big|_{\tau>1} = \bar{\rho}_{ch} \quad \frac{d(\bar{\rho}_{l_c}(\tau))}{d(\tau)}\Big|_{\tau>1} = 0 \quad (6.131)$$

Looking for a smooth transition between those two zones Equations (6.124) and (6.131), it is used a third-degree polynomial Equation (6.132).

$$\bar{\rho}_{l_{BC}}(\tau) = a_{BC} + b_{BC}\tau + c_{BC}\tau^2 + d_{BC}\tau^3 \quad (6.132)$$

Parameters of the points of tangency at ($\tau=1$) have been selected as following:

$$\begin{aligned} \Delta\tau_3 &= 0.003; \\ \Delta\tau_4 &= 0.008; \\ \tau_3 &= 1 - \Delta\tau_3 = 0.997 \\ \tau_4 &= 1 - \Delta\tau_4 = 1.008 \end{aligned} \quad (6.133)$$

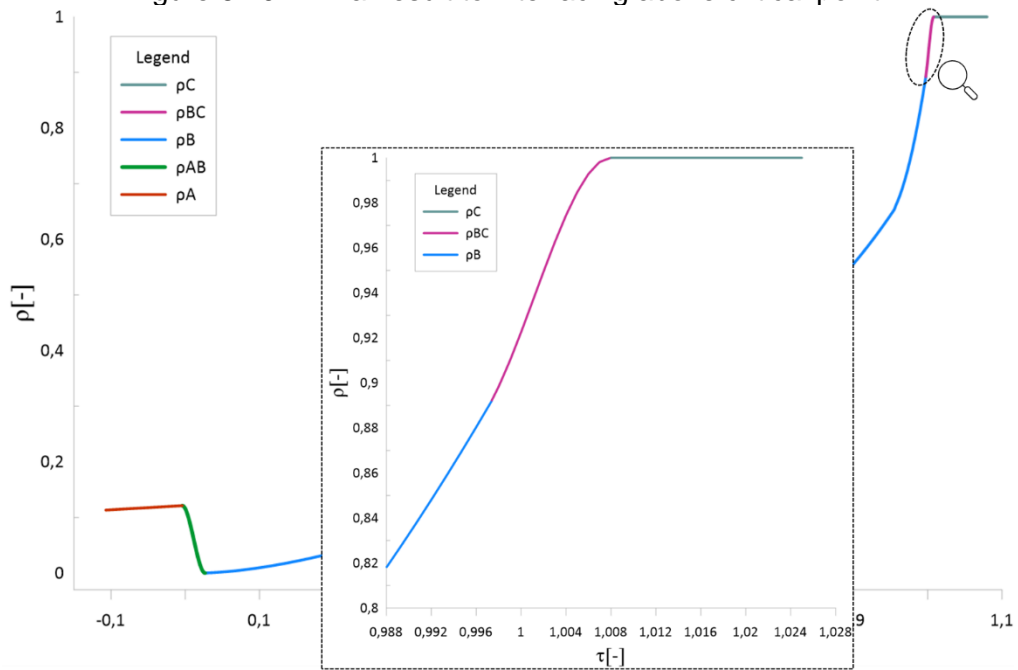
The system of the smooth interfacing conditions is the same as for other properties (Equation 6.52) and does not present here.

The solution for the parameter's values for the interfacing curve, obtained from available analytical solution (Equations 5.29 and 5.32) are presented in (6.134).

$$\begin{cases} a_{BC} = 97196.14 \\ b_{BC} = -291272 \\ c_{BC} = 2909447 \\ d_{BC} = -96868.2 \end{cases} \quad (6.134)$$

Figure 6.70 shows the result of the approximation for this case, then $\bar{\rho}_{ch} = 1$.

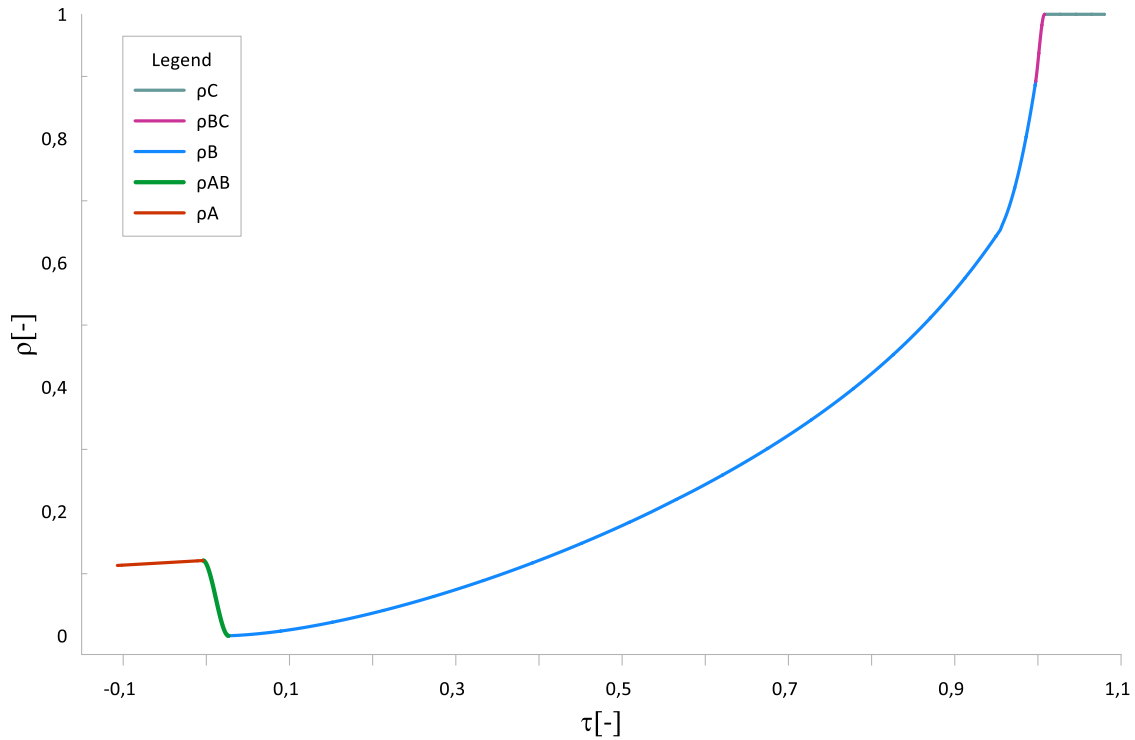
Figure 6.70 – Final result to interfacing above critical point.



6.7.4 Final approximation and pseudo code

The algorithm below that we proposed for the approximation of the entire region is shown in Equation (6.135) as a pseudo code.

Figure 6.71 – Final result for liquid density approximation over entire temperature range.



Therefore, in this chapter we reached an approximation in a wide range of temperature, managing the approximation error in satisfactory levels (no greater than 5%). The pseudo code provides fluid property values starting below the triple point up to beyond critical point.

This code can be implemented in any programming language for use in mathematical models of heat pipes:

$$\left\{ \begin{array}{ll} \text{if } (\tau \leq \tau_1) & \text{then } \bar{\rho}_l(\tau) = a_A + b_A \tau \\ \text{if } (\tau_1 < \tau < \tau_2) & \text{then } \bar{\rho}_l(\tau) = a_{AB} + b_{AB} \tau + c_{AB} \tau^2 + d_{AB} \tau^3 \\ \text{if } (\tau_2 \leq \tau \leq \tau_3) & \text{then } \bar{\rho}_l(\tau) = y_1(\tau) + \chi(\tau_{H1}) y_2(\tau) \\ \text{if } (\tau_3 < \tau < \tau_4) & \text{then } \bar{\rho}_l(\tau) = a_{BC} + b_{BC} \tau + c_{BC} \tau^2 + d_{BC} \tau^3 \\ \text{if } (\tau \geq \tau_4) & \text{then } \bar{\rho}_l(\tau) = \bar{\rho}_{ch} \end{array} \right. \quad (6.135)$$

Table 6.8 – Result algorithm values for the case of $\bar{\rho}_{ch} = 1$.

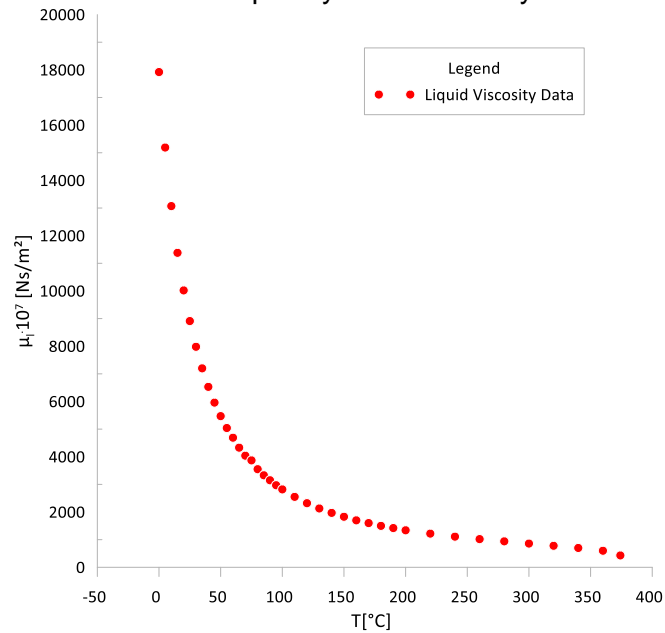
$a_A = 1.22E-01$	$b_B = -2.21E-2$	$i_B = 2$	$\Delta\tau_2 = 2.67E-2$
$b_A = 7.68E-02$	$c_B = 1.4836$	$\tau_{H1} = 0.95$	$\Delta\tau_3 = 5E-3$
$a_{AB} = 1,158E-01$	$d_B = -3.152$	$a_{BC} = 9.72E4$	$\Delta\tau_4 = 8E-3$
$b_{AB} = -2,651$	$e_B = 5.386$	$b_{BC} = -2.913E5$	
$c_{AB} = -2,90E+02$	$f_B = -5.046$	$c_{BC} = 2.909E5$	
$d_{AB} = 8,503E+03$	$g_B = 2.103$	$d_{BC} = -9.687E4$	
$a_B = -2.8E-4$	$h_B = 6.5E1$	$\Delta\tau_1 = 3E-3$	

6.8 Approximations for liquid dynamic viscosity

6.8.1 Approximations for saturated zone

Liquid dynamic viscosity (μ) can be defined as a relation between shear stress and the fluid deformation velocity. This property is essential to set a way as flow is shaped. Therefore, this property is responsible for the fluid interface force between its layers or other fluid or solid surfaces in contact with that flow. (TUREKIAN; HOLLAND, 2014). American Society of Heating, Refrigerating and Air-Conditioning Engineers (ASHRAE) conveyed water data (LEMMON et al., 2023). The original data of the liquid dynamic viscosity behavior with temperature are presented in Figure 6.72.

Figure 6.72 – Water liquid dynamic viscosity number data.



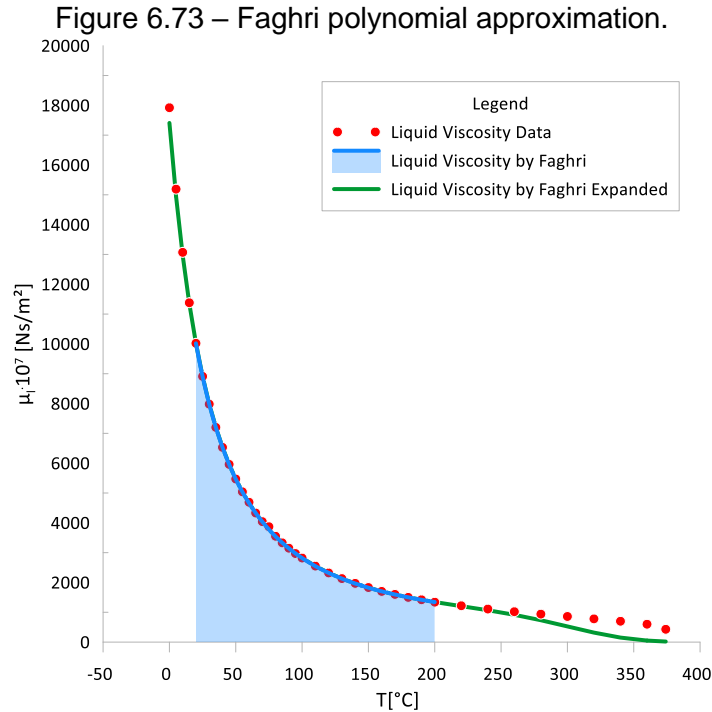
Faghri (2016) suggested the Equation (6.136) to approximate this water property, where the dynamic viscosity is expressed in N·s/m² and the temperature used in equation below in in Celsius.

$$\begin{aligned} \ln(\mu_l(T)) = & -6.3530 - 3.154 \cdot 10^{-2} \cdot T + 2.167 \cdot 10^{-4} \cdot T^2 - \\ & 1.156 \cdot 10^{-6} \cdot T^3 + 3.747 \cdot 10^{-9} \cdot T^4 - 5.219 \cdot 10^{-12} \cdot T^5 \end{aligned} \quad (6.136)$$

It is worth mentioning once again, that this kind of approximation, widely used by other authors, has dimensional numerical coefficients (also known as factors), that is not correct from the point of view of a mathematician. For example, one must keep in mind that the number -6.3530 has dimension ln(Pa·s), but -5.219 · 10⁻¹² has dimension of ln(Pa·s)/C⁵ and, by the way, not ln(Pa·s)/K⁵. Moreover, researchers in UK or USA may not feel comfortable with these coefficients once they use Imperial units instead of SI; another approximation with different coefficients should be elaborated for them.

This equation is valid from 20°C to 200°C; with because the approximation error 0.03% mentioned in (FAGHRI, 2016). The equation covers up to 48% of the entire

two-phase temperature range; out of the range the equation diverges from the experimental tabled data, as shown in Figure 6.73.



Following the same approach to elaborate the approximation over entire two-phase range, from the triple point to the critical point, we use non-dimensional variables for both temperature and liquid dynamic viscosity:

$$\bar{\mu}_l(\tau) = \frac{\mu - \mu_{l_3}}{\mu_{l_{CR}} - \mu_{l_3}} \quad (6.137)$$

For the saturation interval (i.e., two-phase zone, $0 < \tau < 1$), it is difficult to obtain a unique function which approximates the entire zone with acceptable error. Therefore, it was decided to insert one or few interruption points (τ_{Hi}) and join the approximation piece-wise functions by one-by-one by either addition or substitution with the use of Heaviside function.

The best results yielded the following approximation functions:

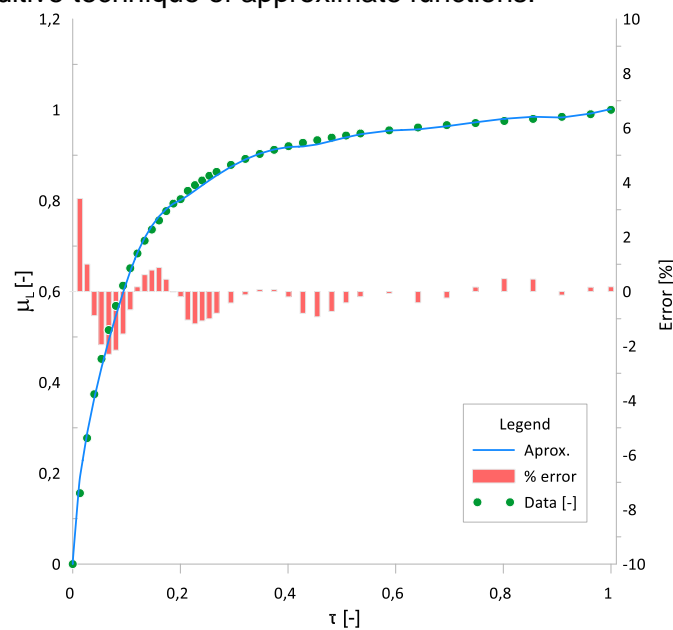
$$\begin{cases} y_1 = b_B \left(1 - \frac{(\tau - c_B)^2}{a_B^2} \right)^{d_B} \\ y_2 = e_B \operatorname{Senh}(\tau - \tau_{H1})^{f_B} \\ y_3 = g_B (\tau - \tau_{H2})^{h_B} \\ y_4 = i_B \operatorname{Senh}(\tau - \tau_{H3})^{j_B} \\ y_5 = k_B \operatorname{Senh}(\tau - \tau_{H4})^{l_B} \\ y_6 = m_B (\tau - \tau_{H5})^{n_B} \end{cases} \quad (6.138)$$

These functions are used in an additive way:

$$\begin{aligned} \mu_l(\tau) = & y_1(\tau) - \chi(\tau - \tau_{H1})y_2(\tau) + \chi(\tau - \tau_{H2})y_3(\tau) + \\ & + \chi(\tau - \tau_{H3})y_4(\tau) + \chi(\tau - \tau_{H4})y_5(\tau) + \chi(\tau - \tau_{H5})y_6(\tau) \end{aligned} \quad (6.139)$$

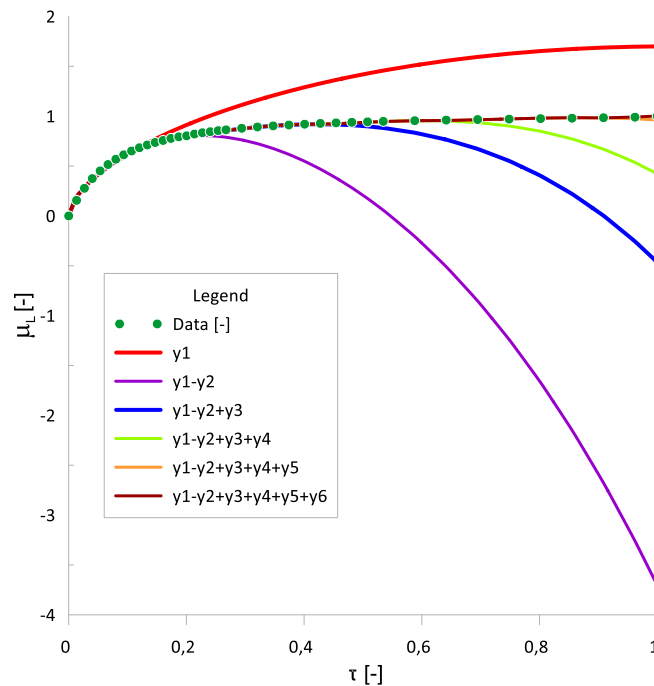
Applying the algorithm above, in the saturation interval of temperature the curve on Figure 6.74 was achieved. The graph shows data from ASHRAE using green circles (LEMMON et al., 2023). The approximation result is shown in the blue line. In red bars we have the deviation error between experimental property table data and the approximation.

Figure 6.74 – Liquid Dynamic Viscosity approximation result in saturated zone using additive technique of approximate functions.



The additive technique of approximate functions, applied step by step, is illustrated in Figure 6.75.

Figure 6.75 – Approximation for saturated zone using additive technique of piece-wise functions.



The conjugate points are $\tau_{H1}=0.11$; $\tau_{H2}=0.20$; $\tau_{H3}=0.43$; $\tau_{H4}=0.60$; $\tau_{H5}=0.91$.

Next, we perform here another approach to do approximation in the same two-phase zone, using substitution of approximate functions instead of addition.

To join two non-linear functions, an intermediate polynomial function must be used. The smoothing (or continuation) conditions should be applied from both sides of this intermediate functions, in the points τ_{H1} and τ_{H2} , having four equations to solve. When the intermediate polynomial function is of third order, having 4 coefficients, the solution is easy and direct.

The best results provide the following combination of two non-linear approximate functions with the intermediate polynomial function of 3rd order:

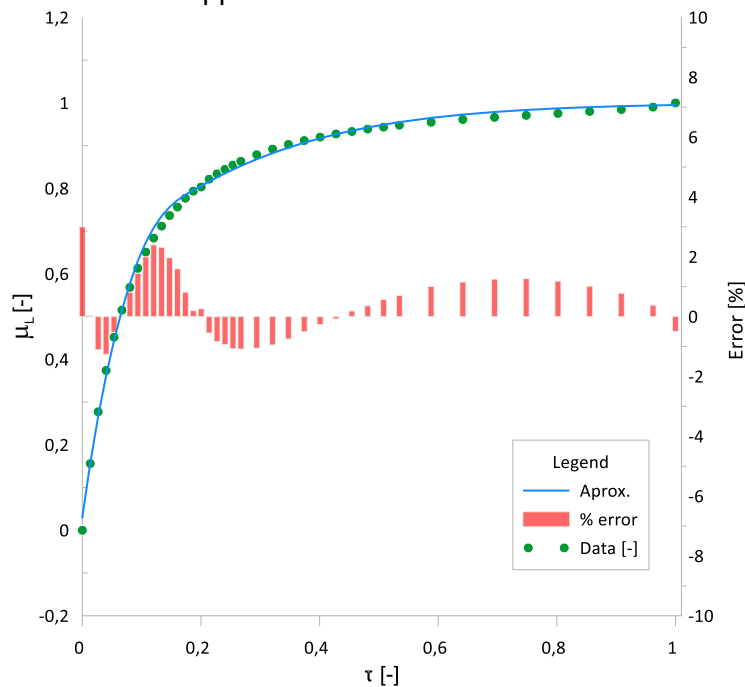
$$\begin{cases} y_1 = a_B - b_B e^{-c_B \tau} \\ y_i = d_B + e_B \tau + f_B \tau^2 + g_B \tau^3 \\ y_2 = \frac{1}{2} \left(1 + \text{Tanh}^{j_B} (h_B (\tau - i_B)) \right) \end{cases} \quad (6.140)$$

These functions are used in substitution way: if $0 < \tau \leq \tau_{H1}$, then $y=y_1$; if $\tau_{H1} < \tau \leq \tau_{H2}$, then $y(\tau)=y_i(\tau)$; if $\tau_{H1} < \tau \leq 1$, then $y(\tau)=y_2(\tau)$. This can be condensed in a unique correlation for our property:

$$\mu_l(\tau) = \chi^{-1}(\tau - \tau_{H1}) y_1(\tau) + \chi(\tau - \tau_{H1}) \chi^{-1}(\tau - \tau_{H2}) y_i(\tau) + \chi(\tau - \tau_{H2}) y_2(\tau) \quad (6.141)$$

The result approximation is shown in Figure 6.76.

Figure 6.76 – Liquid Dynamic Viscosity approximation result in saturated zone using substitution of approximate functions.

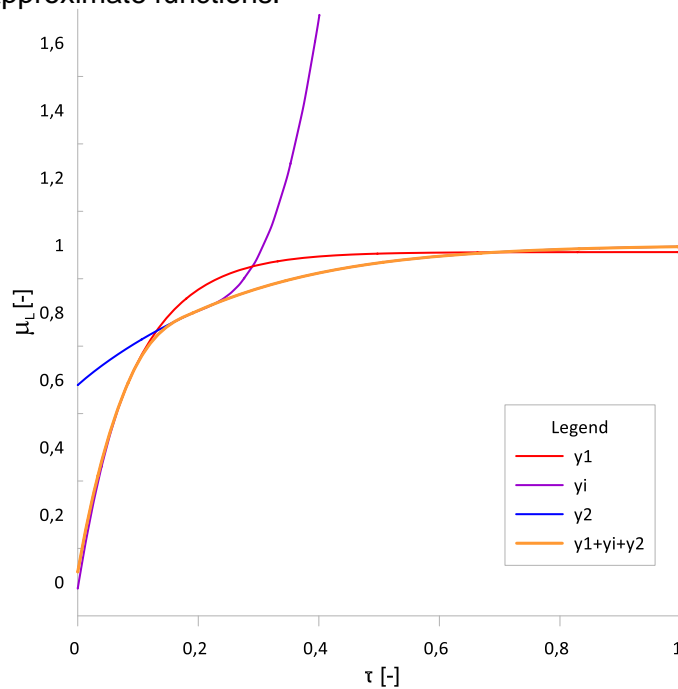


The deviation from data by approximation lies within the usual acceptance criteria in 2% of deviation from the properties table data.

Figure 6.77 shows the components used in the approximation as each contributes to the result. The main reason to use this technique is to reach a

continuous and “smooth” approximation curve, without visible undulation and interruptions.

Figure 6.77 – Components adding used in the approximation using substitution of approximate functions.



The conjugate points are $\tau_{Hi1}=0.084$; $\tau_{Hi2}=0.19$.

For this property, the approach by substitution was used to build the approximation over the entire two-phase zone, with application of two of Heaviside functions to create a curve without ripples.

Basically, this approach consists of creating of two or more curves which correctly describe the property variation within limited intervals and then joint these curves with a fourth-degree polynomial equation.

The addition technique has an intrinsic undesirable effect , when each interruption point, added into the curve, brings an unwelcome side effect that is a local oscillation affecting the error in a local region; this behaves are expressed in Figure 6.79. The substitution technique results in a stable curve, we use this curve to continue the study, doing interfacing between the freezing zone and the super-critical zone.

Figure 6.78 – Step by step components adding used in the approximation

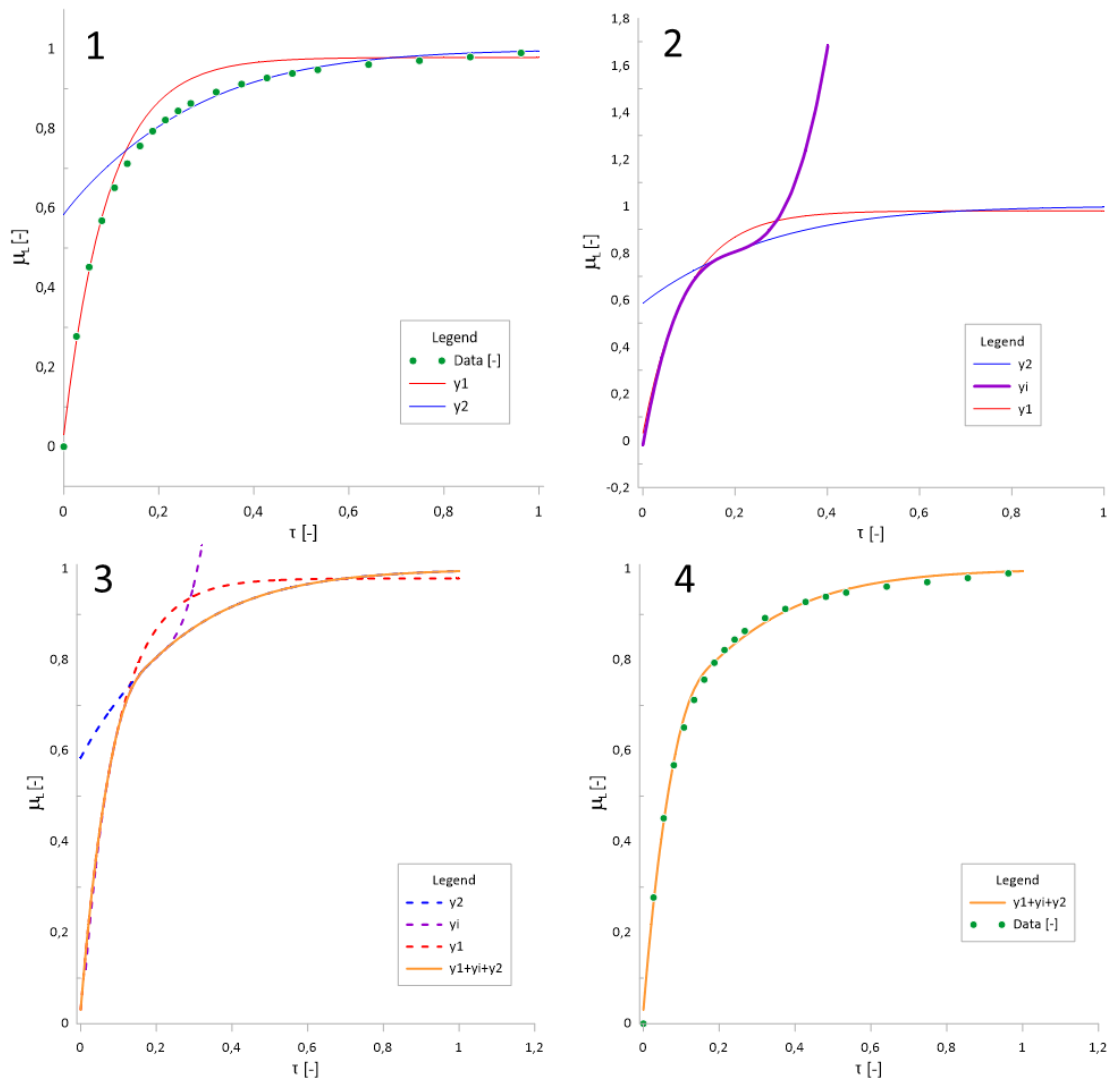
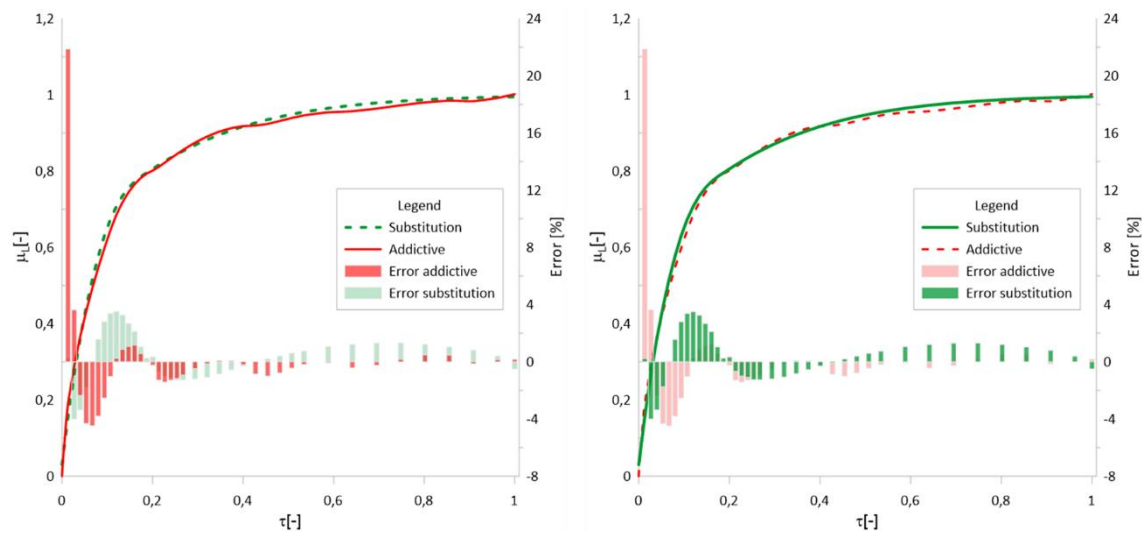


Figure 6.79 – Compare between Heaviside substitution and Heaviside addition techniques.



The comparison show that the substitution technique provide more smooth result for this property.

6.8.2 Approximations for freezing zone and interfacing

The algorithm above that we proposed for the approximation of the entire region shall also include the zones below the freezing point and above critical point.

For the interfacing with the freezing zone and super-critical zone we use the last approximation obtained by substitution technique in the two-phase zone.

A liquid, when freezing, becomes more viscous and actually turns into a solid. Kumagai et al. (1978) defined viscoelastic as a property of many solids; they flow like liquids, however very slowly, even under small stress. Such materials are best described as viscoelastic, that is, possessing both elasticity (reaction to deformation) and viscosity (reaction to rate of deformation). We assume that ice behaves as viscoelastic solid; then viscosity can be characterized through the reaction to the rate of deformation.

The viscous components can be modeled as dashpots such that the stress–strain rate relationship is given in Equation (6.142) (DAY, 1990).

$$\sigma = \eta \frac{d\varepsilon}{dt} \quad (6.142)$$

where σ is the stress (Pa), η is the viscosity (Pa·s), (similar to liquid) , and $d\varepsilon/dt$ is the time derivative of strain (1/s); ε is strain or relative deformation without units (or mm/mm).

This definition is similar to the Newton's law of viscosity, where viscosity μ is introduced as proportional factor to obtain shear stress through shear deformation or shear velocity, du/dy :

$$\tau = \mu \frac{\partial u}{\partial y} \quad (6.143)$$

This mechanical viscosity η we will consider as equivalent of freezing liquid viscosity μ . It is possible to find different values of viscosity of different ice types in diverse sources measured for different conditions. As soon as the value for ice is much higher than the viscosity for liquids, we will use a unique value presented in (SOTIN; POIRIER, 1987) as a reference to use in our interfacing on transition from liquid to solid, equal to $8.4 \cdot 10^9$ Pa s (or $8.4 \cdot 10^{12}$ mPa*s). The value is remarkably high, accounted of about twelve orders of magnitude higher than for the liquid.

$$\mu \equiv \eta = 8.4 \cdot 10^9 [Pa \cdot s] \quad (6.144)$$

Therefore, for the freezing zone we use a constant of high magnitude.

$$\bar{\mu}_{l_A}(\tau) \Big|_{\tau < 0} = -4.8 \cdot 10^{12} \quad \frac{d(\bar{\mu}_{l_A}(\tau))}{d(\tau)} \Big|_{\tau < 0} = 0 \quad (6.145)$$

Another point which deserves attention is the continuity of the values and derivatives in the interrupting points (interface between curves), to guarantee that

the interfacing technique provides a satisfying softening in the conjugate points. It is possible to check the interfacing result in Figure 6.80.

The developed interfacing joins the curves of subcooled zone (i.e., freezing region) with saturated zone.

As usual, we use a third-degree polynomial Equation (6.146) to smooth interfacing even for such different values.

$$\bar{\mu}_{l_{AB}}(\tau) = a_{AB} + b_{AB}\tau + c_{AB}\tau^2 + d_{AB}\tau^3 \quad (6.146)$$

The system owns the following format, which are conditions for tangency and continuity of both curves, which makes a continuous smooth link.

$$\left\{ \begin{array}{l} \bar{\mu}_{l_A}(\tau_1) = a_{AB} + b_{AB}\tau_1 + c_{AB}\tau_1^2 + d_{AB}\tau_1^3 \\ \frac{d(\bar{\mu}_{l_A}(\tau_1))}{d(\tau_1)} = b_{AB} + 2c_{AB}\tau_1 + 3d_{AB}\tau_1^2 \\ \bar{\mu}_{l_B}(\tau_2) = a_{AB} + b_{AB}\tau_2 + c_{AB}\tau_2^2 + d_{AB}\tau_2^3 \\ \frac{d(\bar{\mu}_{l_B}(\tau_2))}{d(\tau_2)} = b_{AB} + 2c_{AB}\tau_2 + 3d_{AB}\tau_2^2 \end{array} \right. \quad (6.147)$$

Where τ_1 and τ_2 are near-zero points from the left and from the right of the central 0 (freezing) point.

Points of tangency have been defined through optimization of the shape of the interfacing curve.

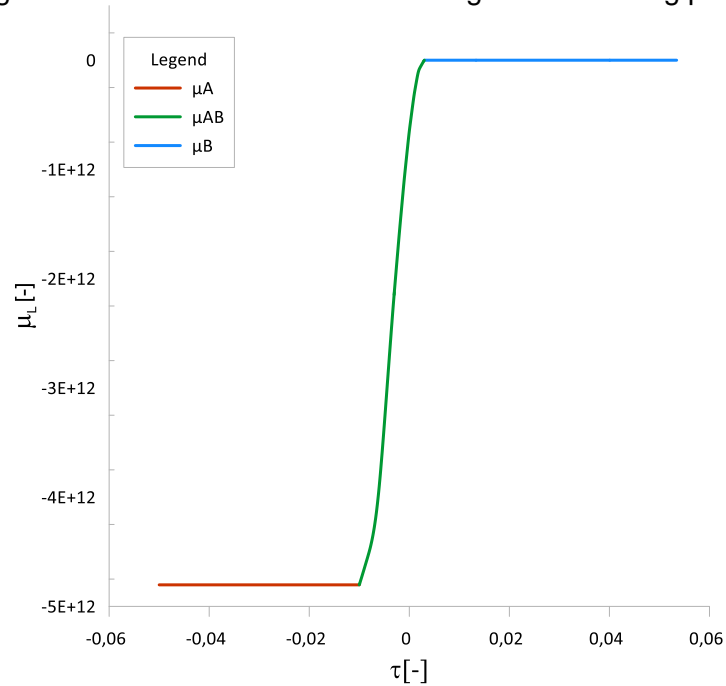
$$\begin{array}{l} \Delta\tau_1 = 0.01; \\ \Delta\tau_2 = 0.003; \\ \tau_1 = -\Delta\tau_1 \\ \tau_2 = +\Delta\tau_2 \end{array} \quad (6.148)$$

The numerical result obtained with available analytical solution for the polynomial coefficients for the interfacing around $\tau=0$ is presented below:

$$\begin{cases} a_{AB} = -6.4926 \cdot 10^{11} \\ b_{AB} = 3.9349 \cdot 10^{14} \\ c_{AB} = -4.5907 \cdot 10^{16} \\ d_{AB} = -4.3721 \cdot 10^{18} \end{cases} \quad (6.149)$$

The result approximations around triple point ($\tau=0$), including the interfacing curve, are shown in Figure 6.80.

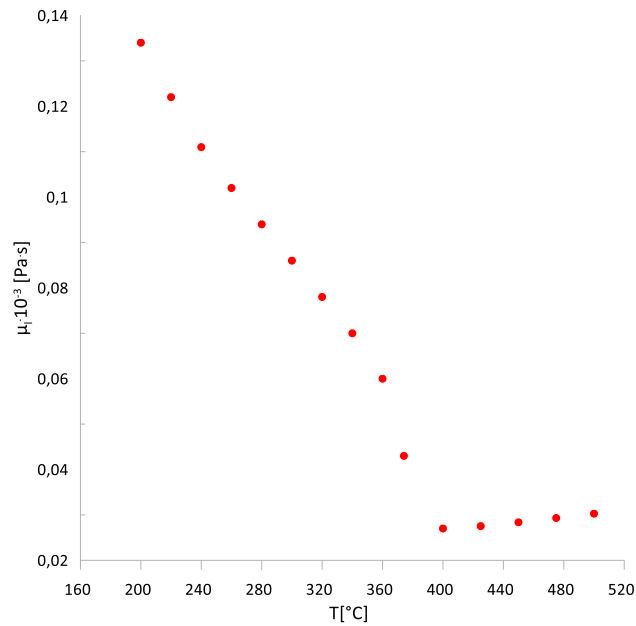
Figure 6.80 – Final Result to interfacing below freezing point.



6.8.3 Approximations for supercritical zone and interfacing

In the super-critical zone, the viscosity suffers sudden drop and then gets a light permanent increasing. Moreover, the behavior above the critical point begins having a dependence of pressure, as shown in Figure 6.81.

Figure 6.81 – Water dynamic viscosity data at critical pressure [220.64 bar].



Therefore, the property has different values at different pressure. When we consider heat pipes, it is most common case when the work pressure cannot exceed the critical value at the critical temperature. Because of that, in the super critical zone our effort will be focused on property value at 220.64 bar (critical pressure). A 2nd order polynomial function approximates the property in the super-critical region with acceptable error:

$$\bar{\mu}_{l_c}(\tau) \Big|_{\tau > 1} = (a_c + b_c \tau + c_c \tau^2) \quad (6.150)$$

For the interfacing, as usual, we use a third-degree polynomial Equation (6.151).

$$\bar{\mu}_{l_{BC}}(\tau) = a_{BC} + b_{BC} \tau + c_{BC} \tau^2 + d_{BC} \tau^3 \quad (6.151)$$

Points of tangency were obtained and shown in Equation (6.152). In this case $\Delta\tau$ defines how far each point lies away from the critical point, ($\tau=1$).

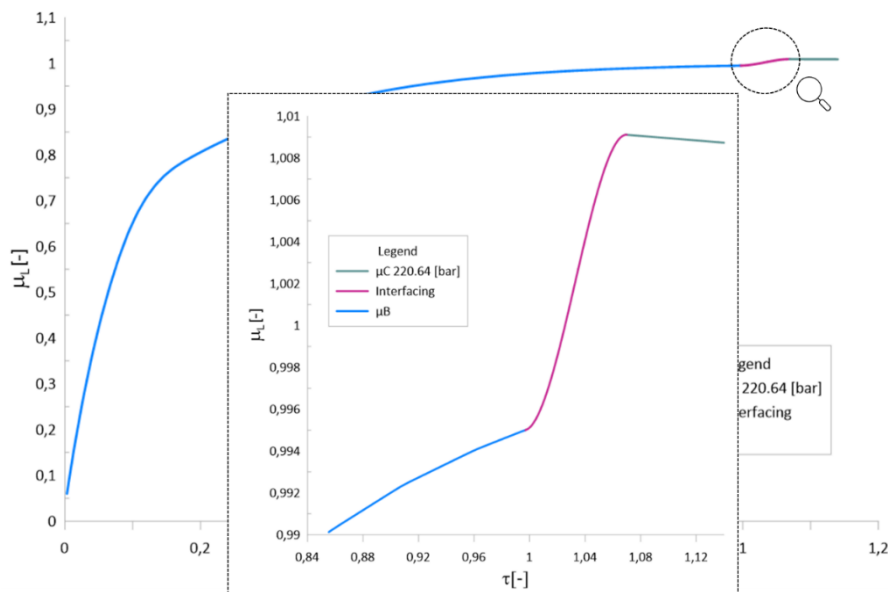
$$\begin{aligned}
\Delta\tau_3 &= 0.003; \\
\Delta\tau_4 &= 0.07; \\
\tau_3 &= 1 - \Delta\tau_3 = 0.997 \\
\tau_4 &= 1 - \Delta\tau_4 = 1.07
\end{aligned}
\tag{6.152}$$

The system of smooth interfacing conditions is the same as usual, for example Equation 6.52 and does not present here. The parameters values are given in Equation (6.153) from the available analytical solution (Equations 5.29 and 5.32).

$$\begin{cases}
a_{BC} = 78.0984 \\
b_{BC} = -224.519 \\
c_{BC} = 217.668 \\
d_{BC} = -70.2521
\end{cases}
\tag{6.153}$$

Figure 6.82 shows the result of the approximation.

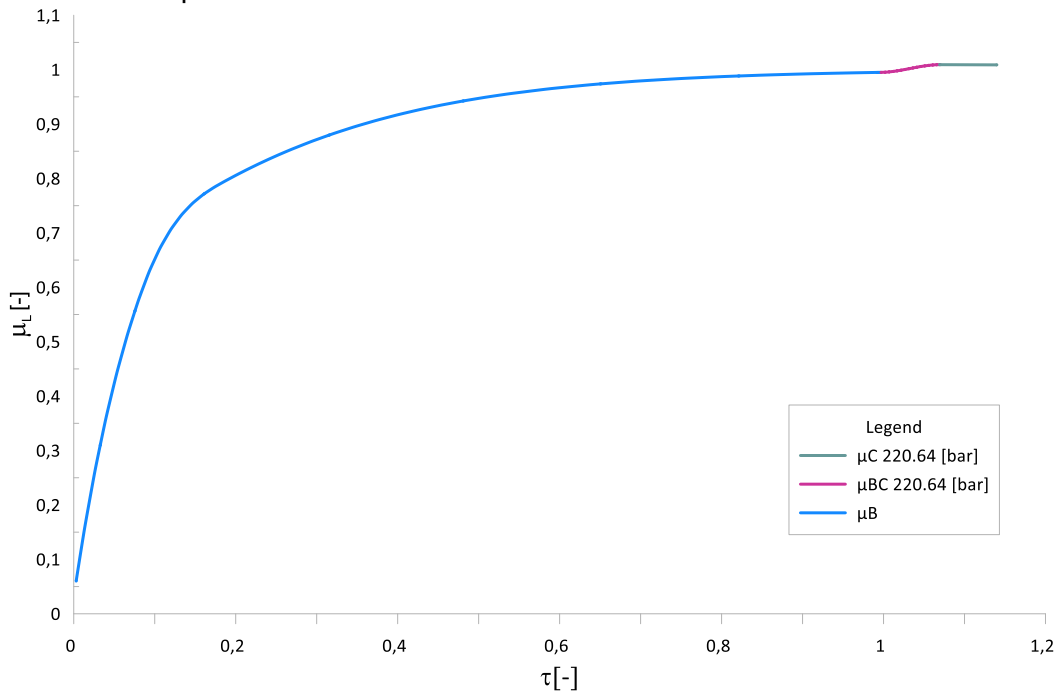
Figure 6.82 – Final result to interfacing above critical point.



6.8.4 Final approximation and pseudo code

The result for different pressure can be seen in Figure 6.83 and shown in Equation 6.154 in the form of pseudo-code.

Figure 6.83 – Result to liquid dynamic viscosity approximation in saturated range and super critical.



This code can be implemented in any programming language:

$$\left\{ \begin{array}{ll}
 \text{if } (\tau \leq \tau_1) & \text{then } \bar{\mu}_l(\tau) = -4.8 \cdot 10^{12} \\
 \text{if } (\tau_1 < \tau < \tau_2) & \text{then } \bar{\mu}_l(\tau) = a_{AB} + b_{AB}\tau + c_{AB}\tau^2 + d_{AB}\tau^3 \\
 \text{if } (\tau_2 \leq \tau \leq \tau_3) & \text{then } \bar{\mu}_l(\tau) = \chi^{-1}(\tau - \tau_{H1})y_1(\tau) + \chi(\tau - \tau_{H1})\chi^{-1}(\tau - \tau_{H2})y_i(\tau) \\
 & \quad + \chi(\tau - \tau_{H2})y_2(\tau) \\
 \text{if } (\tau_3 < \tau < \tau_4) & \text{then } \bar{\mu}_l(\tau) = a_{BC} + b_{BC}\tau + c_{BC}\tau^2 + d_{BC}\tau^3 \\
 \text{if } (\tau \geq \tau_4) & \text{then } \bar{\mu}_l(\tau) = (a_c + b_c\tau + c_c\tau^2)
 \end{array} \right. \quad (6.154)$$

Table 6.9 – Result liquid dynamic viscosity pseudo-code values.

$a_{AB} = -6.493E11$	$d_B = 2.42$	$\tau_{H1} = 8.4E-2$	$b_C = 1.47E-2$
$b_{AB} = 3.934E14$	$e_B = -4E-2$	$\tau_{H2} = 1.9E-1$	$c_C = -9.1E-3$
$c_{AB} = -4.591E16$	$f_B = 7.6E-1$	$a_{BC} = 7.8098E1$	$\Delta\tau_1 = 1E-2$
$d_{AB} = -4.372E18$	$g_B = -3.027E-2$	$b_{BC} = -2.2452E2$	$\Delta\tau_2 = 3E-3$
$a_B = 9.79E-1$	$h_B = 1E14E1$	$c_{BC} = 2.1767E2$	$\Delta\tau_3 = 3E-3$
$b_B = 9.49E-1$	$i_B = -5.539E1$	$d_{BC} = -7.0252E1$	$\Delta\tau_4 = 7E-2$
$c_B = 1.072E1$	$j_B = 9.658E1$	$a_C = 1.0038$	

Table 6.10 – Heaviside Addition coefficient value for liquid dynamic viscosity.

$a_B = 1.02$	$f_B = 1.61$	$k_B = 3.2$	$\tau_{H2} = 0.20$
$b_B = 1.7$	$g_B = 4.6$	$l_B = 2$	$\tau_{H3} = 0.43$
$c_B = 1.02$	$h_B = 1.57$	$m_B = 1.5$	$\tau_{H4} = 0.60$
$d_B = 0.6$	$i_B = 1.9$	$n_B = 1.5$	$\tau_{H5} = 0.91$
$e_B = 5.3$	$j_B = 1.5$	$\tau_{H1} = 0.11$	

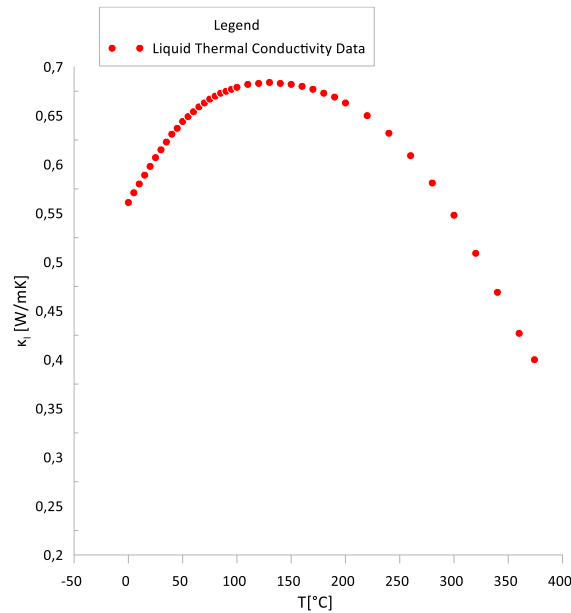
6.9 Approximations for liquid thermal conductivity

6.9.1 Approximations for saturated zone

Liquid thermal conductivity (k_l) can be defined as the ability of a stationary liquid to conduct heat from its one side to the other, without considering any kind of convection. This parameter can be illustrated in Figure 6.34.

American Society of Heating, Refrigerating and Air-Conditioning Engineers (ASHRAE) (LEMMON et al., 2023) conveyed water properties data, including liquid thermal conductivity as a function of temperature; the graph of the liquid thermal conductivity in two-phase zone is presented in Figure 6.84.

Figure 6.84 – Water liquid thermal conductivity numerical data.

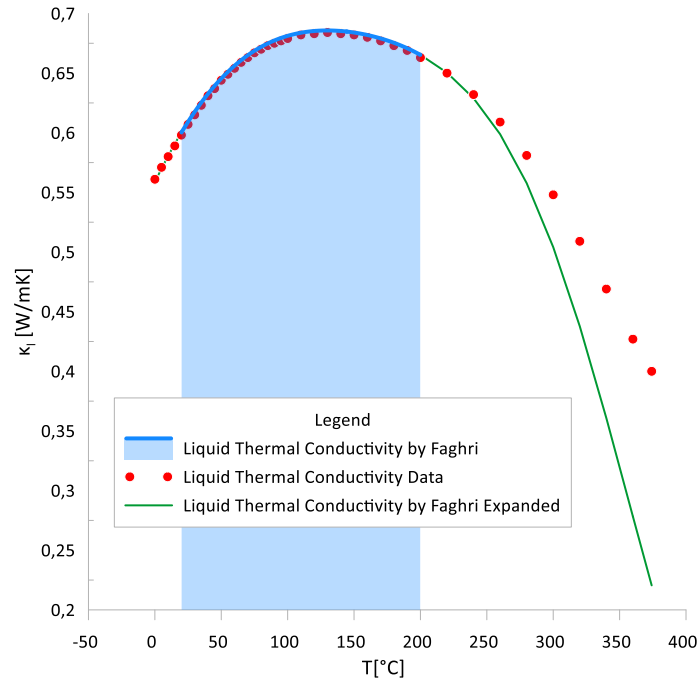


Faghri in his book (2016) suggested the polynomial function (6.155) to approximate this water property, where the liquid thermal conductivity is expressed in W/mK, and the temperature is in Celsius.

$$\begin{aligned} \ln(k_l(T)) = & -5.822 \cdot 10^{-1} + 4.1177 \cdot 10^{-3} \cdot T - 2.7932 \cdot 10^{-5} \cdot T^2 \\ & + 6.5617 \cdot 10^{-8} \cdot T^3 + 4.11 \cdot 10^{-11} \cdot T^4 - 3.822 \cdot 10^{-13} \cdot T^5 \end{aligned} \quad (6.155)$$

This equation is valid between 20°C and 200°C; in this range of temperature this equation can be used for HP modeling with no concern, because of the approximation error mentioned is 0.03% and the equation covers up to 48% of the entire two-phase temperature range. As an example, when we try to use this polynomial equation out of the range, the result has no real behavior. The green line in Figure 6.85 expresses this deviation from the real value.

Figure 6.85 – Faghri polynomial approximation.



Following our approach, non-dimensional variables are used for both temperature and liquid thermal conductivity. This deviation of Faghri's approximation at elevated temperatures shows that the approximation over entire two-phase range cannot be achieved by a unique polynomial function. Several combinations of two or more functions have been evaluated.

To elaborate the approximation over entire two-phase range, from below the triple point to the zone above the critical point, we continue using non-dimensional variables for temperature, τ , as well as for the liquid thermal conductivity:

$$k_l(\tau) = \frac{k - k_{l_3}}{k_{l_{cr}} - k_{l_3}} \quad (6.156)$$

The best result for the approximation within the saturation zone has been achieved with the combination of two functions.

$$\begin{cases} y_1 = a_B + b_B \tau + c_B \tau^2 + d_B \tau^3 + e_B \tau^4 + f_B \tau^5 \\ y_2 = g_B (\tau - \tau_{H1})^{h_B} \end{cases} \quad (6.157)$$

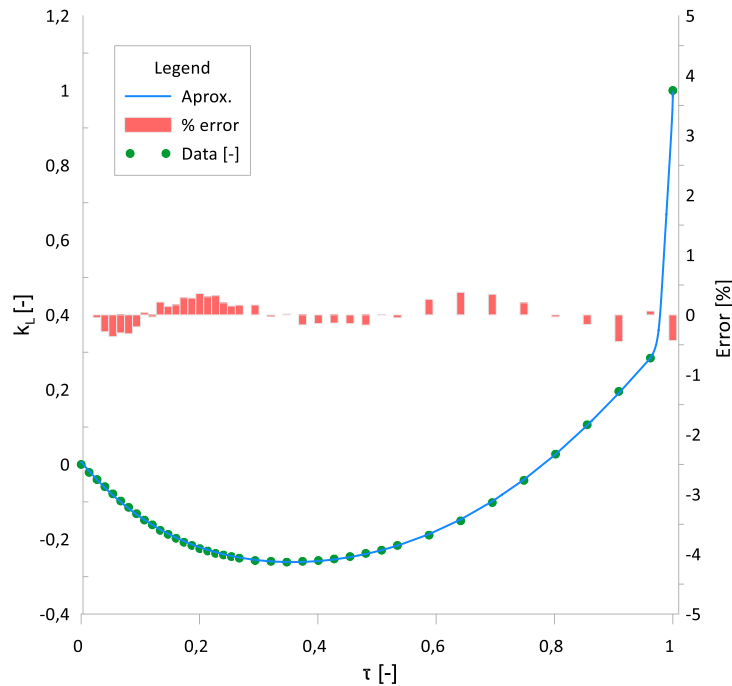
These functions are used in an additive way: when $0 < \tau < \tau_H$, then $y = y_1(\tau)$; when $\tau_{H1} < \tau$, then $y(\tau) = y_1(\tau) + y_2(\tau)$. This can be condensed in a unique correlation for our property:

$$\bar{k}_{l_b}(\tau) = y_1(\tau) + \chi(\tau - \tau_{H1})y_2(\tau) \quad (6.158)$$

The smoothing in the conjugate point (τ_{H1}) has been achieved by the application of continuity conditions for both function and its derivative.

Applying the algorithm above, in the saturation interval of temperature we achieve the curve below. That graph in Figure 6.86 shows data from ASHRAE using green circles (LEMMON et al., 2023). The approximation result is shown in the blue line. In red bars we have the deviation error between property table data and the approximation.

Figure 6.86 – Liquid thermal conductivity approximation results in saturated zone.



We observed that deviation from data by approximation lies within the acceptance criteria in 1% of deviation from the properties table data.

To build this property approximation we used a baseline curve (fifth degree polynomial equation), and we add $y_2(\tau)$ approximate function using the Heaviside function Equation (6.158). The result of that is in Figure 6.86. The main reason to use this technique is reach approximation without sharp interruptions. The technique of the approximation by addition is illustrated in Figures 6.87 and 6.88.

Figure 6.87 –Approximation by two functions for saturated zone.

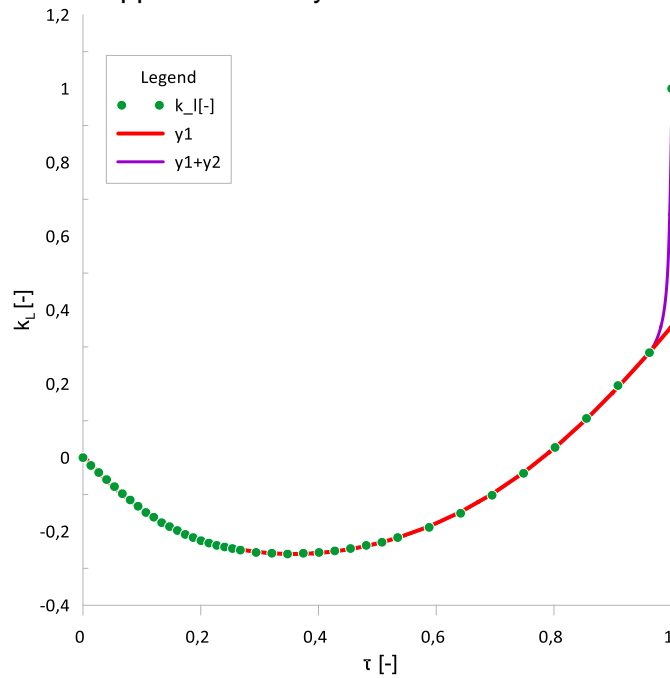
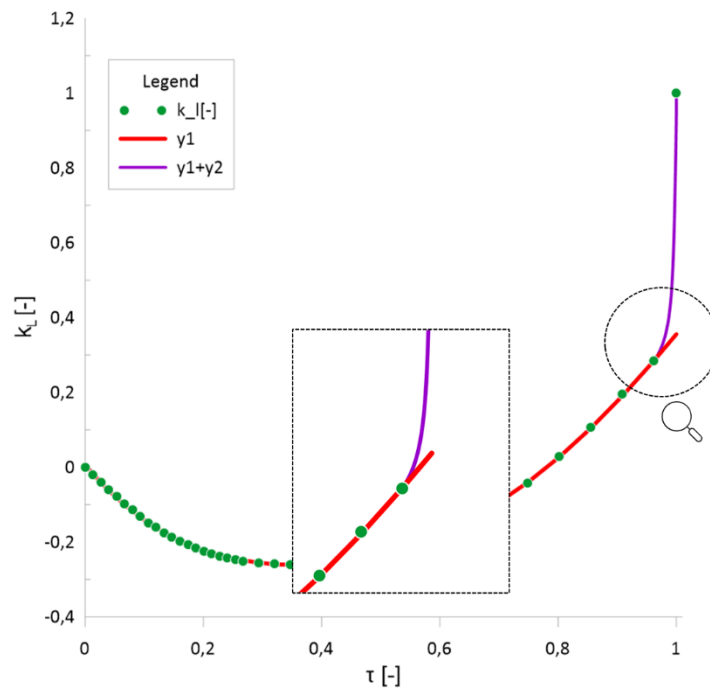


Figure 6.88 – Zoom on conjugate point in the approximation.



6.9.2 Approximations for freezing zone and interfacing

Liley (2005), described this property behavior in the freezing zone, from $-20\text{ }^{\circ}\text{C}$ to $0\text{ }^{\circ}\text{C}$. This data fits the linear type of approximation function. Fukusako (1990) summarized the properties data from 7 different published sources and found the 2nd order polynomial approximation of thermal conductivity of ice in the range from 100 to 273 K (i.e., from $-173\text{ }^{\circ}\text{C}$ to $0\text{ }^{\circ}\text{C}$):

$$k_l = 1.16(1.91 - 8.66 \cdot 10^{-3}T + 2.97 \cdot 10^{-5}T^2) \quad (6.159)$$

or in general form:

$$k_l = a + bT + cT^2 \quad (6.160)$$

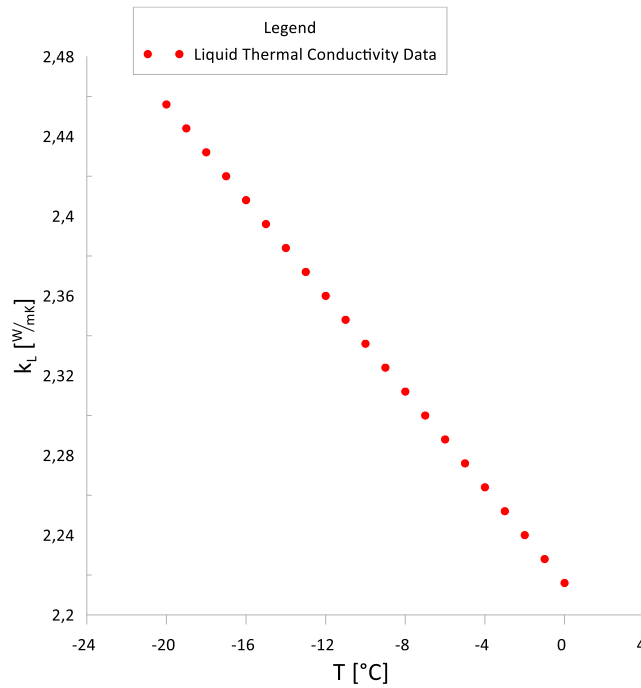
where T is measured in $^{\circ}\text{C}$ and k - in W/m/K , and $a=2.216$; $b=0.01$; $c=3.445 \cdot 10^{-5}$.

Despite wider range of temperature than that by Liley, the Fukusako's approximation is close to linear one, therefore we can continue with linear approximation of Liley:

$$k_{l_A}(T) = 2.216 - 0.0102T \quad (6.161)$$

In this work we used the table presented by Liley (2005) to make an approximation over that data.

Figure 6.89 - Liquid thermal conductivity tabled data in freezing zone.



In this zone, the dimensionless latent heat can be approximated by a linear function:

$$\bar{k}_{l_A}(\tau) = a_A + b_A \tau \quad (6.162)$$

A smooth transition between those two zones is achieved with a third-degree polynomial function (6.163).

$$\bar{k}_{l_{AB}}(\tau) = a_{AB} + b_{AB}\tau + c_{AB}\tau^2 + d_{AB}\tau^3 \quad (6.163)$$

The system of equations of smooth interfacing that touches tangentially both curves and makes a continuous link is the same as for other properties, for example, Equation 6.46.

Points of tangency can be defined by optimizing the approximation result and are presented below.

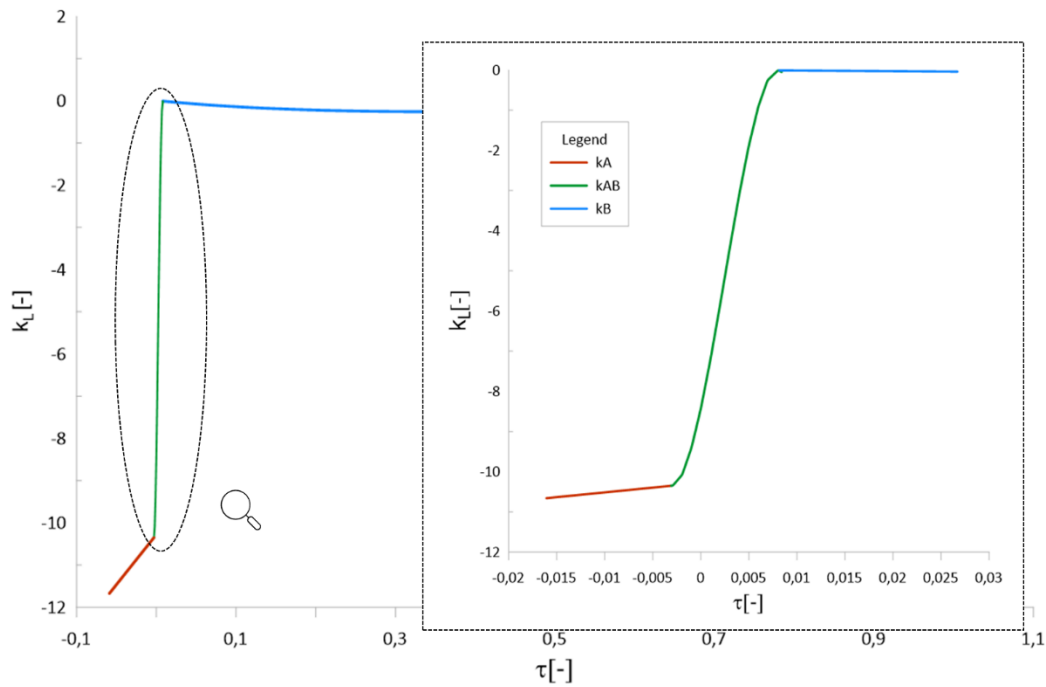
$$\begin{aligned}
 \Delta\tau_1 &= 0.003; \\
 \Delta\tau_2 &= 0.008 \\
 \tau_1 &= -\Delta\tau_1 \\
 \tau_2 &= +\Delta\tau_2;
 \end{aligned}
 \tag{6.164}$$

The resulting interfacing polynomial coefficients, obtained with the available analytical solution (Equations (5.20 and 5.23)), are expressed below:

$$\begin{cases}
 a_{AB} = -8.4248 \\
 b_{AB} = 1.1216 \cdot 10^3 \\
 c_{AB} = 1.1387 \cdot 10^5 \\
 d_{AB} = 1.5359 \cdot 10^7
 \end{cases}
 \tag{6.165}$$

The result approximations around triple point ($\tau=0$), including the interfacing curve, is shown in Figure 6.90.

Figure 6.90 – Final Result to interfacing below freezing point.

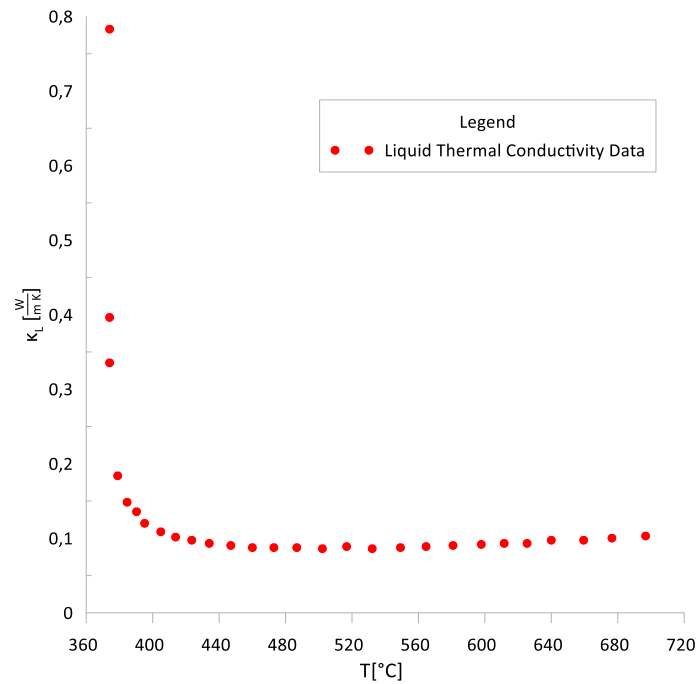


6.9.3 Approximations for supercritical zone and interfacing

In the super-critical zone, the behavior of the thermal conductivity is complex and nonlinear. It is worth mentioning that in the literature, the value of this property in the critical point is either not defined or considered infinity. Therefore, we decide to arbitrate a value for liquid thermal conductivity at critical point as an extrapolation of an interpolation curve of the past 4 points. At temperature above the critical point, the thermal conductivity drops down to the value of about 0.09 W/m/K, shown in the graph in Figure 6.91 as a sudden drop (DHANUSKODI et al., 2011).

We can pick the curve which corresponds to the critical pressure (220.64 bar), as it is close to real heat pipe internal condition near critical point. The same behavior is presented in (PIORO, 2020).

Figure 6.91 – Liquid thermal conductivity data under the critical pressure.



Another point deserving attention is the continuity of the values and derivatives in the interrupting points (interface between curves). To guarantee that, the interfacing technique provides perfect softening in the conjugate points. It is possible to check the interfacing result in figures below.

For super-critical zone we found that the polynomial curve of 5th order fits reasonable the tabled property data:

$$\bar{k}_{l_c}(\tau)\Big|_{\tau>1} = a_c + b_c\tau + c_c\tau^2 + d_c\tau^3 + e_c\tau^4 + f_c\tau^5 \quad (6.166)$$

$$\frac{d(\bar{k}_{l_c}(\tau))}{d\tau}\Big|_{\tau>1} = b_c + 2c_c\tau + 3d_c\tau^2 + 4e_c\tau^3 + 5f_c\tau^4 \quad (6.167)$$

Looking for a smoother transition between those two zones in Equations (6.158), and (6.166), it is used a third-degree polynomial Equation (6.168).

$$\bar{k}_{l_{BC}}(\tau) = a_{BC} + b_{BC}\tau + c_{BC}\tau^2 + d_{BC}\tau^3 \quad (6.168)$$

Points of tangency were obtained through optimization the approximation results:

$$\begin{aligned}\Delta\tau_3 &= 0.003; \\ \Delta\tau_4 &= 0.008; \\ \tau_3 &= 1 - \Delta\tau_3 = 0.997 \\ \tau_4 &= 1 + \Delta\tau_4 = 1.008\end{aligned}\tag{6.169}$$

In this case $\Delta\tau$ defines how far each point will be away from the critical point, ($\tau=1$).

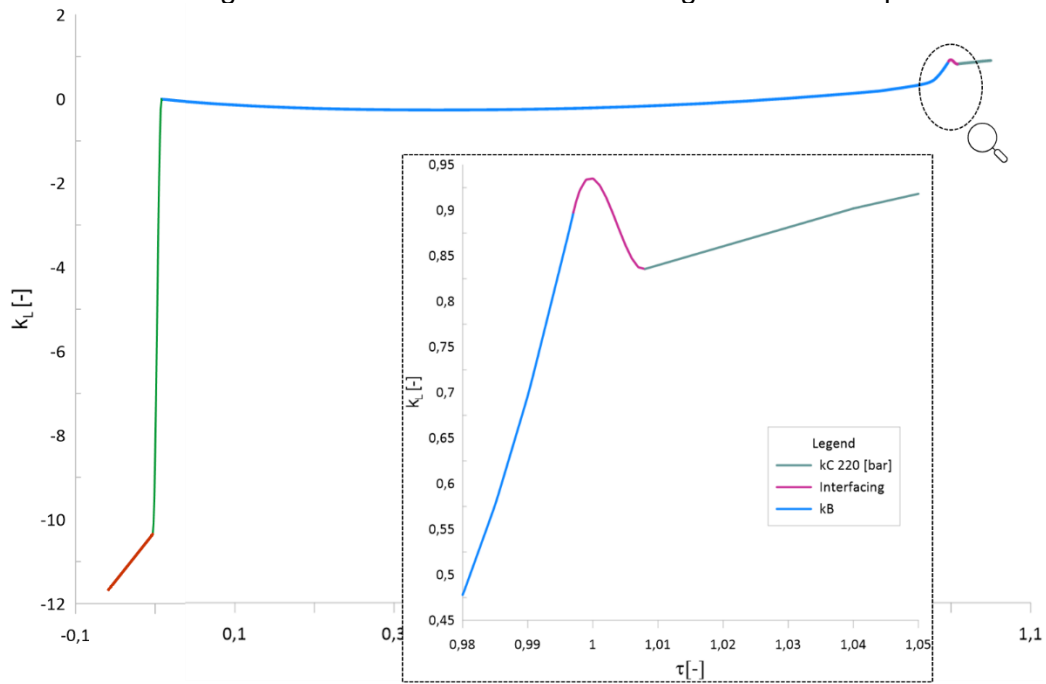
The system has the usual format to the interfacing equation when both curves make a continuous smoothie link (for example, Equation 6.52).

After solving the system, the parameters values are available below:

$$\begin{cases} a_{BC} = -3.7797 \cdot 10^5 \\ b_{BC} = 1.1298 \cdot 10^6 \\ c_{BC} = -1.1257 \cdot 10^6 \\ d_{BC} = 3.7385 \cdot 10^5 \end{cases}\tag{6.170}$$

Figure 6.92 shows the result of the approximation for the critical region.

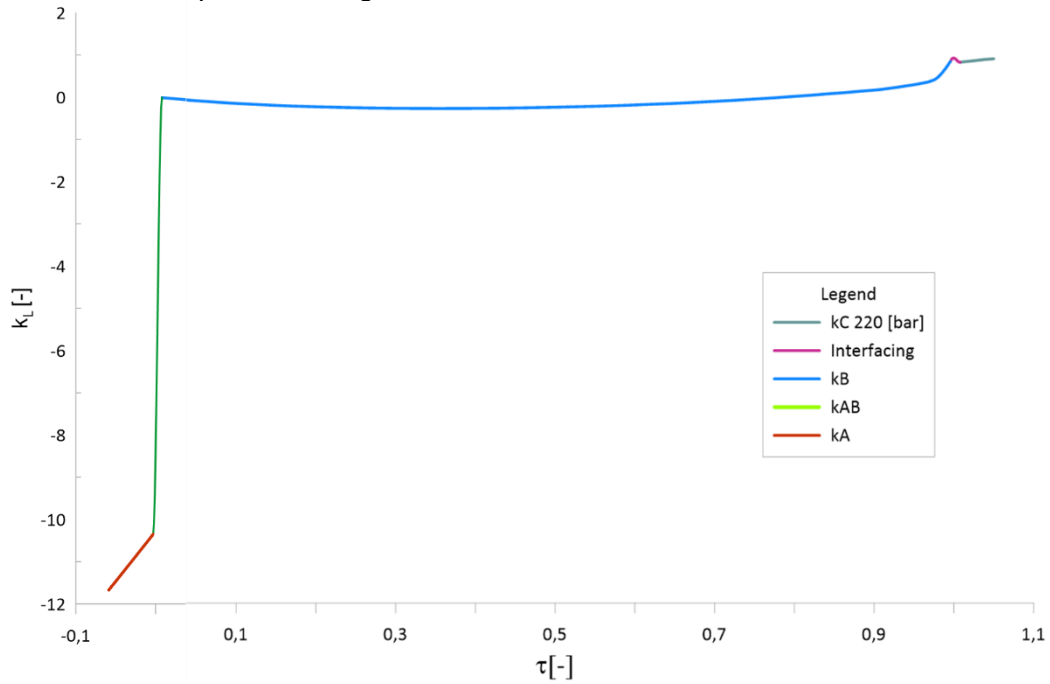
Figure 6.92 – Final result to interfacing above critical point.



6.9.4 Final approximation and pseudo code

The algorithm above that we proposed for the approximation for the entire region which also includes below freezing point and above critical point regions provides the result curve as shown in Figure 6.93.

Figure 6.93 – Final result to liquid thermal conductivity approximation in the entire temperature range.



Therefore, in this chapter we have reached an approximation in the entire range of temperature, managing the approximation error in satisfactory levels (no greater than 5%). The pseudo code provides fluid property values starting below triple point up to above critical point (Figure 6.93).

This code can be implemented in any programming language.

$$\left\{ \begin{array}{ll} \text{if } (\tau \leq \tau_1) & \text{then } \bar{k}_l(\tau) = a_A + b_A \tau \\ \text{if } (\tau_1 < \tau < \tau_2) & \text{then } \bar{k}_l(\tau) = a_{AB} + b_{AB} \tau + c_{AB} \tau^2 + d_{AB} \tau^3 \\ \text{if } (\tau_2 \leq \tau \leq \tau_3) & \text{then } \bar{k}_l(\tau) = y_1(\tau) + \chi(\tau - \tau_{H1}) y_2(\tau) \\ \text{if } (\tau_3 < \tau < \tau_4) & \text{then } \bar{k}_l(\tau) = a_{BC} + b_{BC} \tau + c_{BC} \tau^2 + d_{BC} \tau^3 \\ \text{if } (\tau \geq \tau_4) & \text{then } \bar{k}_l(\tau) = a_C + b_C \tau + c_C \tau^2 + d_C \tau^3 + e_C \tau^4 + f_C \tau^5 \end{array} \right. \quad (6.171)$$

Table 6.11 – Result of liquid thermal conductivity the algorithm values.

$a_A = -1.028E1$	$c_B = 5.0444$	$b_{BC} = 1.1298E6$	$f_C = 1.525E1$
$b_A = 2.37E1$	$d_B = -6.911$	$c_{BC} = -1.1257E6$	$\Delta\tau_1 = 3E-3$
$a_{AB} = -8.423$	$e_B = 6.2103$	$d_{BC} = 3.7385E5$	$\Delta\tau_2 = 8E-3$
$b_{AB} = 1.123E3$	$f_B = -2.075$	$a_C = -1.018E2$	$\Delta\tau_3 = 3E-3$
$c_{AB} = 1.14E5$	$g_B = 4E2$	$b_C = 3.56E2$	$\Delta\tau_4 = 8E-3$
$d_{AB} = -1.536E7$	$h_B = 2$	$c_C = -4.895E2$	
$a_B = 7E-3$	$\tau_{H1} = 0.96$	$d_C = 3.342E2$	
$b_B = -1.92$	$a_{BC} = -3.7797E5$	$e_C = -1.133E2$	

6.10 Approximations for liquid specific heat capacity

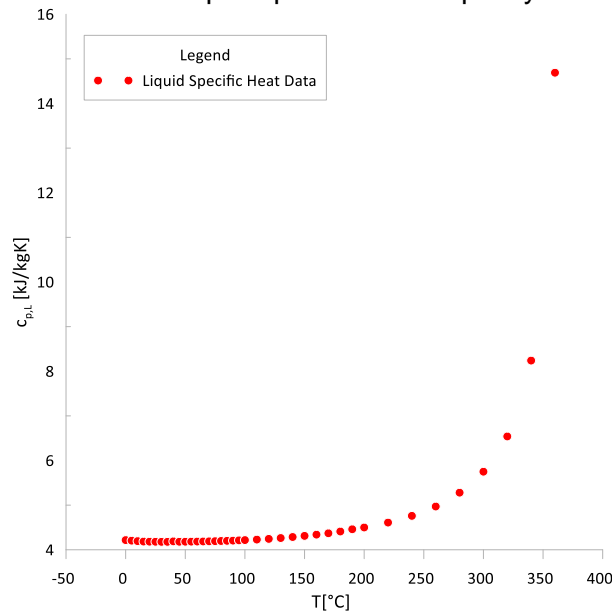
6.10.1 Approximations for saturated zone

Liquid specific heat capacity ($c_{p,l}$) is defined as the amount of heat (dQ) needed to raise the temperature by a small increment (dT) of the sample of unity of mass (M), Equation (6.172).

$$c_{p,l} = \frac{1}{M} \cdot \frac{dQ}{dT} \quad (6.172)$$

The original data of the liquid specific heat capacity behavior for water with temperature in the two-phase zone, presented by ASHRAE (LEMMON et al., 2023), is shown in Figure 6.94.

Figure 6.94 – Water Liquid specific heat capacity number data.



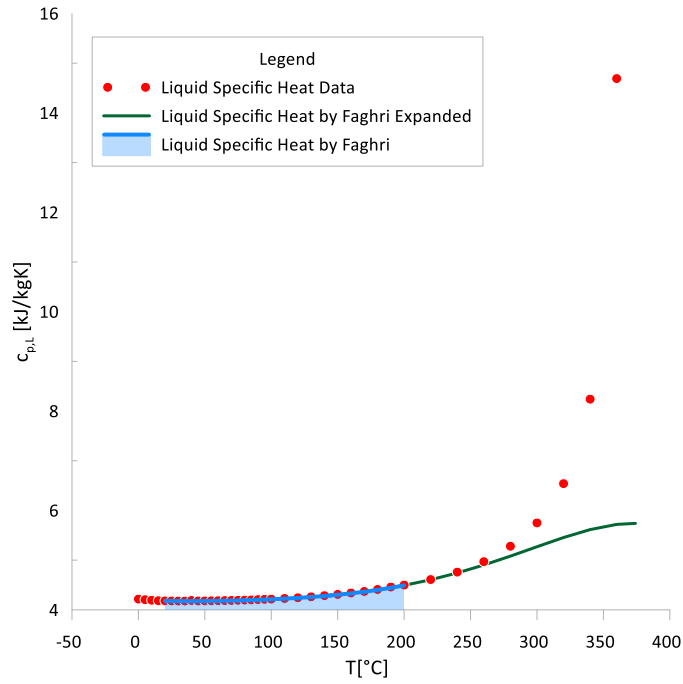
Faghri in his book (2016) suggested an equation to approximate this water property, Equation (6.173).

$$\begin{aligned} \ln(c_{p,l}(T)) = & 1.435 - 3.2231 \cdot 10^{-4} \cdot T + 6.1633 \cdot 10^{-6} \cdot T^2 - \\ & 4.4099 \cdot 10^{-8} \cdot T^3 + 2.0968 \cdot 10^{-10} \cdot T^4 - 3.04 \cdot 10^{-13} \cdot T^5 \end{aligned} \quad (6.173)$$

where T is expressed in °C and Cp_L in kJ/kg/K.

This equation is valid from 20°C to 200°C; for such temperature range this equation can be used for HP modeling with no concern since the approximation error mentioned is 0.03% and the equation covers up to 48% of the entire two-phase temperature range. However, when we try to use this polynomial equation out of the range established, the result run out of the real behavior. The green continuous line in Figure 6.95 expresses this deviation from the real values.

Figure 6.95 – Faghri polynomial approximation.



The dimensionless liquid specific heat capacity follows general dimensionless definition and presented as:

$$\bar{c}_{p,l}(\tau) = \frac{c_{p,l} - c_{p,l_3}}{c_{p,l_{CR}} - c_{p,l_3}} \quad (6.174)$$

For the saturation interval (i.e., two-phase zone, $0 < \tau < 1$), the original curve has a sharp climb as it approaches the critical temperature. It is difficult to obtain a unique function which approximates the entire zone within acceptable error; therefore, we resolved it by applying an interruption point (τ_H) and join two approximation functions in the interval $\tau_H \leq \tau < 1$ by application of Heaviside function. The best results gave the following approximation functions:

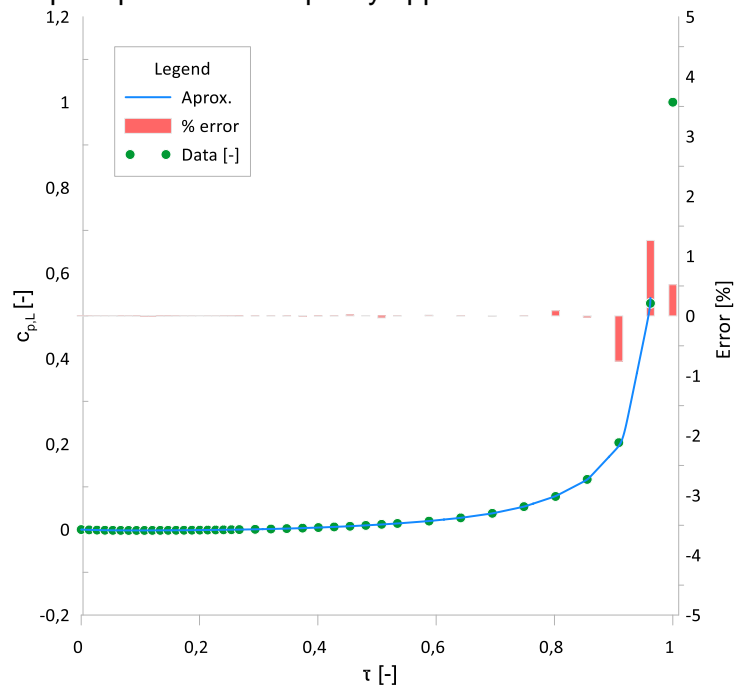
$$\begin{cases} y_1 = a_B + b_B \tau + c_B \tau^2 + d_B \tau^3 + e_B \tau^4 + f_B \tau^5 + g_B \tau^6 \\ y_2 = \frac{h_B (\tau - \tau_{H1})^{i_B}}{1 - j_B (\tau - \tau_{H1})^{k_B}} \end{cases} \quad (6.175)$$

These functions are used in an additive way: when $0 < \tau < \tau_H$, then $y = y_1(\tau)$; when $\tau_{H1} < \tau < \tau_{H2}$, then $y(\tau) = y_1(\tau) + y_2(\tau)$. This can be condensed in a unique correlation for our property:

$$\bar{c}_{p,l}(\tau) = y_1(\tau) + \chi(\tau - \tau_{H1})y_2(\tau) \quad (6.176)$$

Applying the algorithm above, in the saturation interval of temperature we achieve the curve shown below. That chart on Figure 6.96 shows data from ASHRAE using green circles (LEMMON et al., 2023). The approximation results are in the blue line. In red bars we have the deviation error from property table data and approximation.

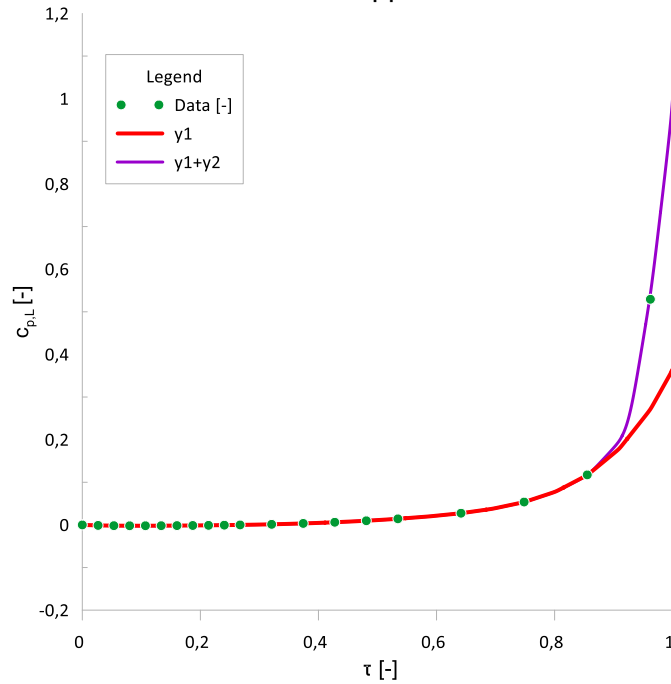
Figure 6.96 – Liquid specific heat capacity approximation results in saturated zone.



We observed the deviation from data by approximation lie within the usual acceptance criteria in 1.5% of deviation from the properties table data.

To build this property approximation we used a baseline curve (4th degree polynomial equation), and we add an auxiliary function in that curve with the use of the Heaviside function. By the use of Equation (6.176) the result of the approximation is shown in Figure 6.97.

Figure 6.97 – Heaviside function in approximation for saturated zone.



The proposed algorithm shall cover the approximation of the entire region which also includes the zones below freezing and above critical points.

6.10.2 Approximations for freezing zone and interfacing

Liley (2005) suggested one approximation to describe that property behavior on freezing zone as presented in Equation 6.177 as a linear function (Figure 6.98). In that case, the equation starts at -20 °C and go to 0°C.

$$c_{p,l}(T) = 2.067 + 6.89 \cdot 10^{-3} \cdot T \quad (6.177)$$

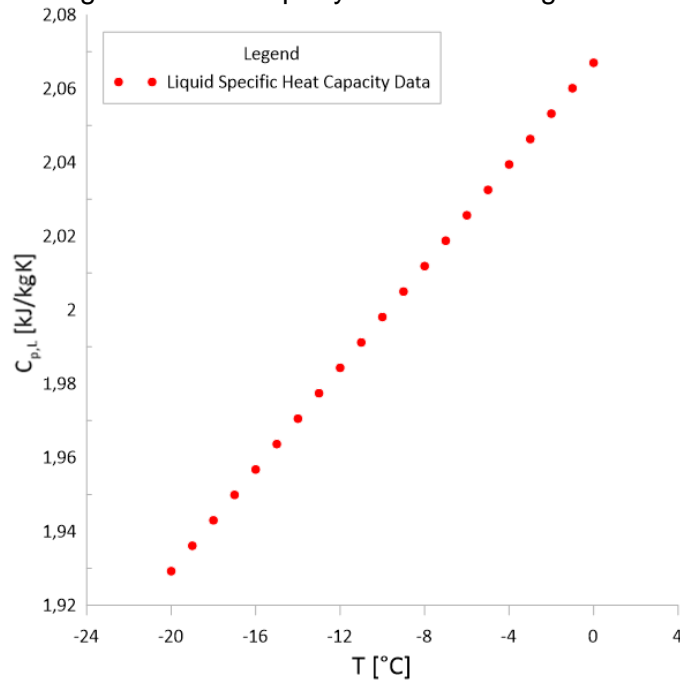
where T is expressed in °C and c_{pl} in kJ/kg/K.

A remarkably similar approximation for $c_{p,l}$ of water ice has been developed by Fukusako (1990) for the temperature range from -183 °C to 0 °C:

$$c_{p,l} = 0.185 + 0.689 \cdot 10^{-2} T \quad (6.178)$$

where $c_{p,l}$ is measured in kJ/kg/K and T - in Kelvin.

Figure 6.98 – Property data in freezing zone.



Another point which deserves attention is the continuity of the values and derivatives in the interface between curves to guarantee that the interfacing technique provides perfect softening.

The interfacing technique is the same that showed in other sections of this work. We start by presenting both equations 6.194 and 6.195 that we intend to connect along with the respective derivatives.

For freezing zone:

$$\bar{c}_{p,l_A}(\tau)\Big|_{\tau < 0} = a_A + b_A \tau \quad (6.179)$$

It is possible to demonstrate a third-degree polynomial function yields the smooth interfacing to join the subcooled zone with saturated zone, Equation (6.180).

$$\bar{c}_{p,l_{AB}}(\tau) = a_{AB} + b_{AB} \tau + c_{AB} \tau^2 + d_{AB} \tau^3 \quad (6.180)$$

The system of smooth interfacing has the similar format as for other properties (for example, Equation 6.46). Points of tangency can will be defined aiming to optimize the approximation result:

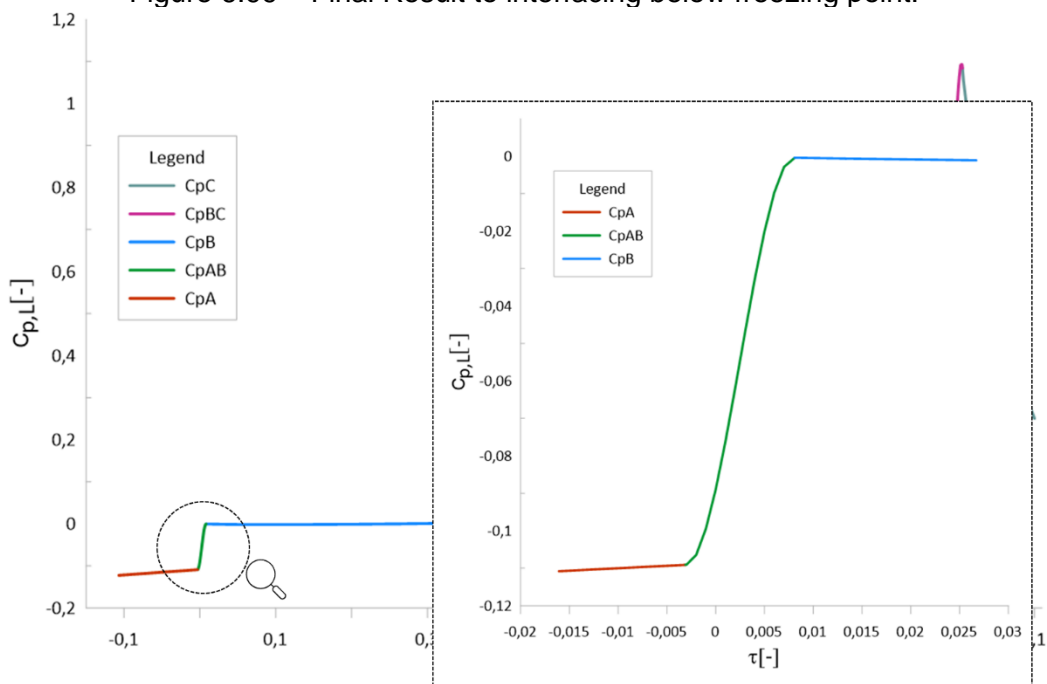
$$\begin{aligned}
 \Delta\tau_1 &= 0.003; \\
 \Delta\tau_2 &= 0.008; \\
 \tau_1 &= -\Delta\tau_1 \\
 \tau_2 &= +\Delta\tau_2
 \end{aligned}
 \tag{6.181}$$

Using the developed universal approach for any property, the result coefficients for c_{pI} interfacing curve is following:

$$\begin{cases}
 a_{AB} = 0.012020 \\
 b_{AB} = -6.237840 \\
 c_{AB} = 958.34396 \\
 d_{AB} = -47962.682
 \end{cases}
 \tag{6.182}$$

The result approximation around triple point ($\tau=0$), including the interfacing curve, is shown in Figure 6.99.

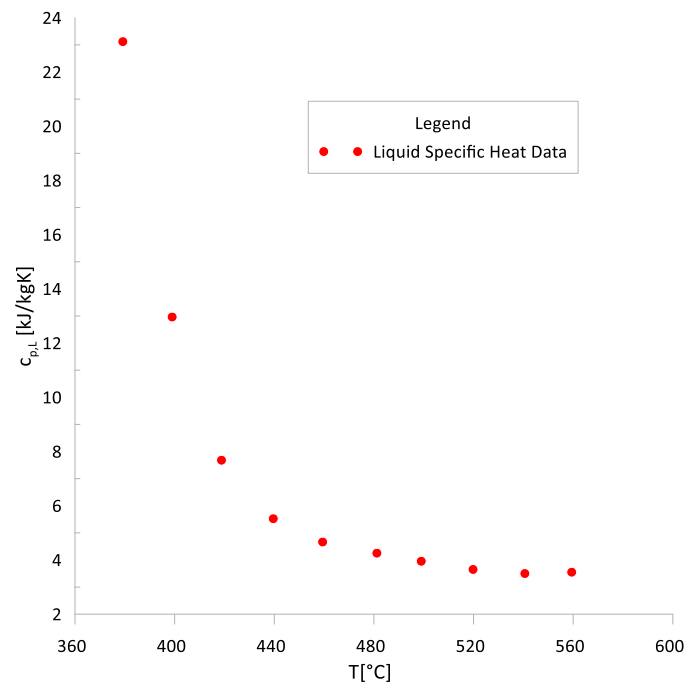
Figure 6.99 – Final Result to interfacing below freezing point.



6.10.3 Approximations for supercritical zone and interfacing

For the supercritical region, the C_{pL} becomes C_{pV} as soon as the difference between the liquid and vapor phases disappears. In various sources this region is referenced as either “superheated vapor” or “steam” or “gas.” The C_{pL} behaves in an overly complicated manner near the critical point: its values get sharp increasing as τ approaches 1 from the left, and then gets sharp falling as τ slightly pass 1 to the right. It also slightly depends on pressure. The chart for near-critical pressure $P=250$ bar is shown in Figure 6.100 (adapted from DHANUSKODI et al., 2011).

Figure 6.100 – Property data in super critical zone.



For super-critical zone a polynomial function of 5th order approximates well the property:

$$\bar{c}_{p,c}(\tau)_{\tau>1} = a_c + b_c\tau + c_c\tau^2 + d_c\tau^3 + e_c\tau^4 + f_c\tau^5 \quad (6.183)$$

The interfacing technique is the same that we used showed in others part of this work, we start with both equation that we want to link and the respective derivatives.

Looking for a smoother transition between those two zones ((6.176) & 6.183), it is used a third-degree polynomial function (6.184).

$$\bar{c}_{p,l_{BC}}(\tau) = a_{BC} + b_{BC}\tau + c_{BC}\tau^2 + d_{BC}\tau^3 \quad (6.184)$$

Points of tangency can be defined aiming to optimize the approximation result. In this case, $\Delta\tau$ defines how far each point is away from the critical point, ($\tau=1$).

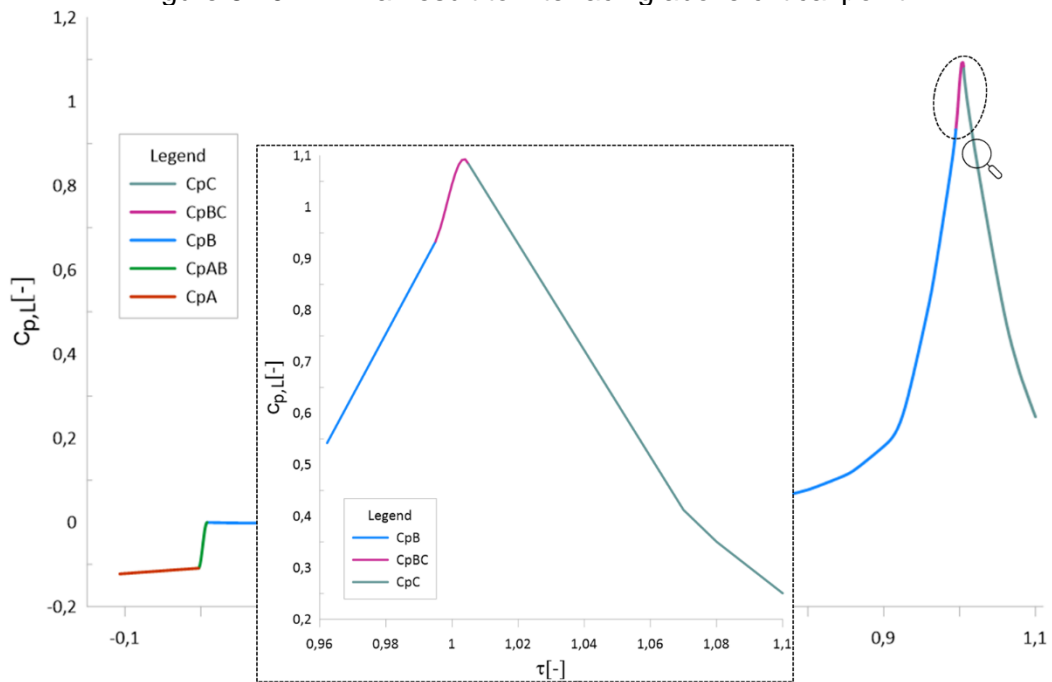
$$\begin{aligned} \Delta\tau_3 &= 0.005; \\ \Delta\tau_4 &= 0.005; \\ \tau_3 &= 1 - \Delta\tau_3 = 0.995 \\ \tau_4 &= 1 - \Delta\tau_4 = 1.005 \end{aligned} \quad (6.185)$$

The system has the usual format to the interfacing equations when both curves make a continuous smooth link (Equations 5.29 and 5.32). Using the values mentioned above, the solution is the following:

$$\begin{cases} a_{BC} = 307310.1729 \\ b_{BC} = -923422.2057 \\ c_{BC} = 924894.2382 \\ d_{BC} = -308781.161 \end{cases} \quad (6.186)$$

Figure 6.101 shows the result of the approximation.

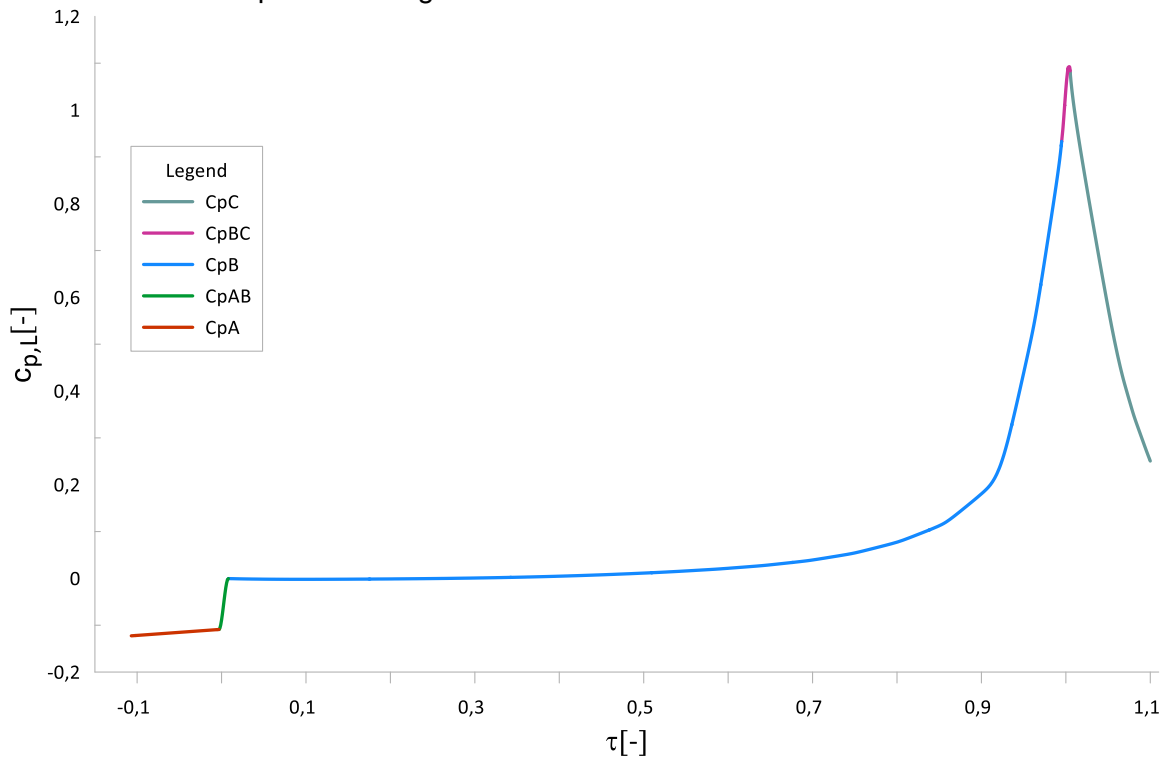
Figure 6.101 – Final result to interfacing above critical point.



6.10.4 Final approximation and pseudo code

Therefore, in this chapter we reached an approximation in a wide range of temperature, managing the approximation error in satisfactory levels (no greater than 5%) Figure 6.102. The pseudo code provides the fluid property values starting below triple point up to above critical point and is presented by Equation (6.187).

Figure 6.102 – Final result for liquid specific heat capacity approximation in the entire temperature range.



This code can be implemented in any programming language.

$$\left\{ \begin{array}{ll} \text{if } (\tau \leq \tau_1) & \text{then } \bar{c}_{p,l}(\tau) = a_A + b_A \tau \\ \text{if } (\tau_1 < \tau < \tau_2) & \text{then } \bar{c}_{p,l}(\tau) = a_{AB} + b_{AB} \tau + c_{AB} \tau^2 + d_{AB} \tau^3 \\ \text{if } (\tau_2 \leq \tau \leq \tau_3) & \text{then } \bar{c}_{p,l}(\tau) = y_1(\tau) + \chi(\tau - \tau_{H1}) y_2(\tau) \\ \text{if } (\tau_3 < \tau < \tau_4) & \text{then } \bar{c}_{p,l}(\tau) = a_{BC} + b_{BC} \tau + c_{BC} \tau^2 + d_{BC} \tau^3 \\ \text{if } (\tau \geq \tau_4) & \text{then } \bar{c}_{p,l}(\tau) = a_C + b_C \tau + c_C \tau^2 + d_C \tau^3 + e_C \tau^4 + f_C \tau^5 \end{array} \right. \quad (6.187)$$

Table 6.12 – Resulting liquid specific heat capacity pseudo code values.

$a_A = -1.087E-1$	$c_B = 5.511E-1$	$k_B = 1$	$c_C = 4.5485E3$
$b_A = 1.305E1$	$d_B = -2.5295$	$\tau_{H1} = 0.89$	$d_C = -3.311E3$
$a_{AB} = -8.9014E-2$	$e_B = 6.4967$	$a_{BC} = 3.073E5$	$e_C = 1.2023E3$
$b_{AB} = 1.1790E1$	$f_B = -7.9777$	$b_{BC} = -9.234E5$	$f_C = -1.7421E2$
$c_{AB} = 1.2116E3$	$g_B = 3.8797$	$c_{BC} = 9.249E5$	$\Delta\tau_1 = 3E-3$
$d_{AB} = -1.6262E5$	$h_B = 5E1$	$d_{BC} = -3.088E3$	$\Delta\tau_2 = 8E-3$
$a_B = -2E-6$	$i_B = 2$	$a_C = 8.536E2$	$\Delta\tau_3 = 5E-3$
$b_B = -5.53E-2$	$j_B = 5E-1$	$b_C = -3,1181E3$	$\Delta\tau_4 = 5E-3$

6.11 Approximations for liquid Prandtl number

6.11.1 Approximations for saturated zone

The Prandtl number makes the correlation between the momentum diffusivity (ν) and the thermal diffusivity (α).

$$\text{Pr} = \frac{\nu}{\alpha} = \frac{\mu / \rho}{\kappa / (c_p \rho)} = \frac{c_p \mu}{\kappa} \quad (6.188)$$

The parameters are defined as following:

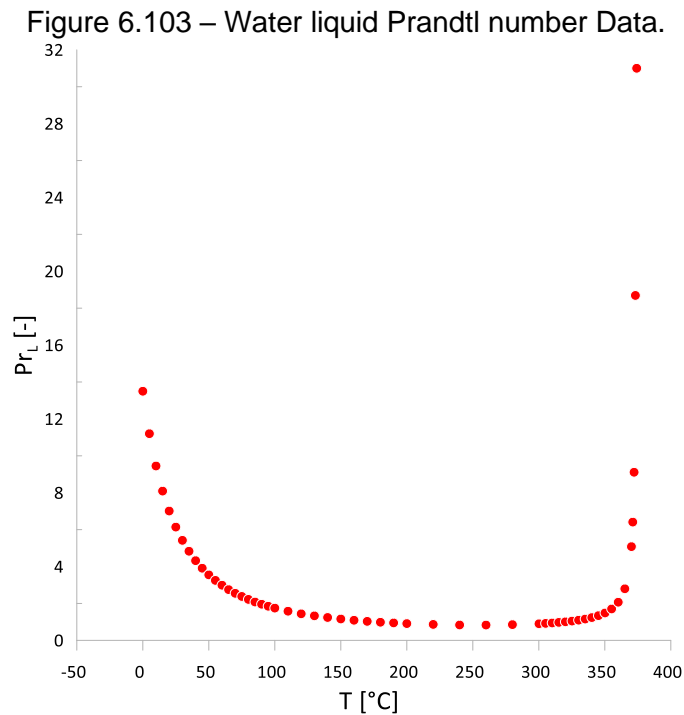
ν is momentum diffusivity or kinematic viscosity, α is thermal diffusivity, μ is dynamic viscosity, κ is thermal conductivity, c_p is specific heat and ρ is density.

By the use of this property initial table, it can be approximated directly from the available points. As an option the Prandtl number approximation can be obtained from the approximations of its components: viscosity, thermal conductivity, and sensible heat.

However, Prandtl number is a dimensionless number that does not means that it is exclusively composed by dimensionless numbers, in fact, to obtain the approximation to Prandtl number using the relations between others dimensionless approximations we need to follow those steps:

- Transform the available dimensionless approximations of Pr components into dimensional values by inverse formulas.
- Build a table of values of Prandtl number, calculated from its components, as a function of temperature and pressure. Then add columns which calculate reduced Pr number as a function of dimensionless temperature and dimensionless pressure.
- Perform approximations of reduced Pr number to result in pseudo-code format.

The Prandtl liquid number behavior with temperature in saturation zone is expressed below in Figure 6.103 (BEATON, 1986).



It is worth to mention that in literature the value of this property in critical point is considered infinite, so we decide to attribute an extrapolated value for Liquid Prandtl Number at critical point by an interpolation curve build from the past 4 points. It resulted in a value of original Pr number equal to 31 (plotted in Figure 6.103).

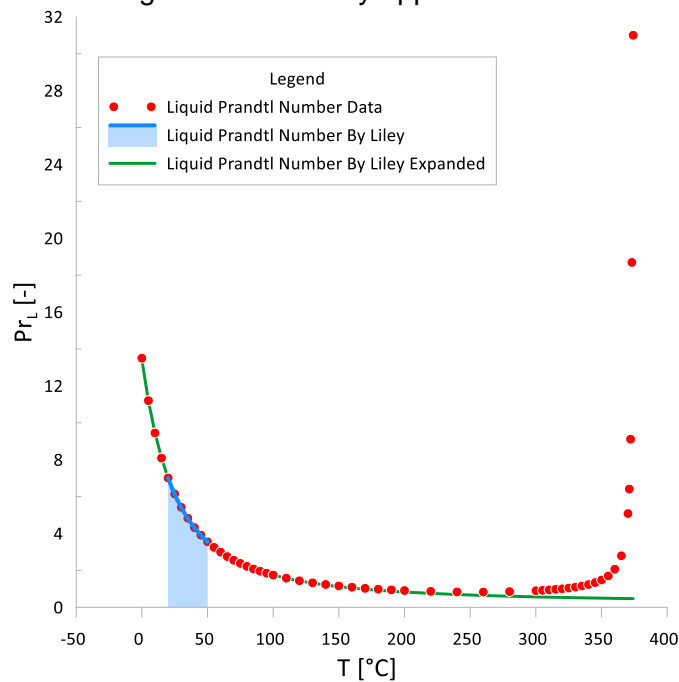
About this property Liley (2005) suggested a group of equations to describe properties behavior with temperature. To build liquid Prandtl number behavior from -20°C up to 50 °C the author breaks its equation in three parts. One starting from -20°C until 0°C, moving to 0°C up to 25°C and from 25°C to 50°C.

All those three equations, that Liley (2005) suggested, represents 13,37% of the saturation range. In order to exemplify the deviation of an equation out of his range of actuation we compared the data, equation suggested by (LILEY, 2005), and that same equation out of temperature range suggested.

$$\text{Pr}(T) = e^{-1.78023 + 501.834 / (T + 114.643)} \quad (6.189)$$

This equation is valid from 25°C to 50°C; that equation covers up to 6.7% of the entire two-phase temperature range. As an example, when we try to use this polynomial equation out of the established range, in that case from 0°C up to 374°C, the result does not follow the real behavior. The green line in Figure 6.104 expresses this deviation from the real data.

Figure 6.104 – Liley approximation.



Following the general approach for all other properties, despite Pr number is already a dimensionless parameter, we introduce “reduced Pr number” defined as:

$$\bar{Pr}_l(\tau) = \frac{Pr_l(T) - Pr_l(T_3)}{Pr_l(T_{cr}) - Pr_l(T_3)} \quad (6.190)$$

Following our approach to elaborate the approximation over entire two-phase range, from the triple point to the critical point, we also continue using non-dimensional variables for temperature.

As shown in Figure 6.103, for the saturation interval (i.e., two-phase zone, $0 < \tau < 1$), the original curve has a sharp climb as it approaches the critical temperature. It is difficult to obtain a unique function which approximates the entire zone within acceptable error: therefore, we will improve it with application of two interruption points (τ_{H1} and τ_{H2}) and join the approximation functions by application of Heaviside functions.

The best results are the following approximate functions:

$$\begin{cases} y_1 = a_B + b_B \tau + c_B \tau^2 + d_B \tau^3 + e_B \tau^4 + f_B \tau^5 + g_B \tau^6 \\ y_2 = h_B (\tau - \tau_{H1})^{i_B} \\ y_3 = j_B \left(\frac{1 - \text{Cos}(\pi(\tau - \tau_{H2}))}{2} \right)^{k_B} \end{cases} \quad (6.191)$$

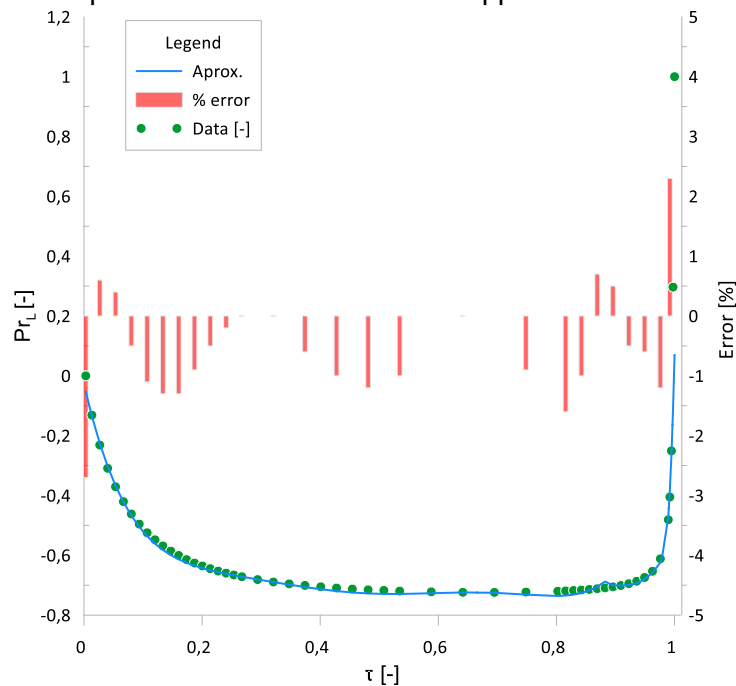
To build such approximation we used a baseline curve (6th degree polynomial equation), and we add in that curves that satisfies continuity and smooth interface conditions.

These functions are used in an additive way: when $0 < \tau < \tau_H$, then $y = y_1(\tau)$; when $\tau_{H1} < \tau < \tau_{H2}$, then $y(\tau) = y_1(\tau) - y_2(\tau)$; when $\tau_{H2} < \tau < 1$, then $y(\tau) = y_1(\tau) - y_2(\tau) + y_3(\tau)$. This can be condensed in a unique correlation for our property:

$$\overline{\text{Pr}}_l(\tau) = y_1(\tau) - \chi(\tau - \tau_{H1})y_2(\tau) + \chi(\tau - \tau_{H2})y_3(\tau) \quad (6.192)$$

Applying the algorithm above, in the saturation interval of temperature we achieve the curve shown in Figure 6.105. This chart also shows data from ASHRAE tables using green circles. The approximation results are shown by the blue line. In red bars we have the deviation error from property table data and the approximation.

Figure 6.105 – Liquid reduced Prandtl number approximation in saturated zone.



We observe that the deviation from the available data by approximation lies within the acceptance criteria of 3% of deviation from the properties table data. The point that deserves attention is the end of range due to the error that point conducts. This point will be smoothed by the link curves that will be result of the interface technique application.

The final curve and contribution of each approximation functions, obtained from Equation (6.192), are shown in Figure 6.106.

Figure 6.106 – Contributions of approximation functions to final approximation for saturated zone.

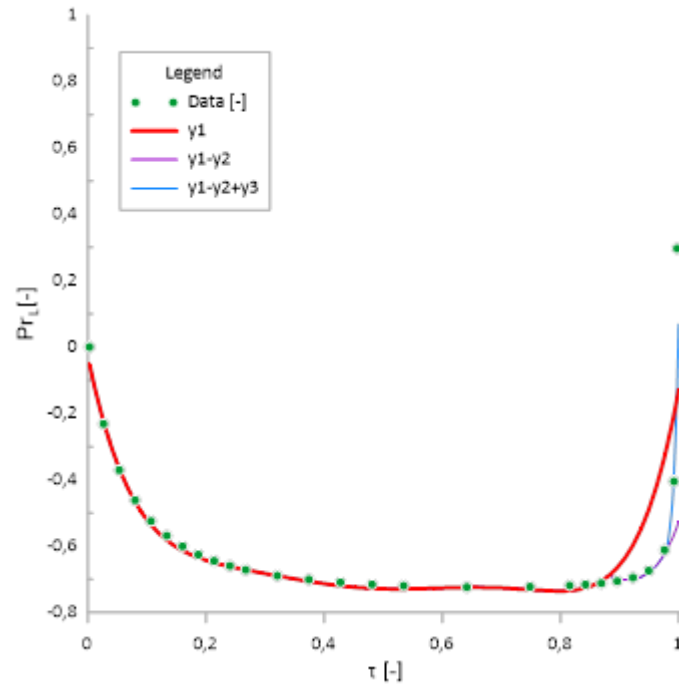
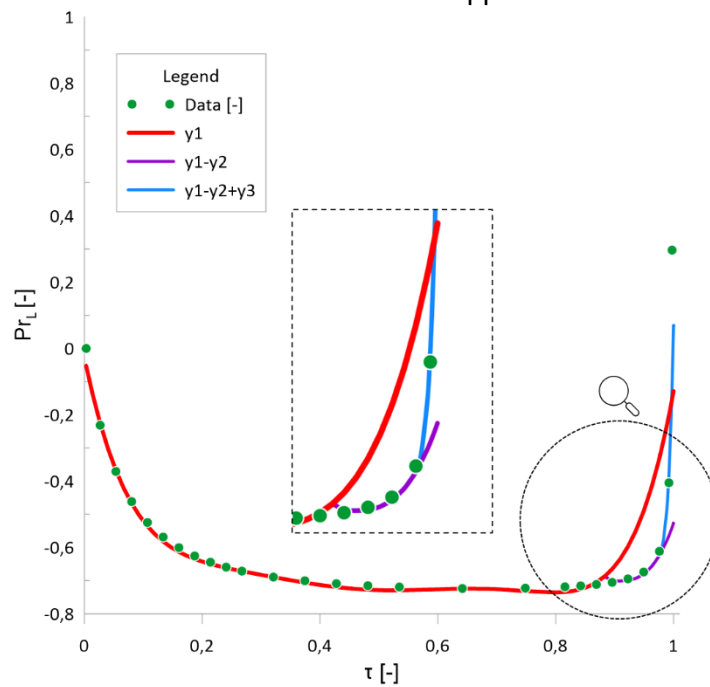
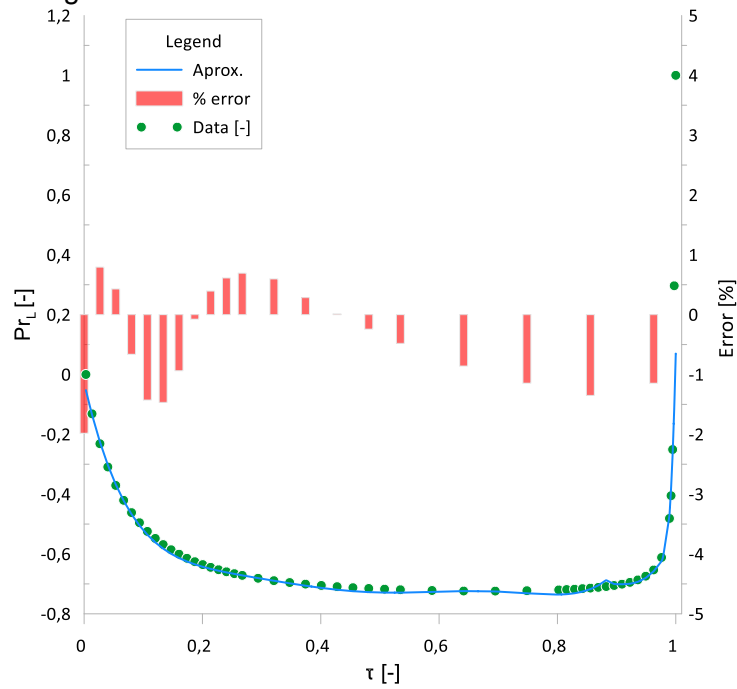


Figure 6.107 – Zoom on individual functions in approximation for saturated zone.



From the other hand, this property is a combination of other properties. When we perform this calculation, we obtain the result shown in Figure 6.108.

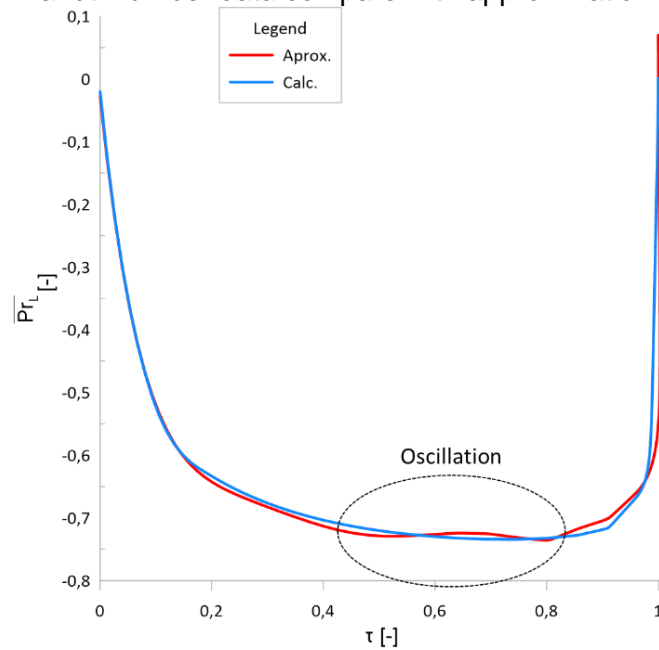
Figure 6.108 – Reduced Prandtl number calculated.



One can see, the maximal error lies within 2 %.

If we put side by side the Prandtl number data, approximation, and calculation, we reach the curves given in Figure 6.109, where it is possible to notice the main difference of obtaining property value by approximation or calculation way. This difference is the oscillation highlighted by dash circle, this phenomenon occurs because of a side effect of using addition Heaviside, in each curve interruption has localized oscillation in a way to best fit.

Figure 6.109 – Prandtl number data compare with approximation and calculation.

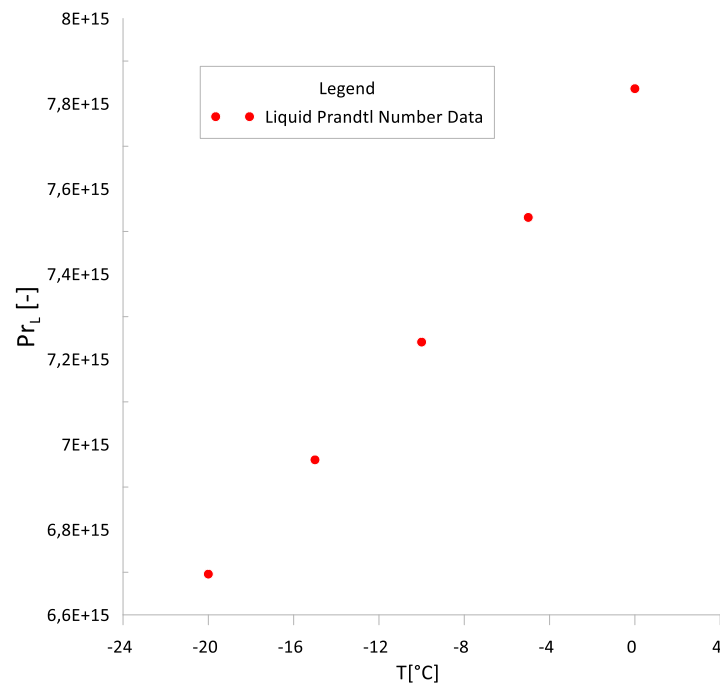


Therefore, calculated approximation of liquid Pr number provides slightly better result than the direct piece-wise approximation.

6.11.2 Approximations for freezing zone and interfacing

In freezing zone, there is not many data available for this property, with that in mind, we calculate the property in this temperature rage using obtained approximations of Pr number components given in Equation (6.188). It is important to expose that in the freezing zone, this property is directly bonded to the dynamic viscosity and Pr behavior is mostly driven by the viscosity of ice. In the case, this value is much higher when compared with the liquid value.

Figure 6.110 – Prandtl Number in freezing zone.



In this zone, the reduced Prandtl number can be approximated by a linear function:

$$\bar{\text{Pr}}_{l_A}(\tau) = a_A + b_A \tau \quad (6.193)$$

Interfacing equation joins the subcooled zone with saturated zone.

Looking for a smooth transition between those two zones, Equations (6.192) and (6.193), it is used a third-degree polynomial Equation (6.194).

$$\text{Pr}_{l_{AB}}(\tau) = a_{AB} + b_{AB} \tau + c_{AB} \tau^2 + d_{AB} \tau^3 \quad (6.194)$$

The system of equations to calculate the coefficients in (6.194) will be of the following format to interface tangency both curves and to make a continuous smooth link.

$$\left\{ \begin{array}{l} \bar{\text{Pr}}_{I_A}(\tau_1) = a_{AB} + b_{AB}\tau_1 + c_{AB}\tau_1^2 + d_{AB}\tau_1^3 \\ \frac{d(\bar{\text{Pr}}_{I_A}(\tau_1))}{d(\tau_1)} = b_{AB} + 2c_{AB}\tau_1 + 3d_{AB}\tau_1^2 \\ \bar{\text{Pr}}_{I_B}(\tau_2) = a_{AB} + b_{AB}\tau_2 + c_{AB}\tau_2^2 + d_{AB}\tau_2^3 \\ \frac{d(\bar{\text{Pr}}_{I_B}(\tau_2))}{d(\tau_2)} = b_{AB} + 2c_{AB}\tau_2 + 3d_{AB}\tau_2^2 \end{array} \right. \quad (6.195)$$

Points of tangency can be defined trying to optimize the approximation result. In this case Δt determines how far each point will be away from the triple point:

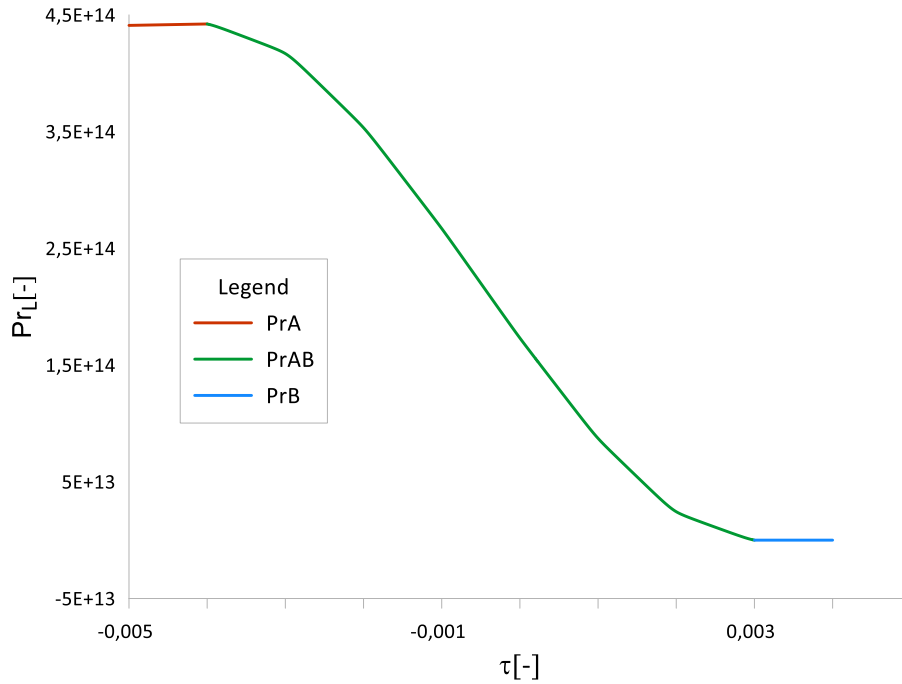
$$\left\{ \begin{array}{l} \Delta\tau_1 = 0.004; \\ \Delta\tau_2 = 0.003; \\ \tau_1 = -\Delta\tau_1 \\ \tau_2 = +\Delta\tau_2 \end{array} \right. \quad (6.196)$$

The solution of system of Equation (6.195) is expressed below.

$$\left\{ \begin{array}{l} a_{AB} = 1.7315 \cdot 10^{14} \\ b_{AB} = -9.245 \cdot 10^{16} \\ c_{AB} = 3.9173 \cdot 10^{18} \\ d_{AB} = 2.5536 \cdot 10^{21} \end{array} \right. \quad (6.197)$$

The result approximation around triple point ($\tau=0$), including the interfacing curve, are shown in Figure 6.111.

Figure 6.111 – Final result to interfacing below freezing point.



6.11.3 Approximations for supercritical zone and interfacing

In super-critical zone, we correlate the pressure variation and temperature variation, resulting in an equation of two variables: dimensionless temperature and pressure.

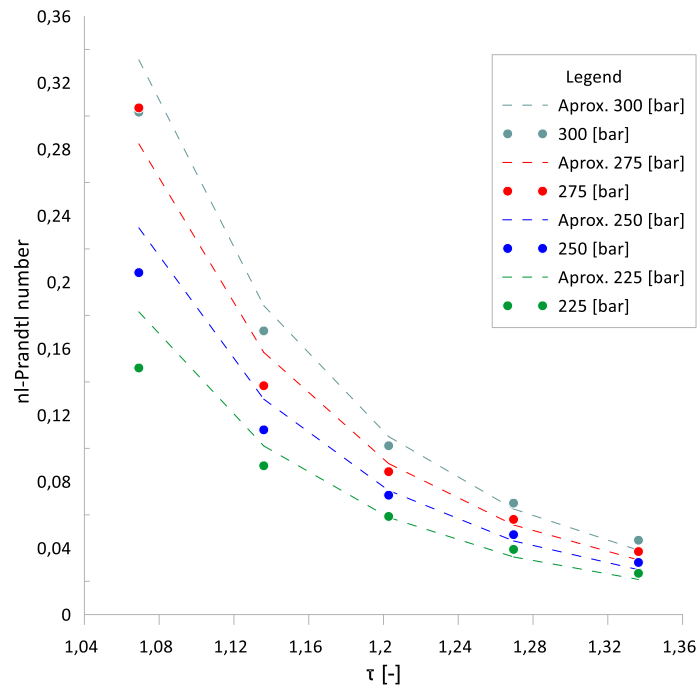
For super-critical zone:

$$\bar{Pr}_{i_c}(\tau, p) \Big|_{\tau > 1} = (a_B + b_B p) (c_B \tau^{d_B}) \quad (6.198)$$

$$\frac{d(\bar{Pr}_{i_c}(\tau, p))}{d(\tau)} \Big|_{\tau > 1} = (a_B + b_B p) (c_B d_B \tau^{d_B - 1}) \quad (6.199)$$

In Figure 6.112 is possible to see the reduced Prandtl number approximation compared with the available data.

Figure 6.112 – Approximation of reduced Prandtl number as a function of dimensionless temperature and pressure for super-critical zone.



Looking for smooth transition between those two zones in Equations (6.192) and (6.198), it is used a third-degree polynomial Equation (6.200).

$$\text{Pr}_{i_{BC}}(\tau) = a_{BC} + b_{BC}\tau + c_{BC}\tau^2 + d_{BC}\tau^3 \quad (6.200)$$

Points of tangency can be defined by trying to optimize the approximation result. In this case $\Delta\tau$ defines how far each point will be away from the critical point, ($\tau=1$).

$$\begin{aligned} \Delta\tau_3 &= 0.003; \\ \Delta\tau_4 &= 0.06913 \\ \tau_3 &= 1 - \Delta\tau_3 = 0.997 \\ \tau_4 &= 1 + \Delta\tau_4 = 1.06913 \end{aligned} \quad (6.201)$$

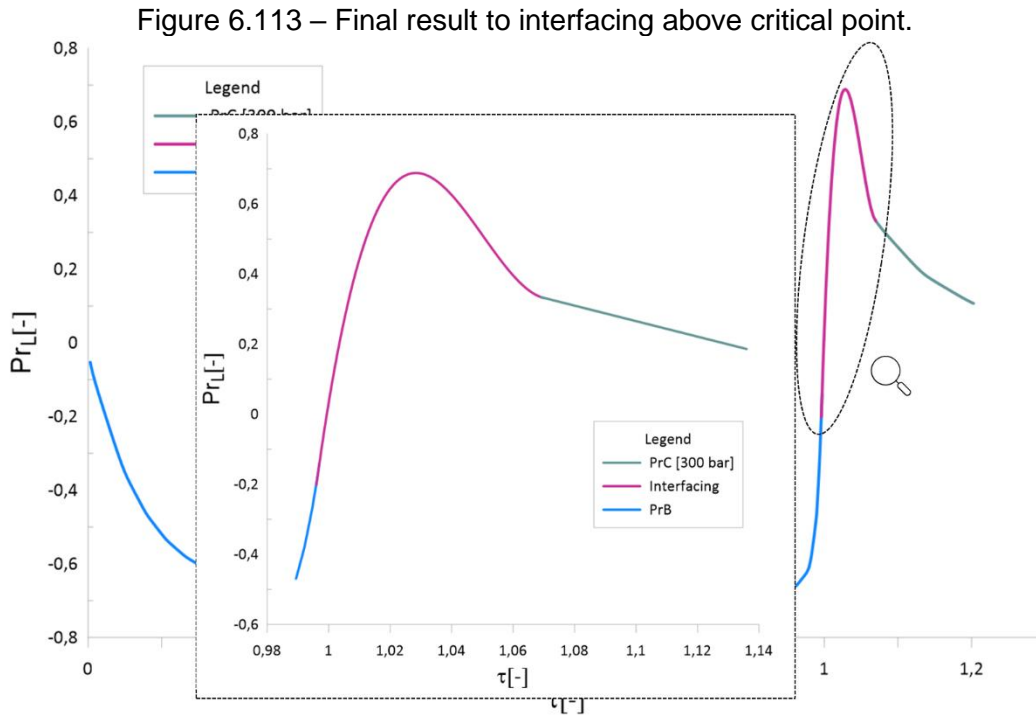
This system has the following format to the interfacing equation tangency when both curves make a continuous smoothie link.

$$\left\{ \begin{array}{l} \bar{Pr}_{l_B}(\tau_3) = a_{BC} + b_{BC}\tau_3 + c_{BC}\tau_3^2 + d_{BC}\tau_3^3 \\ \frac{d(\bar{Pr}_{l_B}(\tau_3))}{d(\tau_3)} = b_{BC} + 2c_{BC}\tau_3 + 3d_{BC}\tau_3^2 \\ \bar{Pr}_{l_C}(\tau_4, p) = a_{BC} + b_{BC}\tau_4 + c_{BC}\tau_4^2 + d_{BC}\tau_4^3 \\ \frac{d(\bar{Pr}_{l_C}(\tau_4, p))}{d(\tau_4)} = b_{BC} + 2c_{BC}\tau_4 + 3d_{BC}\tau_4^2 \end{array} \right. \quad (6.202)$$

Solving the system above, the parameters values are available below.

$$\left\{ \begin{array}{l} a_{BC} = -10028.6257 \\ b_{BC} = 28674.39 \\ c_{BC} = -27315.95 \\ d_{BC} = 8670.22 \end{array} \right. \quad (6.203)$$

Figure 6.113 shows the result of the approximation with this interfacing.

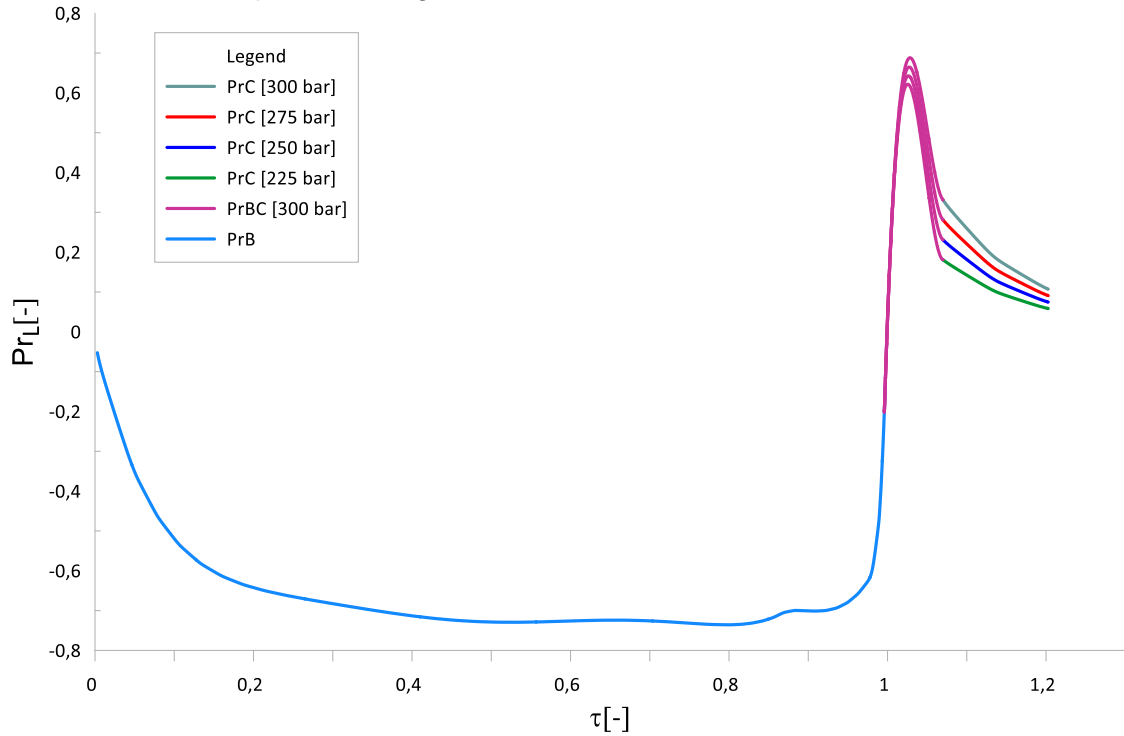


6.11.4 Final approximation and pseudo code

Because of the large magnitude of this property in freezing region, which is much greater than for the others zone, we omit freezing zone from the Figure 6.114 to

the other details be available; but is possible to check the freezing behavior in Figure 6.111.

Figure 6.114 – Final result for liquid reduced Prandtl number approximation in the entire temperature range.



Therefore, in this section we reach an approximation in a wider range of temperature, managing the approximation error in satisfactory levels (no greater than 5%). The pseudo code (Equation 6.204) provides fluid property values starting below triple point up to above critical point.

This pseudo-code can be implemented in any programming language.

$$\left\{ \begin{array}{ll} \text{if } (\tau \leq \tau_1) & \text{then } \bar{Pr}_L(\tau) = a_A + b_A \tau \\ \text{if } (\tau_1 < \tau < \tau_2) & \text{then } \bar{Pr}_L(\tau) = a_{AB} + b_{AB} \tau + c_{AB} \tau^2 + d_{AB} \tau^3 \\ \text{if } (\tau_2 \leq \tau \leq \tau_3) & \text{then } \bar{Pr}_L(\tau) = y_1(\tau) - \chi(\tau - \tau_{H1})y_2(\tau) + \chi(\tau - \tau_{H2})y_3(\tau) \\ \text{if } (\tau_3 < \tau < \tau_4) & \text{then } \bar{Pr}_L(\tau) = a_{BC} + b_{BC} \tau + c_{BC} \tau^2 + d_{BC} \tau^3 \\ \text{if } (\tau \geq \tau_4) & \text{then } \bar{Pr}_L(\tau, p) = (a_B + b_B p)(c_B \tau^{d_B}) \end{array} \right. \quad (6.204)$$

Table 6.13 – Resulting liquid reduced Prandtl number approximation parameters.

$a_A = 4.4707E14$	$d_B = -1.609E2$	$\tau_{H2} = 0.976$	$\Delta\tau_1 = 4E-3$
$b_A = 1.2177E15$	$e_B = 2.743E2$	$a_{BC} = -7.398E3$	$\Delta\tau_2 = 3E-3$
$a_{AB} = 1.7315E14$	$f_B = -2.368E2$	$b_{BC} = 2.106E4$	$\Delta\tau_3 = 3E-3$
$b_{AB} = -9.245E16$	$g_B = 8.097E1$	$c_{BC} = -1.998E4$	$\Delta\tau_4 = 6.913E-2$
$c_{AB} = 3.9173E18$	$h_B = 8.5$	$d_{BC} = 6.317E3$	
$d_{AB} = 2.5536E21$	$i_B = 1.5$	$a_C = -9.66E-1$	
$a_B = -2.7E-2$	$j_B = 9E3$	$b_C = 1.582$	
$b_B = -8.667$	$k_B = 1.467$	$c_C = 5.38E-1$	
$c_B = 5.091E1$	$\tau_{H1} = 0.87$	$d_C = -9.651$	

To return to original Prandtl number from the obtained approximations, use inverse expression:

$$\text{Pr}_l(T) = \text{Pr}_l(T_3) + \text{aprx}(\bar{\text{Pr}}_l(\tau))(\text{Pr}_l(T_{cr}) - \text{Pr}_l(T_3)) \quad (6.205)$$

6.12 Approximations for latent heat

6.12.1 Approximations for saturated zone

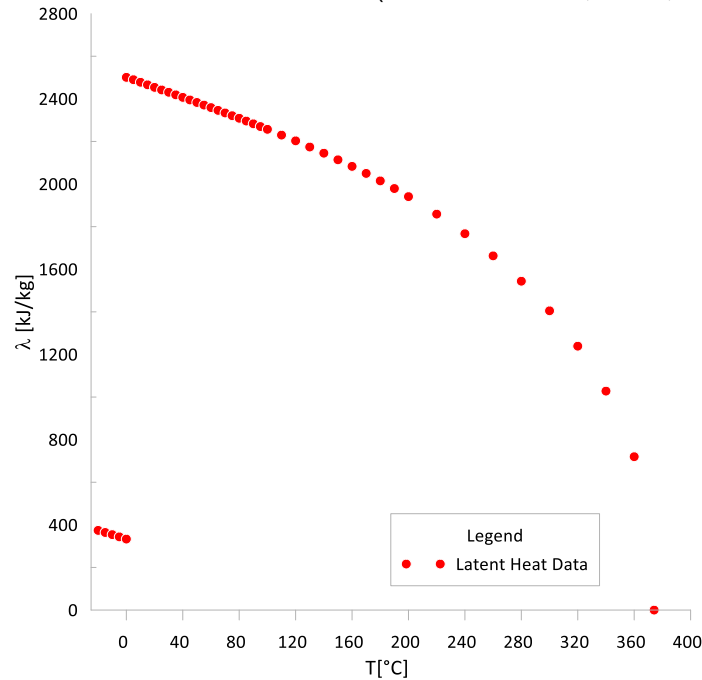
Latent Heat (λ) can be defined as the amount of energy released or absorbed during the phase change of the substance (Q) by unity of mass (M). Latent heat also known as energy released or absorbed by a thermodynamical system during a transmission between phases. It can be applied to evaporation-condensation process (transition of liquid phase to vapor phase, and vice versa), as well as to melting-solidification process (transition of solid phase to liquid phase and vice versa). In the first case it is known as latent heat of vaporization (or enthalpy of vaporization), and in second case it is known as latent heat of fusion (enthalpy of fusion).

The parameter can be defined through the following equation:

$$\lambda = \frac{Q}{M} \quad (6.206)$$

The original data of the latent heat behavior with temperature, published by ASHRAE Lemmon et al. (2023), and data from Liley (2005), are presented in Figure 6.115.

Figure 6.115 – Water Latent Heat Data. (LEMMON et al., 2023; LILEY, 2005).



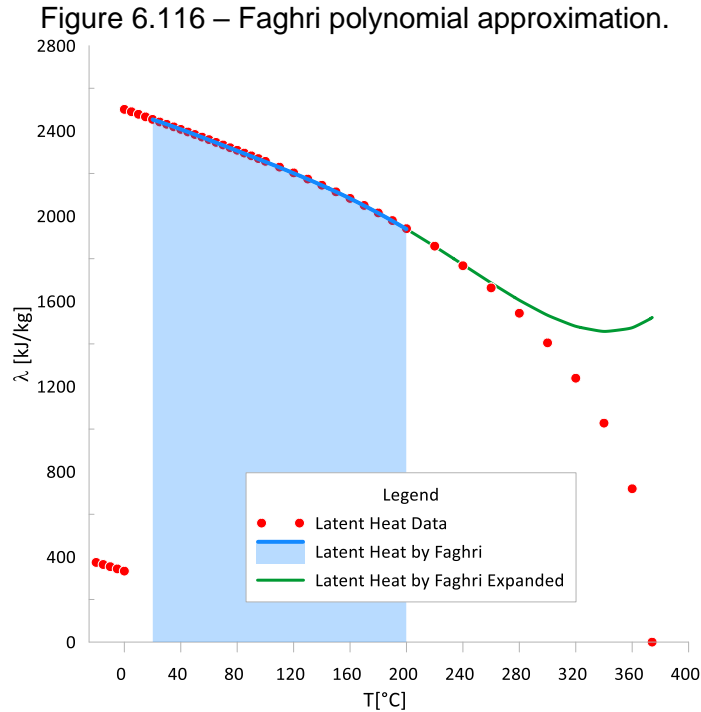
The data presented in Figure 6.115 covers solid state and two-phase coexisting phase zone. At super-critical temperature zone, the latent heat is 0.

Faghri (2016) suggested a polynomial function to approximate logarithm of this water property (6.207). The latent heat is expressed in KJ/kg and the temperature is in Celsius.

$$\begin{aligned} \ln(\lambda(T)) = & 7.8201 - 5.8906 \cdot 10^{-4} \cdot T - 9,1355 \cdot 10^{-6} \cdot T^2 + \\ & 8.4738 \cdot 10^{-8} \cdot T^3 - 3.9635 \cdot 10^{-10} \cdot T^4 - 3.04 \cdot 10^{-13} \cdot T^5 \end{aligned} \quad (6.207)$$

This equation is valid from 20°C up to 200°C, having the approximation error of 0.03%. However, the approximation covers up to 48% of the entire two-phase temperature range. As an example, when we try to use this polynomial equation out of established range, the result does not follow the real behavior. The green

line in Figure 6.116 expresses this deviation from the real value. It is not possible to use such approximation above 200 °C.



Following our approach to elaborate the approximation over entire two-phase range, from below the triple point to the zone above the critical point, we continue using non-dimensional variables for temperature, τ , as well as for the latent heat:

$$\bar{\lambda}(\tau) = \frac{\lambda - \lambda_3}{\lambda_{cr} - \lambda_3} \quad (6.208)$$

At the critical point and above it, the dimensional λ is always equal to 0; therefore, the dimensionless latent heat $\bar{\lambda} = 1$ for this region. At $\tau=0$, $\lambda_3 \approx 2500$ KJ/kg. In the ice (solid) region, the latent heat value drops from ~ 2500 KJ/kg down to ~ 333 KJ/kg. Therefore, in the negative temperature region ($\tau < 0$, i.e., “ice”), the dimensionless latent heat $\bar{\lambda}$ jumps from 0 to the value of ~ 0.867 .

For the saturation interval (i.e., two-phase zone, $0 < \tau < 1$), the original curve has a sharp climb as it approaches the critical temperature. It is difficult to obtain a unique function which approximates the entire two-phase zone within acceptable

error. Therefore, we propose to improve it with application of an interruption point (τ_H) and join two approximation functions in the interval $\tau_H \leq \tau < 1$ by application of Heaviside function.

The best outcome resulted the following combination of two approximate functions:

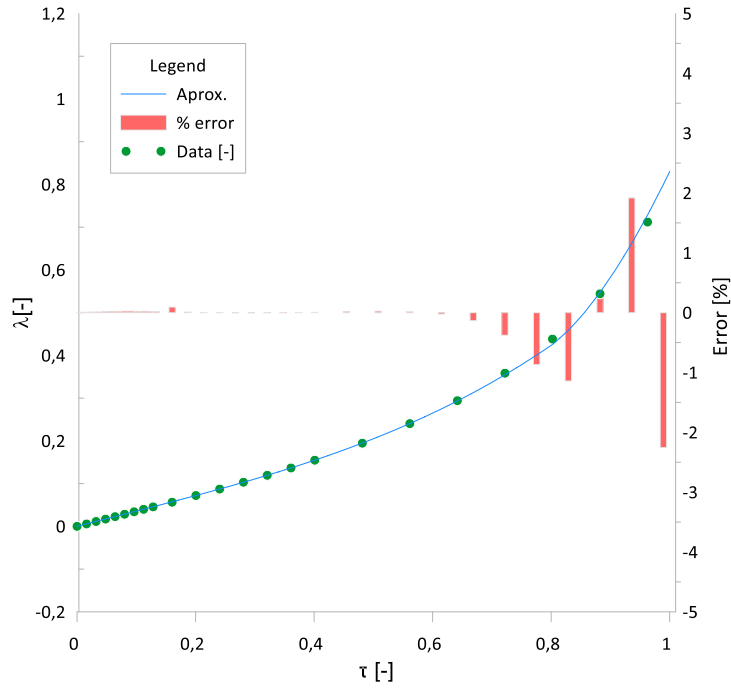
$$\begin{cases} y_1 = a_B + b_B \tau + c_B \tau^2 + d_B \tau^3 + e_B \tau^4 \\ y_2 = g_B (\tau - \tau_{H1})^{h_B} \end{cases} \quad (6.209)$$

These functions are used in an additive way: when $0 < \tau < \tau_H$, then $y = y_1(\tau)$; when $\tau_{H1} < \tau < \tau_{H2}$, then $y(\tau) = y_1(\tau) + y_2(\tau)$. This can be condensed in a unique correlation for our property:

$$\bar{\lambda}(\tau) = y_1(\tau) + \chi(\tau_{H1}) y_2(\tau) \quad (6.210)$$

By applying the algorithm above, in the saturation interval of temperature we achieve the curve shown below. The chart on Figure 6.117 shows data from ASHRAE using green circles (LEMMON et al., 2023). The approximation results are in the blue line. In red bars we have the deviation error from property table data and approximation.

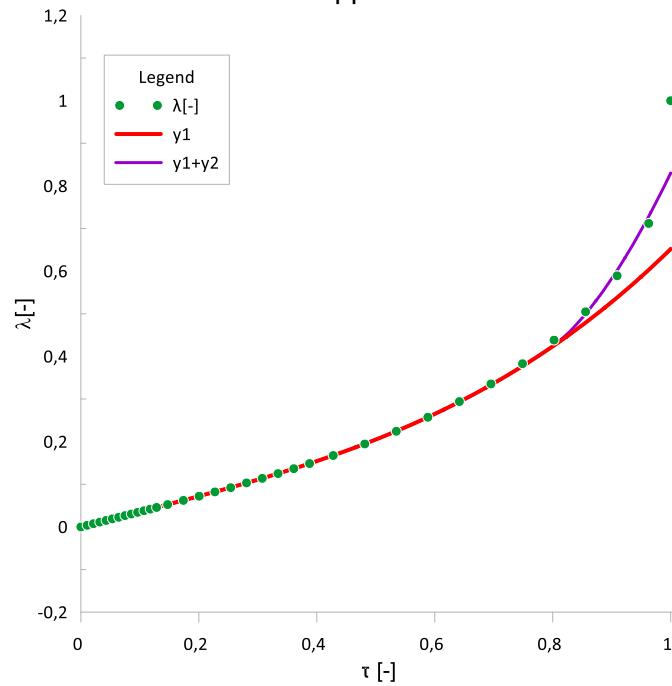
Figure 6.117 – Latent Heat approximation result in saturated zone.



We observe the deviation from the experimental property data by the approximation lie within the acceptance criteria of 3%.

To build this property approximation we used a baseline curve (4th degree polynomial equation), by adding the second function y_2 , that satisfies the criteria of tangency and continuity, by using of the Heaviside function. The result of that is shown in Figure 6.118. The main reason to use this technique is to reach the approximation curve to be continuous and “smooth,” without sharp edges.

Figure 6.118 – Two-functions approximation for saturated zone.



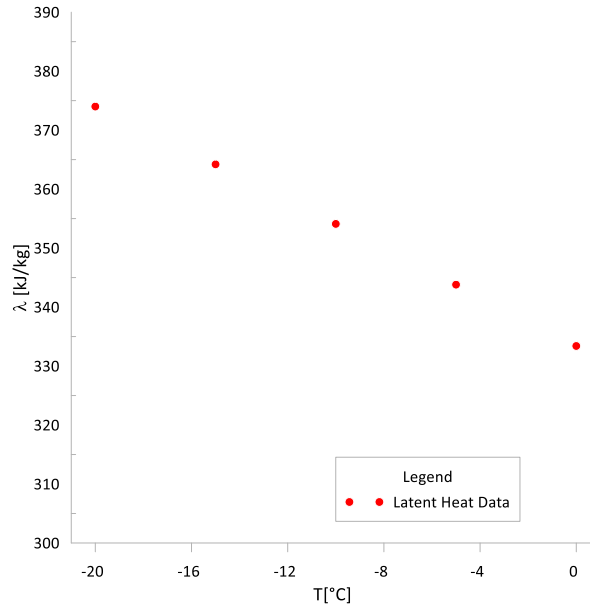
6.12.2 Approximations for freezing zone and interfacing

For the sub-freezing zone, Liley (2005) suggested one approximation to describe that property behavior (Where, λ is in KJ/Kg and T is in Celsius degree, see Figure 6.119). In that case, this equation ranges from -20 °C to 0°C. The approximation is expressed in Equation (6.211).

$$\lambda(T) = -333.4 + 2.11 \cdot T + 4 \cdot 10^{-3} \cdot T^2 \quad (6.211)$$

Where, λ is KJ/Kg and T is Celsius degree.

Figure 6.119 – Property data in freezing zone. (LILEY, 2005).



In this zone, the dimensionless latent heat can be approximated by a linear function:

$$\bar{\lambda}_A(\tau) = a_A + b_A \tau \quad (6.212)$$

Interfacing third-degree polynomial function joins the subcooled zone with saturated zone, Equation (6.213).

$$\bar{\lambda}_{AB}(\tau) = a_{AB} + b_{AB}\tau + c_{AB}\tau^2 + d_{AB}\tau^3 \quad (6.213)$$

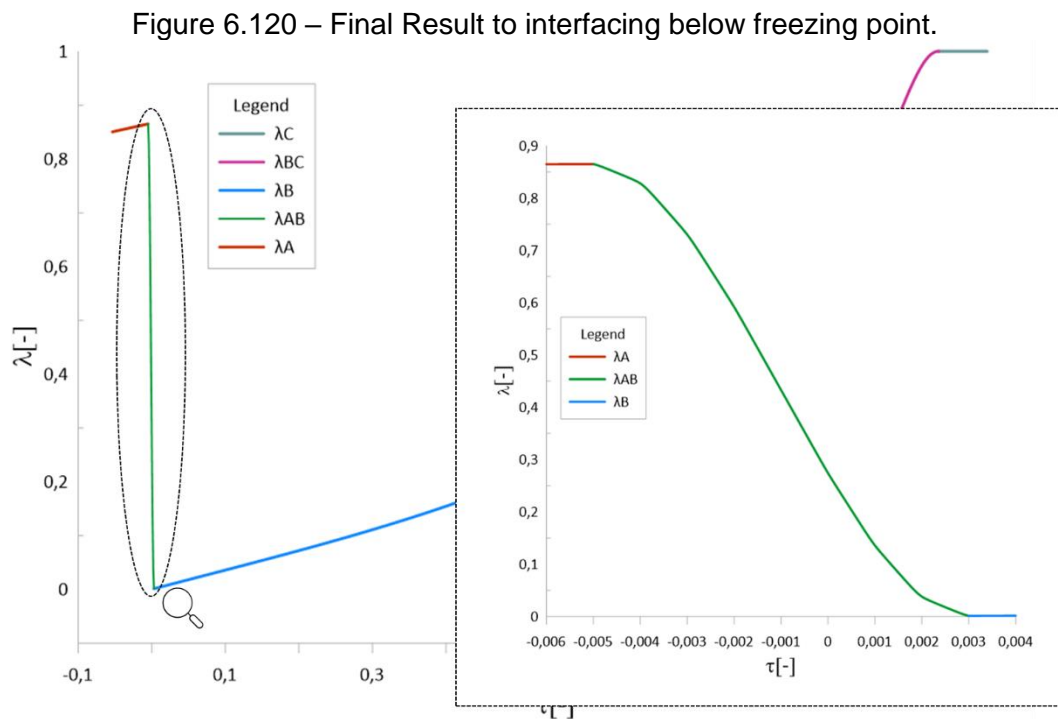
The system of 4 equations for uninterrupted join conditions presents the usual format to the interfacing equations touching tangentially both curves of value and derivative, (as example, see Equation 6.46). The tangency points are defined aiming to optimize the approximation result:

$$\begin{aligned} \Delta\tau_1 &= 0.005; \\ \Delta\tau_2 &= 0.003; \\ \tau_1 &= -\Delta\tau_1 \\ \tau_2 &= +\Delta\tau_2 \end{aligned} \quad (6.214)$$

The solution for interfacing polynomial coefficients is expressed below:

$$\begin{cases} a_{AB} = 0.27425 \\ b_{AB} = -152.0027 \\ c_{AB} = 10159.662 \\ d_{AB} = 3385375.0 \end{cases} \quad (6.215)$$

The result approximations around triple point ($\tau=0$), including the interfacing curve, are shown in Figure 6.120.



6.12.3 Approximations for supercritical zone and interfacing

In super-critical zone, the latent heat is 0, so the equation system follows the steps below.

For super-critical zone dimensional $\lambda=0$, dimensionless $\bar{\lambda} = 1$, and derivative is 0:

$$\bar{\lambda}_c(\tau)|_{\tau=1} = 1 \quad (6.216)$$

$$\left. \frac{d(\bar{\lambda}_c(\tau))}{d(\tau)} \right|_{\tau=1} = 0 \quad (6.217)$$

Looking for a smooth transition between those two zones, Equations (6.210) and (6.216), it is used a third-degree polynomial Equation (6.218).

$$\bar{\lambda}_{BC}(\tau) = a_{BC} + b_{BC}\tau + c_{BC}\tau^2 + d_{BC}\tau^3 \quad (6.218)$$

The tangency points can be defined by optimizing the approximation result. In this case $\Delta\tau$ defines how far each point are from the critical point, ($\tau=1$).

$$\begin{aligned} \Delta\tau_3 &= 0.003; \\ \Delta\tau_4 &= 0.06913; \\ \tau_3 &= 1 - \Delta\tau_3 = 0.997 \\ \tau_4 &= 1 - \Delta\tau_4 = 1.06913 \end{aligned} \quad (6.219)$$

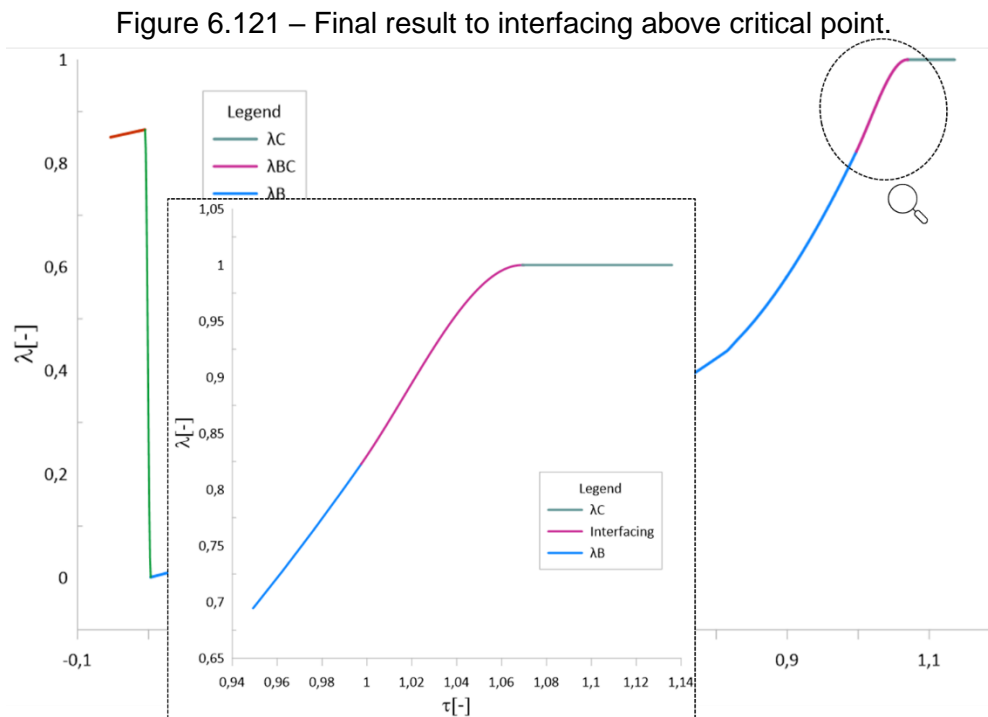
The system of Equation (6.220) has the following format to uninterrupted joining when both curves make a continuous smooth link.

$$\left\{ \begin{array}{l} \bar{\lambda}_B(\tau_3) = a_{BC} + b_{BC}\tau_3 + c_{BC}\tau_3^2 + d_{BC}\tau_3^3 \\ \frac{d(\bar{\lambda}_B(\tau_3))}{d(\tau_3)} = b_{BC} + 2c_{BC}\tau_3 + 3d_{BC}\tau_3^2 \\ \bar{\lambda}_C(\tau_4) = a_{BC} + b_{BC}\tau_4 + c_{BC}\tau_4^2 + d_{BC}\tau_4^3 \\ \frac{d(\bar{\lambda}_C(\tau_4))}{d(\tau_4)} = b_{BC} + 2c_{BC}\tau_4 + 3d_{BC}\tau_4^2 \end{array} \right. \quad (6.220)$$

Solving the system, the parameters values are available below.

$$\left\{ \begin{array}{l} a_{BC} = 421.552 \\ b_{BC} = -1247.8504 \\ c_{BC} = 1230.554 \\ d_{BC} = -403.426 \end{array} \right. \quad (6.221)$$

Figure 6.121 shows the result of the approximation.

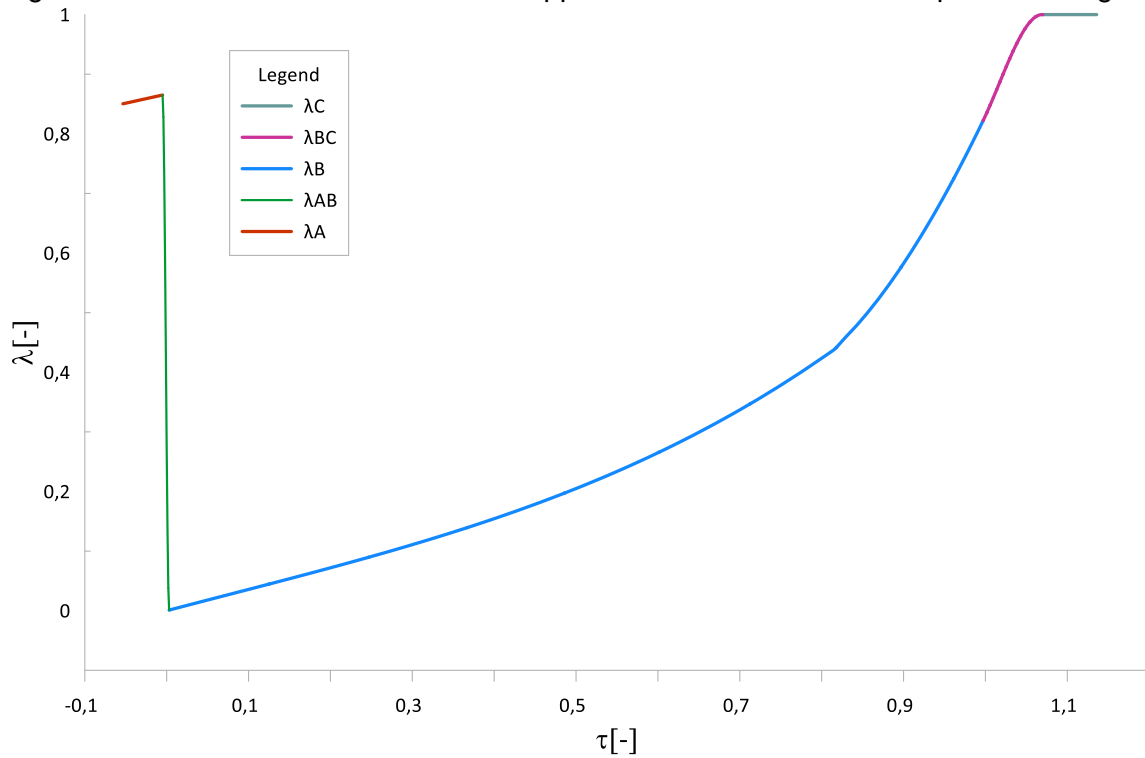


6.12.4 Final approximation and pseudo code

The proposed approximation of the entire region, which includes the regions below freezing and above critical point, is shown in Figure 6.122.

Therefore, the approximation is starting with a negative dimensionless temperature in the freezing region, and $\bar{\lambda}$ achieving a maximum $\bar{\lambda} = 1$ above the critical point, which corresponds the situation of no vapor-liquid interface existence. At the supercritical region, the property has 0 value, translating into $\bar{\lambda} = 1$ on dimensionless rule.

Figure 6.122 – Final result to latent heat approximation in the entire temperature range.



In this section we reach an approximation in a wide range of temperature, with satisfactory error levels (no greater than 3%). The pseudo code provides fluid property values starting below triple point up to above critical point (Figure 6.122).

This code (6.222) can be implemented in any programming language.

$$\left\{ \begin{array}{ll} \text{if } (\tau \leq \tau_1) & \text{then } \bar{\lambda}(\tau) = a_A + b_A \tau \\ \text{if } (\tau_1 < \tau < \tau_2) & \text{then } \bar{\lambda}(\tau) = a_{AB} + b_{AB} \tau + c_{AB} \tau^2 + d_{AB} \tau^3 \\ \text{if } (\tau_2 \leq \tau \leq \tau_3) & \text{then } \bar{\lambda}(\tau) = y_1(\tau) + \chi(\tau - \tau_{H1}) y_2(\tau) \\ \text{if } (\tau_3 < \tau < \tau_4) & \text{then } \bar{\lambda}(\tau) = a_{BC} + b_{BC} \tau + c_{BC} \tau^2 + d_{BC} \tau^3 \\ \text{if } (\tau \geq \tau_4) & \text{then } \bar{\lambda}(\tau) = 0 \end{array} \right. \quad (6.222)$$

Table 6.14 – Resulting latent heat approximation parameters.

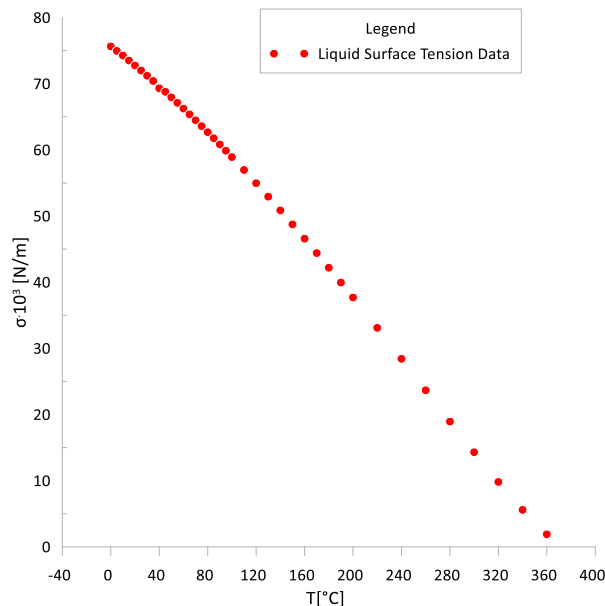
$a_A = 8.67E-1$	$d_{AB} = 3.385E6$	$e_B = 5.3E-2$	$b_{BC} = -1.248E3$	$\Delta\tau_3 = 3E-3$
$b_A = 3.04E-1$	$a_B = 0$	$f_B = 2.75$	$c_{BC} = 1.230E3$	$\Delta\tau_4 = 6.913E-2$
$a_{AB} = 2.74E-1$	$b_B = 3.608E-1$	$g_B = 1.7$	$d_{BC} = -4.034E3$	
$b_{AB} = -1.52E2$	$c_B = -6.84E-2$	$\tau_{H1} = 0.80$	$\Delta\tau_1 = 5E-3$	
$c_{AB} = 1.016E4$	$d_B = 3.06E-1$	$a_{BC} = 4.215E2$	$\Delta\tau_2 = 3E-3$	

6.13 Approximations for surface tension

Surface tension is an important parameter with physical effect, which is observable in two physical phases. This phenomenon becomes noticeable when the liquid surface behaves like an elastic membrane due to molecular cohesive forces between its molecules.

Surface tension, represented by the symbol σ , is measured in force per unit length: N/m. The surface tension behavior with temperature can be seen below (LEMMON et al., 2023) in Figure 6.123.

Figure 6.123 – Water surface tension data.



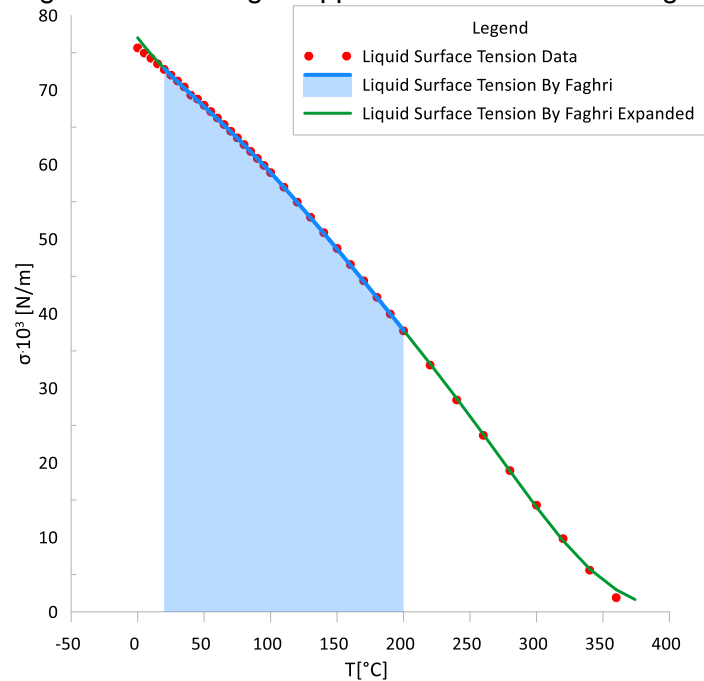
Faghri (2016) suggested equation to approximate the logarithm of this water property by a polynomial function of 5th order.

$$\begin{aligned} \ln(\sigma(T)) = & 4.3438 - 3.0664 \cdot 10^{-3} \cdot T + 2.0743 \cdot 10^{-5} \cdot T^2 - \\ & 2.5499 \cdot 10^{-7} \cdot T^3 + 1.0377 \cdot 10^{-9} \cdot T^4 - 1.7156 \cdot 10^{-12} \cdot T^5 \end{aligned} \quad (6.223)$$

The surface tension is expressed in N/m and the temperature used in the equation is in Celsius.

This equation is valid between 20°C and 200°C; in this range the approximation error mentioned in (FAGHRI, 2016) is 0.03% and the equation (6.223) covers up to 48% of working temperature range.

Figure 6.124 – Faghri approximation available range.



Following the approach to elaborate the approximation over entire two-phase range, from below the triple point to the zone above the critical point, we continue using non-dimensional variables for temperature, τ , as well as for the surface tension:

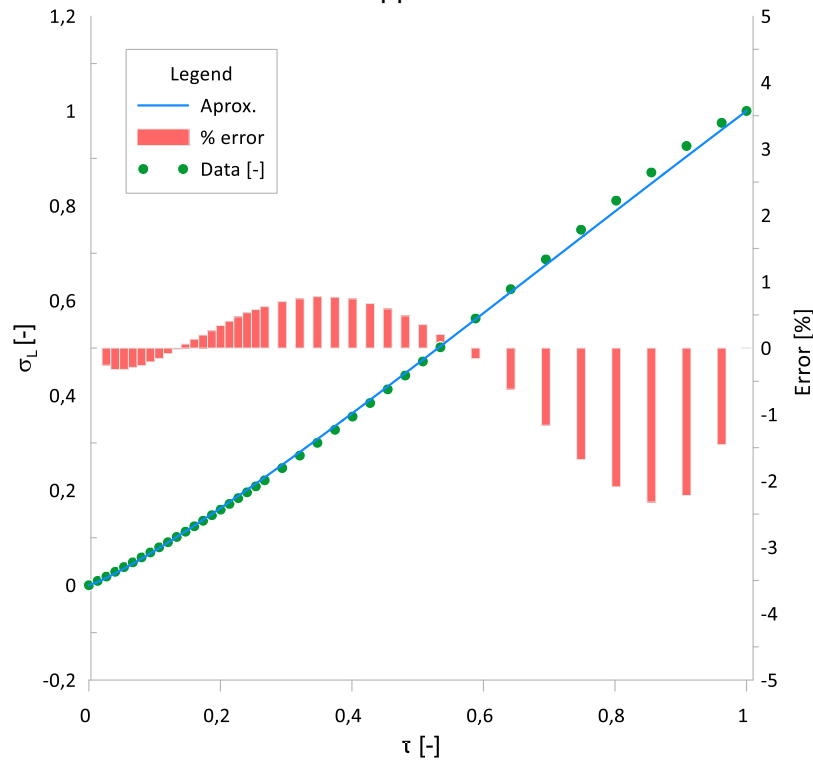
$$\bar{\sigma}(\tau) = \frac{\sigma - \sigma_3}{\sigma_{cr} - \sigma_3} \quad (6.224)$$

As for the approximation, the best results gave the following function:

$$\bar{\sigma}(\tau) = \tau^{a_B(1+b_B\tau)} \quad (6.225)$$

In the saturation interval of temperature, we achieve the curve presented in Figure 6.124. That graph shows data from ASHRAE using green circles (LEMMON et al., 2023). The approximation results in the blue line. In red bars we have the deviation error from property table data and approximation.

Figure 6.125 – Surface tension approximation result in saturated zone.



We observe the deviation from the tabled original property data by the approximation lies within the acceptance criteria of 3% over almost entire range.

In the freezing zone, this property has no value, so the smooth link will be established having a 0 value:

$$\bar{\sigma}_A(\tau) = 0 \quad (6.226)$$

Interfacing equation joins the subcooled zone with saturated zone, used a third-degree polynomial function (6.227).

$$\bar{\sigma}_{AB}(\tau) = a_{AB} + b_{AB}\tau + c_{AB}\tau^2 + d_{AB}\tau^3 \quad (6.227)$$

The system of equations of uninterrupted joining has a usual format, like Equation 6.46, and does not present here.

Points of tangency are the following:

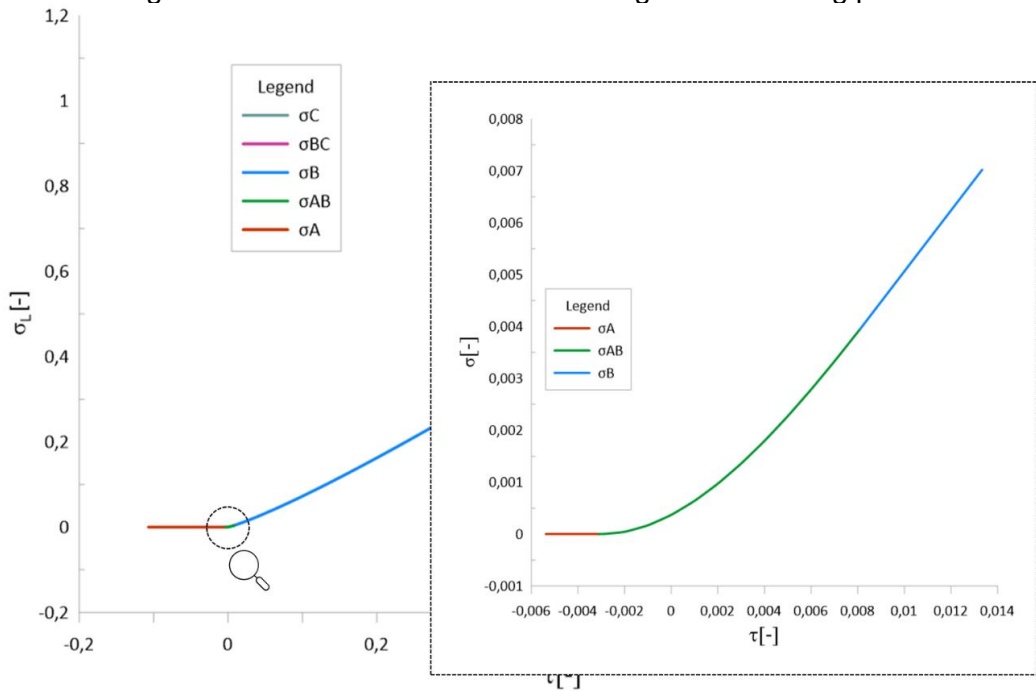
$$\begin{aligned} \Delta\tau_1 &= 0.003; \\ \Delta\tau_2 &= 0.008; \\ \tau_1 &= -\Delta\tau_1 \\ \tau_2 &= +\Delta\tau_2 \end{aligned} \quad (6.228)$$

The solution for interfacing polynomial coefficients is expressed below.

$$\begin{cases} a_{AB} = 0.0003698 \\ b_{AB} = 0.23650 \\ c_{AB} = 34.4026 \\ d_{AB} = -1114.35 \end{cases} \quad (6.229)$$

The result approximations around triple point ($\tau=0$), including the interfacing curve, is shown in Figure 6.126.

Figure 6.126 – Final Result to interfacing below freezing point.



For the super-critical zone, this parameter does not make sense once the vapor-liquid interface does not exist; Therefore, we assume this absolute value to be 0, which corresponds to 1 for the dimensionless surface tension:

$$\bar{\sigma}_c(\tau) = 1 \quad (6.230)$$

A smooth transition between those two zones provides a third-degree polynomial function (6.231).

$$\bar{\sigma}_{BC}(\tau) = a_{BC} + b_{BC}\tau + c_{BC}\tau^2 + d_{BC}\tau^3 \quad (6.231)$$

Chosen points of tangency at critical point, ($\tau=1$), are given below.

$$\begin{aligned} \Delta\tau_3 &= 0.005; \\ \Delta\tau_4 &= 0.005; \\ \tau_3 &= 1 - \Delta\tau_3 = 0.995 \\ \tau_4 &= 1 - \Delta\tau_4 = 1.005 \end{aligned} \quad (6.232)$$

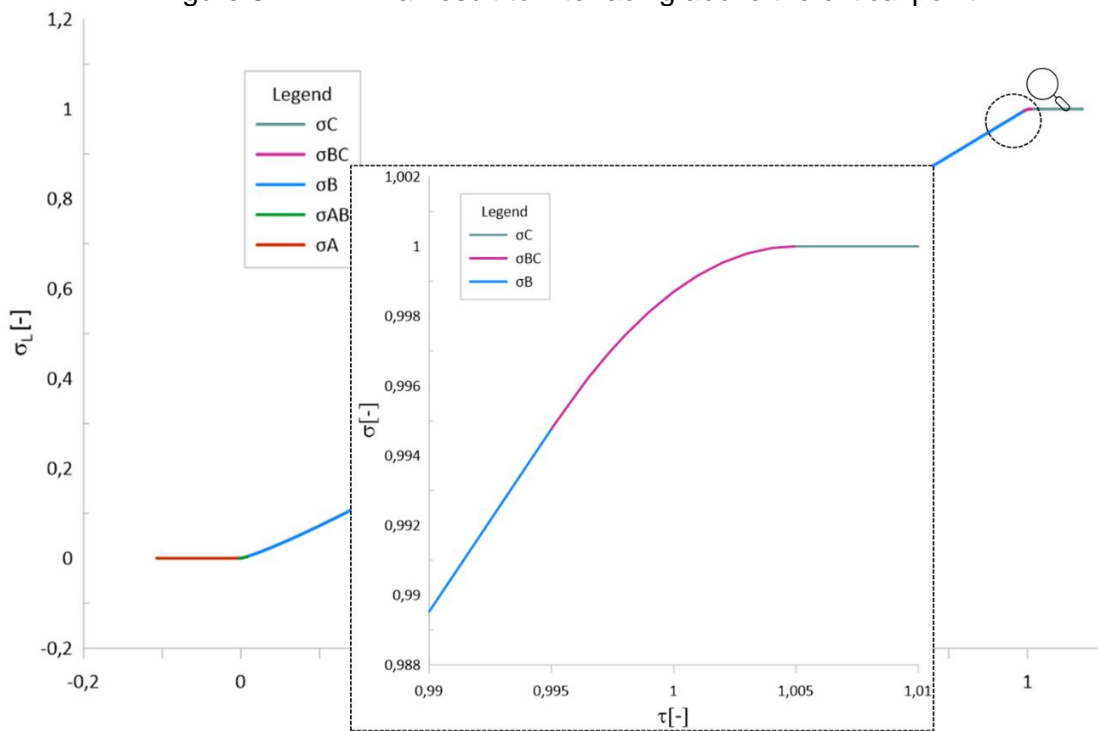
The system has the following similar format to the interfacing equation tangency when both curves make a continuous smooth link.

By solving this system, the parameters values are presented below.

$$\begin{cases} a_{BC} = -107.658 \\ b_{BC} = 272.3035 \\ c_{BC} = -219.159 \\ d_{BC} = 55.5123 \end{cases} \quad (6.233)$$

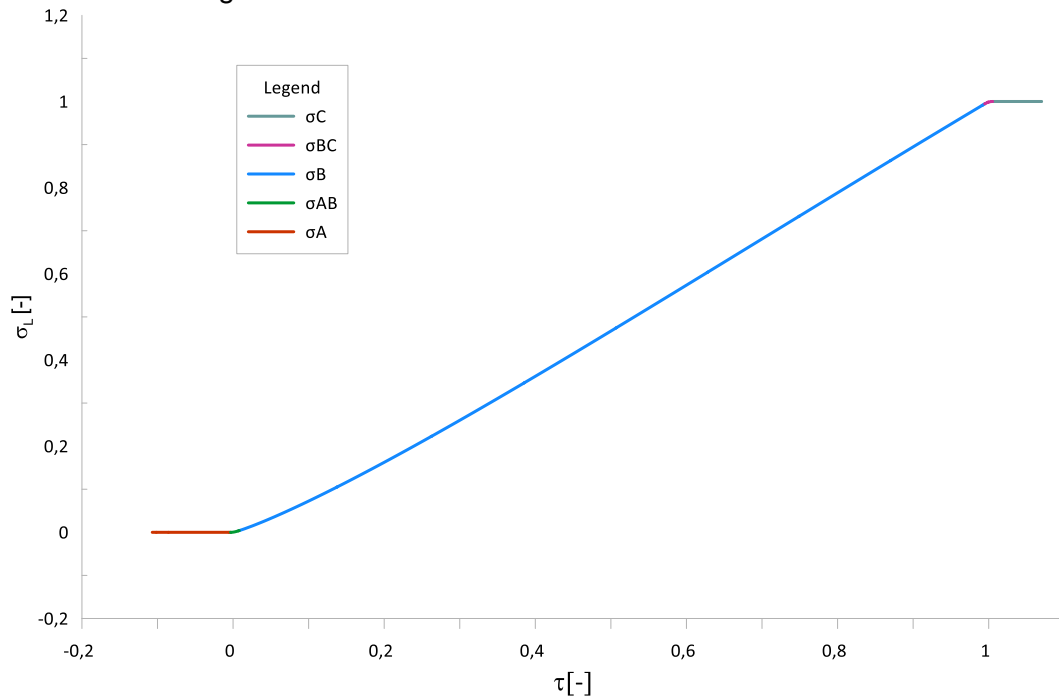
Figure 6.127 shows the result of the approximation with the interfacing curve.

Figure 6.127 – Final result to interfacing above the critical point.



The algorithm above that we proposed for the approximation of the entire region which also includes below freezing and above critical point regions is shown in Figure 6.128.

Figure 6.128 – Final result to surface tension approximation in the entire temperature range.



Therefore, in this chapter we reach an approximation in a wide range of temperature, managing the approximation error at satisfactory levels (no greater than 3%), Figure 6.127. The pseudo code provides fluid property values starting below triple point up to above critical point, (6.234) .

This code can be implemented in any programming language.

$$\left\{ \begin{array}{ll}
 \text{if } (\tau \leq \tau_1) & \text{then } \bar{\sigma}(\tau) = 0 \\
 \text{if } (\tau_1 < \tau < \tau_2) & \text{then } \bar{\sigma}(\tau) = a_{AB} + b_{AB}\tau + c_{AB}\tau^2 + d_{AB}\tau^3 \\
 \text{if } (\tau_2 \leq \tau \leq \tau_3) & \text{then } \bar{\sigma}(\tau) = \tau^{a_B(1+b_B\tau)} \\
 \text{if } (\tau_3 < \tau < \tau_4) & \text{then } \bar{\sigma}(\tau) = a_{BC} + b_{BC}\tau + c_{BC}\tau^2 + d_{BC}\tau^3 \\
 \text{if } (\tau \geq \tau_4) & \text{then } \bar{\sigma}(\tau) = 1
 \end{array} \right. \quad (6.234)$$

Table 6.15 – Resulting to surface tension approximation parameters.

$a_{AB} = 3.698E-4$	$b_{BC} = 2.723E2$
$b_{AB} = 2.365E-1$	$c_{BC} = -2.192E2$
$c_{AB} = 3.440E1$	$d_{BC} = 5.551E1$
$d_{AB} = -1.1143E3$	$\Delta\tau_1 = 8E-3$
$a_B = 1.15$	$\Delta\tau_2 = 5E-3$
$b_B = -9E-2$	$\Delta\tau_3 = 5E-3$
$a_{BC} = -1.077E2$	$\Delta\tau_4 = 5E-3$

7. CONCLUSIONS

This work presents for the first time a methodology for the approximations of 13 thermophysical properties applied for water in the expanded temperature range starting from the freezing zone (below triple point), then passing through entire vapor-liquid coexisting zone (two-phase or saturation zone) and ending at the supercritical zone (above the critical temperature). This is different from the usual approach in which researchers propose approximations to a property in a strict temperature range, aligning with the typical operating limits of heat pipes. The development of methodologies and approximations provides the foundation for complex transient mathematical models applicable to freezable and cryogenic heat pipes. An important feature of these approximations is the uninterrupted and smooth behavior of any thermo-physical property over the entire temperature range, with an acceptable deviation to prevent erroneous modeling and numerical instability. To develop these property approximations over the entire temperature range by a piecewise function with different components, the Heaviside function technique was applied for the first time. Another advance is the interfacing technique, which provides a smooth connection between the curves in different matter state zones.

It is proposed an advanced unique dimensionless format for temperature, pressure, and all other properties, correlating not only the value of the property at the critical point but also at the triple point. To treat the dimensionless temperature as dimensionless values, some authors used only the temperature divided by critical temperature; our approach brings a certain physical sense because the dimensionless temperature is always 0 at the freezing point and 1 at a critical point, keeping the interval between 0 to 1 for the saturation conditions when both vapor and liquid phases coexist. Correspondingly, if temperature is negative, it means the freezing zone; if above 1 - supercritical region. Moreover, all 13 properties behave by a similar way. Such approach provides universal approximations, and we expect the similar correlations can be developed for other working fluids. Another advantage of using dimensionless temperature and dimensionless properties is that the approximation parameters do not depend on

a system of units of measurement, which can be used in International System or Imperial System of Units without any changes.

These approaches establish a solid foundation for developing approximations for other fluids, such as acetone and ammonia, among others. These can be used in mathematical models of heat pipes for transient behavior simulations in a large temperature range. Notably, the developed approximations are not closed-form correlations but as pseudo-codes, which can be implemented in any programming language and applied in mathematical models.

The implemented random optimal search method was applied within MS Excel spreadsheets using the VBA language. The users may actively modify the optimization process by adjusting the variable limits, reducing the time of computation, and improving the approximation precision. The best parameters are obtained by minimizing a combined weighted criterion of the average deviation and the maximum error.

The applicability of the developed technique is not limited by heat pipes, capillary pumped loops, thermosyphons and other two-phase passive heat transfer devices but also every other development that need water property value.

8. PROPOSAL FOR FUTURE RESEARCH

This innovative approach, along with all approximation results, was initially developed for water due to the wide availability of tabulated data for all 13 thermo-physical properties for the saturation zone, overheated steam, and ice. We expect that the format of multiple piecewise functions and pseudo-codes would be similar for other working fluids thanks to the universal dimensionless approach. The optimization algorithm can be improved to not only to calculate the best approximation parameters but also to select the best set of functions used in the piecewise approximation.

REFERENCES

- ACREE, W. E.; CHICKOS, J. S. **Phase transition enthalpy measurements of organic and organometallic compounds**. 69. ed. Gaithersburg MD: National Institute of Standards and Technology, 2023.
- ANDERSON, W. G.; ROSENFELD, J. H.; ANGIRASA, D.; MI, Y. Evaluation of heat pipe working fluids in the temperature range 450 to 700 K. **AIP Conference Proceedings**, p. 20-27, 2004.
- ANGELL, C. A.; SICHINA, W. J.; OGUNI, M. Heat capacity of water at extremes of supercooling and superheating. **The Journal of Physical Chemistry**, v. 86, n. 6, p. 998–1002, 1982.
- ARCHER, D. G.; CARTER, R. W. Thermodynamic properties of the NaCl + H₂O system. 4. heat capacities of H₂O and NaCl(aq) in cold-stable and supercooled states. **The Journal of Physical Chemistry B**, v. 104, n. 35, p. 8563–8584, 2000.
- BEATON, C. F. Steam tables. In: THERMOPEDIA. **A-to-Z guide to thermodynamics, heat and mass transfer, and fluids engineering**. [S.l.]: Begellhouse, 1986.
- BRENNAN, P. J.; KROLICZEK, E. J. **Heat pipe design handbook**. Maryland: [s.n.], 1979.
- BRYSON, C. E.; CAZCARRA, V.; LEVENSON, L. L. Sublimation rates and vapor pressures of water, carbon dioxide, nitrous oxide, and xenon. **Journal of Chemical & Engineering Data**, v. 19, n. 2, p. 107–110, 1974.
- DAY, M. A. The no-slip condition of fluid dynamics. **Erkenntnis**, v. 33, n. 3, p. 285–296, 1990.
- DEVARAKONDA, A. Thermo-physical properties of intermediate temperature heat pipe fluids. In: AIP CONFERENCE, 2005. **Proceedings...** AIP, 2005.
- DHANUSKODI, R.; ARUNAGIRI, A.; ANANTHARAMAN, N. Analysis of variation in properties and its impact on heat transfer in sub and supercritical conditions of water/steam. **International Journal of Chemical Engineering and Applications**, p. 320–325, 2011.
- FAGHRI, A. **Heat pipe science and technology**. 2.ed. [S.l.]: Global Digital Press, 2016.

FLUBACHER, P.; LEADBETTER, A. J.; MORRISON, J. A. Heat capacity of ice at low temperatures. **The Journal of Chemical Physics**, v. 33, n. 6, p. 1751–1755, 1960.

FUKUSAKO, S. Thermophysical properties of ice, snow, and sea ice 1. **International Journal of Thermophysics**, v.11, p. 353 – 372, 1990.

GAKAL, P.; MISHKINIS, D.; LEILANDS, A.; USAKOV, I.; ORLOV, R.; ROGOVIY, Y. Analysis of working fluids applicable for high-temperature loop heat pipe applications. **IOP Conference Series: Materials Science and Engineering**, v. 1226, n. 1, p. 012036, 2022.

GIAUQUE, W. F.; STOUT, J. W. The entropy of water and the third law of thermodynamics. the heat capacity of ice from 15 to 273°K. **Journal of the American Chemical Society**, v. 58, n. 7, p. 1144–1150, 1936.

GOFF, J. A. Saturation pressure of water on the new Kelvin scale. In: CONFERENCE OF THE AMERICAN SOCIETY OF HEATING, REFRIGERATING AND AIR-CONDITIONING ENGINEERS, 1957. **Proceedings...** 1957. p.347-354.

GOFF, J. A. **In Humidity and moisture: measurement and control in science and industry: fundamentals and standards**. New York: Reinhold, 1965.

GOFF, J. A.; GRATCH, S. Low-pressure properties of water from –160 to 212 F. In: CONFERENCE OF THE AMERICAN SOCIETY OF HEATING, REFRIGERATING AND AIR-CONDITIONING ENGINEERS, 1946, New York. **Proceedings...** 1946.

GROVER, G. M.; COTTER, T. P.; ERICKSON, G. F. Structures of very high thermal conductance, **Journal of Applied Physics**, v. 35, n. 6, p. 1990–91, 1964. Doi: 10.1063/1.1713792.

Haskin, W. L. **Cryogenic heat pipe**. [S.l.]: Air Force Flight Dynamics Laboratory, 1967.

HUBER, M. L.; PERKINS, R. A.; LAESECKE, A.; FRIEND, D. G.; SENGERS, J. V.; ASSAEL, M. J.; METAXA, I. N.; VOGEL, E.; MAREŠ, R.; MIYAGAWA, K. New international formulation for the viscosity of H₂O. **Journal of Physical and Chemical Reference Data**, v. 38, n. 2, p. 101–125, 2009.

HYLAND, R. W.; WEXLER, A. Formulations for the thermodynamic properties of the saturated phases of H₂O from 173.15 K to 473.15 K. **Ashrae Transactions**, v. 89, n. 2, p. 500–519, 1983.

JANCOSO, G.; PUPEZIN, J.; VAN HOOK, W. A. Vapor pressure of ice between +10-2 and -1020. **The Journal of Physical Chemistry**, v. 74, n. 15, p. 2984–2989, 1970.

JAWORSKE, D.; SANZI, J.; SIAMIDIS, J. Cold start of a radiator equipped with titanium-water heat pipes. In: INTERNATIONAL ENERGY CONVERSION ENGINEERING CONFERENCE, 6., 2008. **Proceedings...** AIAA, 2008.

JOUHARA, H.; CHAUHAN, A.; NANNOU, T.; ALMAHMOUD, S.; DELPECH, B.; WROBEL, L. C. Heat pipe based systems: advances and applications. **Energy**, v. 128, p. 729–754, 2017.

KALOVA, J.; MARES, R. Crossover equation and the vapor pressure of supercooled water. In: INTERNATIONAL JOURNAL OF THERMOPHYSICS, 2010. **Proceedings...** New York: LLC, 2010.

KESTIN, J.; SOKOLOV, M.; WAKEHAM, W. A. Viscosity of liquid water in the range –8 °C to 150 °C. **Journal of Physical and Chemical Reference Data**, v. 7, n. 3, p. 941–948, 1978.

KISEEV, V.M.; VLASSOV, V.V.; MURAOKA, I.; CANDIDO, P.A. Tri-phase Heat Switch: Application, Development and Test. IN: 15th International Heat Pipe Conference. April 25 to 30, 2010. Clemson, SC, USA. **Proceedings...** 2010

KOOP, T.; LUO, B.; TSIAS, A.; PETER, T. Water activity as the determinant for homogeneous ice nucleation in aqueous solutions. **Nature**, v. 406, n. 6796, p. 611–614, 2000.

KOUTSOYIANNIS, D. Clausius-Clapeyron equation and saturation vapour pressure: simple theory reconciled with practice. **European Journal of Physics**, v. 33, n. 2, p. 295–305, 2012.

KUMAGAI, N.; SASAJIMA, S.; ITO, H. Long-term creep experiment on rocks: results of about 20 years on large specimens and 3 years on small specimens. **Journal of the Society of Materials Science, Japan**, v. 27, n. 293, p. 155–161, 1978.

LE BIDEAU, D.; MANDIN, P.; BENBOUZID, M.; KIM, M.; SELLIER, M. Review of necessary thermophysical properties and their sensitivities with temperature and electrolyte mass fractions for alkaline water electrolysis multiphysics modelling. **International Journal of Hydrogen Energy**, v. 44, n. 10, p. 4553–4569, 2019.

LEE, J.; KIM, D.; MUN, J.; KIM, S. Heat-transfer characteristics of a cryogenic loop heat pipe for space applications. **Energies**, v. 13, n. 7, p. 1616, 2020.

- LEMMON, E. W.; BELL, I. H.; HUBER, M. L.; MCLINDEN, M. O. **Thermophysical properties of fluid systems**. NIST, 2023. Available from: <https://webbook.nist.gov/chemistry/fluid/>. Access on: 23 Feb. 2024.
- LILEY, P. E. Thermophysical properties of ice/water/steam from -20°C to 50°C. **International Journal of Mechanical Engineering Education**, v.33, p. 45-50, 2005.
- MARKOČIČ, E.; KNEZ, Ž. Redlich–Kwong equation of state for modelling the solubility of methane in water over a wide range of pressures and temperatures. **Fluid Phase Equilibria**, v. 408, p. 108–114, 2016.
- MARTI, J.; MAUERSBERGER, K. A survey and new measurements of ice vapor pressure at temperatures between 170 and 250K. **Geophysical Research Letters**, v. 20, n. 5, p. 363–366, 1993.
- MAUERSBERGER, K. Vapor pressure above ice at temperatures below 170 K. **Geophysical Research Letters**, v. 30, n. 3, p. 1121, 2003.
- MISHKINIS, D.; PRADO, P.; SANZ, R.; RADKOV, A.; TORRES IBERESPACIO, A.; TISNA TJIPTAJARDJA, S. **Loop heat pipe working fluids for intermediate temperature range: from -40°C to +125°C**. 2009. Available from: <https://www.researchgate.net/publication/257859443>. Access on: 23 Feb. 2024.
- MONDAL, D.; KARIYA, K.; TUHIN, A. R.; MIYOSHI, K.; MIYARA, A. Thermal conductivity measurement and correlation at saturation condition of HFO refrigerant trans-1,1,1,4,4,4-hexafluoro-2-butene (R1336mzz(E)). **International Journal of Refrigeration**, v. 129, p. 109–117, 2021.
- MURPHY, D. M.; KOOP, T. Review of the vapour pressures of ice and supercooled water for atmospheric applications. **Quarterly Journal of the Royal Meteorological Society**, v. 131, n. 608, p. 1539–1565, 2005.
- OCHTERBECK, J. M.; MISHKINIS, D. Loop heat pipes: criteria approach. In: MINSK INTERNATIONAL SEMINAR HEAT PIPES, HEAT PUMPS, REFRIGERATORS, 5., 2003, Minsk. **Proceedings...** 2015.
- PÁTEK, J.; HRUBÝ, J.; KLOMFAR, J.; SOUČKOVÁ, M.; HARVEY, A. H. Reference correlations for thermophysical properties of liquid water at 0.1MPa. **Journal of Physical and Chemical Reference Data**, v. 38, n. 1, p. 21–29, 2009.
- PIORO, I. L. **Advanced supercritical fluids technologies: supercritical-fluids thermophysical properties and heat transfer in power-engineering applications**. UK: Intechopen, 2020.

POLASEK, F.; STULC, P. Heat pipe for the temperature range from 200 to 600°C. In: INTERNATIONAL HEAT PIPE CONFERENCE, 2., 1976.

Proceedings... Hanover, 1976.

POLING, B. E.; PRAUSNITZ, J. M.; O'CONNELL, J. P. **The Properties of Gases and Liquids**. 5.ed. [S.l.]: McGraw-Hill, 2001.

POPIEL, C. O.; WOJTKOWIAK, J. Simple formulas for thermophysical properties of liquid water for heat transfer calculations (from 0°C to 150°C).

Heat Transfer Engineering, v. 19, n. 3, p. 87–101, 1998.

REDLICH, O.; KWONG, J. N. S. On the thermodynamics of solutions. v. an equation of state. fugacities of gaseous solutions. **Chemical Reviews**, v. 44, n. 1, p. 233–44, 1949. Doi: 10.1021/cr60137a013.

QASEM, N. A. A.; GENEROUS, M. M.; QURESHI, B. A.; ZUBAIR, S. M. A Comprehensive review of saline water correlations and data: part ii— thermophysical properties. **Arabian Journal for Science and Engineering**, v. 46, n. 3, p. 1941–1979, 2021.

QIAN, S.; LOU, S.; GE, C.; WANG, W.; TIAN, X.; CAI, Y. The influence of temperature dependent fluid properties on topology optimization of conjugate heat transfer. **International Journal of Thermal Sciences**, v. 173, 2022.

SAASKI, E. U.; SAASKI, E. W. Two-phase working fluids for the temperature range 100-350°C. In: AIAA THERMOPHYSICS CONFERENCE, 12., 1977, Albuquerque. **Proceedings...** 1977.

SAUL, A.; WAGNER, W. international equations for the saturation properties of ordinary water substance. **Journal of Physical and Chemical Reference Data**, v. 16, n. 4, p. 893–901, 1987.

SHUKLA, K. N. Heat pipe for aerospace applications: an overview. **Journal of Electronics Cooling and Thermal Control**, v. 5, n. 1, p. 1–14, 2015.

SMITH, C. J. An experimental study of the viscous properties of water vapour. **Proceedings of the Royal Society of London. Series A, Containing Papers of a Mathematical and Physical Character**, v. 106, n. 735, p. 83–96, 1924.

SMITH, R.; PETERS, C.; INOMATA, H. Equations of state and formulations for mixtures. **Supercritical Fluid Science and Technology**, v. 4, p. 333–480, 2013.

SOAVE, G. Equilibrium constants from a modified Redlich-Kwong equation of state. **Chemical Engineering Science**, v. 27, n. 6, p. 1197–1203, 1972.

SONNTAG, D. Important new values of the physical constants of 1986, vapour pressure formulations based on the ITS-90 and Psychrometer Formulae.

Meteorologische Zeitschrift, v. 40, p. 340–344, 1990.

SOTIN, C.; POIRIER, J. P. Viscosity of ice v. **Le Journal de Physique**

Colloques, v. 48, n. C1, p. C1-233-C1-238, 1987.

STRAUB, J.; ROSNER, N.; GRIGULL, U. Oberflächenspannung von leichtem und schwerem Wasser. **Wärme- und Stoffübertragung**, v. 13, n. 4, p. 241–252, 1980.

TOMBARI, E.; FERRARI, C.; SALVETTI, G. Heat capacity anomaly in a large sample of supercooled water. **Chemical Physics Letters**, v. 300, n. 5/6, p. 749–751, 1999.

TOURNIER, J.-M. AND EL-GENK, M. S. A heat pipe transient analysis model.

International Journal of Heat and Mass Transfer, v. 37, n. 5, p. 753–62, 1994. Doi: 10.1016/0017-9310(94)90113-9.

TUREKIAN, K. K.; HOLLAND, H. D. **Treatise on geochemistry**. 2. ed. [S.I.]: Elsevier, 2014.

URNS, S. R.; KRAIGE, D. R.; TURNS, S. R.; TURNS, S. R. **Property tables for thermal fluids engineering : SI and US customary units**. Cambridge: Cambridge University Press, 2007. 219 p.

VARGAFTIK, N. B.; VOLKOV, B. N.; VOLJAK, L. D. International tables of the surface tension of water. **Journal of Physical and Chemical Reference Data**, v. 12, n. 3, p. 817–820, 1983.

VLASSOV, V. V., Analysis of heat spreading performance of acetone-filled heat pipe at low temperatures for using in satellite honeycomb panels. **Journal of Aerospace Engineering, Sciences and Applications**, v. 1, p. 1–17, 2008.

VLASSOV, V. V. **Transient model of a grooved heat pipe embedded in the honeycomb structural panel**. [S.I.]: SAE, 2005. Doi: 10.4271/2005-01-2936.

VLASSOV, V. V.; RIEHL, R. R. Mathematical model of a loop heat pipe with cylindrical evaporator and integrated reservoir. **Applied Thermal Engineering**, v. 28, n. 8/9, p. 942–54, 2008. Doi: 10.1016/j.applthermaleng.2007.07.016.

WAGNER, W.; PRUSS, A. International equations for the saturation properties of ordinary water substance. revised according to the international temperature scale of 1990. **Journal of Physical and Chemical Reference Data**, v. 22, n. 3, p. 783–787, 1993.

WAGNER, W.; SAUL, A.; PRUSS, A. International equations for the pressure along the melting and along the sublimation curve of ordinary water substance. **Journal of Physical and Chemical Reference Data**, v. 23, n. 3, p. 515–527, 1994.

XIN, F.; LYU, Q.; WANG, Q. Three-dimensional numerical analysis of mini-grooved flat heat pipe filled with different working fluids with experimental validation. **Heat Transfer Engineering**, v. 44, n. 4, p. 317–333, 2023.

ZAYTSEV, I. D.; ASEYEV, G. G. **Properties of aqueous solutions of electrolytes**. [S.I.]: CRC Press, 1992.

APPENDIX A – EQUATIONS AND ITS DERIVATIVES

This appendix relies on a foundation of key mathematical equations and derivatives, presented in the work. These essential expressions serve as a guidance to build the approximations and its derivatives used for the interfacing.

$$y(x) = x^{a(1+bx)} \rightarrow \frac{\partial y(x)}{\partial x} = x^{a(1+bx)} \left(\frac{a(1+bx)}{x} + a \cdot b \cdot \ln[x] \right)$$

$$y(x) = (a \operatorname{Tanh}^b(x-c)) \rightarrow \frac{\partial y(x)}{\partial x} = (ab \cdot \operatorname{Sech}(c-x)^2) \cdot (-\operatorname{Tanh}(c-x))^{b-1}$$

$$y(x) = (a(x-b)^c + d) \rightarrow \frac{\partial y(x)}{\partial x} = ac \cdot (x-b)^{c-1}$$

$$y(x) = ((1 - \operatorname{Tanh}(e \cdot x))^a)^b + c \rightarrow \frac{\partial y(x)}{\partial x} = -ab \cdot e^1 \cdot (\operatorname{Sech}(e \cdot x))^2 \operatorname{Tanh}(e \cdot x)^{a-1}$$

$$y(x) = a \left(\frac{1 - \operatorname{Cos}(\pi(x-b))}{2} \right)^c \rightarrow \frac{\partial y(x)}{\partial x} = \frac{ac\pi}{2^c} (1 - \operatorname{Cos}(\pi(x-b)))^{c-1} (\operatorname{Sen}(\pi(x-b)))$$

$$y(x) = \frac{1}{2} (1 + \operatorname{Tanh}^c(a(x-b))) \rightarrow \frac{\partial y(x)}{\partial x} = \left(\frac{1}{2} ac \cdot \operatorname{Sech}(a(c-x))^2 \right) \cdot (1 + \operatorname{Tanh}(a(c-x)))^{b-1}$$

$$y(x) = a \operatorname{Senh}(x-b)^c \rightarrow \frac{\partial y(x)}{\partial x} = ac \cdot \operatorname{Cosh}(x-b) \cdot (-\operatorname{Senh}(b-x))^{c-1}$$

$$y(x) = a \left(1 - \frac{(x-b)^2}{c^2} \right)^d \rightarrow \frac{\partial y(x)}{\partial x} = -\frac{2ad(x-b) \left(1 - \frac{(x-b)^2}{c^2} \right)^{d-1}}{c^2}$$

$$y(x) = \frac{a(x-b)^c}{1-d(x-b)^e} \rightarrow \frac{\partial y(x)}{\partial x} = \frac{a(x-b)^{c-1} (c - c \cdot d \cdot (x-b)^e + d \cdot e \cdot (x-b)^e)}{(-1 + d(x-b)^e)^2}$$

$$y(x) = a \cdot \operatorname{Exp} \left(b \cdot \left(1 - \frac{c}{dx} \right) \right) + e \rightarrow \frac{\partial y(x)}{\partial x} = \frac{a \cdot b \cdot c \cdot \operatorname{Exp} \left(b \cdot \left(1 - \frac{c}{dx} \right) \right)}{d \cdot x^2}$$

$$y(x) = \operatorname{Ln} \left(a \cdot \operatorname{Exp} \left(b \cdot \left(1 - \frac{c}{dx} \right) \right) + e \right) \rightarrow \frac{\partial y(x)}{\partial x} = \frac{a \cdot b \cdot c \cdot \operatorname{Exp} \left(b \cdot \left(1 - \frac{c}{dx} \right) \right)}{d \cdot \left(e + a \cdot \operatorname{Exp} \left(b \cdot \left(1 - \frac{c}{dx} \right) \right) \right) \cdot x^2}$$

$$y(x) = a(b \cdot x + c)^{-d} \rightarrow \frac{\partial y(x)}{\partial x} = -a \cdot b \cdot d \cdot (b \cdot x + c)^{-d-1}$$

APPENDIX B – FUNCTIONS AND GRAPHS FOR THE APPROXIMATIONS

This appendix is related to be a visual collection which may be helpful to build the appropriate approximations. The figures show the functions and its behaviors varying x (as dimensionless temperature τ), and other parameters.

In Figures B.1-B7 first we present functions that obey addition Heaviside conditions which is the functions and its derivates must be equal to zero at $x=0$.

Figure B.1 – Equation behavior example $y = ax^n$ (Function meets conditions $y(0)=0$; $y'(0)=0$ at $n > \sim 1.5$).

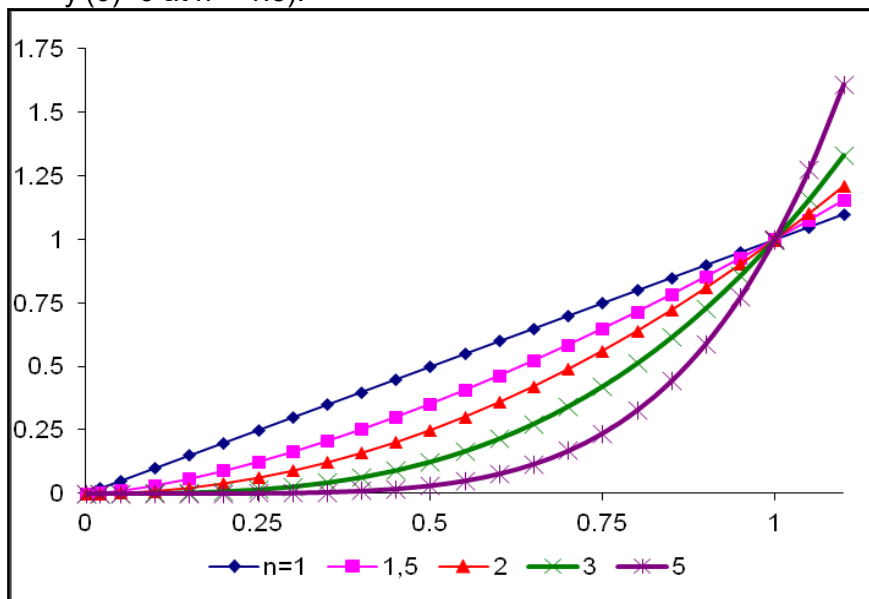


Figure B.2 – Equation behavior example $y = \frac{ax^n}{1-bx^m}$, Function meets conditions $y(0)=0$; $y'(0)=0$ at $n > \sim 1.5$; $0.1 < b < 0.9$

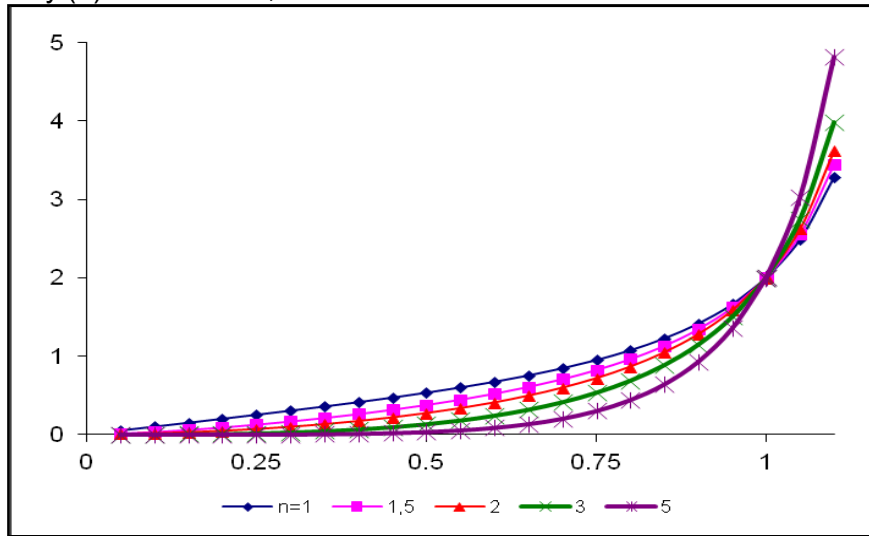


Figure B.3 – Equation behavior example, $y = a_2x^2 + a_3x^3 + a_4x^4$, Function meets conditions $y(0)=0$; $y'(0)=0$.

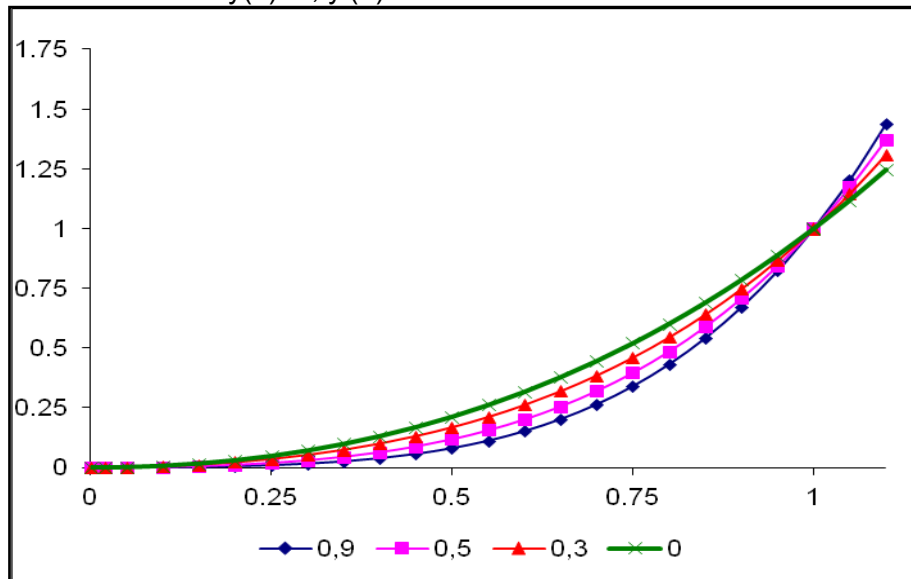


Figure B.4 – Equation behavior example $y = aTanh^n(ex)$, Function meets conditions $y(0)=0; y'(0)=0$ at $n > \sim 1.5$.

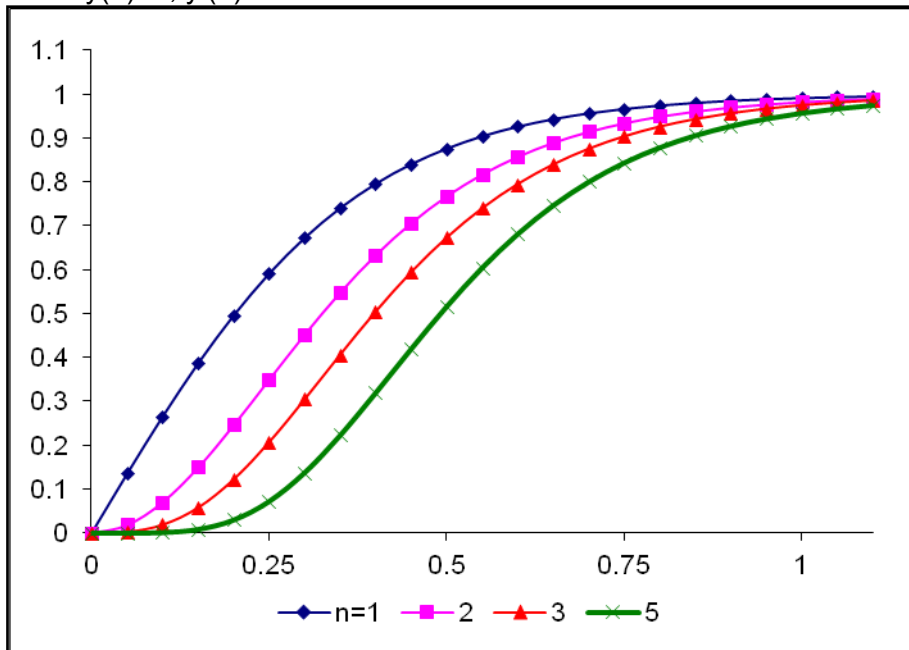


Figure B.5 – Equation behavior example $y = aSinh^n(x)$, Function meets conditions $y(0)=0; y'(0)=0$ at $n > \sim 1.5$.

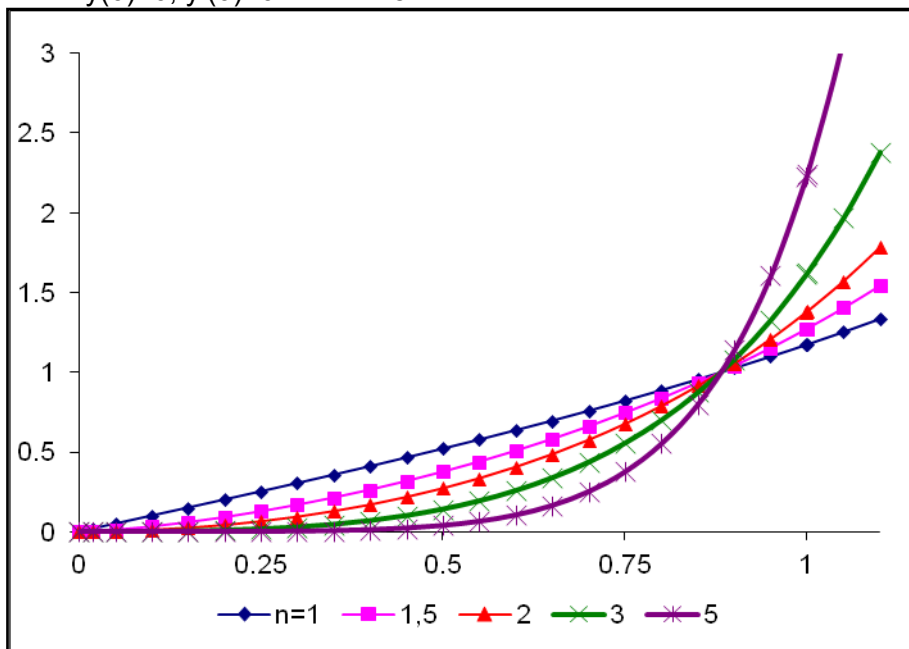


Figure B.6 – Equation behavior example $y = a \left(\frac{1 - \cos(\pi x)}{2} \right)^n$, Function meets conditions $y(0)=0$; $y'(0)=0$.

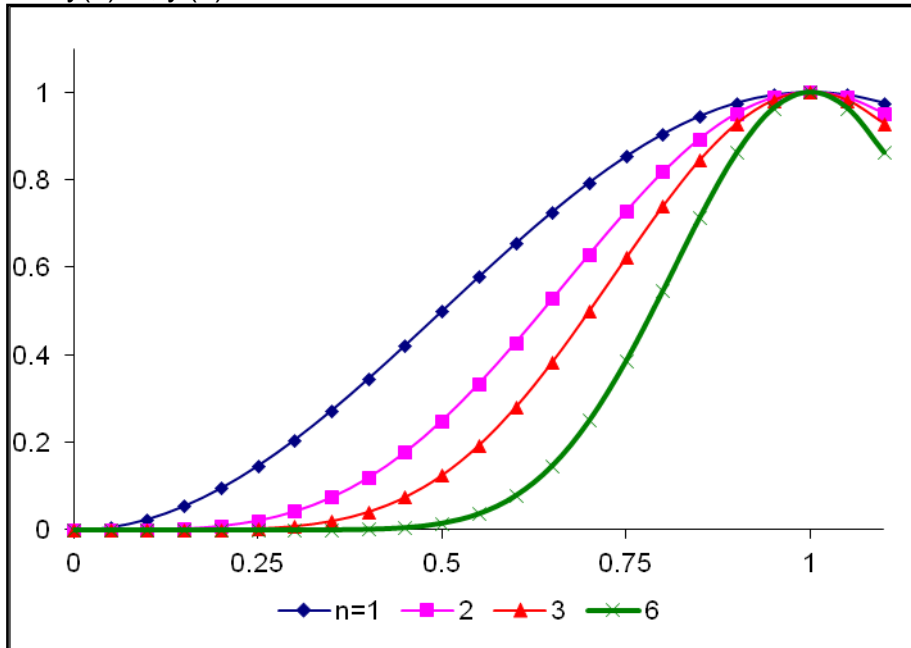
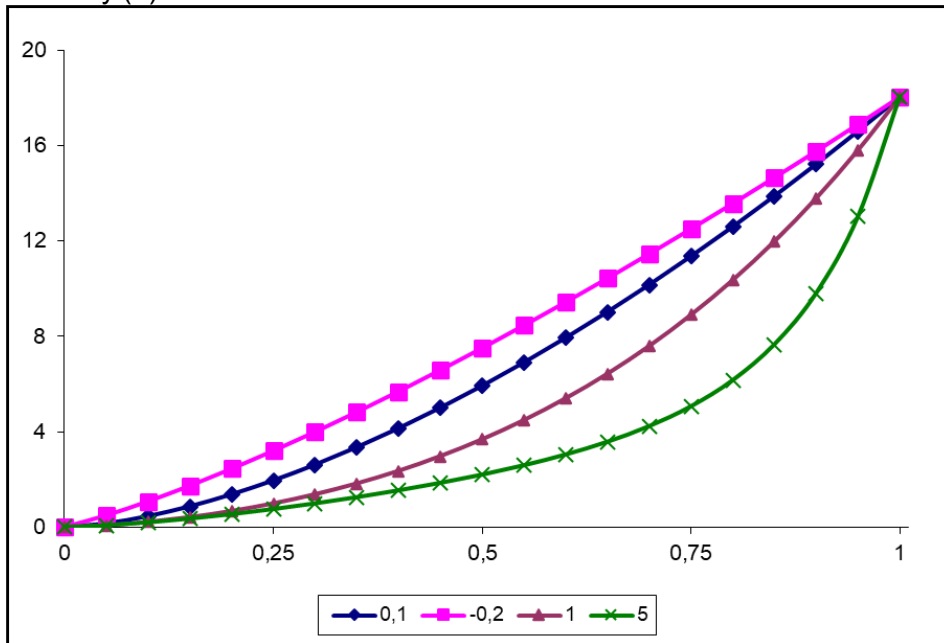


Figure B.7 – Equation behavior example $y = ax^b e^{cx^n}$, Function meets conditions $y(0)=0$; $y'(0)=0$ at $b > \sim 1.5$ & $n > 0$.



The functions below do not necessarily need satisfy the Heaviside conditions.

Figure B.8 – Equation behavior example $y = \text{Tanh}^n(ex)$.

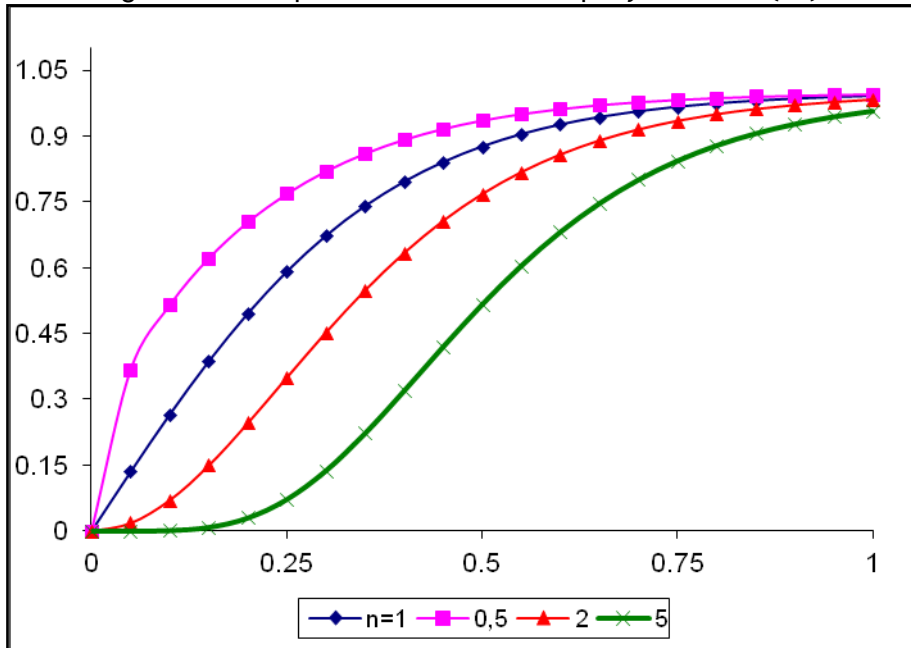


Figure B.9 – Equation behavior example $y = 1 - \text{Tanh}^n(ex)$.

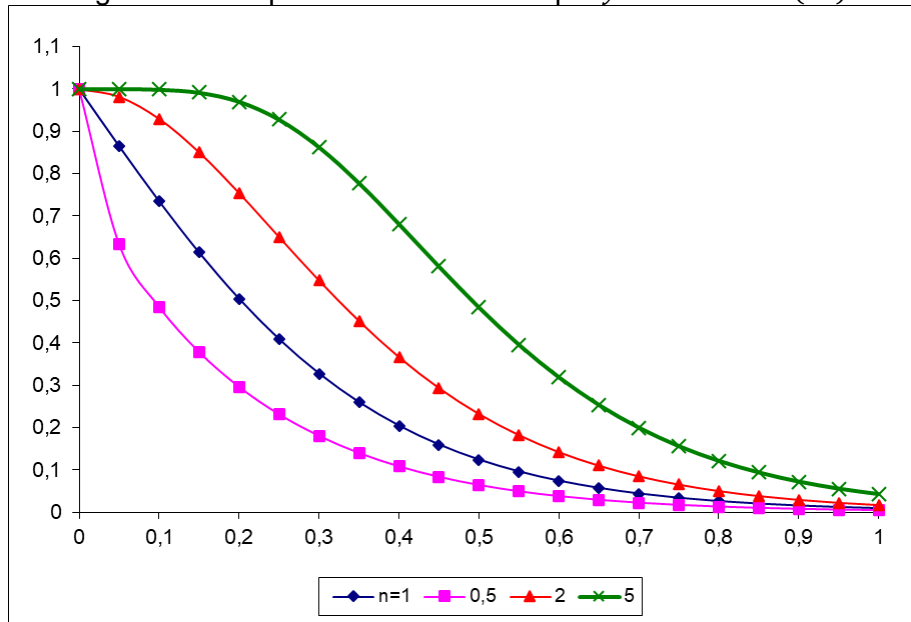


Figure B.10 – Equation behavior example $y = (1 - \text{Tanh}^n(ex))^n$.

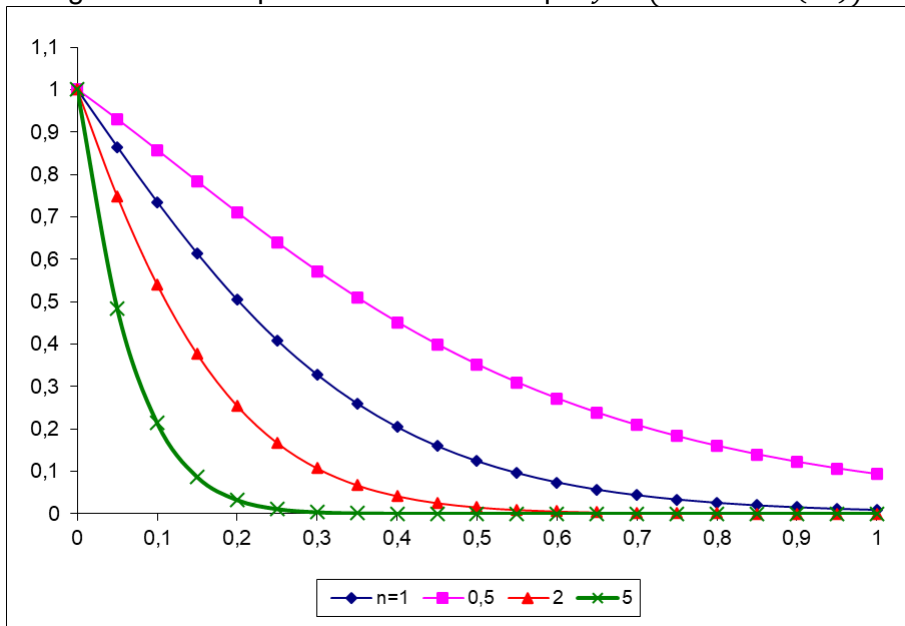


Figure B.11 – Equation behavior example $y = \frac{1}{2}(1 + \text{Tanh}(n(x - 0.5)))$.

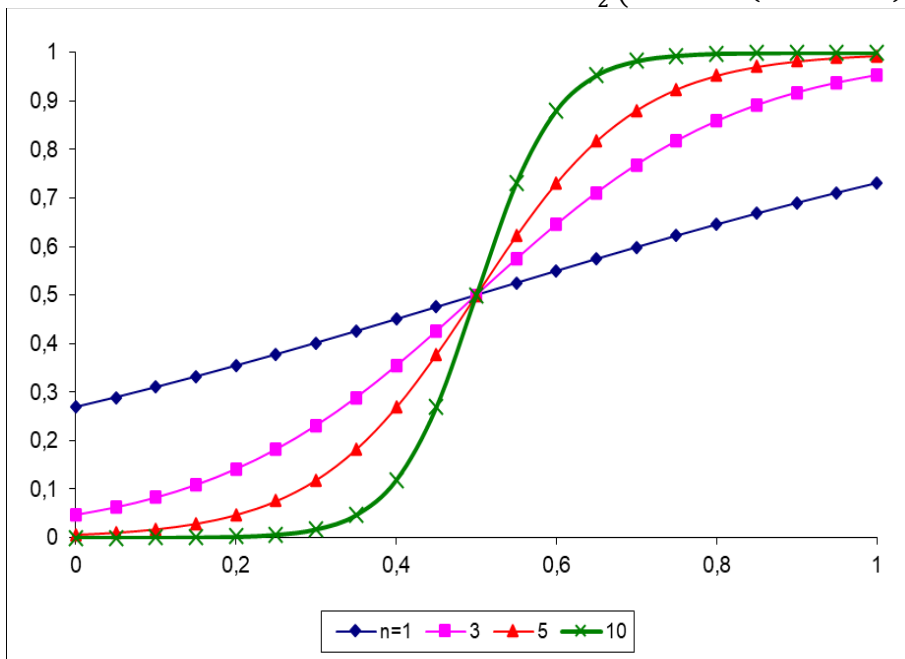


Figure B.12 – Equation behavior example $y = (1 - x)^n$.

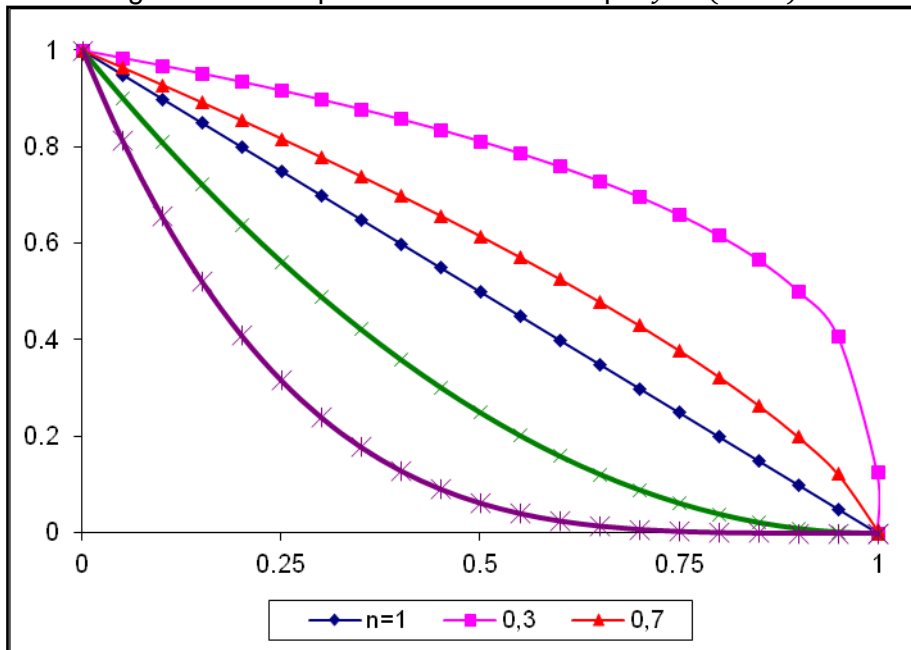


Figure B.13 – Equation behavior example $y = \frac{1-x}{1-x^n}$.

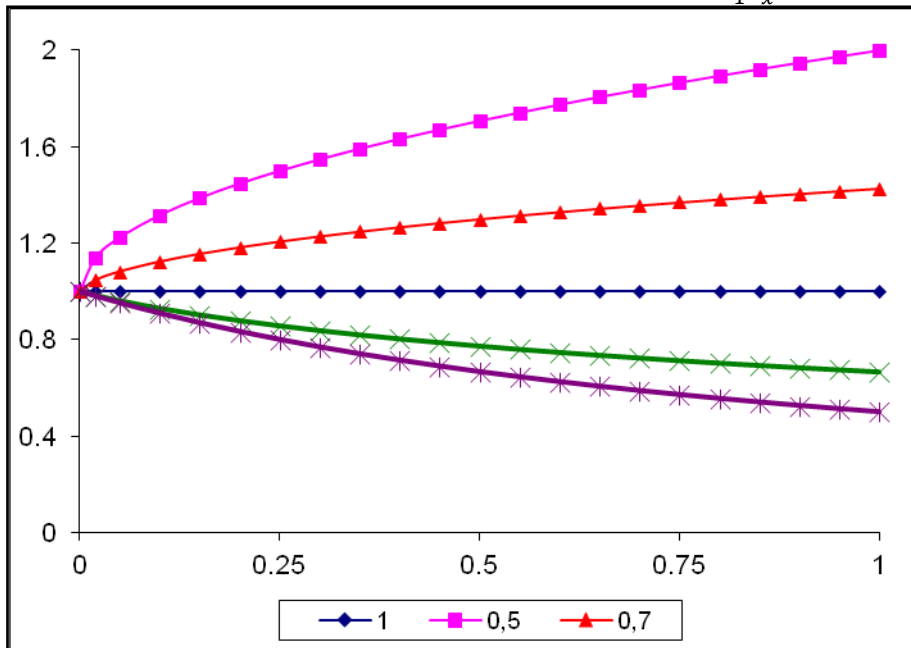


Figure B.14 – Equation behavior example $y = \text{Sech}^n(x)$.

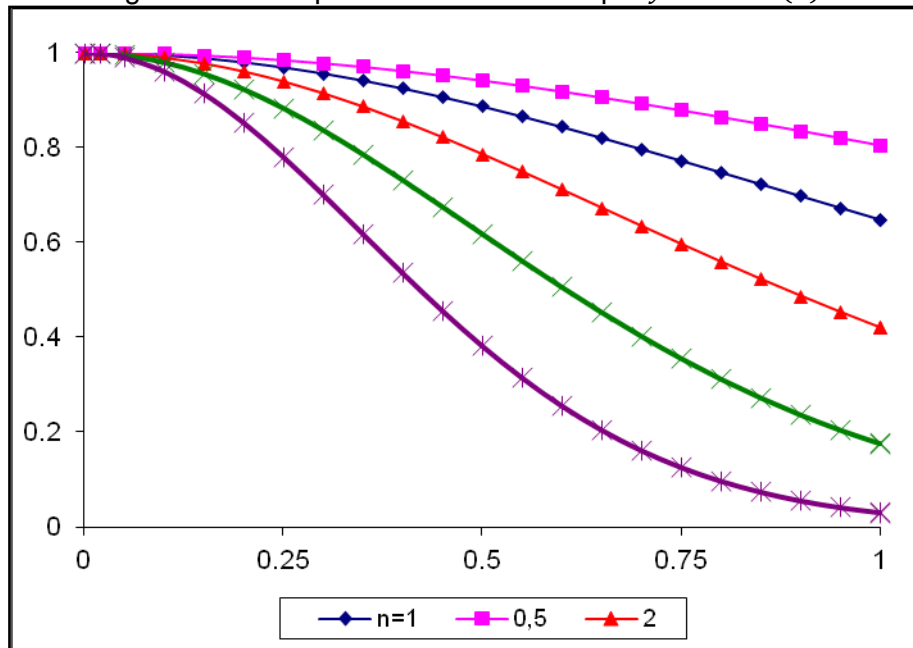


Figure B.15 – Equation behavior example $y(x) = a \left(1 - \frac{(x-b)^2}{c^2}\right)^n$.

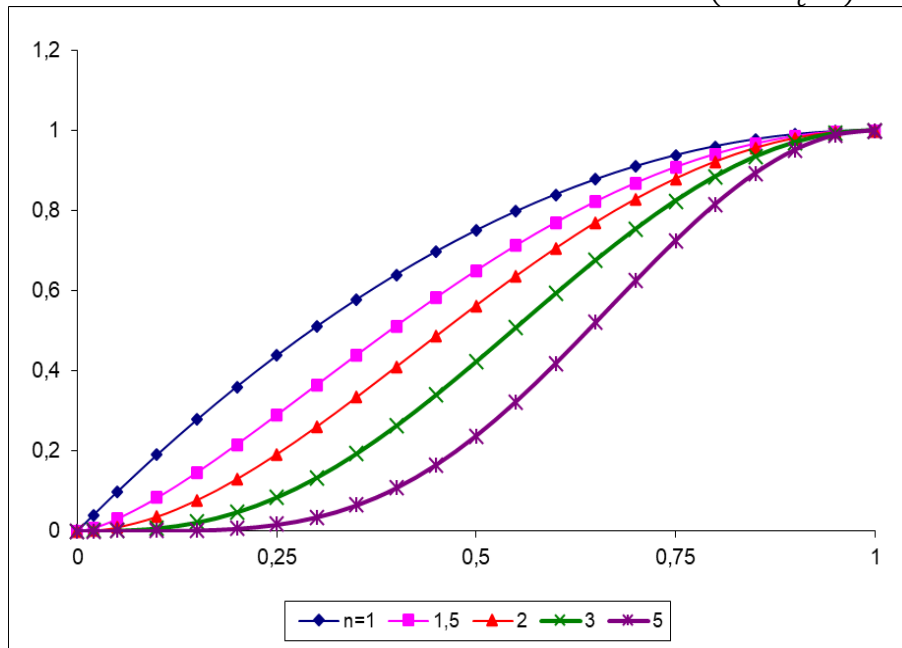
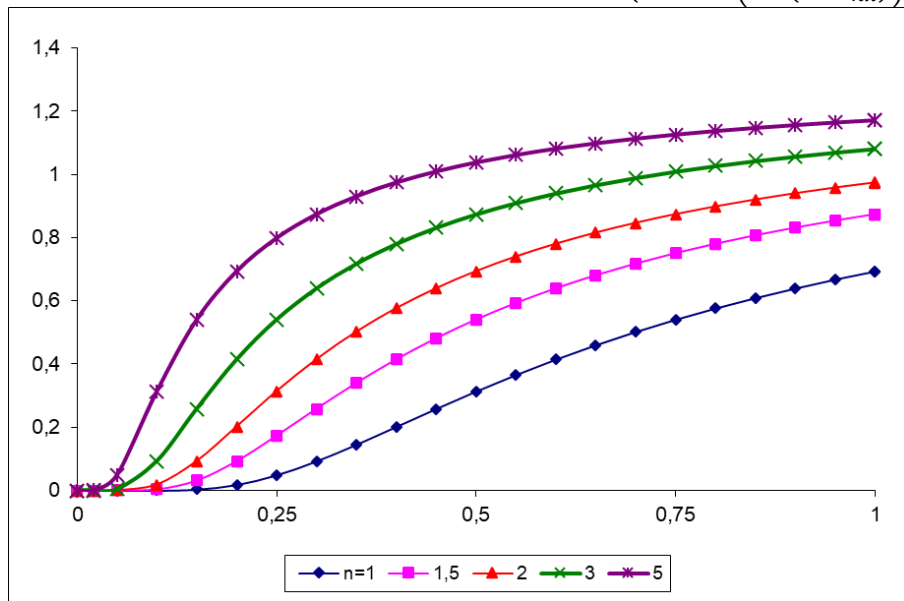


Figure B.16 – Equation behavior example $y(x) = \text{Ln} \left(a \cdot \text{Exp} \left(b \cdot \left(1 - \frac{c}{nx} \right) \right) + e \right)$.



APPENDIX C – EXCEL VISUAL BASIC CODE FOR RANDOM SEARCH

This part presents a developed VBA code built within EXCEL table to help the User to reach the best approximation results by minimizing the weighted error of the approximation. The parameters of approximations are optimized variables. This code applies random search within values, chosen by User, on the approximation parameters and place the 10th better result interactively in a rank. At any moment User may interrupt the execution to narrow the range of variation of any variable. The algorithm of this code was described in section 4.5 of Methodology capture.

```

Dim continuarExecucao As Boolean
Public b As Integer
Sub EncontrarMelhoresValores()
    continuarExecucao = True

    On Error GoTo ErrorHandler ' Lidar com erros
    continuarExecucao = True
    Dim melhorResultado As Double
    Dim erroMaximo As Double
    Dim desvioO10 As Double
    Dim variaveis(1 To 13) As Double
    Dim Interacoes, loops, p As Long
    Dim i, t, CONTROLE, j As Integer
    Dim numeroDeColunas As Integer
    Dim melhoresResultados(1 To 10) As Double
    Dim melhoresVariaveis(1 To 10, 1 To 13) As Double
    Dim ResultAtual As Double

    Range("AC9:AD100").Value = ""
    Interacoes = 30000
    loops = 500
    p = 0
    b = 8
    Range("N8").Value = p
    Range("AC9:AD100").Value = ""
    For t = 1 To loops
        '-----Inicialmente coloca valores aleatorios-----
        ' Inicialize o melhorResultado
        If t = 1 Then
            For j = 1 To 13
                variaveis(j) = RndRange(LimiteInferior(j), LimiteSuperior(j))
            Next j
            For j = 11 To 23
                Range("N" & j).Value = variaveis(j - 10)
            ' Ajuste o índice da variável para corresponder às células
            Next j
            For j = 10 To 23
                Range("O" & j).Value = Range("N" & j).Value
            Next j
            ' Y->Z
            For j = 10 To 23
                Range("Z" & j).Value = Range("N" & j).Value
            Next j
            ' X->Y
            For j = 10 To 23
                Range("Y" & j).Value = Range("N" & j).Value
            Next j
            ' W->X
            For j = 10 To 23

```

```

Range("X" & j).Value = Range("N"
& j).Value
Next j
' V->W
For j = 10 To 23
Range("W" & j).Value = Range("N"
& j).Value
Next j
' U->V
For j = 10 To 23
Range("V" & j).Value = Range("N"
& j).Value
Next j
' T->U
For j = 10 To 23
Range("U" & j).Value = Range("N"
& j).Value
Next j
' S->T
For j = 10 To 23
Range("T" & j).Value = Range("N"
& j).Value
Next j
' R->S
For j = 10 To 23
Range("S" & j).Value = Range("N"
& j).Value
Next j
' Q->R
For j = 10 To 23
Range("R" & j).Value = Range("N"
& j).Value
Next j
' N->Q
For j = 10 To 23
Range("Q" & j).Value = Range("N"
& j).Value
Next j
End If
melhordesvio = Range("O10").Value

Desvio1 = Range("Q10").Value
Desvio2 = Range("R10").Value
Desvio3 = Range("S10").Value

Desvio4 = Range("T10").Value
Desvio5 = Range("U10").Value
Desvio6 = Range("V10").Value
Desvio7 = Range("W10").Value
Desvio8 = Range("X10").Value
Desvio9 = Range("Y10").Value
Desvio10 = Range("Z10").Value

melhorResultado = melhordesvio

Result1 = Desvio1
Result2 = Desvio2
Result3 = Desvio3
Result4 = Desvio4
Result5 = Desvio5
Result6 = Desvio6
Result7 = Desvio7
Result8 = Desvio8
Result9 = Desvio9
Result10 = Desvio10

' Array para rastrear os 10 melhores
resultados e suas variáveis

For i = 1 To Interacoes
Do Until Not continuarExecucao

' Defina os limites iniciais das variáveis
For j = 1 To 13
variaveis(j) =
RndRange(LimiteInferior(j), LimiteSuperior(j))
Next j

' Inserir valores aleatórios nas células
N11 a N21
For j = 11 To 21
Range("N" & j).Value = variaveis(j - 10)
' Ajuste o índice da variável para corresponder às
células

Next j
p = p + 1
Range("N8").Value = p

```

' Verificar se os resultados atendem aos critérios

desvioAtual = Range("N10").Value

If desvioAtual < melhordesvio Then

b = b + 1

' Calcular a multiplicação de N9 e N10

ResultAtual = desvioAtual

If ResultAtual < melhorResultado Then

'-----Separar dados para grafico

Range("AC" & b).Value = p

Range("AD" & b).Value = desvioAtual

melhorResultado = ResultAtual

' Copiar os valores de N9 a N21 para as células O9 a O21

For j = 10 To 23

Range("O" & j).Value = Range("N" & j).Value

Next j

melhordesvio = Range("O10").Value

End If

End If

Desvio1 = Range("Q10").Value

Desvio2 = Range("R10").Value

Desvio3 = Range("S10").Value

Desvio4 = Range("T10").Value

Desvio5 = Range("U10").Value

Desvio6 = Range("V10").Value

Desvio7 = Range("W10").Value

Desvio8 = Range("X10").Value

Desvio9 = Range("Y10").Value

Desvio10 = Range("Z10").Value

melhorResultado = melhordesvio

Result1 = Desvio1

Result2 = Desvio2

Result3 = Desvio3

Result4 = Desvio4

Result5 = Desvio5

Result6 = Desvio6

Result7 = Desvio7

Result8 = Desvio8

Result9 = Desvio9

Result10 = Desvio10

'-----ERRO 1-----

If melhordesvio < Desvio1 Then

' Y->Z

For j = 10 To 23

Range("Z" & j).Value = Range("Y" & j).Value

Next j

' X->Y

For j = 10 To 23

Range("Y" & j).Value = Range("X" & j).Value

Next j

' W->X

For j = 10 To 23

Range("X" & j).Value = Range("W" & j).Value

Next j

' V->W

For j = 10 To 23

Range("W" & j).Value = Range("V" & j).Value

Next j

' U->V

For j = 10 To 23

Range("V" & j).Value = Range("U" & j).Value

Next j

' T->U

For j = 10 To 23

Range("U" & j).Value = Range("T" & j).Value

Next j

' S->T

For j = 10 To 23

Range("T" & j).Value = Range("S" & j).Value

```

Next j
' R->S
For j = 10 To 23
  Range("S" & j).Value = Range("R"
& j).Value
Next j
' Q->R
For j = 10 To 23
  Range("R" & j).Value = Range("Q"
& j).Value
Next j
' N->Q
For j = 10 To 23
  Range("Q" & j).Value = Range("O"
& j).Value
Next j
Else
'-----ERRO 2-----
If Range("N10").Value < Desvio2 Then
  ' Y->Z
  For j = 10 To 23
    Range("Z" & j).Value = Range("Y"
& j).Value
  Next j
  ' X->Y
  For j = 10 To 23
    Range("Y" & j).Value = Range("X"
& j).Value
  Next j
  ' W->X
  For j = 10 To 23
    Range("X" & j).Value = Range("W"
& j).Value
  Next j
  ' V->W
  For j = 10 To 23
    Range("W" & j).Value = Range("V"
& j).Value
  Next j
  ' U->V
  For j = 10 To 23
    Range("V" & j).Value = Range("U"
& j).Value
  Next j
' T->U
For j = 10 To 23
  Range("U" & j).Value = Range("T"
& j).Value
Next j
' S->T
For j = 10 To 23
  Range("T" & j).Value = Range("S"
& j).Value
Next j
' R->S
For j = 10 To 23
  Range("S" & j).Value = Range("R"
& j).Value
Next j
' N->R
For j = 10 To 23
  Range("R" & j).Value = Range("N"
& j).Value
Next j
Else
'-----ERRO 3-----
If Range("N10").Value < Desvio3 Then
  ' Y->Z
  For j = 10 To 23
    Range("Z" & j).Value = Range("Y"
& j).Value
  Next j
  ' X->Y
  For j = 10 To 23
    Range("Y" & j).Value = Range("X"
& j).Value
  Next j
  ' W->X
  For j = 10 To 23
    Range("X" & j).Value = Range("W"
& j).Value
  Next j
  ' V->W
  For j = 10 To 23
    Range("W" & j).Value = Range("V"
& j).Value
  Next j
  ' U->V

```



```

Range("U" & j).Value = Range("N"
& j).Value
Next j
Else
'-----ERRO 6-----
If Range("N10").Value < Desvio6 Then
' Y->Z
For j = 10 To 23
Range("Z" & j).Value = Range("Y"
& j).Value
Next j
' X->Y
For j = 10 To 23
Range("Y" & j).Value = Range("X"
& j).Value
Next j
' W->X
For j = 10 To 23
Range("X" & j).Value = Range("W"
& j).Value
Next j
' V->W
For j = 10 To 23
Range("W" & j).Value = Range("V"
& j).Value
Next j
' N->V
For j = 10 To 23
Range("V" & j).Value = Range("N"
& j).Value
Next j
Else
'-----ERRO 7-----
If Range("N10").Value < Desvio7 Then
' Y->Z
For j = 10 To 23
Range("Z" & j).Value = Range("Y"
& j).Value
Next j
' X->Y
For j = 10 To 23
Range("Y" & j).Value = Range("X"
& j).Value
Next j
' W->X
For j = 10 To 23
Range("X" & j).Value = Range("W"
& j).Value
Next j
' N->W
For j = 10 To 23
Range("W" & j).Value = Range("N"
& j).Value
Next j
Else
'-----ERRO 8-----
If Range("N10").Value < Desvio8 Then
' Y->Z
For j = 10 To 23
Range("Z" & j).Value = Range("Y"
& j).Value
Next j
' X->Y
For j = 10 To 23
Range("Y" & j).Value = Range("X"
& j).Value
Next j
' N->X
For j = 10 To 23
Range("X" & j).Value = Range("N"
& j).Value
Next j
Else
'-----ERRO 9-----
If Range("N10").Value < Desvio9 Then
' Y->Z
For j = 10 To 23
Range("Z" & j).Value = Range("Y"
& j).Value
Next j
' N->Y
For j = 10 To 23
Range("Y" & j).Value = Range("N"
& j).Value
Next j
Else
'-----ERRO 10-----

```

```

    If Range("N10").Value < Desvio10
Then
    ' Y->Z

    For j = 10 To 23
        Range("Z" & j).Value = Range("N"
& j).Value
    Next j
End If
DoEvents
Loop
Next i
Next t
Exit Sub ' Sair em caso de sucesso

```

```

ErrorHandler:
    MsgBox "Ocorreu um erro: " & Err.Description
End Sub

```

```

Function LimiteInferior(ByVal index As Integer)
As Double
' Defina os limites inferiores para as variáveis
Select Case index
    Case 1
        LimiteInferior = Range("P11").Value
    Case 2
        LimiteInferior = Range("P12").Value
    Case 3
        LimiteInferior = Range("P13").Value
    Case 4
        LimiteInferior = Range("P14").Value
    Case 5
        LimiteInferior = Range("P15").Value

```

```

Case 6
    LimiteInferior = Range("P16").Value
Case 7
    LimiteInferior = Range("P17").Value
Case 8
    LimiteInferior = Range("P18").Value
Case 9
    LimiteInferior = Range("P19").Value
Case 10
    LimiteInferior = Range("P20").Value
Case 11
    LimiteInferior = Range("P21").Value
Case 12
    LimiteInferior = Range("P22").Value
Case 13
    LimiteInferior = Range("P23").Value
End Select
End Function

```

```

Function LimiteSuperior(ByVal index As Integer)
As Double
' Defina os limites superiores para as variáveis
Select Case index
    Case 1
        LimiteSuperior = Range("AA11").Value
    Case 2
        LimiteSuperior = Range("AA12").Value
    Case 3
        LimiteSuperior = Range("AA13").Value
    Case 4
        LimiteSuperior = Range("AA14").Value
    Case 5
        LimiteSuperior = Range("AA15").Value
    Case 6
        LimiteSuperior = Range("AA16").Value
    Case 7
        LimiteSuperior = Range("AA17").Value
    Case 8
        LimiteSuperior = Range("AA18").Value
    Case 9
        LimiteSuperior = Range("AA19").Value

```

```

Case 10
    LimiteSuperior = Range("AA20").Value
Case 11
    LimiteSuperior = Range("AA21").Value
Case 12
    LimiteSuperior = Range("AA22").Value
Case 13
    LimiteSuperior = Range("AA23").Value
End Select
End Function

```

```

Function RndRange(ByVal MinValue As Double,
ByVal MaxValue As Double) As Double
    ' Gera um número aleatório entre MinValue e
MaxValue
    RndRange = (MaxValue - MinValue) * Rnd +
MinValue
End Function

```

```

Sub PararMacro()
    continuarExecucao = False
    Dim j As Integer
    For j = 11 To 23
        Range("N" & j).Value = Range("o" &
j).Value
    Next j
End Sub

```

```

Sub EncontrarMelhoresValoresPause_cont()
    continuarExecucao = True

    On Error GoTo ErrorHandler ' Lidar com erros
    continuarExecucao = True
    Dim melhorResultado As Double
    Dim erroMaximo As Double
    Dim desvioO10 As Double
    Dim variaveis(1 To 13) As Double
    Dim Interacoes, loops, pcont As Long
    Dim i, t, CONTROLE As Integer
    Dim numeroDeColunas As Integer
    Dim melhoresResultados(1 To 10) As Double
    Dim melhoresVariaveis(1 To 10, 1 To 13) As
Double

```

```

Dim ResultAtual As Double
Interacoes = 30000
loops = 500
For t = 1 To loops
    melhordesvio = Range("O10").Value
    Desvio1 = Range("Q10").Value
    Desvio2 = Range("R10").Value
    Desvio3 = Range("S10").Value
    Desvio4 = Range("T10").Value
    Desvio5 = Range("U10").Value
    Desvio6 = Range("V10").Value
    Desvio7 = Range("W10").Value
    Desvio8 = Range("X10").Value
    Desvio9 = Range("Y10").Value
    Desvio10 = Range("Z10").Value
    melhorResultado = melhordesvio
    Result1 = Desvio1
    Result2 = Desvio2
    Result3 = Desvio3
    Result4 = Desvio4
    Result5 = Desvio5
    Result6 = Desvio6
    Result7 = Desvio7
    Result8 = Desvio8
    Result9 = Desvio9
    Result10 = Desvio10

    ' Array para rastrear os 10 melhores
resultados e suas variáveis
    For i = 1 To Interacoes
        Do Until Not continuarExecucao

            ' Defina os limites iniciais das variáveis
            For j = 1 To 13
                variaveis(j) =
                RndRange(LimiteInferior(j), LimiteSuperior(j))
            Next j

            ' Inserir valores aleatórios nas células
N11 a N21
            For j = 11 To 23

```

```

Range("N" & j).Value = variaveis(j - 10)
' Ajuste o índice da variável para corresponder às
células

```

```

Next j

```

```

pcont = Range("N8").Value

```

```

pcont = pcont + 1

```

```

Range("N8").Value = pcont

```

```

' Verificar se os resultados atendem aos
critérios

```

```

desvioAtual = Range("N10").Value

```

```

If desvioAtual < melhordesvio Then

```

```

    b = b + 1

```

```

    ' Calcular a multiplicação de N9 e N10

```

```

    ResultAtual = desvioAtual

```

```

    If ResultAtual < melhorResultado Then

```

```

'-----Separar dados para grafico

```

```

    Range("AC" & b).Value = pcont

```

```

    Range("AD" & b).Value = desvioAtual

```

```

    melhorResultado = ResultAtual

```

```

    ' Copiar os valores de N9 a N21 para
as células O9 a O21

```

```

    For j = 10 To 23

```

```

        Range("O" & j).Value = Range("N" &
j).Value

```

```

    Next j

```

```

    melhordesvio = Range("O10").Value

```

```

End If

```

```

End If

```

```

Desvio1 = Range("Q10").Value

```

```

Desvio2 = Range("R10").Value

```

```

Desvio3 = Range("S10").Value

```

```

Desvio4 = Range("T10").Value

```

```

Desvio5 = Range("U10").Value

```

```

Desvio6 = Range("V10").Value

```

```

Desvio7 = Range("W10").Value

```

```

Desvio8 = Range("X10").Value

```

```

Desvio9 = Range("Y10").Value

```

```

Desvio10 = Range("Z10").Value

```

```

melhorResultado = melhordesvio

```

```

Result1 = Desvio1

```

```

Result2 = Desvio2

```

```

Result3 = Desvio3

```

```

Result4 = Desvio4

```

```

Result5 = Desvio5

```

```

Result6 = Desvio6

```

```

Result7 = Desvio7

```

```

Result8 = Desvio8

```

```

Result9 = Desvio9

```

```

Result10 = Desvio10

```

```

'-----ERRO 1-----

```

```

    If melhordesvio < Desvio1 Then

```

```

        ' Y->Z

```

```

        For j = 10 To 23

```

```

            Range("Z" & j).Value = Range("Y"
& j).Value

```

```

        Next j

```

```

        ' X->Y

```

```

        For j = 10 To 23

```

```

            Range("Y" & j).Value = Range("X"
& j).Value

```

```

        Next j

```

```

        ' W->X

```

```

        For j = 10 To 23

```

```

            Range("X" & j).Value = Range("W"
& j).Value

```

```

        Next j

```

```

        ' V->W

```

```

        For j = 10 To 23

```

```

            Range("W" & j).Value = Range("V"
& j).Value

```

```

        Next j

```

```

        ' U->V

```

```

        For j = 10 To 23

```

```

            Range("V" & j).Value = Range("U"
& j).Value

```

```

        Next j

```

```

' T->U
For j = 10 To 23
    Range("U" & j).Value = Range("T"
& j).Value
Next j
' S->T
For j = 10 To 23
    Range("T" & j).Value = Range("S"
& j).Value
Next j
' R->S
For j = 10 To 23
    Range("S" & j).Value = Range("R"
& j).Value
Next j
' Q->R
For j = 10 To 23
    Range("R" & j).Value = Range("Q"
& j).Value
Next j
' N->Q
For j = 10 To 23
    Range("Q" & j).Value = Range("O"
& j).Value
Next j
Else
'-----ERRO 2-----
If Range("N10").Value < Desvio2 Then
' Y->Z
For j = 10 To 23
    Range("Z" & j).Value = Range("Y"
& j).Value
Next j
' X->Y
For j = 10 To 23
    Range("Y" & j).Value = Range("X"
& j).Value
Next j
' W->X
For j = 10 To 23
    Range("X" & j).Value = Range("W"
& j).Value
Next j
' V->W
For j = 10 To 23
    Range("W" & j).Value = Range("V"
& j).Value
Next j
' U->V
For j = 10 To 23
    Range("V" & j).Value = Range("U"
& j).Value
Next j
' T->U
For j = 10 To 23
    Range("U" & j).Value = Range("T"
& j).Value
Next j
' S->T
For j = 10 To 23
    Range("T" & j).Value = Range("S"
& j).Value
Next j
' R->S
For j = 10 To 23
    Range("S" & j).Value = Range("R"
& j).Value
Next j
' N->R
For j = 10 To 23
    Range("R" & j).Value = Range("N"
& j).Value
Next j
Else
'-----ERRO 3-----
If Range("N10").Value < Desvio3 Then
' Y->Z
For j = 10 To 23
    Range("Z" & j).Value = Range("Y"
& j).Value
Next j
' X->Y
For j = 10 To 23
    Range("Y" & j).Value = Range("X"
& j).Value
Next j
' W->X
For j = 10 To 23

```

```

Range("X" & j).Value = Range("W"
& j).Value
Next j
' V->W
For j = 10 To 23
Range("W" & j).Value = Range("V"
& j).Value
Next j
' U->V
For j = 10 To 23
Range("V" & j).Value = Range("U"
& j).Value
Next j
' T->U
For j = 10 To 23
Range("U" & j).Value = Range("T"
& j).Value
Next j
' S->T
For j = 10 To 23
Range("T" & j).Value = Range("S"
& j).Value
Next j
' N->S
For j = 10 To 23
Range("S" & j).Value = Range("N"
& j).Value
Next j
Else
'-----ERRO 4-----
If Range("N10").Value < Desvio4 Then
' Y->Z
For j = 10 To 23
Range("Z" & j).Value = Range("Y"
& j).Value
Next j
' X->Y
For j = 10 To 23
Range("Y" & j).Value = Range("X"
& j).Value
Next j
' W->X
For j = 10 To 23

```

```

Range("X" & j).Value = Range("W"
& j).Value
Next j
' V->W
For j = 10 To 23
Range("W" & j).Value = Range("V"
& j).Value
Next j
' U->V
For j = 10 To 23
Range("V" & j).Value = Range("U"
& j).Value
Next j
' T->U
For j = 10 To 23
Range("U" & j).Value = Range("T"
& j).Value
Next j
' N->T
For j = 10 To 23
Range("T" & j).Value = Range("N"
& j).Value
Next j
Else
'-----ERRO 5-----
If Range("N10").Value < Desvio5 Then
' Y->Z
For j = 10 To 21
Range("Z" & j).Value = Range("Y"
& j).Value
Next j
' X->Y
For j = 10 To 23
Range("Y" & j).Value = Range("X"
& j).Value
Next j
' W->X
For j = 10 To 23
Range("X" & j).Value = Range("W"
& j).Value
Next j
' V->W
For j = 10 To 23

```

```

Range("W" & j).Value = Range("V"
& j).Value
Next j
' U->V
For j = 10 To 23
Range("V" & j).Value = Range("U"
& j).Value
Next j
' N->U
For j = 10 To 23
Range("U" & j).Value = Range("N"
& j).Value
Next j
Else
'-----ERRO 6-----
If Range("N10").Value < Desvio6 Then
' Y->Z
For j = 10 To 23
Range("Z" & j).Value = Range("Y"
& j).Value
Next j
' X->Y
For j = 10 To 23
Range("Y" & j).Value = Range("X"
& j).Value
Next j
' W->X
For j = 10 To 23
Range("X" & j).Value = Range("W"
& j).Value
Next j
' N->W
For j = 10 To 23
Range("W" & j).Value = Range("N"
& j).Value
Next j
Else
'-----ERRO 8-----
If Range("N10").Value < Desvio8 Then
' Y->Z
For j = 10 To 23
Range("Z" & j).Value = Range("Y"
& j).Value
Next j
' X->Y
For j = 10 To 23
Range("Y" & j).Value = Range("X"
& j).Value
Next j
' N->X
For j = 10 To 23
Range("X" & j).Value = Range("N"
& j).Value
Next j
Else
'-----ERRO 9-----
If Range("N10").Value < Desvio9 Then
' Y->Z
For j = 10 To 23

```

```

Range("Z" & j).Value = Range("Y"
& j).Value
Next j
' N->Y
For j = 10 To 23
Range("Y" & j).Value = Range("N"
& j).Value
Next j
Else
'-----ERRO 10-----
If Range("N10").Value < Desvio10
Then
' Y->Z

For j = 10 To 23
Range("Z" & j).Value = Range("N"
& j).Value
Next j
End If

End If
End If
End If
DoEvents
Loop

Next i
Next t
Exit Sub ' Sair em caso de sucesso

ErrorHandler:
MsgBox "Ocorreu um erro: " & Err.Description

End Sub
Function HV(val)
'Heaviside user function
If val > 0 Then HV = 1 Else HV = 0
End Function
Function HVR(val)
'Reverse Heaviside user function
If val >= 0 Then HVR = 0 Else HVR = 1
End Function

```